NIOSH

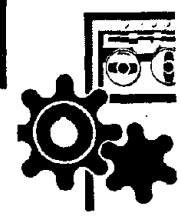

TECHNICAL REPORT

VIBRATION WHITE FINGER DISEASE in U.S. WORKERS USING PNEUMATIC CHIPPING and GRINDING HAND TOOLS

II: ENGINEERING TESTING

U.S. DEPARTMENT OF HEALTH AND HUMAN SERVICES
Public Health Service
Centers for Disease Control
National Institute for Occupational Safety and Health

VIBRATION WHITE FINGER DISEASE IN U.S. WORKERS USING PNEUMATIC CHIPPING AND GRINDING HAND TOOLS

II: ENGINEERING TESTING

Project Director
DONALD WASSERMAN

Team Leaders
D. REYNOLDS, Engineering Testing
V. BEHRENS, Epidemiology
W. TAYLOR, Medical-Clinical Testing
S. SAMUELOFF, Clinical-Objective Testing

R. BASEL

U. S. DEPARTMENT OF HEALTH AND HUMAN SERVICES
Public Health Service
Centers for Disease Control
National Institute for Occupational Safety and Health
Division of Biomedical and Behavioral Science
Cincinnati, Ohio 45226

August 1981

1-b

DISCLAIMER

Mention of company names or products does not constitute endorsement by the National Institute for Occupational Safety and Health.

OMB Project Approval Number 68-S77056

DHHS (NIOSH) Publication No. 82-101

VIBRATION STUDY TEAM *

D. E. Wasserman, MSEE (Project Director)

MEDICAL-CLINICAL TESTING

Team Leader:
W. Taylor, M.D., Ph.D.[1]
R. Miday, M.D.[4]

CLINICAL-OBJECTIVE TESTING

Team Leader:
S. Samueloff, M.D., Ph.D.[2]
W. Carlson, B.S.
R. James, M.S.
G. Peterson, B.S., M.E.

ENGINEERING TESTING

Team Leader:
D. Reynolds, Ph.D.[3]
D. Wasserman, MSEE
R. Basel, M.S.
T. Doyle
W. Asburry

EPIDEMIOLOGY

Team Leader:
V. Behrens, M.S.
S. Spaeth

QUESTIONAIRE/INTERVIEW

C. Cottrill, M.S.

RADIOLOGY

Team Leader:
G. Howie, M.D.[5]
M. Rappaport, M.D.[6]
W. Parr, Ph.D.
S. Langenbrunner
D. Nurrie

STATISTICS & DATA PROCESSING

Team Leader:
J. Morrison, B.S.
N. Lalich, M.S.
R. Smith, B.S.
K. Hicks

[1]Visiting Scientist, University of Dundee Medical School, Dundee, Scotland
[2]Visiting Scientist, Hebrew University, Hadassah Medical School, Jerusalem, Israel
[3]Mechanical Engineering Department, University of Pittsburgh, now with Pelton-Blum Inc., Dallas, Texas
[4]Kettering Institute, University of Cincinnati Medical School, Cincinnati, Ohio
[5]Consultant Radiologist, University of Dundee Medical School, Dundee, Scotland
[6]Consultant Radiologist, Univ. of Cincinnati, Medical School, Cincinnati, Ohio

*The report contained herein represents only one portion of a large multidisciplined vibration study. This report is complete in itself, however, the reader is advised to consult the other volumes comprising the entire study effort, in order to gain a complete understanding of the scope of the project.

ABSTRACT

This report represents the engineering and measurements portion of a larger comprehensive epidemiological and medical field study evaluating 74 control workers and 311 vibration-exposed workers who use pneumatic hand-held tools. In this study chipping and grinding tools were examined: (a) acceleration measurements were made while workers operated chipper and grinding tools, and (b) dynamic compliance measurements were obtained on 67 vibration exposed workers and 8 control workers.

Acceleration measurements of pneumatic chippers showed (over a frequency range of 6.3 Hz-1000 Hz) 2,400 g(rms) [23,544 m/sec^2] on the chisel, and 30 g(rms) [294.3 m/sec^2] on the rear handle taken at the points where workers normally grip these tools. Reducing the tool from full to 1/2-3/4 throttle resulted in a chisel acceleration of 200 g(rms) [1962 m/sec^2] on the chisel and 4 g(rms) [39.2 m/sec^2] on the rear handle. Acceleration levels on pneumatic grinders (operating at full throttle) were 0.5-2 g(rms) [4.9- 19.62 m/sec^2] over the same frequency range. Dynamic compliance measurements suggest that more than a 5 degree of freedom mechanical model is necessary to characterize the human hand-arm system. Total instantaneous energy into the hand appeared mostly at frequencies below 80 Hz and showed approximately 7 x 10^5 Joules/sec. on the chipping tool chisel and 157 Joules/sec. on the rear handle.

This report forms the engineering portion of the overall chipper and grinder study report.

CONTENTS

ACKNOWLEDGMENTS

The National Institute for Occupational Safety and Health's Vibration Study Team gratefully acknowledges the interest and help the following people and organizations gave throughout the various phases of planning, preparing, and performance of this study: Dr. E. S. Harris, Dr. F. Dukes-Dobos, Dr. B. Craft, Dr. C. Xintaras, Mr. W. Kelley, Mr. T. Sandlin, Mr. A. Laumann, Mrs. D. Hamilton, Mrs. M. Swenk, Dr. G. Lawton, Dr. D. Hoeffler, Dr. T. Markham, Dr. H. Hursh, Mr. W. Cochran, Dr. J.C. Guignard, Dr. J. Pearson, Mr. J. Wolfe, Dr. D. Kerr, The Bedford Indiana Chamber of Commerce, Bedford Times Mail Newspaper, radio station WBIW, Mr. G. Rasmussen, Mr. A. Romo, and those companies, unions, and volunteer worker subjects without whose help this study could not have taken place. A special acknowledgement is extended to The Indiana Laborers' Training Institute, Bedford, Indiana, and its Director, (Mr. T. Stigall) for their help and guidance with the stonecutting and carving environmental measurements.

ENGINEERING MANUSCRIPT TECHNICAL REVIEWERS

Finland

M. Hoikkala, M.S.

U.S

H. Scarton, Ph.D.
D. Clapp, Ph.D.
J. C. Barton, M.S.
T. Mueller, M.S.

INTRODUCTION

Historical Background

In 1862, Dr. Maurice Raynaud wrote an M.D. thesis entitled "Local Asphyxia and Symmetrical Gangrene of the Extremities."[1] In this thesis we find the first description of a "condition, a local syncope, where females are found to have one or more fingers becoming white and cold all at once. The determining cause is often the impression of cold. The cutaneous sensibility also becomes blunted and then annihilated." This clinical condition of "white finger" or "dead hand," which affects about 5% to 8% of the general population (many of the affected being female), has now passed into the terminology of clinical medicine as PRIMARY RAYNAUD'S DISEASE. These blanching attacks, usually affecting the fingers symmetrically, are relatively trivial in the early stages of the disease. A small proportion (1% to 3%) may, however, become progressively more severe and, over a period of years, lead to blue cold fingers, wherein the skin becomes atrophic, later ulcerated, and finally gangrenous. Dr. Raynaud also noted that there was an emotional or psychosomatic factor present in this "white finger syndrome;" the number and severity of blanching attacks increase during emotional stress.

By the end of the 19th century, other conditions giving rise to Raynaud's disease were recognized, particularly the association of vibratory tools with intermittent attacks of cold-induced pallor. Loriga[2] first described "vascular spasm" or white finger in the hands of miners using pneumatic tools. Hamilton[3] studied carvers and cutters using drills in the limestone quarries of Indiana and described "spastic anaemia of the hands." In the 1930s reports by Seyring[4], who studied fettlers in iron foundries; by Hunt[5], who studied riveters using pneumatic tools; and by Telford et al.,[6], who described white fingers in men working with electrically driven high-speed rotating tools in a warm environment, showed that white finger syndrome was on the increase. In 1946 and 1949, Agate and Druett[7] examined 230 men who were grinding excess metal from small castings that were hand-held against 2 foot diameter grinding wheels. Of this total, 163 (70%) had a history of white fingers. At this time, the "white finger" condition appeared to be arising from the effects of prolonged exposure to vibration entering the hands and was now referred to as "RAYNAUD'S PHENOMENON OF OCCUPATIONAL ORIGIN," and later as "VIBRATION-INDUCED WHITE FINGER" or VWF. With further research into VWF in the 1960s, signs and symptoms associated with vibrating tools were reported in other systems such as nerves, bones, joints, and muscles. The association of VWF with these disabilities now became known as the "VIBRATION SYNDROME."

In 1962 and 1964, Ashe and his colleagues[8, 9] investigated a small group of hard-rock mine drillers from Saskatchewan, seven of whom were examined in the hospital. As part of the clinical investigations, arteriography and biopsy of the digital arteries were done. In the worst cases, extensive damage to the digital artery with narrowing of the lumen was demonstrated. Whereas the majority of cases of VWF could be described as trivial, these investigations illustrated that in severe cases extensive pathological damage to the arteries of the fingers could arise as a result of prolonged exposure to vibration transferred from the tool to the hand.

From 1964 onward, there appeared an association between Raynaud's Phenomenon and gasoline-powered chain saws then being extensively used in British forestry for felling, delimbing or debranching (snedding), and cross-cutting timber. By 1968-1969, when chain saw operators had accumulated 12 to 14 years of continuous chain saw use, complaints of VWF were reported in Britain. The vibration of the two-stroke internal combustion engine (reciprocating forces of the single cylinder two-stroke) transmitted through the handles to hands was causing white fingers with prevalence rates in certain forests (where sawyers were working 5 to 6 hours per day, 5 days a week) greater than 90%.

The VWF prevalence rates were rising in Britain and the clinical state of the hands of workers using these chain saws was deteriorating to such an extent that the British Forestry Commission in 1970 issued workers newly designed anti-vibration (A/V) saws. The first A/V saws were based on vibration criteria thought to be safe with exposure times of 6 to 7 hours per day, 5 days a week.

Hand-Arm Vibration Research in the United States

As early as 1918, studies of Raynaud's Phenomenon in the United States were reported among stone cutters[10,11] using vibrating hand tools. These workers were studied by Alice Hamilton[3], Rothstein[12], Edsall[13], and Leake[14]. Very few studies in the United States were reported until 1946 when Dart[15] described the effects of vibrating hand tools on 112 workers in the aircraft industry. He noticed these workers complained of pain and swelling, and also showed an abnormal response to a cold provocation test; as well as tenosynovitis. Once again, there was a hiatus of occupational studies in this area in the United States until the early 1960s when Ashe et al.,[8] and Ashe and Williams[9] reported that Raynaud's Phenomenon had been clinically diagnosed on seven hard-rock miners. Surprisingly, however, Pecora[16] conducted a questionnaire-type survey of a group of occupational physicians in the United States and concluded: "A preliminary survey of the literature on the incidence of Raynaud's Phenomenon of occupational origin in this country revealed a conspicuous lack of information concerning both the number of workers affected and the number using small hand-held vibratory tools. An attempt was made to estimate the number of workers using vibrating tools and the number afflicted with Raynaud's Phenomenon of occupational origin. All of

the information thus gathered indicates that Raynaud's Phenomenon of occupational origin may not be completely evaluated, but it may have become an uncommon occupational disease approaching extinction in this country."

Once again, there was a lack of occupational hand-arm vibration studies in the United States until 1974 when a survey carried out by the National Institute for Occupational Safety and Health (NIOSH) indicated that an estimated 8 million workers were exposed to occupational vibration in U.S. industries[17]. Some 6.8 million were exposed to whole-body vibration and some 1.2 million to hand-arm vibration. These estimates were based on a multi-worksite survey from a multiplicity of U.S. industries. In 1974, the late Dr. Norman Williams (who had collaborated with Ashe in the early 1960s) and Byrne completed another study for NIOSH[18]. This study was an attempt to determine the quality, quantity, and availability of suitable health records (from which NIOSH might later conduct epidemiological studies in an attempt to determine the quality, quantity, and quantify the extent of the occupational hand-arm vibration problem). Although this study was not totally exhaustive, the results indicated that of the sparse records available for an epidemiological study in the United States, the records of those companies, employing workers who almost exclusively use hand tools, were the best. Particularly disturbing, however, were Williams' reports of informal talks with some workers whose hands appeared blanched. Many of these workers told him that they knew they had Raynaud's Phenomenon but lived with it and tolerated it because they feared loss of employment should they report the malady[18].

In October 1975, NIOSH organized and held a week-long international occupational hand-arm conference where the epidemiological, medical, clinical, physiological, and engineering aspects of VWF and vibration measurements were discussed in depth. The presentations and discussions were later published as a Proceedings[19]. The conference summary and recommendations comprised ten points, two of which applied to the engineering aspects of the vibration problem:

1. There were extreme difficulties in performing vibration measurements on percussive pneumatic tools (because the attendant acceleration levels were very high and resulted in actual destruction of the measuring transducers), and

2. there was the need to validate an engineering model (i.e., simulation of the hand and arm) to assist the engineering tool designer in producing a more accurate vibration-free tool.

Before addressing these points, some introductory remarks are in order. For a more rigorous treatment of the technical terms discussed below, the interested reader is referred to appropriate engineering texts [20,21].

Vibration Parameters

Measurement of vibration and the human response to it depend on several elements -- elements that Griffin[22] has called "extrinsic and intrinsic variables;" these are given in Table II-1. Since vibration is a vector quantity (e.g., it has a magnitude and directionality), nearly all of the extrinsic variables given in Table II-1 must be extended to multiple axes depending on the nature of the vibration being examined. Throughout this report, we have attempted to account for as many of these variables as possible and practical.

Table II-1*

Extrinsic variables

1. Frequency of vibration
2. Amplitude of vibration
3. Time history of vibration
4. Direction of vibration
5. Point of application of vibration
6. Interaction between body and vibration input
7. Effect of clothing, etc.

Intrinsic Variables

1. Body size (height, weight, build, etc.)
2. Body posture
3. Body tension

Definitions and Technical Remarks

When we speak of mechanical vibration, we generally refer to motion about some equilibrium position. Displacement refers to the position of an object in the vibration cycle with reference to its normal resting position (expressed in feet or meters). Sinusoidal motion is given by the following:

$$\text{Displacement} = X \sin \omega t$$

where: X = peak displacement
$\omega = 2 \pi f$ (f = cyclic frequency in Hz)
t = time in seconds (sec)

* All remaining tables and figures discussed in this report can be found at the end of this report.

Velocity refers to the time rate of change of displacement (expressed in feet/second or meters/second) and represents the first derivative of the displacement function given above. This is given by the following:

$$\text{Velocity} = \frac{dx}{dt} = \omega X \cos\omega t$$

where: ωX = peak velocity

The velocity and displacement functions are separated by 90° in phase.

Acceleration refers to the time rate of change of velocity (expressed in either feet/second^2, given in "g" gravitational units or meters/second^2, where 1g = 9.81 m/sec^2 = 32.2 ft/sec^2). Acceleration represents the second derivative of the displacement function and is given by the following:

$$\text{Acceleration} = \frac{d^2x}{dt^2} = \frac{dv}{dt} = -\omega^2 X \sin\omega t$$

Where:

$\omega^2 X$ = peak acceleration

Frequency (in Hz) refers to the cyclic nature of the vibration. (Note that the velocity function is proportional to frequency, whereas the acceleration function is proportional to the square of the frequency.)

Resonance (or natural frequency) in this case refers to the human body as a whole (or various body parts) acting in concert with externally generated vibration and actually amplifying certain vibration frequencies impinging on the body. In the case of hand-arm vibration, resonance is thought to occur around 100-200 Hz, for whole-body (head-to-toe) vibration this occurs about 5 Hz.

Vibration found in the workplace and other environments usually contains multiple vibration frequencies, all contributing various amounts to the aggregate vibration measured by vibration transducers. An approach to analyzing such data is to separate this vibration aggregate into its constituent parts in frequency and amplitude--this is referred to as Fourier Spectrum Analysis.

Mathematically, one expression of the Fourier series is:

$$F(t) = a_o + a_1 \sin\omega t + a_2 \sin 2\omega t +$$
$$a_3 \sin 3\omega t + \ldots a_n \sin n\omega t +$$
$$b_1 \cos\omega t + b_2 \cos 2\omega t +$$
$$b_3 \cos 3\omega t + \ldots b_n \cos n\omega t$$

where, a_o is the average (or DC) term and the $a_1 - a_n$ and $b_1 - b_n$ terms define the amplitude of each of the vibration frequencies present in a

given spectrum; the sin and cos terms give the actual vibration frequency components comprising the spectrum and their phases. The spectrum is thus a frequency "fingerprint" of the vibration present in a given situation. Spectra are usually derived via computer analysis and graphically displayed as follows:

a. The horizontal axis represents frequency,
b. The vertical axis represents either of the following amplitudes: acceleration, velocity, displacement, energy.
c. The horizontal axis position of each spectral peak, displayed as a vertical line gives its vibration frequency.
d. The total number of these vertical lines in the spectrum indicates all of the vibration frequencies present.
e. The height of each of these vertical lines indicates the amplitude of a parameter (given in b. above) that each respective frequency element contributes to the total spectrum.

If a vibratory stimulus is applied to a human being, mechanical structure, etc., there is resulting motion (at the same frequency) at the point of vibration application as well as other points on the structure. Mechanical impedance is the ratio of the applied vibrating force to the resulting motion (velocity) at the same frequency.

$$\text{Mechanical impedance} = \frac{\text{Force}}{\text{Velocity}} = \frac{F}{V}$$

Measuring both the applied force and the resulting velocity at the same point is referred to as "point impedance." Or, measuring the force at the point of excitation and measuring the resulting velocity at another point on the structure is referred to as "transfer impedance." Mechanical impedance has been extensively used[23-39] in both human and structural vibration to determine resonances, stiffness, and damping characteristics and other system dynamics. In actuality, impedance is a measure of the total dynamic opposition the human body offers to the movement imparted by the vibration and can reflect body resonances without interfering with normal body functions[35].

Instead of velocity system dynamics in opposition (impedance) to movement, one can view vibration as a form of movement or dynamic compliance, which is defined as:

$$\text{Dynamic Compliance} = \frac{\text{Displacement}}{\text{Force}} = \frac{X}{F}$$

Mechanical and human systems can be simulated (i.e., modeled) by the use of three elements: mass, dampers, and springs. Both the spring and the mass elements are capable of storing mechanical energy[20]. The energy in the mass, kinetic energy, is due to the velocity associated with a moving mass. The energy of the spring, potential energy, due to its deformation and, lastly, the damper is a dissipator of energy into heat, and cannot store mechanical energy.

Test Methods

Two types of basic tests were performed during this study:

1. Vibration acceleration measurements using volunteer workers as they actually worked with the pneumatic tools; and

2. dynamic compliance measurements.

Both measurements are relatable to a standardized coordinate system established by the International Standards Organization (ISO) Document 5349 and shown in Figure 15. All field tests were performed by a combined NIOSH and University of Pittsburgh* engineering team on site, as described in Appendix H.

During the course of the overall study, 385 workers who chip and grind metal in two foundries and a shipyard were medically tested. Of that number, 75 workers were randomly chosen (white finger cases and controls) to be tested using dynamic compliance. Acceleration measurements were made for the most part on-site using experienced chipper and grinder workers.

The medical team also examined 30 limestone cutters, carvers, and drillers in a related study reported elsewhere[40]. In this limestone study only acceleration measurements were performed (at the Indiana Laborers' Training Institute, Bedford, Indiana).

Details of the worksites, work practices, and tools used on the job are given in Appendix G.

This report contains ALL of the acceleration amd mobility measurements made on both studies. Details of measurements follow:

A. Acceleration Testing

Acceleration was used as the measurement of choice in this study because of:

1. the ability to obtain three parameters (acceleration, velocity, and displacement) from one measurement (if acceleration is measured, then through electronic integration the velocity function is obtained. Through a second integration the displacement function is obtained).

2. The large variety of accelerometers available.

* Portions of this report have been extracted from NIOSH Contract Report #210-77-0165 (Analysis of Segmental Vibration Impinging on Chipping and Grinding Workers). Led by Dr. Reynolds, field study data was obtained principally by NIOSH engineering team members and recorded on tape to be analyzed at the University of Pittsburgh.

Three types of accelerometers are used in vibration measurements: strain gage, piezoresistive, and piezoelectric. The first two employ a balanced Wheatstone Bridge principle where the accelerometer elements form two or more of the four resistance elements of a balanced electrical bridge. Vibration impinging on this balanced bridge temporarily deforms one or more of the bridge elements thereby changing the resistance in these elements and, thus, unbalancing the bridge. This unbalance is precisely measured with the use of solid-state differential amplifiers. When the vibration is removed, the bridge returns to the original balanced state. Strain gage and piezoresistive accelerometers are suitable for very low frequency to mid frequency ($\leq$ 1 kHz) measurements depending on the type of device used.
The third type of device is a piezoelectric accelerometer. It operates on a different principle and is well suited for mid to high frequency measurements (20 Hz to 20 KHz). It is not truly suitable for low frequency acceleration measures. In principle, when vibration impinges upon a piezoelectric accelerometer, the vibration moves a small mass against the face of a crystal element. This crystal element produces an electrical voltage proportional to the compression of the mass against the crystal. This voltage is proportional to acceleration. Because the voltage produced is small and loss in signal can easily occur, a "charge amplifier" is used in conjunction with the crystal accelerometer. This amplifier overcomes signal loss problems by measuring changes in the electrical charge (or capacitance) of the crystal. Since crystal charge simultaneously varies in unison with the aforementioned signal voltage, a measure of acceleration is obtained.

Because of the large acceleration levels and sharp acceleration "spikes" expected from pneumatic tools, a wide frequency range was anticipated (approximately 6 Hz to 3 KHz)[64] stem from the very high impulsive vibration levels that produce actual destruction of the accelerometers as well as problems of spectrum accuracy at the low frequency end (referred to as DC shift). The methods of attack on these measurement problems have been two-fold:

1. Use of a "mechanical (damping) filter" between the tool and accelerometer and/or:

2. modifying the design of the accelerometer itself to try to operate with this enormous vibration abuse.

Using a mechanical filter prevents destruction of the accelerometer, but the acceleration measurement made by the accelerometer in series with a mechanical filter is modified and altered by the characteristics of the filter. Thus, this measurement is of limited value. It seemed to us that modifications would need to be made to the accelerometers, thus eliminating mechanical filters.

We contacted some of the leading accelerometer manufacturers and found that only the Danish-based Bruel & Kjaer (B & K) Company was interested in this problem. The B & K Model 8309 compression-type piezoelectric accelerometer (1 Hz to 60 KHz range, sensitivity 0.3 mv/g or 0.04 pC/g, wt. 3 grams) was chosen as the best device for our application, knowing in advance that it might be necessary to have this device factory modified.

ACCELERATION MEASUREMENTS AND ANALYSIS

Description of Tools

Acceleration levels were obtained from four so-called Type 2 pneumatic chipping hammers (of various manufacturers) and two different pneumatic grinders. The chipping hammers were of the type shown in Figure 1. The grinders used are shown in Figures 2 and 3. Chipping hammers A, B, and C and the vertical grinder are used in an engine foundry to remove excess metal (i.e., burrs and flash) from nodular cast iron castings. Chipping hammer D and the vertical grinder are used by the shipyard workers to shape and finish propeller blades and smooth welds on ships. A small limestone chipping hammer is used for decorative carving and finishing limestone blocks and monuments. This chipping hammer was also measured. A complete description of these tools and how they are used on the job is given in Appendix G.

Chipper Tool Testing Methods and Difficulties

One of the major operations performed in the grey iron foundry is the chipping and grinding of burrs and flash from slots in the cast iron castings. For this operation a "Type 2" chipping hammer is used. This chipping hammer is operated at full throttle with the chisel directed into a corner of the casting. Slot chipping data was taken for chipping hammers A, B, C, and D so that a comparison could be made between the various types of chipping hammers. To indicate the influence of work material on the acceleration levels produced by the tool, data was also taken for chipping hammer D, used for chipping nickel-aluminium-bronze (Ni-Al-Br) and mild steel. For these tests chipping hammer D was operated at 1/2 to 3/4 throttle to cut a groove in the material 0.76 inches (1.9 cm) wide and 0.10 inches (0.25 cm) deep. Acceleration levels were measured for the small limestone chipping hammer chipping on limestone at full throttle. We again note that the chipping hammer data was taken under actual field conditions and the tools were operated by the workers who normally use them.

Chipping hammers B, C, and D were all of roughly the same size and weight. Chipping hammer A was somewhat larger and heavier than chippers B, C, and D. The limestone chipping hammer was much smaller and lighter than any of the chippers. The chisels used with chipping hammers A, B, and C were 10 to 12 inches (25 - 30 cm) long. The chisels used with the limestone chipping hammer and chipping hammer D were 3 - 5 inches (7.5 - 12.5 cm) long.

The testing set-up is shown in Figure 7. Two B & K 8309 measuring accelerometers were used, one at the chisel end of the tool, the other at the rear handle of the tool. At the chisel end, a steel block was welded directly to the chisel and positioned where the worker would normally hold

his chisel. The mounting block (Figure 4) had a tapped hole with the accelerometer screwed into it and held by a tension stud and castle nut. The accelerometer sensed vibration in the axial direction, parallel to the axis of the chisel. Block welding to the chisel was necessary due to the extremely high acceleration levels generated on the chisel end of the chipping hammer. Similarly, a steel mounting block welded to a stainless steel hose clamp (jubilee clip) as shown in Figure 5 was found to be effective on the handle. The accelerometer was equipped with a mounting stud for attachment to the mounting block. The hose clamp was securely tightened around the handle of the chipping hammer as close as possible to the operator's hand. In the case of the small limestone chipper the accelerometer was mounted on the barrel of the tool.

We initially tried attaching hose clamps to the chisel. They broke or slipped while on the chisel. As a solution, steel mounting blocks were then welded to the various chisels. Also, various accelerometer failures occurred and were believed caused by fatigue which resulted in shearing of the studs or stripping of the threads and loosening of welds of the "top hat" which protects the crystal element. Damaged accelerometers were sent back to the B & K factory, who in turn replaced the damaged 8309 accelerometers. All accelerometers eventually failed after a finite exposure time to chisel acceleration. Average accelerometer life was around 30 minutes for chisel testing.

It is important to note that the accelerometers must be screwed tightly into the mounting holes in order to avoid artifactual noise in the measurement. In order to reduce the accelerometer fatigue problem, tension in the mounting stud, however, should not be excessive. The mounting arrangement shown in Figure 4 was found effective and used to obtain the data in this study. A hole was drilled into the mounting block at right angles to the accelerometer mounting hole. A stud loading pin was inserted into the hole, then drilled and tapped to accept the accelerometer mounting stud. The pin was threaded at its outer end to accept a castle nut. After the accelerometer was screwed finger tight into the mounting block, the tensioning pin was pulled tightly against the accelerometer mounting stud using the castle nut. In this manner, the accelerometer was attached securely to the mounting block without tensioning the mounting stud. The resulting shear load which was generated in the mounting stud was much more advantageous than tension from the standpoint of fatigue failure.

The use of the mounting arrangement shown in Figure 4 was effective in eliminating mounting stud failures. However, failures of the electrical cable connectors occurred after several minutes of testing. The failures occurred in the electrical connectors both in the attachment threads and in shearing of the center contact pins. The lifetime of the electrical connectors was finally extended to an acceptable value by changing cable manufacturers to Endevco, and by carefully strain relieving and taping the leads to the chisel. In most cases, after several minutes of repeated shocks from the chisel, the accelerometer crystals would be excited at resonance and fail. As mentioned above, even these B & K 8309, 100,000g accelerometers would eventually fail after 30 minutes of chisel testing.

For the most part, professional chipper, grinder, and stonecutter workers were used for testing and asked to work as they would normally. Most chipping tools were operated at the normal full throttle (using 100 psi air supply),* a few were tested at 1/2-3/4 throttle as described in later sections. Data was obtained for three operators. Because of the problems stated above, only vibration levels parallel to the chisel axis were measured. Although it is generally agreed that transverse vibration (vibration perpendicular to the chisel axis) is excited on a chisel during normal chipping operations. However, it was felt that over most of the frequency range of interest, the amplitudes of the transverse vibration levels on the chisel would be lower than the vibration levels parallel to the chisel axis. However, the main reason chisel transverse vibration measurements were not made is the fact that at the time when the tests were conducted, it was not possible to attach an accelerometer to a chisel in the transverse direction without failing another mounting stud and another costly accelerometer crystal.

Grinding Tool Testing

Two types of pneumatic grinders were examined: vertical and horizontal (Figures 2 and 3). Grinder acceleration levels were taken while grinding on cast iron. The vertical grinder was operated with a 6 inch sanding pad and medium grit paper. Data was obtained for the horizontal grinder for three, 6 inch grinding wheels: a coarse radial wheel, a fine radial wheel, and a coarse flared cup wheel.

A triaxial accelerometer block was mounted on each grinder handle as shown in Figures 2 and 3. Each block consisted of three Columbia Research Model 6063 accelerometers mounted on three perpendicular faces of a steel cube. These cubes were glued to the grinders using epoxy cement. The accelerometer leads were strain relieved, bundled, and taped to the handles to avoid electrical noise due to movement of the leads. The measurement coordinate systems used and given in Figures 2 and 3 are consistent with ISO 5349.

The grinders were 6000 RPM units and were operated at full throttle with 100 psi supply air pressure. Data was obtained for two operators.

Acceleration Data Acquisition System and Testing

A system block diagram used to obtain, measure, and record acceleration levels of both the pneumatic chipping hammers and the grinders is shown in Figure 6. The charge output from the accelerometers is converted to voltage signals in charge amplifiers (Ithaco Model 461) and recorded on a Honeywell Model 5600 C, multichannel FM tape recorder. In order to constantly monitor for amplifier clipping due to possible input overloads, the charge amplifier signals and tape recorder outputs were observed on a multichannel Tektronix 5103 oscilloscope. A Nicolet 444A Fourier spectrum analyzer was also used to observe spectra on-line, as the measurements were being obtained.

* 1psi = 6.89476kPa

All crystal accelerometers were calibrated before use in our field mobile unit with the use of a minishaker (B & K Model 4809), driven by a B & K Model 2706 amplifier, and swept by a Spectral Dynamics Model SD104 sweep oscillator. These crystal accelerometers were calibrated against a known piezoresistive accelerometer (Entran EGAL 125).

Before actual data was recorded, trial data was played through the tape recorder to establish the maximum signal levels. No DC shift was observed from the crystal accelerometers. The tape recorder input gain was adjusted to give recorded levels large enough to be easily read but small enough to avoid over-ranging the tape recorder input amplifiers. Static and dynamic calibration signals were later used to scale the data during digitization. For the most part, measurements were made while professional and experienced chippers and grinders worked under actual working conditions using metal castings taken directly from the given workplace.* In order that the accelerometers would not be overly abused, measurements were limited to 1 minute runs. Tool operators were instructed to begin chipping or grinding before the tape recorder was started. Approximately one minute runs of data were then recorded. Handle and chisel vibration measurements were taken, and the subjects' hand motions were simultaneously video taped for later observation.

Acceleration Digitization and Plotting

Data obtained in the field was sent for a complete data analysis to the University of Pittsburgh where another Honeywell 5600 tape recorder was located. The 1/3 octave band acceleration levels for the grinder and chipping hammers were obtained using the system shown in Figure 7. The FM tape recording of the analog acceleration data for the various tools was played into a General Radio Model 1921 1/3 octave band real-time analyzer. The 1/3 octave band frequency spectrum output from the frequency analyzer was digitized using a Hewlett-Packard analog/digital converter and the 9820A calculator. The digital data was stored on cassette tapes. The accelerometer digitization program listing and chronology is listed in Appendix A.

The acceleration levels were plotted as a function of frequency using the acceleration plotting program given in Appendix A. The acceleration plots are given in Appendix C, Figures C-1 through C-32. The overall acceleration level for each acceleration plot may be determined as:

$$A = \left[\sum_{i=1}^{23} \ddot{X}_i^2 \right]^{1/2}$$

* In the case of pneumatic grinders, where insufficient acceleration data was obtained in the field, supplemental data was obtained at the University of Pittsburgh's mechanical engineering laboratory, using the same tool types with similar metal castings as that found in the field.

Where X_i are the acceleration levels for each center frequency. The chipping hammer and grinder overall acceleration levels are given in Tables II-2 & II-3 respectively. The calculator program listing is given in Appendix A.

RESULTS AND DISCUSSION OF ACCELERATION DATA

Chipping Hammer Acceleration

The chipping hammer is an impact type tool. The 1/3 octave band acceleration levels for various Type 2 pneumatic chipping hammers are given in Figures C-1 through C-6. C7-C8 are levels for the smaller limestone chipping hammer. Both chisel and rear handle acceleration levels are given for hammer A, hammer D and the small limestone chipping hammer. Only handle data is given for hammers B and C. The overall acceleration levels from 6.3 Hz to 1000 Hz are given in Table II-2. A representative spectrum is given in Figure 8. It is to be noted that little acceleration was noted beyond 1000 Hz in our tests; hence the choice of a 1000 Hz upper frequency cutoff during the analysis.

The plots for hammers A, B, C, and D have peaks at 31.5 Hz and 63 Hz. The small limestone chipper has peaks at 80 Hz and 160 Hz. The first peaks, at 31.5 Hz and 80 Hz, are the first harmonics of the excitation frequency for each respective tool.

Of the Type 2 chipping hammers, hammer A exhibits the highest chisel acceleration levels. The chisel acceleration levels for chipping hammer D and the limestone chipper are comparable to each other and considerably less than chipping hammer A.

Data was taken for chipping hammer D slot chipping on cast iron and chipping on mild B steel and Ni-Al-Br to assess the influence of material and operating conditions on acceleration levels. The levels for mild B steel and Ni-Al-Br are generally the same. The levels for slot chipping are approximately 10 times higher. Foundry slot chipping is generally a more severe operation since the chisel is operated at full throttle. When chipping on Ni-Al-Br or mild steel, we found shipyard workers use 1/2 to 3/4 throttle.

The acceleration levels for the chipper handles are considerably lower than for the chisels. The amount of attenuation of acceleration transmitted from the chisel to the handle varies with each chipper. Chipping hammer A shows an attenuation of 1/150 for the peaks and 1/65 for the general acceleration level. Chipping hammer D shows an attenuation of 1/150 for peaks and 1/60 for the general level. The small limestone chipper, which is the smallest of the five chipping hammers, shows the least attenuation of all: 1/3 for the peaks and 1/2 for the general level.

The insignificant acceleration attenuation from chisel to handle of the small limestone chipper leads to an interesting situation. The chisel

acceleration levels for the small limestone chipping hammer are the smallest measured, comparable to those for hammer D and much less than for hammer A, but the handle accelerations are the largest, approximately four times the levels for the handle of hammer A. This situation is probably associated with the relative size of the masses of the chipping hammer handles relative to the masses of the chisels. The larger hammers have more mass in their handles than does the limestone chipper. The larger the mass of the chipping hammer handle, the less the acceleration of the handle required to absorb the impact transmitted from the chisel. So it appears that it is not necessarily true that smaller chipping hammers, by virtue of delivering lighter chisel blows, expose the operator to lower acceleration levels. On the contrary, the highest handle accelerations measured were for the smallest chipping hammer.

It is quite possible that the handle acceleration levels are far more significant to the operator than are the chisel levels. Perhaps only a small part of the chisel acceleration is transmitted to the hand since the chisel is usually guided by resting on the open palm or by cradling between the thumb and index finger. The handle on the other hand must be grasped firmly, which results in good mechanical coupling and good acceleration transfer from the handle to the hand-arm system.

Grinder Acceleration

The grinder is not an impact tool, rather it produces a type of continuous vibration. The grinder accelerations are shown in Figures C-9 through C-37 The grinder acceleration levels are very much less than those measured for the chipping hammer chisels and most of the handles. The grinder acceleration levels vary between .003-1 g(rms) [.03 m/s^2 and 10 m/s^2]. Chipping hammer handle accelerations generally range between 1-10 g(rms) [10 m/s^2 and 100 m/s^2]. The overall grinder acceleration levels are given in Table II-3. A representative spectrum is given in Figure G-9.

Peaks occur in many of the horizontal grinder plots at 63 Hz, 250 Hz and 1000 Hz (1/3 octave bands). These may be the operating frequencies of mechanical parts within the tools. Peaks occur frequently at 40, 80 and 250 Hz in the vertical grinder plots, but these plots are difficult to characterize.

It is interesting to note that the acceleration levels for some of the horizontal grinder coarse radial wheel and flared cup data are comparable in magnitude to the handle acceleration levels of chipping hammer D chipping on mild B steel and Ni-Al-Br. This can be seen in Figures C-9, C- 11, C-14, C-21, C-22, and C-23. Above 100 Hz the left hand plots for the horizontal grinder with the coarse flared cup wheel, Figures C-21 through C-23, have general acceleration levels between 63 Hz and 250 Hz which are lower but close to those for the handle of chipping hammer D chipping on Ni-Al-Br. It can be seen that for discrete frequency ranges, workers using chipping hammer D and the horizontal grinder with the coarse wheels, are receiving similar acceleration exposure.

Displacement Determination

In order to serve as a check on the acceleration data, the displacements of the chisels and handles of the chipping hammers were determined from Fourier series approximations of the accelerations.

Any periodic function, f(t), may be expressed as a Fourier series, one expression of which is as follows[45]:

$$f(t) = a_0 + \sum_{n=1}^{\infty} a_n \cos(n\omega t) + \sum_{m=1}^{\infty} b_m \sin(m\omega t) \qquad (1)$$

Where:

$$a_0 = \frac{\omega}{2\pi} \int_{t_0}^{\left[t_0 + \frac{2\pi}{\omega}\right]} f(t)dt \qquad (2)$$

$$a_n = \frac{\omega}{\pi} \int_{t_0}^{\left[t_0 + \frac{2\pi}{\omega}\right]} f(t) \cos(n\omega t)dt \qquad (3)$$

$$b_m = \frac{\omega}{\pi} \int_{t_0}^{\left[t_0 + \frac{2\pi}{\omega}\right]} f(t) \sin(m\omega t)dt \qquad (4)$$

$$\omega = \frac{2\pi}{T_1} \qquad (5)$$

Where T_1 is the time for one cycle, and n and m are the number of terms, and a_0 is the average value.

The acceleration time histories are shown in Figures E-1 through E-6 of Appendix E. The time histories were obtained using a Nicolet Model 1090A digital storage oscilloscope as shown in Figure 10. The plotting program for use with the 9820A calculator is given in Appendix A.

The acceleration time histories are of two types. Figures E-1, E-5, and E-6 may be simulated as decaying exponentials where:

$$f(t) = Ye^{-at} \qquad (6)$$

Y is the magnitude of the spike and a is the time constant of decay. Substituting into equations (3) and (4) and integrating we obtain:

$$a_n = \frac{Ya\left[1 - e^{-aT_1}\right]}{a^2 + \left(\frac{2n\pi}{T_1}\right)^2} \tag{7}$$

$$b_n = \frac{4\pi nY\left[1 - e^{-aT_1}\right]}{T_1^2\left[a^2 + \left[\frac{2n\pi}{T_1}\right]^2\right]} \tag{8}$$

Figures E-2, E-3 and E-4 can be simulated as a single sinusoidal cycle of

$$a_n = \frac{2Y}{T_1}\left[\frac{\cos(\omega_0 - n\omega)t_1 - 1}{2(\omega_0 - n\omega)} + \frac{\cos(\omega_0 + n\omega)t_1 - 1}{2(\omega_0 + n\omega)}\right] \tag{9}$$

$$b_n = \frac{2Y}{T_1}\left[\frac{\sin(\omega_0 + n\omega)t_1}{2(\omega_0 + n\omega)} - \frac{\sin(\omega_0 - n\omega)t_1}{2(\omega_0 - n\omega)}\right] \tag{10}$$

The 9820A calculator programs used to find the Fourier coefficients for Figures E-1 through E-6 are given in Appendix A. The displacements were found using equations (1) and the fact that $X = \frac{-\ddot{x}}{\omega^2}$ (derived as equation (16) in a later section of this report).

The computer program used to plot the displacements is given in Appendix A. The calculated displacement time histories are plotted in Figures E-7 through E-12. The Fourier series levels for acceleration are found as:

$$C_n = (a_n^2 + b_n^2)^{\frac{1}{2}} \tag{11}$$

It can be seen from the displacement plots that the calculated handle displacements are small. This agrees with operating experience. The same is true for the chisel displacements for chipping hammer D and the small limestone chipper. However, the displacements for the chipping hammer A chisel, are very much larger than those experienced under operating conditions. The maximum displacement experienced with chisels during operation is one or two centimeters. The predicted value of 20 cm is in disagreement.

A likely source of the error is the nature of the chisel impact. A basic assumption associated with use of Fourier series is that the principle of superposition applies to the case under consideration[45]. Superposition does not apply if nonlinear effects or finite deformations are present[46, 47]. One source of nonlinearity is gross plastic deformation due to the high acceleration levels. By the very nature of the chipping operation, plastic deformation will probably occur in the workpiece and not on the chisel (due to its hardness). As acceleration levels become large, the plastic deformation of the chisel may become general enough to significantly influence the nature of the acceleration pulses [48]. Since the chisel acceleration levels for chipping hammer D and the small limestone chipper are very much smaller than for chipping hammer A, the nonlinearity effects may not be large enough to be significant.

It is possible that the displacement time history for the chisel of chipping hammer A cannot be reconstructed using a Fourier series. This does not mean to say that the acceleration time history is incorrect. The accelerometer measured the acceleration occurring in the chisel. The 1/3 octave band levels for the chipping hammer A chisel accelerations are still accurate for the time histories recorded. However, since the principle of superposition does NOT apply when gross nonlinear plastic deformation occurs, it is possible that the displacement time history calculated from the Fourier series for the chisel of chipping hammer A is in error. Also, our inability to measure the aforementioned transverse vibration component may also be a contributing source of error[64].

COMPARISON OF ACCELERATION LEVELS

Some years ago an International Standards Organization subcommittee on human vibration was formed in an effort to determine safe and healthy levels for persons exposed to vibration exposure. This committee has proposed a hand-arm vibration standard (ISO 5349). For the most part, the data used to generate this proposed hand-arm vibration standard is based principally on subjective studies and some chain saw data, and not on "hard medical data", it therefore has been seriously challenged[49]. The standard has yet to be universally adopted at this time, however, since it represents the single international attempt to develop a standard in this area we believe it is useful to compare the acceleration levels obtained in this study to the ISO document. However, let the reader be cautioned that comparison of this data to ISO 5349 does NOT necessarily imply endorsement of this document by these authors or NIOSH. The proposed ISO limits are given in Figure 11.

Chisel Acceleration

Our data indicates that all of the chipping hammer chisel acceleration levels in Figures B-1 through B-8 are in excess of the ISO 30 minute exposure levels. The peak at 31.5 Hz for the chisel of chipping hammer A is 1500 times the exposure limit. None of the chisel acceleration levels fall below the 30 minute exposure limit within the 6.3 Hz to 1000 Hz range investigated.

Since no accelerometers were actually placed on the test subject's hands or arms, it is difficult to determine how much acceleration is actually transmitted from the chisel to the open palm of an operator. A recent study by Farkkila et al.,[51] included 16 male stonecutters, 4 of which had a history of white fingers. The acceleration measurements (10Hz = 1kHz) were made on the pneumatic hammer chisel and barrel as well as the subject's wrists. They showed a reduction (attenuation factor) of approximately 1600 between the chisel and wrist of the chisel hand (2,755 g(rms) [27,000 m/sec^2] to 1.7 g(rms) [17 m/sec^2]), and a reduction of approximately 8 between the barrel and wrist of the barrel hand (3.16 g(rms) [3 m/sec^2] to 0.4 g(rms) [4 m/sec^2]). This suggests that the fingers and palms locally absorb much vibration energy. Similarly, our chisel acceleration levels transmitted to the hand from chipping hammer D and the small limestone chipper for example, may be reduced by a factor of 1/50 or 1/100 (depending on worker/tool hand grip strength and work practices employed). However, these reductions would barely bring the acceleration levels down to the 30-minute ISO exposure limit.

For handle acceleration levels, chipping hammers A, B and C acceleration levels in the low and middle frequency ranges susbstantially exceed the 30 minute levels. For hammer A, Figure C-1, acceleration levels for all

frequencies below 300 Hz are in excess of the 30 minute limit. For hammers B and C, the minimum frequency within the 30 minute exposure limit is 80 Hz. It should be noted that for hammer B, Figure C-2, the acceleration levels for 80 Hz, 125 Hz and 160 Hz are all very near the 30 minute exposure limit. The worst chipping hammer for handle vibration is the small limestone chipper which exceeds the 30 minute exposure limits over the entire 6.3 Hz to 1000 Hz frequency range. The acceleration levels are 1.5 times to 65 times the exposure limit with most of the range being more than 10 times the limit.

On the other hand, the handle acceleration levels for chipping hammer D chipping on Ni-Al-Br operating at 1/2-3/4 full throttle and shown in Figure C-5, lie entirely within suggested ISO acceleration exposure limits for 30 minutes. The acceleration level at 31.5 Hz would limit continuous exposure to approximately 1.5 hours per day. For chipping hammer D chipping on mild steel only, the peak at 31.5 Hz, exceeds the 30-minute exposure limits. For full throttle slot chipping on cast iron, (Figure C-4), all acceleration levels below 1000 Hz are in excess of the 30 minute limit. This demonstrates the severity of the slot chipping operation together with the work practice of operating the tool at full throttle in order to get the work completed in a specified time.

Grinder Acceleration

The grinder acceleration levels given in Figures C-5 through C-32 are all below the 30 minute exposure limit. The horizontal grinder with the fine radial wheel has acceleration levels for both handles in all directions and at all frequencies, which are lower than the 8-hour exposure limits. The horizontal grinder with the coarse radial wheel is limited by the left hand x and z directions, which have acceleration levels at approximately the 2-hour exposure limit. The right x and z directions also exceed the 8-hour limit, but are within the 7-hour limit. The horizontal grinder with the coarse flared cup wheel is limited to 4 hours exposure by the left hand y direction. The left hand z direction and the right hand y direction barely exceed the 8-hour exposure limit.

It would appear from the data presented here, that workers operating chipping hammer D (running 1/2 to 3/4 throttle) on Ni-Al-Br, or any of the grinders should be able to stay within the ISO proposed exposure limits if operating time limits are observed. Chipping hammer D (and the vertical grinder) are also used by shipyard workers to shape propeller blades.

The small margin between the suggested limits and several of the peaks in the various figures shows that accuracy is of considerable importance. Before data reduction of the 1/3 octave band acceleration levels, considerable exploratory work was done with integration time constants applicable to the spectrum analysis. As a general rule, integration time constants are inversely proportional to the lowest center frequency of interest. Since the acceleration peaks for successive strikes of the chisel are generally not the same, it was necessary to choose integration times which were long enough to include sufficient peaks in each 1/3 octave band to obtain a good average during integration. It was found that if 30 or more

peaks were included in each 1/3 octave band repeatable results were obtained For half these number of peaks, repeated reduction of the same data gave different and poorer results.

CONCLUSIONS FROM ACCELERATION MEASUREMENTS *

Vibration acceleration measurements (axial axis) were obtained on four large Type 2 chipping hammers and a small stone chipper during actual work conditions. The results indicate that when these Type 2 hammers are operated at full throttle chipping grey iron, Ni-Al-Br, or mild steel castings, acceleration levels on the chisel were approximately 2400 g(rms) [23,544 m/sec^2] and 30 g(rms) [294.3 m/sec^2] on the rear handle, (taken at points where workers grip these tools). In the case of one chipping hammer (A), the ratio of chisel to rear handle acceleration was approximately 78/1. When the Type 2 chipping hammer throttle was reduced from full to 1/2 - 3/4 throttle, the chisel acceleration levels significantly reduced by a factor of 12 (2400 g(rms) [23,544 m/sec^2] down to 200 g(rms) [1960 m/sec^2]). Correspondingly, rear handle accelerations went from 30 g(rms) [294.3 m/sec^2] down to approximately 4 g(rms) [39.2 m/sec^2]. Thus, the ratio of chisel to rear handle acceleration at 1/2-3/4 throttle was reduced to 50/1, as compared to 78/1 at full throttle.

The levels measured on the small stone chipper were approximately 500 g(rms) [4900 m/sec^2] on the chisel, and 200 g(rms) [1960 m/sec^2] on the rear handle (a factor of 2.5/1). These levels are quite high, especially on the rear handle. This is apparently due to the very little mass damping of this light weight tool. Thus, the attenuation of acceleration transmitted from chipping hammer chisels to handles is larger for large chipping hammers than for small chipping hammers. At the same operating conditions, substantially more energy is transmitted to the hand-arm system from the handles of small chipping hammers than from the handles of large chipping hammers. Spectra for each tool extended from approximately 6.3 Hz-1kHz

For illustrative purposes only, acceleration measurements were compared to ISO 5349 (proposed hand-arm vibration standard). In no case did the chipping hammer chisel acceleration measurements fall within an acceptable ISO exposure limit. In some instances at 1/2-3/4 throttle the chipping handle acceleration levels did fall within the ISO acceptable exposure limits. Similarly, triaxial acceleration measurements were obtained on pneumatic horizontal and vertical grinders using a variety of grinding wheels. All grinders were operated at full throttle. The vector summed acceleration levels ranged from a low of 0.56 g(rms) [5.49 m/sec^2] on the vertical grinder to a high of 2.09 g(rms) [20.50 m/sec^2] on the horizontal grinder. These levels are considerably lower than the chipping hammer levels and are distributed within the ISO 5349 acceptability range of 30 minutes to 8-hour exposures.

* The relationship of these engineering findings to the prevalence of VWF found in the workers studied medically will be discussed in other volumes of this report.

VIBRATION ENERGY MEASUREMENTS AND ANALYSIS*

The previously cited 1975 NIOSH Hand-Arm Vibration Conference[19] stated in its summary and recommendations: "The medical researchers emphasized the vital need to develop standardized methods of measuring vibration energy entering workers' hands and to correlate vibration spectrum with clinical tests and symptoms. Engineering models of the hand-arm system and their relation to vibratory tools have been devised. However, their practical validity rests on the combined results of epidemiological, medical, and engineering field study data."

A paper presented at this Conference by Lidstrom[50], who studied Swedish rock drillers, chiseling and grinding workers, suggested that the occurrence and severity of VWF was vibration energy and frequency dependent. It was found that the studied worker groups had the same relative ranking when ranked: (a) according to percentage of workers in each group who contracted symptoms of VWF and (b) by the vibration energy per unit time measured for the various pneumatic tools used by these workers.

The Lidstrom energies are single value exposure criterion for the tools in question. While a single number criterion is convenient to use, it says little about frequency dependency. Also, it has been established in the literature that indeed it appears that the vibration response of the hand-arm system may be frequency dependent. Extensive subjective equal sensation data presented by Miwa[57-63] indicates this, as do mechanical impedance models and test data presented by Reynolds[32], Suggs[36], Keith[52], and others. Thus, energy frequency spectrum data is needed to help determine the role of frequency dependency in the development of VWF in workers.

The remainder of this report will address the following topics: Energy frequency spectra will be experimentally determined for the chipping and grinding pneumatic tools used in this study. The dynamic compliance (X/F) and phase angle between X and F will be obtained for the previously cited group of 75 foundry workers. From the handle and chisel acceleration spectra for chipping hammers and grinders (discussed in the first part of this report), values of instantaneous energy will be calculated using the acceleration and X/F data. The energies will be plotted for 1/3 octave band frequencies between 6.3 Hz and 1000 Hz. Relationships will be developed for energy per unit time and cumulative energy. A table of these values will be given for each tool. Energy spectra determined from the acceleration levels will be compared to the proposed ISO standard for illustrative purposes.

---

* The analytical work presented in this part of the report was performed at the University of Pittsburgh (contract #210-77-0165) and formed the principal part of R. Basel's M.S. Thesis. This Thesis later became part of the contract final report. Salient parts have been extracted for presentation herein.

ENERGY DERIVATION *

Instantaneous Energy

To measure the total energy incident on the hand-arm system, Lidstrom used a specially designed handle equipped with force transducers and accelerometers[50]. In many measurement situations, there is concern that the measurement device will alter the characteristics of the system to be studied In this instance, the handle was designed with low mass and high stiffness to reduce the possibility of distortion due to resonance effects. Other factors which may affect the measurement are size, shape and surface finish of the handle, not only as they relate to distortion, but also in the way they affect an operator's reaction to the tool.

An alternate approach to direct force measurement is to calculate the force using the input displacement and the driving point dynamic compliance, X/F, determined for the hand-arm system. The driving point dynamic compliance may be measured experimentally using a shaker attached to an instrumented handle. Displacement may be found by integrating acceleration twice with respect to time. If the driving point dynamic compliance is experimentally determined for three mutually orthogonal directions, then the force transmitted from a vibrating tool to the hand-arm system may be determined by measuring the acceleration of the tool handle in the same three mutually orthogonal directions. Since displacement may be determined by integrating the acceleration, force can then be determined using the displacement and the X/F data.

The instantaneous energy incident on the hand-arm system is:

$$E(t) = \overline{F} \cdot \overline{X}$$

* Mechanical work as produced by an object is defined as the product of its displacement times the force applied to that object (in the direction of the displacement). Power is the rate of doing work (i.e. work, divided by the time necessary to do the work). Thus, power is the product of the velocity of an object times the force applied to that object. The energy of an object is its ability to do work. This can be in the form of: potential energy (i.e., the ability of an object to do work because of its state or position); kinetic energy (i.e., the ability of an object to do work because of its motion); or dissipative energy (i.e., energy converted and lost as heat). Energy (and work) are scalar quantities and are expressed in terms of Joules, where 1 Joule = 1 Newton-meter = 0.7376 foot-pounds.

Let

$$\overline{F} = F\cos(\omega t) \tag{12}$$

$$\overline{X} = X\cos(\omega t + \phi) \tag{13}$$

Where F and X are the amplitudes of force and displacement, respectively, ω is the circular frequency in radians per second, and ϕ is the phase angle in radians between force and displacement.

Since the force and displacement are measured in the same direction, the spatial angle between the vectors is zero. Then, the dot product is a simple product of the time varying magnitudes:

$$E(t) = FX\cos(\omega t)\cos(\omega t + \phi) = \frac{FX}{2}\{\cos(\phi) + \cos(2\omega t + \phi)\} \tag{14}$$

Now

$$\overline{F} = \overline{X}(F/X)$$

Keith[52] has shown that the hand-arm system may be modeled as a three-degree-of-freedom, mass-spring-damper, lumped parameter system with constant coefficients. From Keith's equations it can be shown that:

$$F/X = \frac{1}{X/F}$$

Then

$$\overline{F} = \frac{\overline{X}}{X/F} \tag{15}$$

The energy can be determined in terms of the acceleration.

Acceleration is:

$$\ddot{\overline{X}} = \frac{d^2\overline{X}}{dt^2} = \frac{d}{dt}\{-\omega X\sin(\omega t + \phi)\} = -\omega^2 X\cos(\omega t + \phi)$$

Let

$$\ddot{\overline{X}} = \ddot{X}\cos(\omega t + \phi).$$

Then

$$X = \frac{-\ddot{X}}{\omega^2} \tag{16}$$

Now combining equations (3), (4), and (5) the instantaneous energy incident on the hand-arm system in a given direction is:

$$E(t) = \frac{\ddot{X}^2}{2\omega^4(X/F)} \{\cos(\phi) + \cos(2\omega t + \phi)\} \tag{17}$$

It can be seen that the instantaneous energy has an average value due to the $\cos(\phi)$ term and a time varying component due to the $\cos(2\omega t + \phi)$ term. The amplitude of the time varying component is:

$$|E| = \frac{\ddot{X}^2}{2\omega^4(X/F)} \tag{18}$$

This quantity has physical significance in that it may be obtained using existing instrumentation systems and may be run through a spectrum analyzer or read on an AC voltmeter or oscilloscope. With Lidstrom's instrumentation this value is the product of the force and double integrated acceleration. This value might also be obtained using an analog computer simulation of the hand-arm system based on Keith's three-degree-of-freedom model and the measured tool handle acceleration. In this study, the energy will be calculated using digital data for displacement mobility and frequency spectra for the tool handle accelerations.

Real and Imaginary Parts of Instantaneous Energy

The dynamic compliance may be thought of mathematically as a complex quantity, having both real and imaginary parts. In complex notation, dynamic compliance is expressed in terms of an amplitude and a phase angle:

$$(X/F) = |X/F| \, e^{j\phi} \tag{19}$$

The phase angle is defined as[23]:

$$\phi = \tan^{-1} \frac{\mathrm{Im}(X/F)}{\mathrm{Re}(X/F)}$$

The phase angle, ϕ , can also be shown to be the time phase shift between the displacement and the force.

Substituting, we get:

$$|E| = \frac{\ddot{X}^2}{2\omega^4 |X/F| \, e^{j\phi}} = \frac{\ddot{X}^2 e^{-j\phi}}{2\omega^4 |X/F|}$$

Complex numbers may also be expressed using Euler's formula as:

$$|E| = \frac{\ddot{X}^2}{2\omega^4 |X/F|} \{\cos(\phi) - j \sin(\phi)\} \tag{20}$$

The amplitude of the incident energy given in equation (20) is a complex quantity having both real and imaginary parts. To determine the significance of the real and imaginary parts of the incident energy a simplified model of the hand-arm system will be used.

Keith has modeled the hand-arm system as a three-degree-of-freedom, lumped parameter, mass-spring-damper system (52). Since the three-degree-of-freedom equations are somewhat unmanageable, consider the simpler case of a single-degree-of-freedom mass-spring-damper system shown in Figure 12. Dynamic compliance for this system may be expressed as:

$$\frac{X}{F} = \frac{1}{(k - \omega^2 m) + j\omega b} \tag{21}$$

The energy input to the mass-spring-damper system is:

$$E = \overline{F} \cdot \overline{X} \tag{22}$$

Where

$$\overline{F} = F \cos(\omega t)$$

$$\overline{X} = \overline{F}(X/F)$$

$$= F \, |X/F| \cos(\omega t + \phi)$$

$$= X \cos(\omega t + \phi) \tag{23}$$

Then

$$X = F\ |X/F| \tag{24}$$

Substituting into equation (23)

$$E = FX \cos(\omega t)\cos(\omega t + \phi)$$

$$= \frac{F^2\ |X/F|}{2}\ \{\cos(\phi) + \cos(2\omega t + \phi)\} \tag{25}$$

The magnitude of the energy is:

$$|E| = \frac{F^2\ |X/F|}{2} \tag{26}$$

Substituting equation (21) into equation (26) and multiplying by the complex conjugate of the denominator

$$|E| = \frac{F^2\ \{(k - \omega^2 m) - j\omega b\}}{2\ \{(k - \omega^2 m)^2 + \omega^2 b^2\}} \tag{27}$$

In the mass-spring-damper system energy is dissipated in the damper and stored in the mass and spring. The instantaneous dissipated energy, E_D, is:

$$E_D = \bar{F}_D \cdot \bar{X} \tag{28}$$

Where the force in the damper, F_D, is:

$$\bar{F}_D = b\dot{\bar{X}} \tag{29}$$

When "b" is a constant and

$$\dot{\bar{X}} = \frac{d\bar{X}}{dt} = -\omega X \sin(\omega t + \phi) \tag{30}$$

Substituting equations (24), (29), and (30) into (28) yields

$$E_D = \frac{-b\omega F^2 (X/F)^2}{2} \sin(2\omega t + 2\phi) \tag{31}$$

Then the amplitude of the instantaneous dissipated energy is

$$|E_D| = \frac{b\omega F^2}{2} (X/F)^2 \tag{32}$$

Substituting equation (21) into (32) and simplifying

$$|E_D| = \frac{b\omega F^2}{2} \left[\frac{1}{\{(k - \omega^2 m)^2 - \omega^2 b^2\} + 2j\omega b(k - \omega^2 m)} \right]$$

Now, multiply numerator and denominator by the complex conjugate of the denominator to obtain

$$|E_D| = \frac{b\omega F^2}{2} \left[\frac{\{(k - \omega^2 m)^2 - \omega^2 b^2\} - 2j\omega b(k - \omega^2 m)}{\{(k - \omega^2 m)^2 - \omega^2 b^2\}^2 + 4\omega^2 b^2 (k - \omega^2 m)^2} \right]$$

The amplitude of this complex quantity is:

$$|E_D| = \frac{b\omega F^2}{2} \left[\frac{\{(k - \omega^2 m)^2 - \omega^2 b^2\}^2 + 4\omega^2 b^2 (k - \omega^2 m)^2}{\{[(k - \omega^2 m)^2 - \omega^2 b^2]^2 + 4\omega^2 b^2 (k - \omega^2 m)^2\}^2} \right]^{1/2}$$

$$= \frac{b\omega F^2}{2} \left[\frac{1}{\{(k - \omega^2 m)^2 - \omega^2 b^2\}^2 + 4\omega^2 b^2 (k - \omega^2 m)^2} \right]^{1/2}$$

$$= \frac{b\omega F^2}{2} \left[\frac{1}{(k - \omega^2 m)^4 - 2\omega^2 b^2 (k - \omega^2 m)^2 + \omega^4 b^4 + 4\omega^2 b^2 (k - \omega^2 m)^2} \right]^{1/2}$$

$$= \frac{b\omega F^2}{2} \left[\frac{1}{(k - \omega^2 m)^4 + 2\omega^2 b^2 (k - \omega^2 m)^2 + \omega^4 b^4} \right]^{1/2}$$

Then

$$|E_D| = \frac{b\omega F^2}{2} \left[\frac{1}{\{(k - \omega^2 m)^2 + \omega^2 b^2\}} \right] \tag{33}$$

It can be seen that the amplitude of the instantaneous dissipated energy expressed in equation (33) is equal to the amplitude of the imaginary part of the instantaneous incident energy, equation (27).

The instantaneous stored and kinetic energy for the mass and spring is:

$$E_s = \overline{F}_m \cdot \overline{X} + \overline{F}_k \cdot \overline{X} \tag{34}$$

Where the inertia force (using Newton's second law) is:

$$\overline{F}_m = m\ddot{\overline{X}}$$

$$= -\omega^2 m X \cos(\omega t + \phi) \tag{35}$$

The spring force is:

$$\overline{F}_k = k\overline{X}$$

$$= kX \cos(\omega t + \phi) \tag{36}$$

Substituting equations (35) and (36) into equation (34) and simplifying

$$|E_s| = \frac{F^2(X/F)^2}{2} (k - \omega^2 m) \{\cos(\phi) + \cos(2\omega t + \phi)\} \tag{37}$$

The amplitude of the instantaneous stored energy is

$$|E_s| = \frac{F^2(k - \omega^2 m)}{2} (X/F)^2 \tag{38}$$

Using the same steps used for the dissipated energy above, it can be shown that

$$|E_s| = \frac{F^2(k - \omega^2 m)}{2\{(k - \omega^2 m)^2 + \omega^2 b^2\}} \tag{39}$$

The amplitude of the instantaneous stored energy given in equation (39) is identical to the amplitude of the real part of the instantaneous incident energy given in equation (27). Then, the real and imaginary parts of the amplitude of the instantaneous energy incident on a single degree of freedom mass spring damper system are significant in that the amplitude of the real part is equal to the amplitude of the energy stored in the system and the amplitude of the imaginary part is equal to the amplitude of the energy dissipated in the system. It is reasonable to expect that for systems with higher degrees of freedom this will also be true. Then for the hand-arm system the magnitude of the instantaneous dissipated energy, E_D, is the imaginary part of the equation (20)

$$|E_D| = \frac{\ddot{X}^2 \sin(\phi)}{2\omega^4 |X/F|} \tag{40}$$

The magnitude of the instantaneous stored energy, E_S, is the real part of the equation (20):

$$|E_S| = \frac{\ddot{X}^2 \cos(\phi)}{2\omega^4 |X/F|} \tag{41}$$

The relations for instantaneous energy developed above are one-half those given by Reynolds[19]. It is difficult to determine where the discrepancy lies since the equations in reference[25] are given without proof. However, if the value of displacement or acceleration input to Reynolds equation is a root-mean-square (RMS) value, the equations are identical.

Total Energy Incident on Hand-Arm System

Lidstrom determined the quantity of energy transferred to the hand-arm system from a vibrating power tool over a given period of time. This is expressed as the work done on the hand-arm system by the tool. Work is defined as:

$$W = \int \bar{F} \cdot d\bar{X} \tag{42}$$

If force and displacement are as given in equations (12) and (13), $d\bar{X}$ is:

$$d\bar{X} = \frac{d\bar{X}}{dt} dt = -\omega X \sin(\omega t + \phi) dt \tag{43}$$

Substituting equations (12), (15), (16), and (43) into equation (42):

$$W = -\int_0^t F \cos(\omega t)\, \omega X \sin(\omega t + \phi)\, dt$$

$$= \frac{-\bar{\ddot{X}}^2}{2\omega^3 |X/F|}\left[\sin(\phi)\, t - \frac{1}{2\omega}\{\cos(2\omega t + \phi) - \cos(\phi)\}\right] \tag{44}$$

It can be seen that the cosine terms in equation (44) drop out if t is chosen to give a whole number of complete cycles. Then the work per unit time is:

$$\left|\frac{W}{t}\right| = \frac{\bar{\ddot{X}}^2 \sin(\phi)}{2\omega^3 |X/F|} \tag{45}$$

From equations (45) and (40) the relationship between the amplitude of the instantaneous dissipated energy and the amplitude of the work per unit time is:

$$\left|\frac{W}{t}\right| = \omega |E_D| \tag{46}$$

METHODS

General

To determine the energy transmitted from a vibrating tool to the hand-arm system, two types of information are necessary: the acceleration levels of the tool and the dynamic compliance of the hand-arm system. The levels of acceleration, dynamic compliance, and energy will be determined for the 1/3 octave band frequencies from 6.3 Hz to 1000 Hz.

Since the proposed ISO standard 5349 is expressed as acceleration levels at 1/3 octave band center frequencies, data for this study will also be expressed in terms of 1/3 octave band center frequencies.

Dynamic Compliance Data Acquisition - Data Recording

The dynamic compliance for the hand-arm system was obtained for a group of 75 foundry workers at the worksites. A block diagram for the experimental set-up is shown in Figure 13.

The workers were asked to grasp an instrumented handle which was then vibrated using an electromechanical shaker. The linkage between the handle and the shaker was a Wilcox (Z-602) impedance head (measuring both force and acceleration). To measure grip force, the handle was instrumented with a narrow metal beam equipped with strain gages as shown in Figure 14. The beam was calibrated for grip force by applying a point force at the center of the span using a point loading device. The workers wore their usual work clothing so that any influence of clothing on the response of the hand-arm system was typical of that which would occur under normal working conditions. Two handles were used. A 1.52 in (3.8 cm) diameter large handle and a 0.76 in (1.9 cm) diameter small handle simulated the handle and chisel of a pneumatic chipping hammer, respectively. The large handle was hollow with a 6.25 in (15.63 cm) wall thickness and the small handle was solid. Both handles were constructed of aluminum for low mass.

The workers were instructed to grasp the instrumented handle in the manner they would normally hold the handle or chisel of a chipping hammer. The subjects maintained their grip force at a constant level throughout the test and were asked to watch a large meter which displayed the output of the handle strain gages(53). A grip force of 5.7 lb (25.4N) was used. *

* With no vibration present, 12 chipper/grinder workers were each asked to grip the larger and then smaller handles (simulating the chipper rear handle and chisel, respectively) the way they would actually work with the tool. Their grip strength (for both handles) varied very little, using an average grip force of 5.7 lb or 25.4N.

Each handle was vibrated in a single direction while the vibration frequency was varied continuously from 5 Hz to 1000 Hz. The sweep rate was adjusted such that in the log sweep function mode, the time required for the frequency to logarithmically sweep from 5 Hz to 1000 Hz was 30 seconds. The normal sweep time should have been around 150 seconds; however, this was too long for the workers to be required to clasp the vibrating handle with a constant grip force. Thus, it was necessary for the sweep time to be as short as possible and still give accurate and reliable results. The 30 second sweep time was experimentally shown to meet these requirements.

The Spectral Dynamics instrumentation used in this study had a mass-cancel circuit. This circuit was used to cancel and eliminate the effects of the mass of the vibrating handle above the force transducer in the impedance head. Thus, the outputs of this system were the amplitude and phase of the dynamic compliance as a function of frequency as measured at the hand-handle interface.

Six tests, representing vibration in three orthogonal directions for each handle, were conducted for each subject. The coordinate system used is shown in Figure 15. This system is derived from the ISO 5349, and has its origin at the head of the third metacarpal. In the ISO standard the Z (horizontal) direction is defined by the longitudinal axis of that bone. In this study the Z axis is defined as perpendicular to the axis of the instrumented handle. This difference in general is slight.

The signals from the force transducer and accelerometer of the impedance head were inputs to a Spectral Dynamics mechanical impedance transfer function measurement system. The X/F signal, the phase angle between the displacement and the acceleration, and the frequency of the signal were the outputs from the system. The amplitudes of these values were recorded on magnetic tape as DC signal voltages using an FM tape recorder. Simultaneously, a real time plot of X/F and phase as a function of frequency was made at the time the data was taken. Eleven test days were required to obtain the data for 75 subjects in the field. Calibration information was recorded on the tape at the start of each day. The information included a calibration sweep from 5 Hz to 1000 Hz using a known reference mass on the shaker; X/F at 5 Hz and a phase equal to 0 degrees; X/F at 151 Hz and phase angle equal to 180 degrees; and X/F at 1 kHz and phase angle equal to 180 degrees. This information was essential for scaling the data during the digitization process. Field data was later sent to the University of Pittsburgh for analysis.

Dynamic Compliance Digitization - Date Reduction

The dynamic compliance data was digitized using a Hewlett-Packard 9820A calculator and the peripheral equipment shown in Figure 16. The analog data was obtained from the FM tape recorder through a low pass filter into an analog to digital (A/D) converter. The digital data was sampled, converted to engineering units and stored in the memory of the calculator using the digitization program listed in Appendix A. The program was started manually at the beginning of each recorded frequency sweep. The data channels for frequency, X/F and phase were sampled in rapid succession and the data was

stored in the calculator memory. The program was terminated automatically when 1000 Hz was reached. The digital data was then recorded onto magnetic tape cassette data files for storage. Six data files, representing three directions for each hand, were obtained for each of the 75 foundry workers.

Determination of 1/3 Octave Band Data Using Spline Function

The X/F and phase data was sampled at sequential frequencies, but at essentially random intervals. The values of X/F and phase for the 1/3 octave band center frequencies were calculated and the data was plotted using a "spline function interpolation program" adapted from the calculator user library[54]. The program chronology and listing is given in Appendix A. The program uses a third-degree natural spline function routine as developed by T.N.E. Greville[55]. The spline function has continuous first and second derivatives and results in a unique curve which is the smoothest path passing through all of the data points.

The values of X/F and phase at the 1/3 octave band center frequencies were recorded on cassette tapes. Twelve X/F and phase plots made using the spline function program were compared with the real-time plots to establish the validity of the data.

Dynamic Compliance Average and Confidence Limit Plots

The mean and 90% confidence limits were found at each center frequency for the X/F and phase data of the 75 foundry workers. The mean, or average, value, $\bar{y}$, of a group of n measurements, y_i, is given as[56]:

$$\bar{y} = \frac{\sum_{i=1}^{n} y_i}{n} \tag{47}$$

It should be recognized that for less than an infinite number of measurements $\bar{y}$ is only an estimate of the actual value of the mean. Using the student's "t statistic," it can be stated with a certain confidence level the interval in which the actual value of the mean lies. The t statistic is defined as[56]:

$$t = \frac{\bar{y} - \eta}{(s^2/n)^{1/2}} \tag{48}$$

In this expression, s^2 is the estimate of the variance of the data.

$$\eta = \bar{y} \pm t(s^2/n)^{1/2} \tag{49}$$

The estimate of the variance is defined as[56]:

$$s^2 = \frac{\sum_{i=1}^{n} (y_i - \bar{y})^2}{n - 1} \tag{50}$$

where y_i is the value of each data point. Expanding this expression and simplifying it you get:

$$s^2 = \frac{\left[\sum_{i=1}^{n} y_i^2 - n\bar{y}^2\right]}{n - 1} \tag{51}$$

Then

$$\eta = \bar{y} \pm t \left[\frac{\sum_{i=1}^{n} y_i^2 - n\bar{y}^2}{n(n-1)}\right]^{1/2} = \bar{y} \pm c\left[\sum_{i=1}^{n} y_i^2 - n\bar{y}^2\right]^{1/2} \tag{52}$$

Where,

$$c = \frac{1}{\{n(n-1)\}^{1/2}} \tag{53}$$

The t statistic has been tabulated as a function of the confidence percentage and the number of degrees of freedom. The number of degrees of freedom is equal to the number of data points minus 1. For 90% confidence level and 74 degrees of freedom, student's t is 1.668 and C = .02239[56]. Then equation (52) becomes:

$$\eta = \bar{y} \pm .02239\left[\sum_{i=1}^{n} y_i^2 - n\bar{y}^2\right]^{1/2} \tag{54}$$

The average and confidence limits and the X/F and phase data were obtained using the sum and sum of squares program and the average and confidence limit program given in Appendix A. The sum and sum of squares program was used to combine the 1/3 octave band data files of all 75 subjects. The sum and sum of the squares of the X/F and phase data were obtained for each center frequency in the vertical, horizontal and axial directions for both large and small handles. The results, recorded on cassette tapes, were used as input to the average and confidence limits program. The average and

confidence limits program calculated the average value of X/F and phase at each center frequency as well as the 90% confidence limits. This data was then arranged into a format suitable for input to the spline function program using the plotting file assembly program listed in Appendix A. The dynamic compliance and phase in the vertical, horizontal and axial directions were plotted for both large and small handles using the spline function program. The resulting plots are Figures B-1 through B-12 contained in Appendix B. Figures B-1 through B-6 are in English units, and Figures B-7 through B-12 are in metric units. Table B-1 contains a numerical listing of the values of dynamic compliance and phase at the 1/3 octave band center frequencies.

Energy Data - Instantaneous Energy Plots

It has been previously shown in this report that the magnitude of the instantaneous energies in the hand-arm system may be determined given the magnitude of the acceleration, dynamic compliance, and phase angle of the dynamic compliance. We have just shown how these quantities were determined experimentally at each 1/3 octave band center frequency, then stored in digital form on cassette magnetic tapes. The magnitudes of the instantaneous incident energy, instantaneous dissipated energy and the instantaneous stored energy may be determined using equations (20), (40) and (41), respectively.

The magnitudes of the instantaneous energies were calculated from the digital acceleration levels, X/F, and phase data using the 9820A calculator and peripheral equipment as shown in Figure 14. The listing and program chronology for the energy calculation program is given in Appendix A. The energy plots are given in Appendix D, Figures D-1 through D-35.

Work per Unit Time on Hand-Arm System

It has also been shown that the magnitude of the work per unit time done on the hand-arm system by a vibrating tool may be calculated from the magnitude of the instantaneous dissipated energy. The sum of the work per unit time for all frequencies is the total work per unit time for the given tool and direction. The work per unit time for each tool was calculated from the instantaneous dissipated energies using the work per unit time program given in Appendix A. These results are summarized in Tables II-4 and II-5 with plots given in Appendix F.

RESULTS AND DISCUSSION OF DYNAMIC COMPLIANCE DATA

The dynamic compliance plots are given in Figures B-1 through B-12 of Appendix B. Figures B-1 through B-6 give the average values and the 90% confidence limits in English units. Figures B-7 through B-12 give the average values in metric units.

The data presented in Figures B-1 through B-3 was obtained using the 1.50 in (3.8 cm) diameter handle. The 0.75 in (1.9 cm) diameter handle was used to obtain the data in Figures B-4 through B-6. While the general shape and the natural frequencies of the X/F and phase curves are the same for the same directions on both handles, there are also pronounced differences. The X/F curves for the large handle are generally lower than the corresponding curves for the small handle curves.

The data presented in Figures B-1 through B-6 is in general agreement with the dynamic compliance data presented by Reynolds and Keith[31] and Reynolds and Soedel[32]. The X/F and phase data most nearly match Reynolds' and Keith's data for palm grip with an 8 lb_f (35.6 N) grip force. The 5.7 lb_f (25.4 N) grip force data presented here lies between the 8 lb_f grip force data and the 2 lb_f (8.9 N) grip force data presented by Reynolds and Keith.

The confidence limits for dynamic compliance shown in Figures B-1 through B-6 are generally 6% to 8% above and below the average value. The widest variation occurs in Figure B-6 between 35 Hz and 100 Hz where the confidence limits are approximately $\pm$ 12%. Over much of the data the confidence limits are as low as $\pm$ 3% to $\pm$ 5%.

The confidence limits for the phase data range from $\pm$ 1.4 to $\pm$ 5.1 degrees. For most of the phase data the confidence limits are approximately $\pm$ 2.5 degrees.

The confidence limits are significant in that 90% of the time, the average X/F and phase value for similar populations can be expected to lie between the upper and lower confidence limits. The differences between the data for the large and small handles are likely not due to experimental error since the confidence limits do not overlap.

When the X/F data was taken, the worker subjects were instructed to grasp the large handle with the hand normally used to grasp the handle of a chipping hammer and to grasp the small handle with the hand used to grasp the chisel. Since most of the workers were right-handed, this usually resulted in the workers grasping the large handle with their right hand. Perhaps 95% of the large handle data is for the right hand, although both left and right hand data is present.

Reynolds[51] investigated the effects of grip force, grip type, handle size, clothing, and left and right hand on the response of the hand-arm system. He found that grip force, grip type, and handle size had pronounced effect on the system response but that differences between left and right hand effects were small. It is likely then that the differences between the large and small handle data are due to handle size.

In addition to the confidence limits, another statistic of interest when considering the dynamic compliance data is the tolerance limit. The tolerance limit for a given body of data is given by Hunter[56] as:

$$T = \pm Ks$$

where K is a tabulated constant which is a function of the desired probability and the number of sample points, and s is the standard deviation. It can be seen from equation (48) that the tolerance limit differs from the confidence limit by the coefficient, K, which replaces t/n. Values of K for 95% confidence level are tabulated by Hunter. For 75 subjects, 90% of the data lies within a band on either side of the average which is $\pm$ 1.918 s wide. Then, the tolerance limits are 10 times larger than the confidence limits.

The tolerance limits for dynamic compliance range from $\pm$ 30% to $\pm$ 120% of the average value. But over most of the range the tolerance limits are $\pm$ 60% to $\pm$ 80%. These tolerance limits are nearly the same as the width of the data envelope reported by Reynolds and Keith[31,52] for the dynamic compliance data of eight test subjects. For most of the frequency range the ratio between the upper and lower envelope of Reynolds' and Keith's data is two or more. At the low frequency end the ratio is approximately five. Reynolds and Keith used all healthy subjects not exposed to high hand acceleration levels. Their data was obtained using equipment and methods similar to those used in this study. In Reynolds' and Keith's study, variables such as handle size, grip type and grip force were held constant for each plot. The variation in Reynolds' and Keith's data then was due primarily to differences in the response of the hand-arm system from one individual to another. It is apparent from a comparison of Reynolds' and Keith's data, to the data presented here, that the tolerance limits for the X/F and phase data in this study are comparable to those to be expected due to variation between individuals. The size of the tolerance limits is quite significant when the nature of the population surveyed is considered. The group of 7 5 foundry workers from whom this data was obtained consisted of vibration exposed workers suffering from various stages of VWF -- from those showing no symptoms at all to those experiencing advanced stages of the disorder. If the vibration response of the hand-arm system were strongly dependent upon the severity of VWF in the individual, then the tolerance limits for 75 subjects in various stages of the disorder would be expected to be large. The fact that the tolerance limits presented here are no greater than those experienced by Reynolds and Keith suggests that the vibration response of the hand-arm system is <u>not</u> strongly dependent upon the presence of VWF in the individual. In fact, <u>if</u> there is a dependency, it is not distinguishable from the normal scatter of data experienced in Reynolds' and Keith's study.

Reynolds and Keith[31,52] developed a three-degree-of-freedom,mass-spring-damper model from their data. While they had considerable success matching the X/F data with the model, large discrepancies were present over wide ranges of the phase data. This strongly indicates that considerably more than three degrees of freedom are necessary to model the hand-arm system. This present study data suggests that perhaps a five-or-more-degree-of-freedom model is necessary to characterize the hand-arm system.

CONCLUSIONS FROM DYNAMIC COMPLIANCE DATA

1. The influence of handle size on response of the hand-arm system appears significant. The larger handle size gave lower X/F values.

2. No evidence was found to indicate that mechanical response of the hand-arm system is significantly influenced by the presence of VWF.

3. The X/F plots presented indicate that a five-or-more-degree-of-freedom model is necessary to adequately characterize the hand-arm system.

RESULTS AND DISCUSSION OF ENERGY DATA

Chipping Hammer Instantaneous Energies

The 1/3 octave band instantaneous energy levels for the pneumatic chipping hammer chisels and handles are given in Appendix D, Figures D-1 through D-11. Each figure contains plots of the amplitudes of the total incident energy, the energy stored in the masses and springs, and the energy dissipated by damping. The energy levels are expressed in Joules (J) (1 Joule = 1 Newton meter = Nm). A representative plot is shown in Figure 17.

The highest energies were found for the chisels at the chipper operating frequencies. Approximately 3000 J was obtained at 31.4 Hz for the chisel of chipping hammer A. The second peak at 63 Hz is approximately 100 J, while the third peak at 100 Hz is 10 J. The incident energies for the chisel of chipping hammer A at all frequencies below 31.5 Hz are in excess of 60 J. By contrast the maximum chisel peaks for chipping hammer D chipping on mild B steel and Ni-Al-Br are 1.8 J and 10 J, respectively. Both peaks for hammer D occur at 31.5 Hz. The maximum peak for the chisel of the small limestone chipper is approximately 6 J at 80 Hz. It can be seen that over a very substantial portion of the frequency range the energy levels for the chisel of hammer A are much higher than the highest peaks for the chisels of the other hammers. Hammer A was measured at full throttle slot chipping cast iron.

Overall, the plots in Appendix D indicate that the handle instantaneous energy levels are all much lower than the levels for the chisels. For chipping hammer A, the handle energy level at 31.5 Hz is reduced by 1/10,000 from the chisel level. The general energy levels are reduced by 1/1000. A reduction of 1/1000 is also experienced between the chisel and handle energies of chipping hammer D on both mild B steel and on Ni-Al-Br. For the small limestone chipper the reduction between the chisel and handle energies is only 1/10. This is consistent with the acceleration data discussed earlier.

An interesting fact is that the general instantaneous energy levels for the slot chipping case are of nearly the same magnitude for all of the chipping hammer handles. The general energy levels for hammers A and B are nearly equal. The levels for the small limestone chipper and for hammer D are comparable to each other. Both are somewhat higher than the levels for hammers A and B. The energy levels for hammer C are somewhat less than for the other hammers.

On the other hand, the energy levels for chipping hammer D, chipping on mild B steel and on Ni-Al-Br, are comparable to each other, but are at least a factor of 100 less than for the slot chipping case. Chipping hammer D, when slot chipping at full throttle produced some of the highest handle energy

levels. When the chipper was operated at 1/2 to 3/4 throttle, as in chipping on mild B steel and Ni-Al-Br, the levels for chipping hammer D were much lower. Another interesting aspect of the handle instantaneous energy data is that for all of the chipping hammers except the small limestone chipper, the maximum energy levels occurred at either 6.3 Hz or 8 Hz and not at the principle striking frequency of the tool. For the small limestone chipper the energy peak at 80 Hz is slightly larger than at 6.3 Hz. As a general rule, for all of the handle and chisel data, the magnitudes of the instantaneous energy levels decrease sharply as the frequency increases. The slope of the trend is approximately -2.5 decades/decade. Of course, peaks do occur at the principle striking frequencies and their harmonics. All of this tends to indicate that the majority of the instantaneous energy transmitted to the hand-arm system from the chisels and handles of the chipping hammers surveyed, is contained in the lower frequencies (125 Hz). It is also significant to note that for both handles and chisels at 31.5 Hz and above, the incident energy is essentially equal to the dissipated energy. It appears that a very large portion of the incident energy is absorbed by the hand, probably as heat.

Grinder Instantaneous Energies

The 1/3 octave band instantaneous energy levels for the vertical and horizontal pneumatic grinders are plotted in Figures D-12 through D-35 of Appendix D. A representative plot is given in Figure 18.

The grinder energy levels and peaks are all very much less than for the chipping hammers. The energies for chipping hammer D chipping on mild B steel and Ni-Al-Br are 10 to 100 times larger than the grinder energies at most frequencies. For the horizontal grinder with the coarse radial wheel and flared cup wheel some energy peaks are comparable to the hammer D energy levels at the same frequency.

The maximum grinder energy level is 3.3×10^{-4} J which occurs at 63 Hz for the left hand z direction of the horizontal grinder with the coarse radial wheel. All of the coarse radial wheel plots have the largest peak at 63 Hz. The largest energy levels for the horizontal grinder data generally occur at some principle frequency which seems to vary with the type and condition of the grinding wheel used. For the coarse radial wheel the principle frequency occurs at 63 Hz. The fine radial wheel has large peaks at 31.5 Hz. The principle frequency for the flared cup wheel is 40 Hz.

The vertical grinder with the sanding pad has a peak at 40 Hz in each plot. However, for the right hand data and the left hand z direction the maximum energy levels occur at 6.3 Hz.

All of the grinder energy data tends to have higher energy levels at the low frequencies. With the exception of the peak at the principle frequency, the energy levels decrease with increasing frequency. As with the chipping hammers, this indicates that the majority of the energy transmitted to the hand and arm from the grinders is contained in the lower frequencies.

The energy levels for the horizontal grinders with the coarse radial wheel and flared cup wheel are of comparable magnitude. The energies for the horizontal grinder with the fine radial wheel and the vertical grinder with the sanding pad have comparable magnitudes and are slightly less than for the coarse radial wheel and the flared cup wheel.

The energy levels for the left hand data of the horizontal grinder are higher than for the right hand data. This is probably because the left hand is closer to the grinding wheel on the horizontal grinder. The horizontal grinder y direction levels are considerably less than the x and z direction levels. The opposite is true for the vertical grinder. The vertical grinder y direction energy levels are slightly higher than for the x and z directions. The general energy levels for the vertical grinder y direction are comparable to the general levels for the horizontal grinder coarse radial and flared cup wheels.

Energies Compared to the ISO 8-Hour Acceleration Limits

Instantaneous energies for the x, y, and z directions for both large and small handles were calculated using the ISO 8-hour exposure limits as the acceleration input. The results are plotted in Figures 19 through 24. In general, the instantaneous energy plots for each direction of the large handle are very similar to the small handle plots for the same direction. The large handle energy levels are usually slightly higher than those for the small handle. It is interesting to note that the plots for the same direction of large and small handle have the same shape and slope throughout the frequency range.

Nothing has been said in previous discussions of the energy plots about the variation in the relative sizes of incident, stored, and dissipated energy with frequency. It is apparent from equations (18), (36) and (41) that the relationship between the magnitudes of these three quantities is dependent only upon the phase angle of dynamic compliance at the frequency of interest (see Appendix B). Therefore, those trends between incident, stored and dissipated energy at a given frequency which are observed in the ISO energy data are true for any instantaneous energy data, regardless of the acceleration input.

Using the data from Figures 19-24 and Appendix B, we observe that the x direction data for both small and large handles shows the dissipated energy larger than the stored energy at low frequencies. At some intermediate frequency, 16 Hz for the large handle and 31.5 Hz for the small handle, these two energies reverse their relative magnitudes and stored energy becomes larger than dissipated energy. At 80 Hz for the large handle and 100 Hz for the small handle, the dissipated energy again becomes larger than the stored energy. For frequencies above 100 Hz for the large handle and above 160 Hz for the small handle, the dissipated energy is essentially equal to the incident energy and much greater than the stored energy. For the large handle, in the frequency range between 250 Hz and 800 Hz, the dissipated energy is slightly less than the incident energy, but still much greater than the stored energy. The same thing occurs at 800 Hz and 1000 Hz in the small handle plot. It is interesting to note that these changes occur in frequency

ranges where energy is essentially constant. The frequency range where stored energy is larger than dissipated energy is also a constant energy region.

For the y direction plots at frequencies below 25 Hz the dissipated energy is larger than the stored energy. For frequencies of 31.5 Hz and above, the dissipated energy is equal to the incident energy. For the large handle plot the dissipated energy is greater than the stored energies at frequencies between 500 and 800 Hz. The same is true at 800 and 1000 Hz for the small handle plot. At 100 Hz, the large handle stored energy is larger than the dissipated energy. As with the x direction, data changes in the size relationship between stored and dissipated energy seem to coincide with regions of constant energy.

For the z direction, the dissipated energy is greater than the stored energy at frequencies below 31.5 Hz. For frequencies between 40 Hz and 630 Hz the dissipated energy is equal to, or nearly equal to, the incident energy. In the frequency range between 160 and 200 Hz the dissipated energy is somewhat less than the incident energy, but much greater than the stored energy. At 100 Hz the dissipated energy is greater than the stored energy. Once again, it can be seen that changes in the relationship between stored and dissipated energy occur at regions of essentially constant energy.

Thus, it can be seen that a pattern exists for all of the ISO energy plots. It appears that all of these curves can be divided into a minimum of four regions. Each curve begins at low frequency with a region of steeply descending energy levels which leads into a constant energy region beginning at 16 Hz. The constant energy region is followed at intermediate frequencies by a second region of descending energy, whose slope is not as steep as the slope of the first region. A second region of constant energy occurs at high frequency. The z direction plots are unique in that a third region of descending energy levels follows the second region of constant energy. The slope of the third descending region is again not as steep as the slope of the descending region preceeding it. One is led to wonder whether these patterns of alter- nately descending and constant energy levels would continue if data were available above 1000 Hz.

The physical significance of these very distinct regions in the energy plots is not clear. It appears that the region below 16 Hz is the region of constant acceleration in the ISO 8-hour limits. The constant energy portions of the plots are those frequency ranges where the input acceleration spectrum corresponding to a constant velocity at all frequencies will result in constant energy transfer to the hand-arm system. Two different constant energy levels are seen in each plot. The intermediate and high frequency descending regions are those frequency ranges where the dissipative energy equals the incident energy. In these ranges, essentially all of the energy entering the hand-arm system is dissipated internally by damping. It appears there is some relationship between acceleration spectra characterized by constant velocity at all frequencies and the energy transferred to the hand-arm system.

Work Per Unit Time

The work per unit time for the chipping hammers and grinders listed in Tables II-4 and II-5 is a measure of the cumulative energy transferred to the operator from the tool. The numbers given in the tables for each tool represent the total quantity of energy contained in the frequencies between 6.3 Hz and 1000 Hz which is transferred to the hand-arm system over a period of one second.

As would be expected, the highest energies are for the chipping hammer chisels. Referring to Table II-4, the largest energy is for chipping hammer A, followed by the small limestone chipper and chipping hammer D. The handle data is generally much lower than the chisel data. The ranking of the various chipping hammers by handle cumulative energies is quite different than the ranking by chisel energies. The cumulative energy for the handle of the small limestone chipper is more than 10 times the value for the handle of hammer A. The work per unit time for chipping hammer D slot chipping is almost 30% greater than the value for hammer A. As in the case of the instantaneous energies, it is apparent that the energies transferred to the hand-arm system from the handles of the small chipping hammers are substantially more severe than from larger hammers operated under similar conditions.

The cumulative energies for chipping hammers B and C are much less than for hammer A. The lowest chipping energies were experienced for the handle of hammer D chipping on Ni-Al-Br and mild B steel. The value for chipping on mild B steel is approximately three times that for Ni-Al-Br. It appears from Table II-4, that these work practices of using the chipping hammer at less than full throttle plays a significant role in reducing the amount of energy entering the worker's hands.

Referring to Table II-5, it appears that the grinder cumulative energies are much lower than the energies for the handle of chipping hammer D. Even the largest total energy for all three directions on one hand is approximately 25% of the energy for hammer D chipping on Ni-Al-Br.

The largest grinder total cumulative energy for one hand is for the left hand of the horizontal grinder with the coarse radial wheel. For this case the left hand value is approximately six times the right hand value. For all the other grinder cases, the total left hand cumulative energy is approximately three times the right hand value. The horizontal grinder with the flared cup wheel has energies approximately equal to those for the coarse radial wheel. Similarly, the horizontal grinder with the fine radial wheel has energy values roughly equal to those for the vertical grinder with the sanding pad.

For the horizontal grinder cases the z direction energy is usually the largest and the x direction is the smallest. The left hand total energy is always larger than the right hand.

Lidstrom[50] presents cumulative energy levels for rock chiseling and grinding of 2.7 J/s and 0.07 J/s, respectively. The rock chiseling data was

measured for chipping hammer handles only. This value is consistent with the handle data in Table II-4 for chipping on Ni-Al-Br or mild B steel. The grinding value is definitely consistent with the data in Table II-5.

The cumulative energy values make it convenient to comment on the distribution by frequency of the instantaneous energies in Figures D-2 through D-35. For all of the chipping hammers and for the horizontal grinders with the coarse wheels, the majority of the energy is contained at the lower frequencies. For chipping hammers A, B, C, and D, 70% to 95% of the energy is contained in the frequencies of 40 Hz and below. For the small limestone chipper, where the principle frequency is 80 Hz, 88% of the energy is contained at 80 Hz and below.

A surprising amount of the total energy can be contained in a very few energy peaks. A typical example is Figure D-15, the left hand x direction for the horizontal grinder with the coarse radial wheel, where 93% of the cumulative energy is contained in the peak at 63 Hz. Similar situations exist for most of the plots for the horizontal grinder with the coarse radial wheel and the coarse flared cup wheel.

Acceleration Levels Which Produce Constant Energy

In light of the previous discussion where it was found that acceleration levels representative of constant velocity produced constant instantaneous energy over certain frequency ranges, we have calculated and plotted the values of acceleration which produce constant values of instantaneous energy and work per unit time. Figures 25 through 27 are the acceleration levels for the large handle x, y and z directions which produce constant instantaneous energy equal to 1.0 J at each center frequency. Figures 28 through 30 are the acceleration levels which produce constant work per unit time equal to 1.0 J/s at each center frequency. Only data for the X/F large handle case have been plotted.

The slope of the increasing acceleration levels at low frequencies for the constant instantaneous energy acceleration, shown in Figures 25 through 27, is 1 decade/decade. In other words, the acceleration curve is for constant velocity. Above 160 Hz for the x direction and above 40 Hz for the y and z directions the slope of the plot increases slightly. At higher frequencies the slope returns once again to 1 decade/decade.

The acceleration levels for constant work per unit time shown in Figures 28 through 30 are quite different from those for constant instantaneous energy. All of the curves possess definite peaks and valleys and the slopes are difficult to determine.

Also included in Figure 28 is a plot of equal sensation data for the vertical direction obtained by Suggs and Mishoe[36]. The similarity between the shape of their data and the x direction constant work per unit time data is quite remarkable. For frequencies below 250 Hz the data is very similar. For frequencies above 250 Hz, the equal sensation data slope is much steeper than for the constant work per unit time data. There is, however, very good agreement of frequencies at which the slope changes occur.

Plots of annoyance level data obtained by Reynolds, Standlee and Angevine[37] for 8-pound grip force in the vertical, horizontal and axial direction are plotted along with the 1.0 J/s constant work per unit time data in Figures 28 through 30. This data is essentially a special case of equal sensation data.

Once again the agreement between shape of the constant work per unit time plot and the annoyance level data is quite surprising. In this case, the agreement in slope at higher frequencies is quite good and the agreement in slope at lower frequencies is reasonable.

Comparison of the z direction data in Figure 30 indicates very good slope agreement over most of the frequency range. Deviation appears likely at the extreme ends of the range. Only the y direction data in Figure 29 shows a substantial disagreement between the constant work per unit time data and Reynolds', et al.,[37] data. The disagreement in the plots concerns the frequencies at which the slope changes occur. The slope changes are shifted to lower frequencies for constant work per unit time than for Reynolds', et al.,[37] data. However, if frequencies are shifted so that 10 Hz on the equal work per unit time plot corresponds to 25 Hz on the annoyance level plot, excellent agreement is obtained in the shape of the curves. This might suggest a shift in the phase data between the X/F data presented here and the annoyance level plots presented by Reynolds, et al.,[37]. It is interesting to note that in Figures B-2 and B-5, the shape of the phase plot is similar to large and small handles, but a peak which occurs at 10 Hz for the large handle data is shifted far to the left for the small handle data. Thus, there appears to be some relationship between equal sensation data and constant work per unit time.

CONCLUSIONS FROM ENERGY DATA*

1. In looking at the distribution by frequency of the instantaneous energies for all of the chipping hammers and for the horizontal grinders with the coarse wheels, the majority of the energy is contained at the lower frequencies (80 Hz). For chipping hammers A, B, C, and D, 70% to 95% of the energy is contained in the frequencies of 40 Hz and below. For the small limestone chipper where the principle frequency is 80 Hz, 88% of the energy is contained at 80 Hz and below.

2. In the tool types studied, the amount of energy into the hand appears to be correlated to: work practices; how hard the tool impacts on the work-piece; and throttle setting.

3. There is an apparent relationship between constant velocity and acceleration limits and instantaneous energy levels.

4. There is evidence to suggest that equal sensation acceleration data results in constant work per unit time.

* The relationship of these engineering findings to the prevalence of VWF found in the workers studied medically will be discussed in other volumes of this report series.

REFERENCES

1. Raynaud, M. 1888. Local Asphyxia and Symmetrical Gangrene of the Extremities. M.D. Thesis, Paris, 1862. IN: Selected Monographs. London, New Sydenham Society.
2. Loriga, G. 1934. Pneumatic Tools: Occupation and Health. In: Encyclopedia of Hygiene, Pathology, and Social Welfare, Vol. 2, International Labour Office, Geneva, Switzerland.
3. Hamilton, A. 1918. A Study of Spastic Anemia in the Hands of Stonecutters: An Effect of the Air Hammer on the Hands of Stonecutters. Bulletin 236, United States Department of Labor, Bureau of Labor Statistics, Industrial Accidents. and Hygiene Series, No. 19.
4. Seyring, M. 1930. Disease Resulting from Work with Compressed Air Tools. Arch. Gewerbepathol. Gewerbehy. 1:359.
5. Hunt, J.J. 1936. Raynaud's Phenomenon in Workmen using Vibrating Instruments. Proc. Royal Soc. Med. 30:171.
6. Telford, E.D., M.B. McCann, and D.H. MacCormack. 1945. Dead Hand in Users of Vibrating Tools. Lancet. 2:359.
7. Agate, J.N. and N.A. Druett. 1947. A Study of Portable Vibrating Tools in Relation to the Clinical Effects They Produce. Brit. J. Ind. Med. 4:141
8. Ashe, W.F., W.T. Cook, and J.W. Old. Raynaud's Phenomena of Occupational Origin. Arch. Environ. Health. 5:333.
9. Ashe, W.F. and N. Williams. 1964. Occupational Raynaud's. Arch. Environ. Health. 9:425.
10. Cargile, C.H. 1915. Raynaud's Disease in Stonecutters using Pneumatic Tools. J. Am. Med. Assoc. 64:582.
11. Cottingham, C.C. May 1917. Cited in the President's Monthly Report, Stonecutters Journal. 32:5. May 1917, comments on the President's Monthly Report, ibid., 32:9.
12. Rothstein, T. 1918. Report of the Physical Findings in Eight Stonecutters from the Limestone Region of Indiana: An Effect of the Air Hammer on the Hands of Stonecutters. Bulletin 236, U.S. Department of Labor, Bureau of Labor Statistics. Industrial Accidents and Hygiene Series, No. 19.
13. Edsall, D.L. March 1918. Supposed Physical Effects of the Pneumatic Hammer on Various Workers in Indiana Limestone. Public Health Reports. 33:394.
14. Leake, J.P. March 1918. Health Hazards from the Use of the Air Hammer in Cutting Indiana Limestone. Public Health Reports. 33:379.
15. Dart, E.E. 1946. Effects of High Speed Vibrating Tools on Operators Engaged in the Airplane Industry. Occup. Med. 1:515.
16. Pecora, L.J. 1960. Survey of Current Status of Raynaud's Phenomenon of Occupational Origin. J. Am. Ind. Hyg. Assoc. 21:80.
17. Wasserman, D., D.W. Badger, T.E. Doyle and L. Margolies. 1974. Industrial Vibration An Overview. J. Am. Soc. Saf. Eng. 19(6):19.

18. Williams, N. and E.B. Byrne. 1974. An Investigation to Determine the Qualitative and Quantitative Extent of Health Records and Injury Claim Records of Workers Exposed to Hand Tool Vibration in U.S. Industry. Final Report, NIOSH Contract No. HSM-99-73-56.
19. Wasserman, D.E., W. Taylor and M.G. Curry, Eds. April 1977. Proceedings of the International Occupational Hand-Arm Vibration Conference. DHEW (NIOSH) Publication No. 77-170.
20. Tse, F.S., MI.E. Morse and R.T. Hinkle. 1971. Mechanical Vibrations. Allyn & Bacon, Boston.
21. Jenkins, G.M. and D.G. Watts. 1968. Spectral Analysis. Holden-Day, Inc., San Francisco.
22. Griffin, M.J. 1946. Some Problems Associated with the Formulation of Human Response to Vibration. In: W. Taylor, Ed. The Vibration Syndrome. Academic Press, London.
23. Coermann, R.R. 1961. The Mechanical Impedance of the Human Body in Sitting and Standing Position at Low Frequencies. AMRL Technical Report No. ASD-TR-61-492.
24. Reynolds, D.D. and W. Soedel. July 1971. Dynamic Response of the Hand-Arm System to a Sinusoidal Input. Purdue University Noise Control Conference, West Lafayette, Indiana.
25. Abrams, C.F., Jr. 1971. Modeling the Vibration Characteristics of the Human Hand by the Driving Point Mechanical Impedance Method. Unpublished Ph.D. dissertation, North Carolina State University.
26. Dieckmann, D. 1958. Ein Mechanisches Modell fur das Schwengungserregte Hand-Arm System des Menschen. Intl. Z. Angew. Physiol. Einshcl. Arbeitsphysuik. 17:25.
27. Reynolds, D.D. and W. Soedel. 1972. Dynamic Response of the Hand-Arm System to a Sinusoidal Input. J. Sound & Vibration. 21(3):339.
28. Reynolds, D.D. and C.R. Jokel. 1976. Hand-Arm Vibration--An Engineering Approach. America Industrial Hygiene Journal, 35,10.
29. Suggs, C.W. 1974. Modeling of the Dynamic Characteristics of the Hand-Arm System. In: W. Taylor, Ed. The Vibration Syndrome. Academic Press, London.
30. Reynolds, D.D. and C.R. Jokel. Feb 1974. Modeling the Hand-Arm System's Response to Vibration. Report No. 1: Vibration Characteristics of the Hand and Arm. Grant OH 00470-01. National Institute for Occupational Safety and Health, Cincinnati, Ohio.
31. Reynolds, D.D. and R.H. Keith. 1977. Hand-Arm Vibration - Part I: Analytical Model of the Vibration Response Characteristics of the Hand. J. Sound & Vibration, 51(2):237.
32. Reynolds, D.D. 1972. Vibration Interaction of the Human Hand-Arm System with Vibrating Power Tools (especially Chain Saws). Unpublished Ph.D. dissertation. Purdue University, West Lafayette, Indiana.
33. Kazarian, L. 1972. Dynamic Response Characteristics of the Human Vertebral Column. Acta Orthopaedia Scandinavica. Supplement No. 146.
34. Miwa, T. 1975. Mechanical Impedance of the Human Body in Various Postures. Ind. Health (Japan). 13:1.
35. Broderson, A.B. and H.E. Von Gierke. 1971. Mechanical Impedance in the Restrained Primate during Prolonged Vibration. Report No. AMRL-TR-71-67.

36. Suggs, C.W. and J.W. Mishoe. April 1977. Hand-Arm Vibration: Implications Drawn from Lumped Parameter Models. In: Proceedings of the International Hand-Arm Vibration Conference. pp. 136-141. DHEW (NIOSH) Publication No. 77-170.
37. Reynolds, D.D., K. G. Standlee and E. N. Angevine. 1977. Hand-Arm Vibration - Part III: Subjective Response Characteristics of Individuals to Hand-Induced Vibration, J. Sound & Vibration, 51(2):267.
38. Wood, L.A. and C.W. Suggs. April 1977. A Distributed Parameter Dynamic Model of the Human Forearm. In: Proceedings of the International Hand-Arm Vibration Conference. pp. 142-145. DHEW (NIOSH) Publication No. 77-170.
39. Kerfoot, R.E. 1966. Solutions for Mechanical Impedance Measurement Problems. Spectral Dynamics Corporation. Technical Report No. M-1. San Diego, California.
40. Taylor, W., D. Wasserman, V. Behrens, and D. Reynolds. Effect of the Air Hammer on the Hands of Stonecutters. The Limestone Quarries of Bedford, Indiana, revisited. (In Press)
41. Hempstock, T.I. and D.April 1977. E. O'Connor. Evaluation of Human Exposure to HandTransmitted Vibration. In: Proceedings of the International Hand-Arm Vibration Conference. pp. 129-135. DHEW (NIOSH) Publication No. 77-170.
42. Frood, A.D.M. April 1977. Testing Methods and Some of the Problems Involved in Measuring the Vibration of Hand-Held Pneumatic Tools. In: Proceedings of the International Hand-Arm Vibration Conference. pp. 146-152. DHEW (NIOSH) Publication No. 77-170.
43. Kitchener, R. April 1977. The Measurement of Hand-Arm Vibration in Industry. In: Proceedings of the International Hand-Arm Vibration Conference. pp. 153-159. DHEW (NIOSH) Publication No. 77-170.
44. Rasmussen, G. April 1977. Measurement Techniques for Hand-Arm Vibration. In: Proceedings of the International Hand-Arm Vibration Conference. pp. 173-178. DHEW (NIOSH) Publication No. 77-170.
45. Shearer, J.L., A.T. Murphy and H.H. Richardson. 1967. Introduction to System Dynamics. Addison-Wesley Publishers, Reading, Mass.
46. Sokolnikoff, I.S. and R.1966. M. Redheffer. Mathematics of Physics and Modern Engineering (2nd Edition). McGraw-Hill Publishers, New York, N.Y.
47. Sokolnikoff, I.S. 1956. Mathematical Theory of Elasticity (2nd Edition). McGraw-Hill Publishers, New York, N.Y.
48. Harris, C.M. and C.E. Crede. Eds. 1976. Shock and Vibration Handbook (2nd Edition). McGraw-Hill Publishers, New York, N.Y. 1976.
49. Taylor, W. and D. Wasserman. 1979. Relationship between Occupational Vibration and Morbidity. J. Envir. Path. and Toxicology 2(5):67.
50. Lidstrom, I.J. April 1977. Vibration Injury in Rock Drillers, Chiselers, and Grinders. In: Proceedings of the International Hand- Arm Vibration Conference. pp. 77-83. DHEW (NIOSH) Publication No. 77- 170.
51. Farkkila, M., J. Starck, J. Hyvarinen, and K. Kurppa. 1978. Vasospustic Symptoms Caused by Asymmetrical Vibration Exposure at the Upper Extremities to a Pneumatic Hammer, Scand. J. Work Wnviron. & Health. 4:330.
52. Keith, R.H. 1975. Analytical Model of the Vibration Characteristics of the Hand-Arm System. Unpublished M.S. Thesis. School of Engineering, University of Texas at Austin.

53. Wasserman, D.E., T. Germann, D.V. Goulding and F. Pizzo. 1974. An Instrument for Testing Isometric Strength and Endurance. DHEW (NIOSH) Publication No. 74-109.
54. Hewlett-Packard Calculator 9820A Math Pac. 1978. "Numerical Integration with Unequally Spaced Base Points, Interpolation, First and Second Derivatives and Curve through Points using Spline Functions" Hewlett-Packard Products Division, Loveland, Colorado. pp. 119-124.
55. Ralston, A. and H.S. Wilf. Eds. 1967. Mathematical Methods for Digital Computers - Spline Functions, Interpolations, and Numerical Quadrature. T.N.E. Greville, Wiley Publishers, New York, N.Y.
56. Hunter, J.S. 1968. Design of Experiments Course, Vol. 1: Introduction to Statistics. Westinghouse Learning Press.
57. Miwa, T. 1967. Evaluation Methods for Vibration Effects. Part 1: Measurement of Threshold and Equal Sensation Contours of Whole Body for Vertical and Horizontal Vibrations. Ind. Health (Japan). 1967.
58. Miwa, T. 1967. Evaluation Methods for Vibration Effects. Part 2: Measurement of Equal Sensation Level for Whole Body Vibrations Between Vertical and Horizontal Sinusoidal Vibrations. Ind. Health (Japan). 5:206.
59. Miwa T. Evaluation Methods for Vibration Effects. Part 3: Measurement of Threshold and Equal Sensation Contours on Hand for Vertical and Horizontal Vibrations. Ind. Health (Japan). 5:213.
60. Miwa, T. 1968. Evaluation Methods for Vibration Effects. Part 4: Measurement of Vibration Greatness for Whole Body and Hand in Vertical and Horizontal Vibrations. Ind. Health (Japan). 6:1
61. Miwa, T. 1968. Evaluation Methods for Vibration Effects. Part 5: Measurement of Vibration Greatness Level on Compound Vibrations. Ind. Health (Japan). 6:11.
62. Miwa, T. 1968. Evaluation Methods for Vibration Effects. Part 6: Measurement of Unpleasant and Tolerance Limit Levels for Sinusoidal Vibration. Ind. Health (Japan). 6:19.
63. Miwa, T. 1968. Evaluation Methods for Vibration Effects. Part 7: The Vibration Greatness of the Pulses. Ind. Health (Japan).6:143.
64. Scarton, H.A., W. C. Kennedy, and J. A. Lacey. 1980. Sources of Noise Produced During Pneumatic Chipping Hammer Operation, ASME Paper No. 80-WA-NC-11.

Table II-2: Overall Acceleration Levels for Chipping Hammers (axial direction-Y) (6.3 Hz - 1000 Hz)

Tool and Direction	Throttle	Overall RMS Acceleration*	
Type 2		m/s^2	g
Chipping Hammer A			
Slot Chipping (cast iron)			
Handle	Full	2.99×10^2	30.51
Chisel		2.34×10^4	2,390.00
Chipping Hammer B			
Slot Chipping (cast iron)			
Handle	Full	3.52×10^2	35.84
Chipping Hammer C			
Slot Chipping (cast iron)			
Handle	Full	1.20×10^2	12.25
Chipping Hammer D			
Slot Chipping (cast iron)			
Handle	Full	6.47×10^2	65.96
Chipping Hammer D			
Ni-Al-Br			
Handle	1/2-3/4	3.71×10^1	3.78
Chisel		1.91×10^3	194.29
Chipping Hammer D			
Mild B Steel			
Handle	1/2-3/4	3.97×10^1	4.05
Chisel		1.99×10^3	203.34
Small Limestone Chipper			
Slot Chipping			
Handle	Full	2.01×10^3	205.32
Chisel		4.85×10^3	494.28

*1g = 9.81 m/sec^2

Table II-3: Overall Acceleration Levels for Grinders (6.3 Hz - 1000 Hz)

Tool and Direction	Overall RMS Acceleration*		
	m/sec^2	Total (m/sec^2)	Total (g)
Horizontal Grinder with Coarse Radial Wheel			
Right Hand	x 4.53 y 2.49 z 5.20	7.30	0.74
Left Hand	x 1.05×10^1 y 3.17 z 1.14×10^1	15.83	1.61
Horizontal Grinder with Fine Radial Wheel			
Right Hand	x 4.21 y 2.46 z 4.08	6.36	0.64
Left Hand	x 3.73 y 2.30 z 6.40	7.75	0.79
Horizontal Grinder with Flared Cup Wheel			
Right Hand	x 7.00 y 7.77 z 1.32×10^1	16.71	1.71
Left Hand	x 9.29 y 8.54 z 1.62×10^1	20.50	2.09
Vertical Grinder with Standing Pad			
Right Hand	x 3.81 y 6.96 z.5.34	9.56	0.97
Left Hand	x 3.51 y 3.58 z 2.29	5.51	0.56

*1g =9.81 m/sec^2 and $A_T = \sqrt{A_x^2 + A_y^2 + A_z^2}$

Table II-4: (Total Energy) Work per Unit Time for Chipping Hammers

Chipping Hammer	Throttle	Work per Unit Time, J/s
Chipping Hammer A,		
Slot Chipping	Full	
Handle		1.57×10^{2}
Chisel		7.23×10^{5}
Chipping Hammer B,		
Slot Chipping	Full	
Handle		6.71×10^{1}
Chipping Hammer C,		
Slot Chipping	Full	
Handle		2.99×10^{1}
Chipping Hammer D,		
Slot Chipping	Full	
Handle		2.04×10^{2}
Chipping Hammer D,		
Ni-Al-Br	1/2-3/4	
Handle		8.52×10^{-1}
Chisel		3.18×10^{3}
Chipping Hammer D		
Mild B Steel	1/2 - 3/4	
Handle		2.28
Chisel		1.08×10^{3}
Small Limestone Chipping Hammer		
Slot Chipping	Full	
Handle		1.99×10^{3}
Chisel		4.14×10^{3}

Table II

Table II-5: (Total Energy) Work per Unit Time for Grinders

Grinder	Work per Unit Time, J/s
Horizontal Grinder with Coarse Radial Wheel	
Right Hand	x 1.21×10^{-2}
	y 2.57×10^{-3}
	z 2.71×10^{-2}
	Total 4.17×10^{-2}
Left Hand	x 8.13×10^{-2}
	y 2.94×10^{-3}
	z 1.51×10^{-1}
	Total 2.35×10^{-1}
Horizontal Grinder with Fine Radial Wheel	
Right Hand	x 1.84×10^{-3}
	y 1.12×10^{-3}
	z 3.62×10^{-3}
	Total 6.58×10^{-3}
Left Hand	x 4.95×10^{-3}
	y 6.99×10^{-4}
	z 1.84×10^{-2}
	Total 2.41×10^{-2}
Horizontal Grinder with Flared Cup Wheel	
Right Hand	x 4.44×10^{-3}
	y 1.93×10^{-2}
	z 1.79×10^{-2}
	Total 4.16×10^{-2}
Left Hand	x 1.31×10^{-2}
	y 4.62×10^{-2}
	z 6.67×10^{-2}
	Total 1.26×10^{-1}
Vertical Grinder with Sanding Pad	
Right Hand	x 2.51×10^{-3}
	y 4.52×10^{-3}
	z 1.29×10^{-3}
	Total 8.32×10^{-3}
Left Hand	x 1.89×10^{-3}
	y 8.58×10^{-3}
	z 1.01×10^{-2}
	Total 2.06×10^{-2}

FIGURES

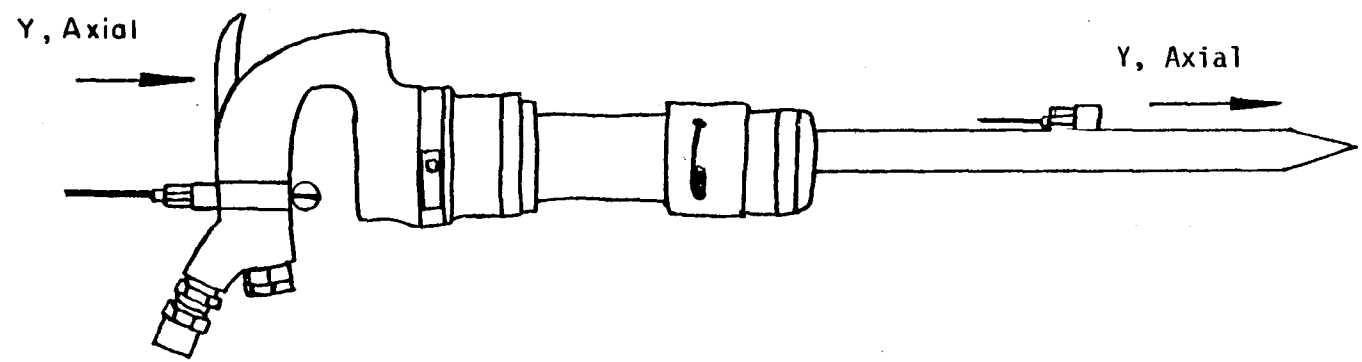

Figure 1. Pneumatic chipping hammer accelerometers and coordinate system.

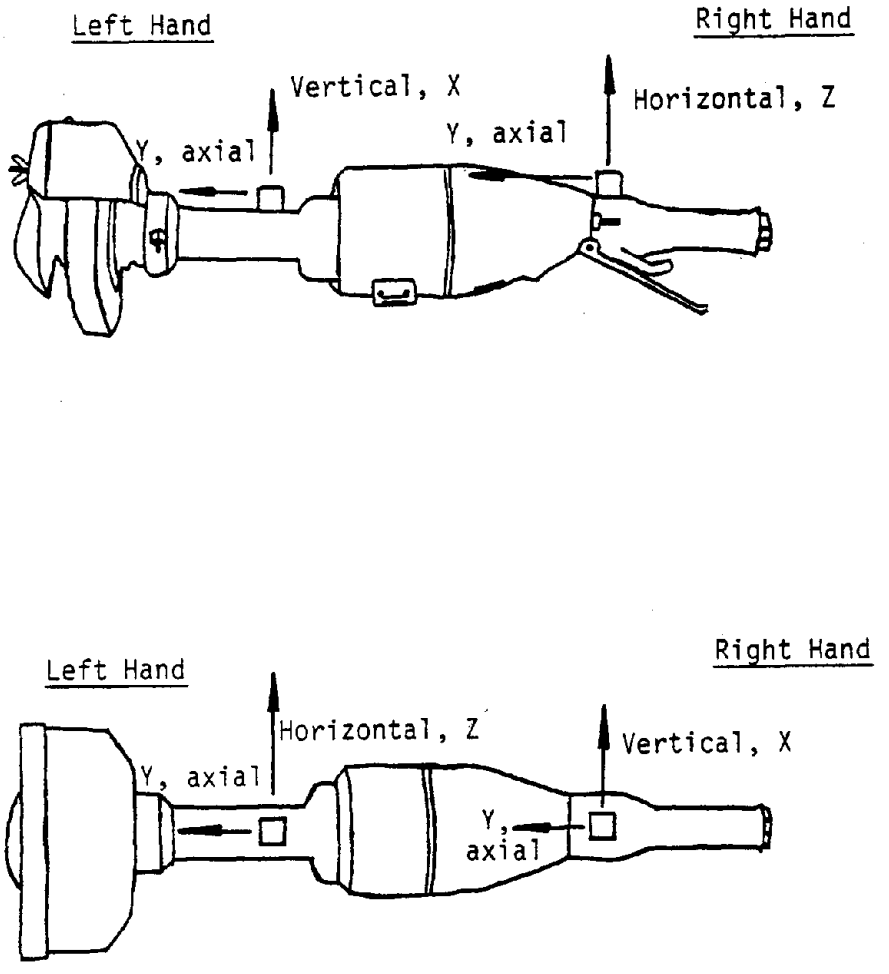

Figure 2. Horizontal grinder accelerometers and coordinate system.

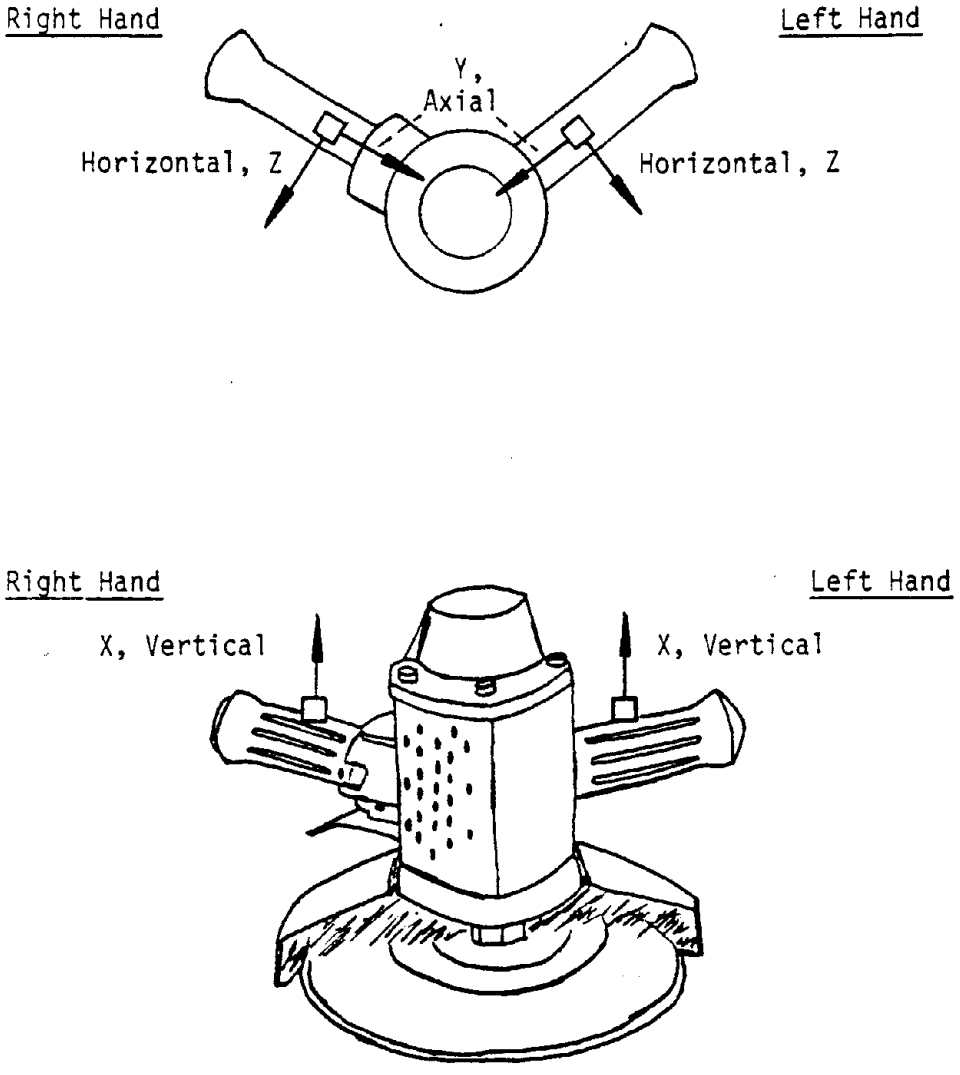

Figure 3. Vertical grinder accelerometers and coordinate system.

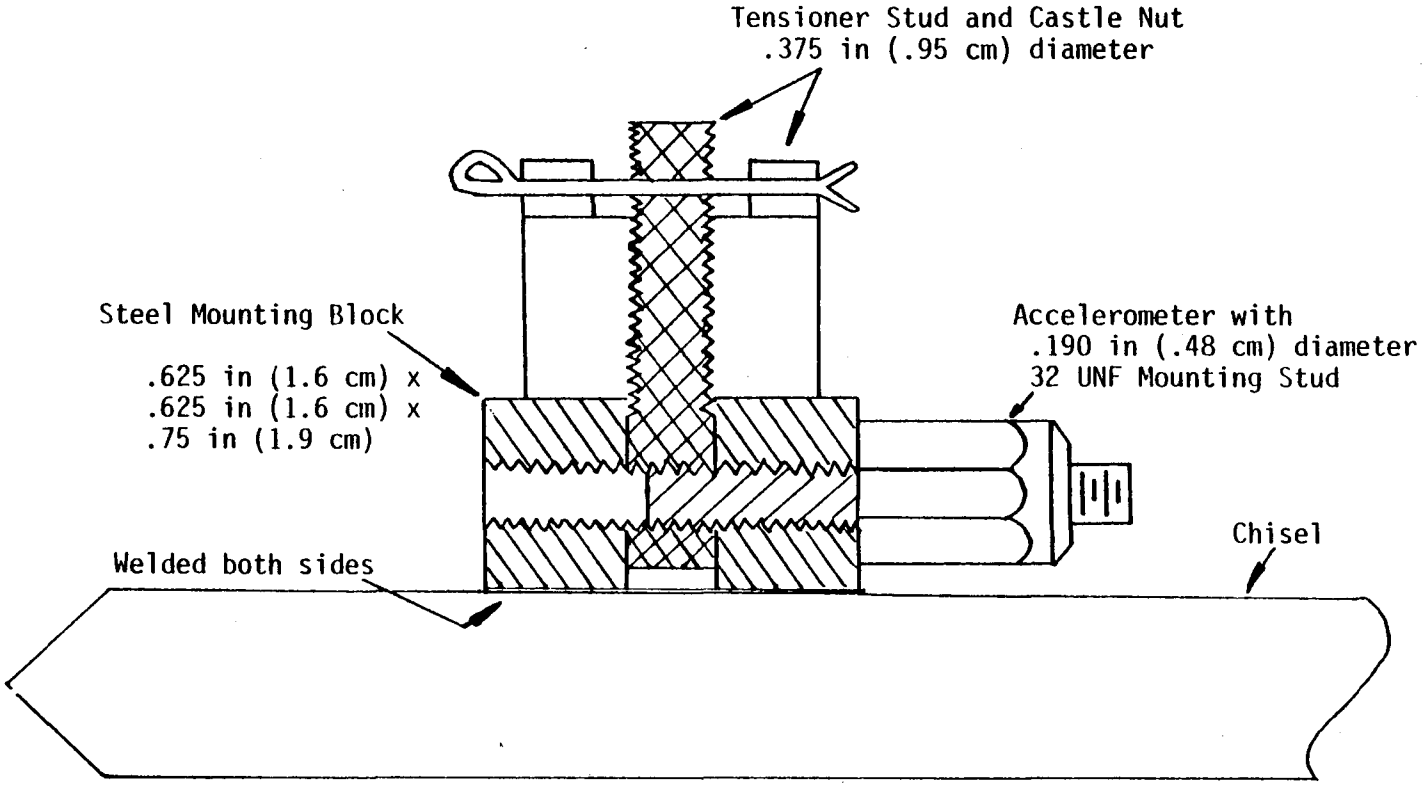

Figure 4. Acceleration mounting block for chipping hammer chisels.

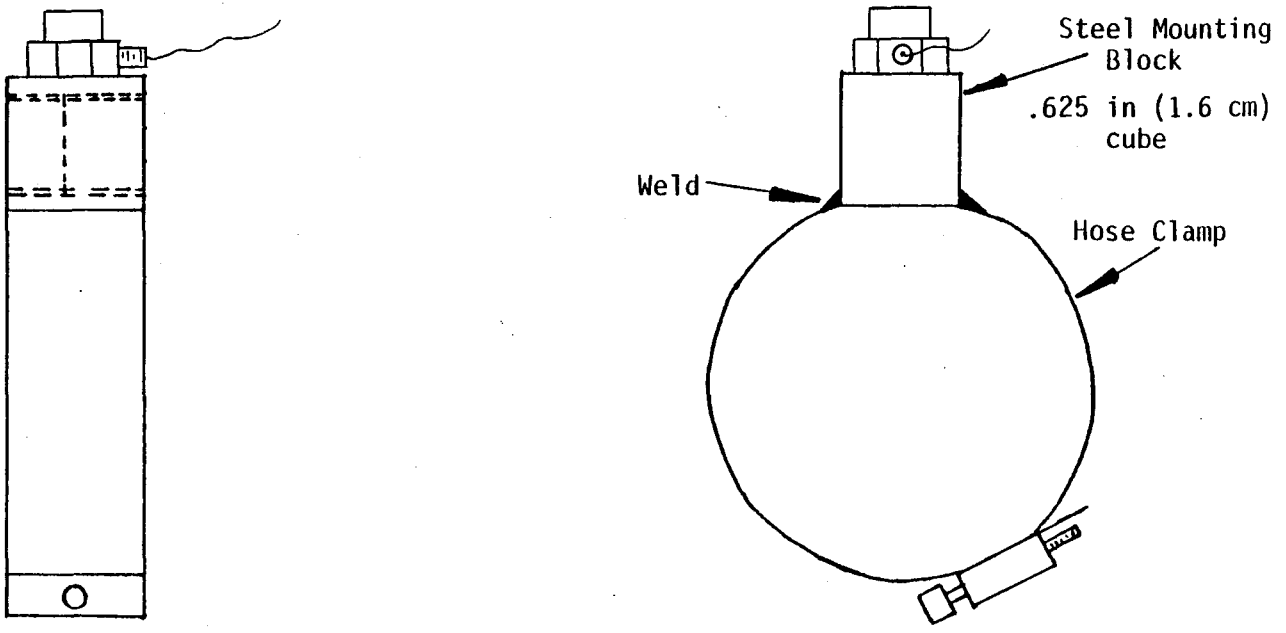

Figure 5. Accelerometer mounting block for chipping hammer handles.

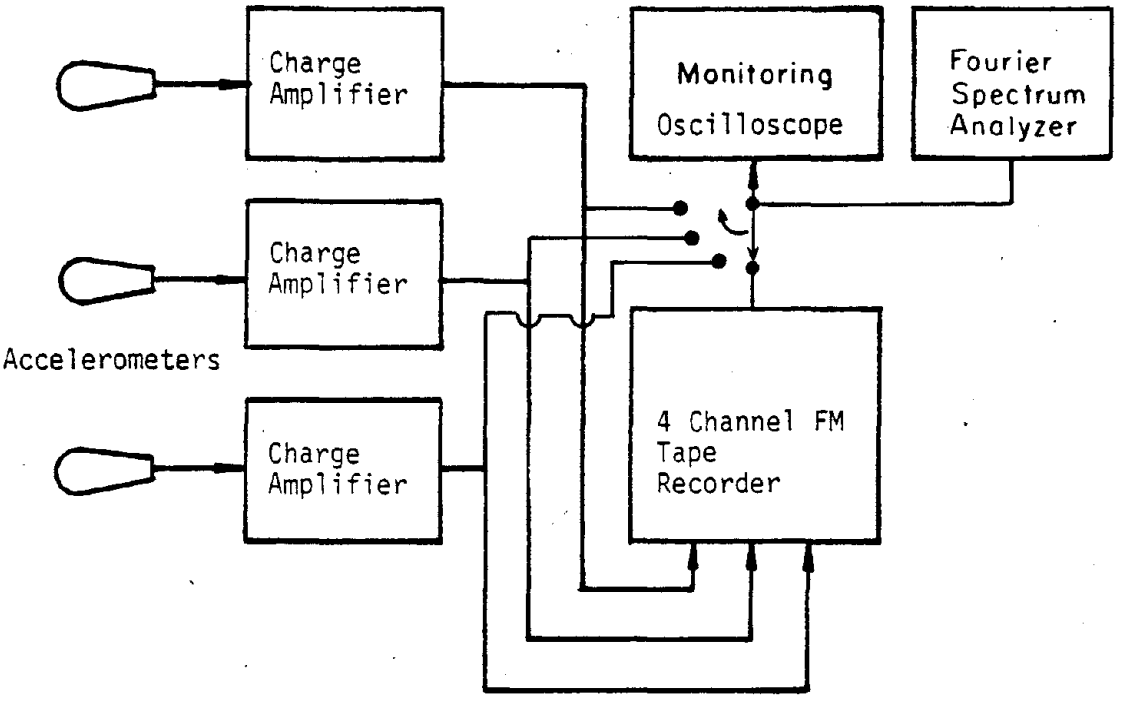

Figure 6. Acceleration measurement system block diagram.

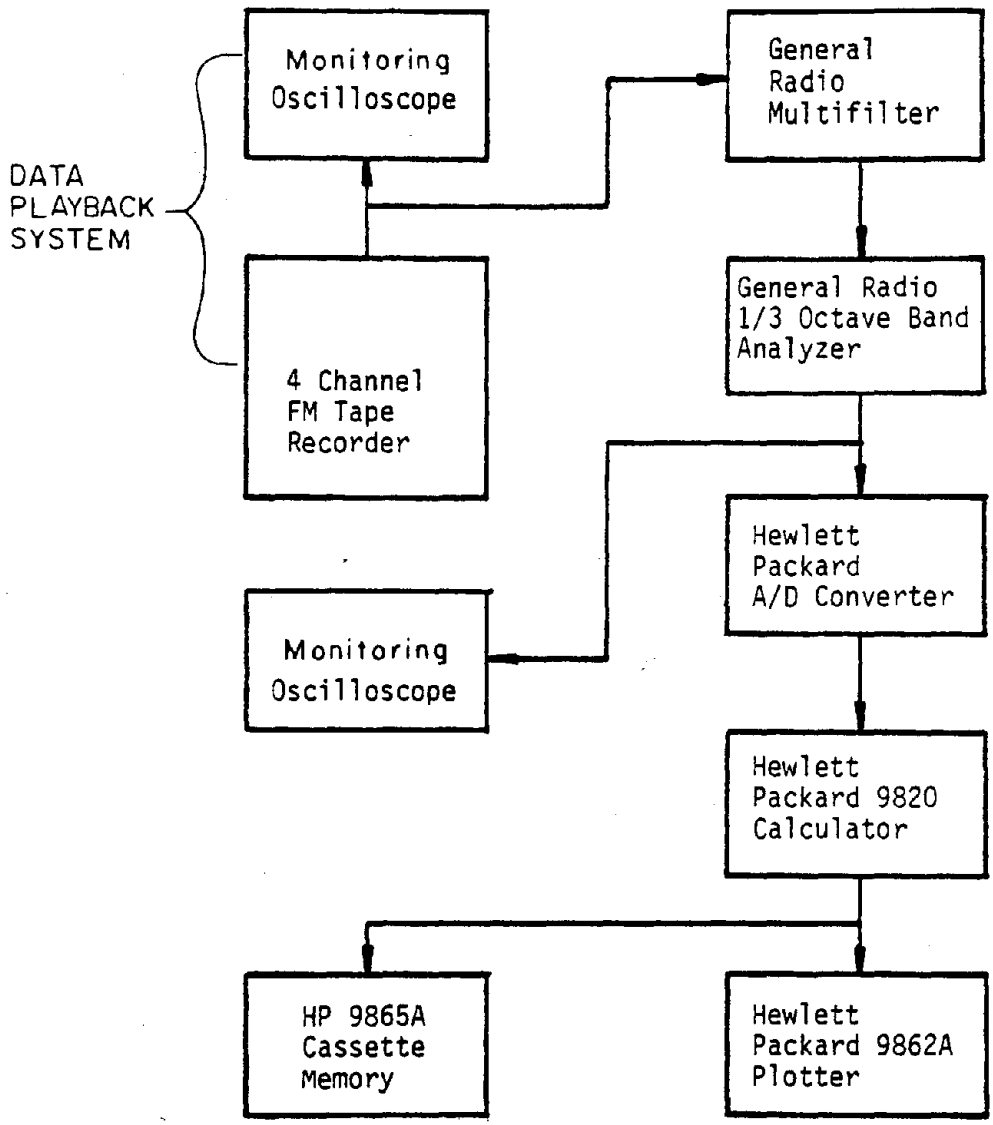

Figure 7. Acceleration spectrum analysis and digitization system block diagram.

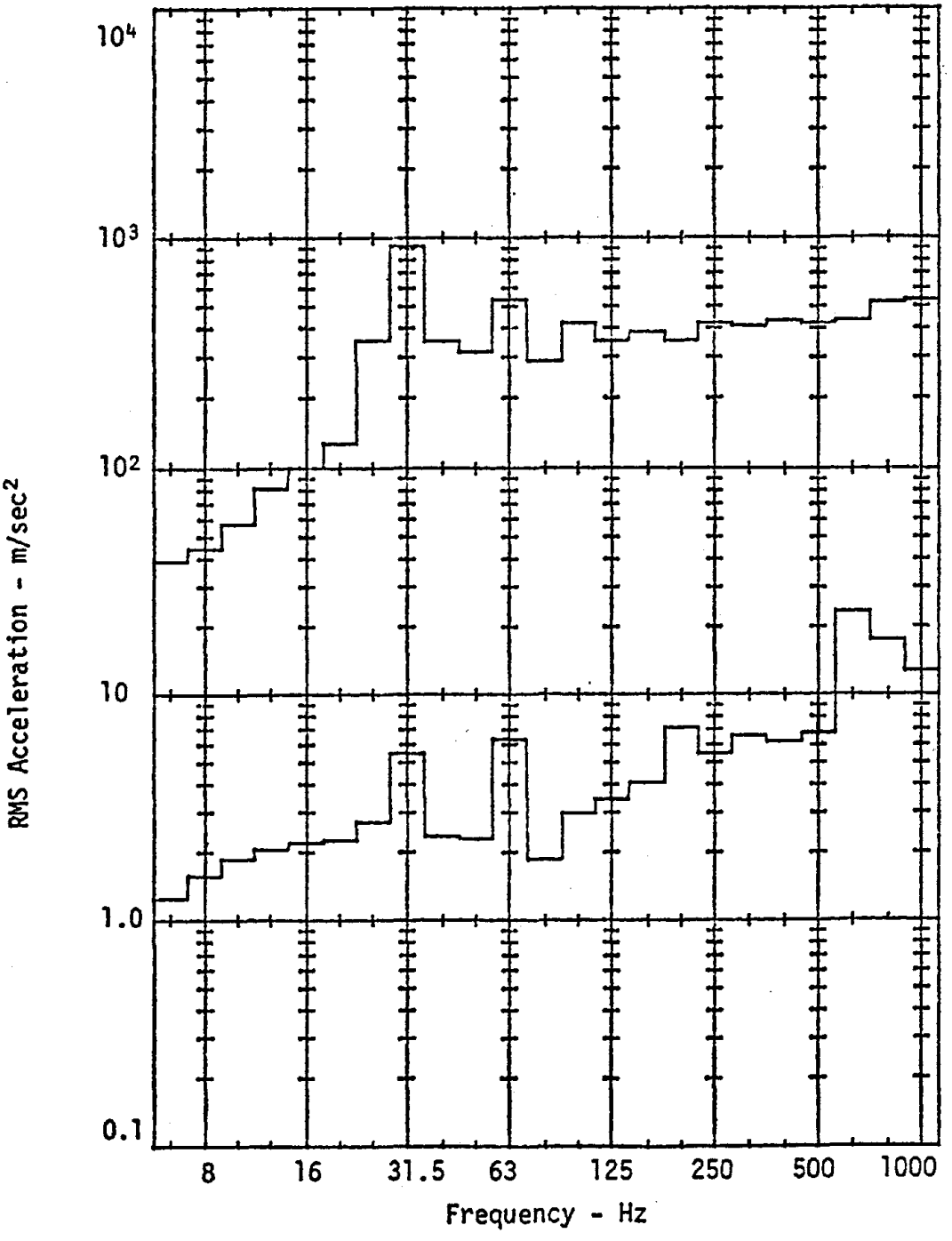

Figure 8. RMS acceleration levels for chipping hammers D used to shape propeller blades. Chipping on Ni-Al-Br. Top - chisel. Bottom - handle. Chipping hammer operated at 1/2-3/4 throttle.

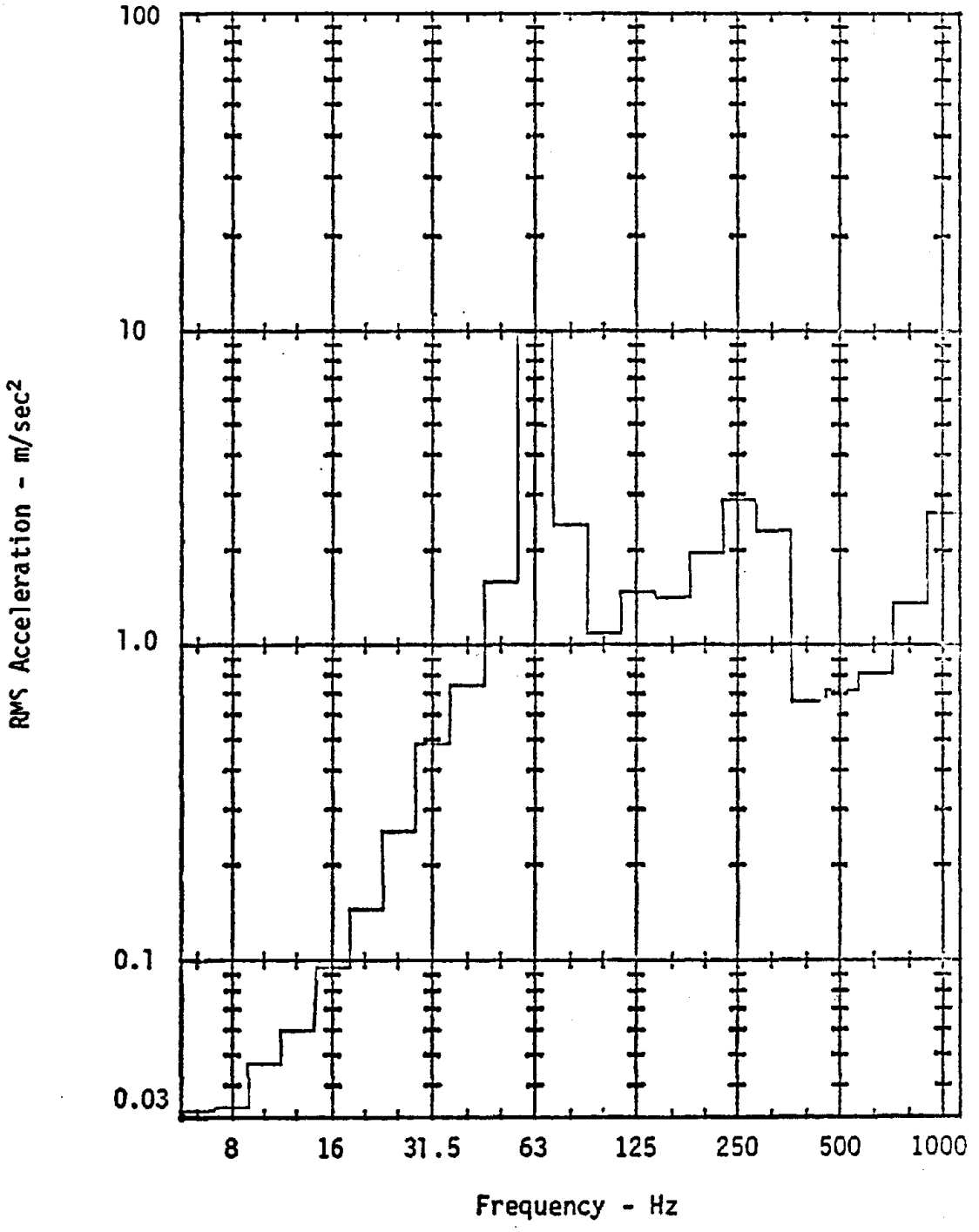

Figure 9. RMS acceleration levels for horizontal grinder with coarse radial wheel. Left hand, Z-direction.

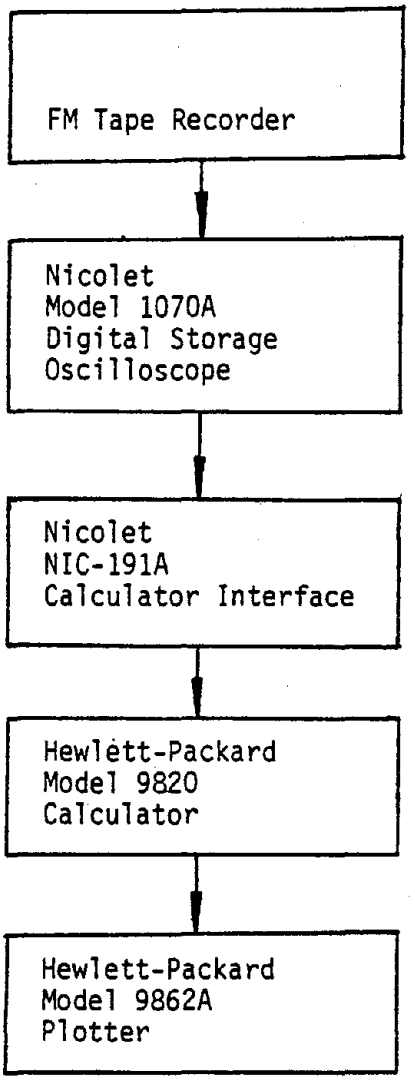

Figure 10. Block diagram for chipping hammer acceleration time history plots.

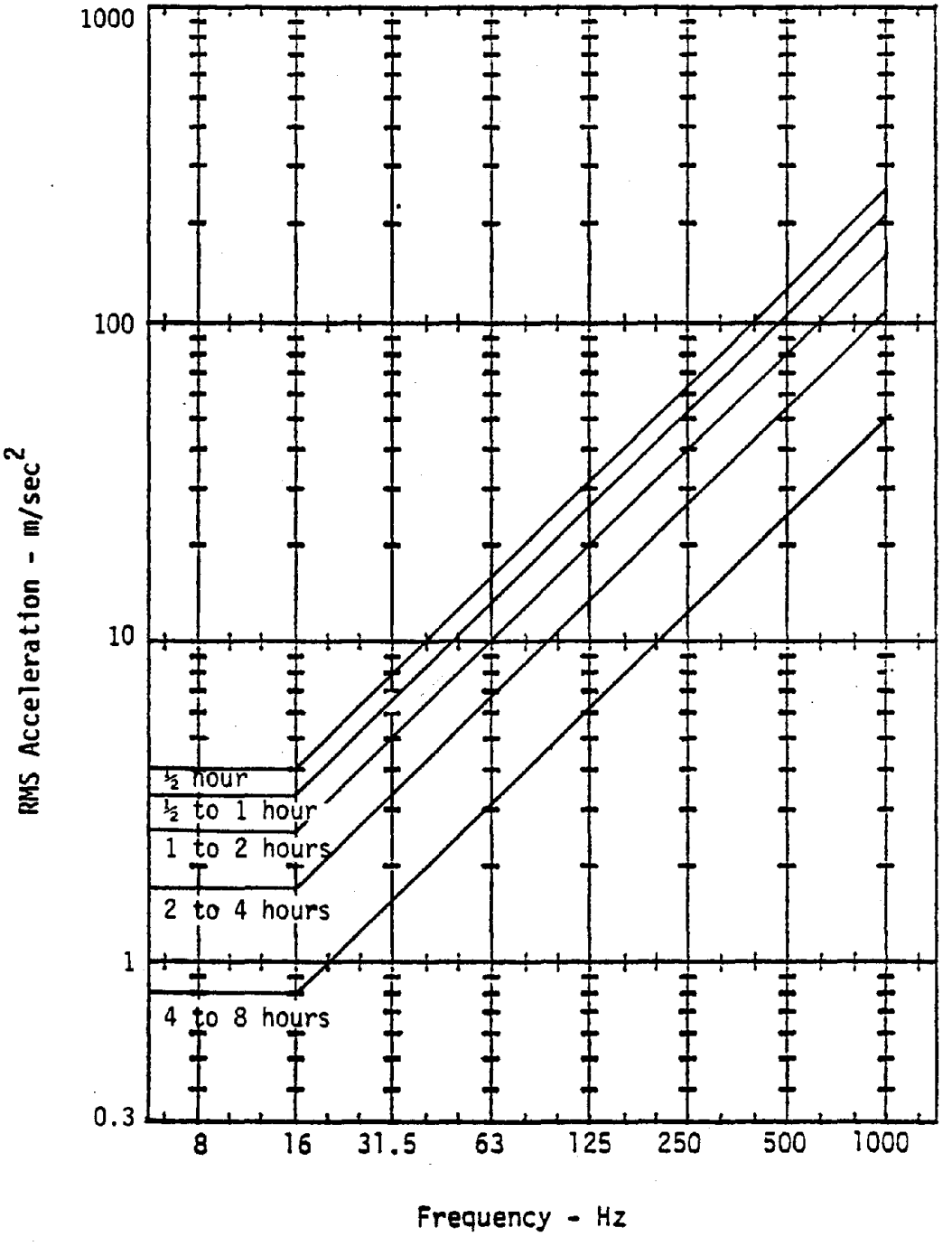

Figure 11. Proposed International Standards Organization 1/3 octave band RMS acceleration limits.

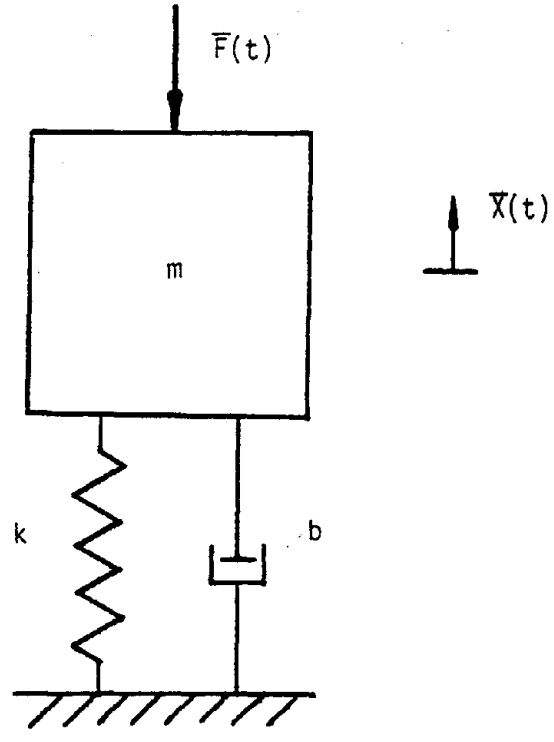

Figure 12. Single degree of freedom mass-spring-damper system.

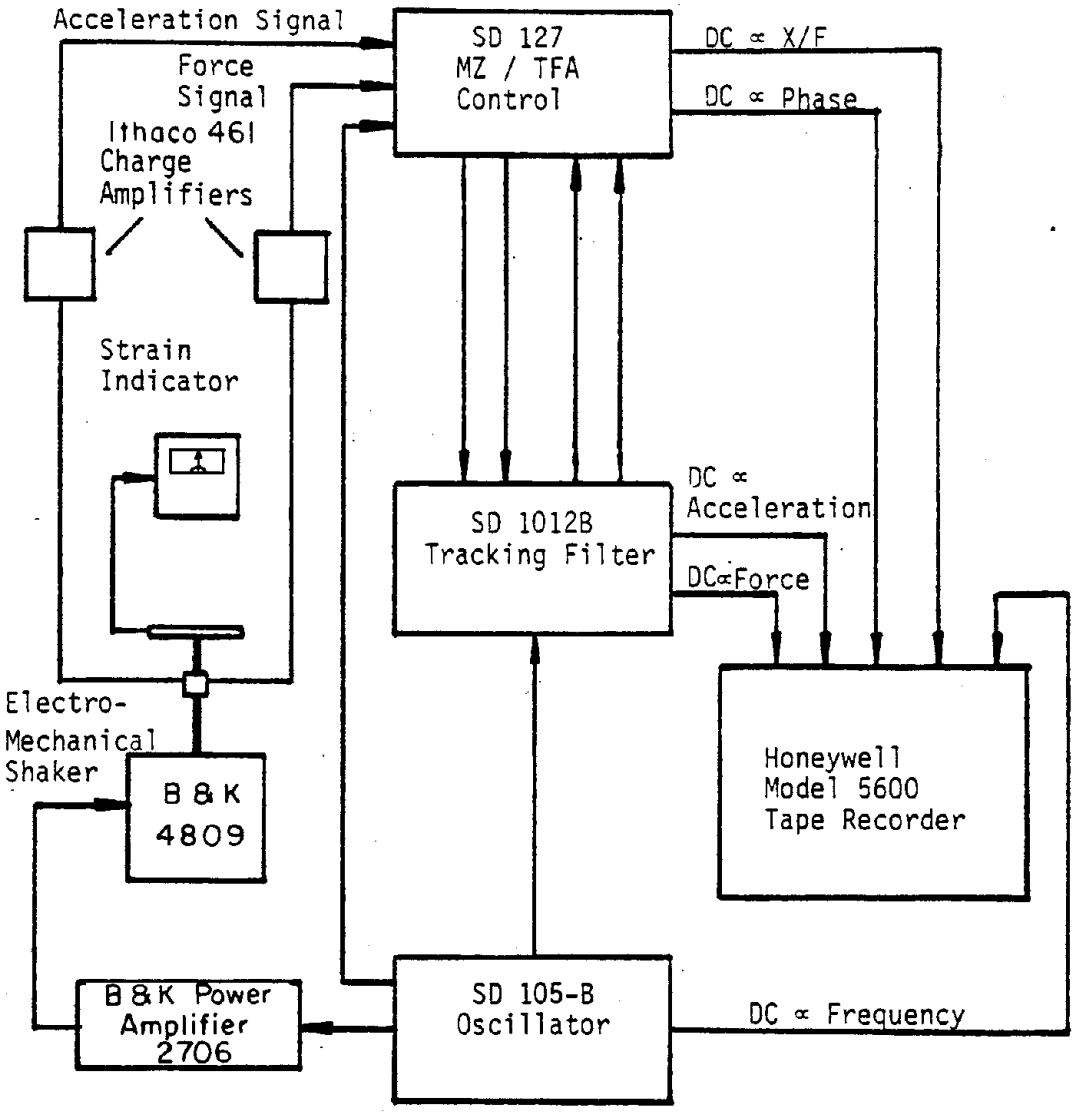

Figure 13. Mechanical compliance data acquisition system block diagram.

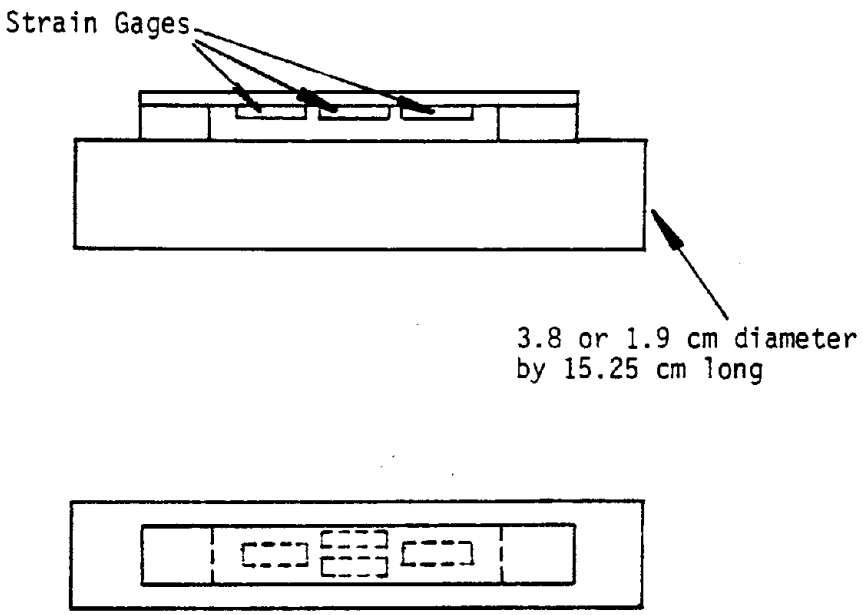

Figure 14. Instrumented shaker handle.

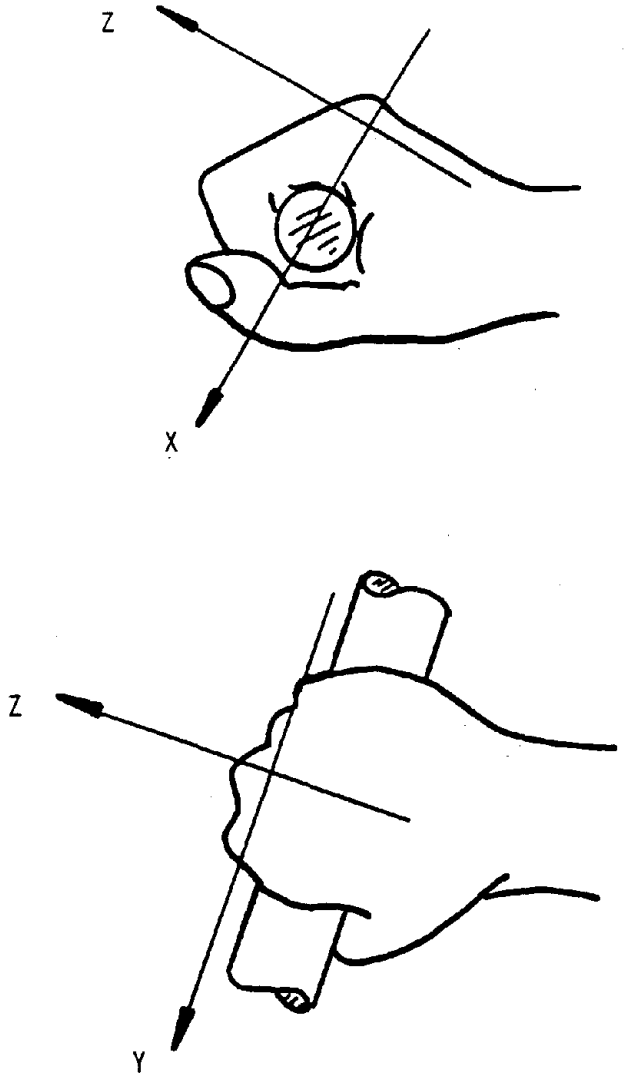

Figure 15. Coordinate system for the hand-arm system.

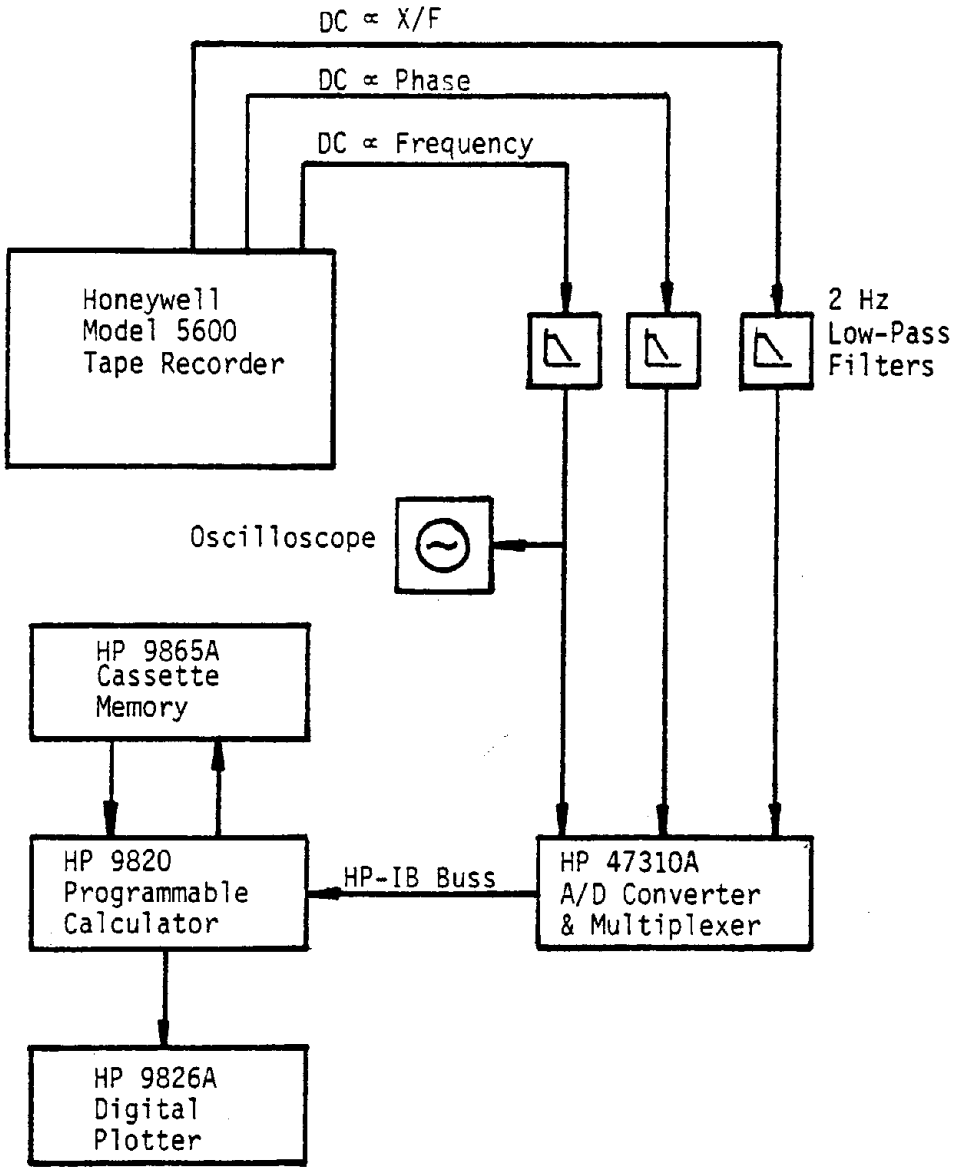

Figure 16. 9820 calculator and peripheral equipment block diagram.

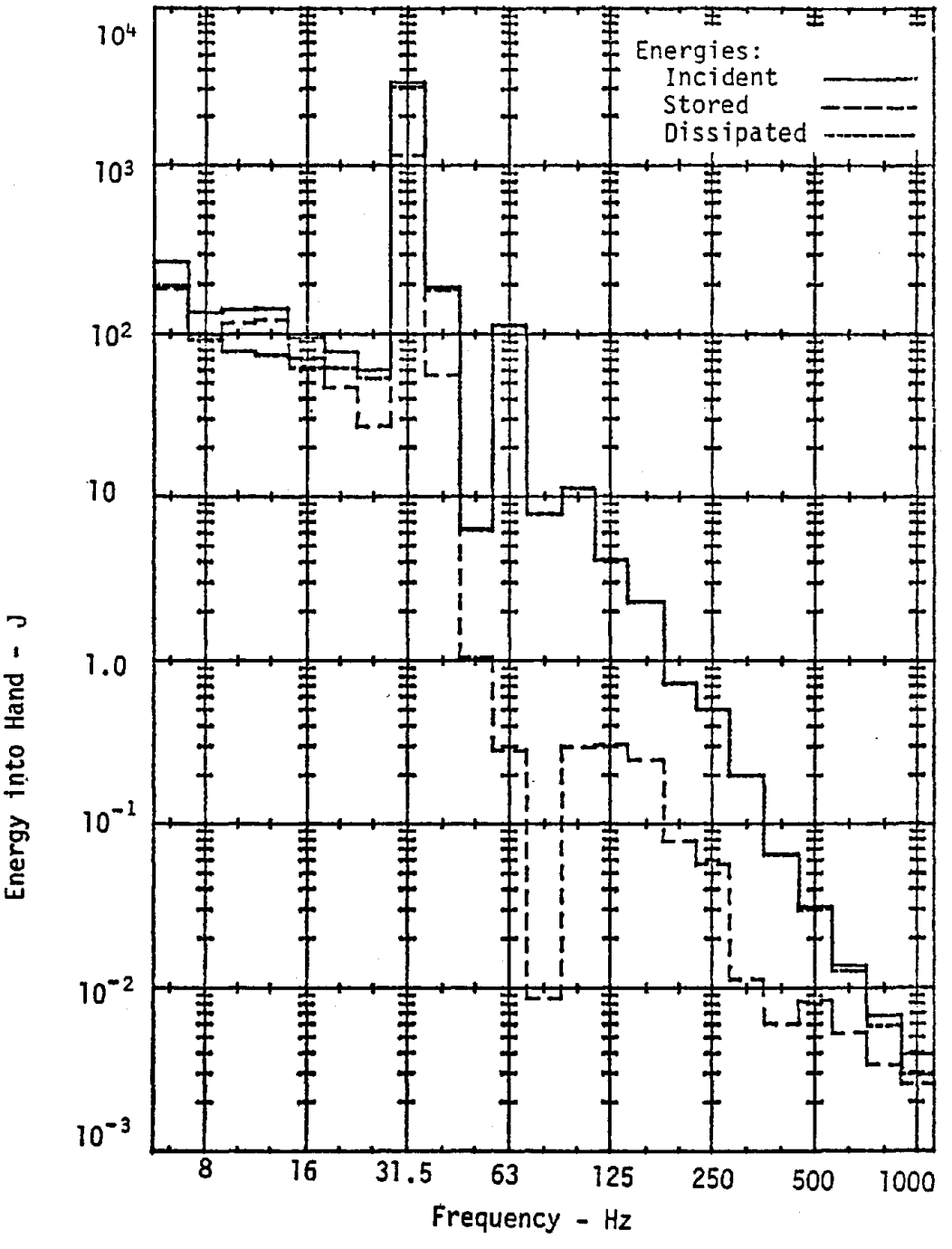

Figure 17. RMS amplitude of instantaneous energy directed into hand from the chisel of chipping hammer A used to clean castings. Slot chipping on nodular cast iron. Chipping hammer operated at full throttle.

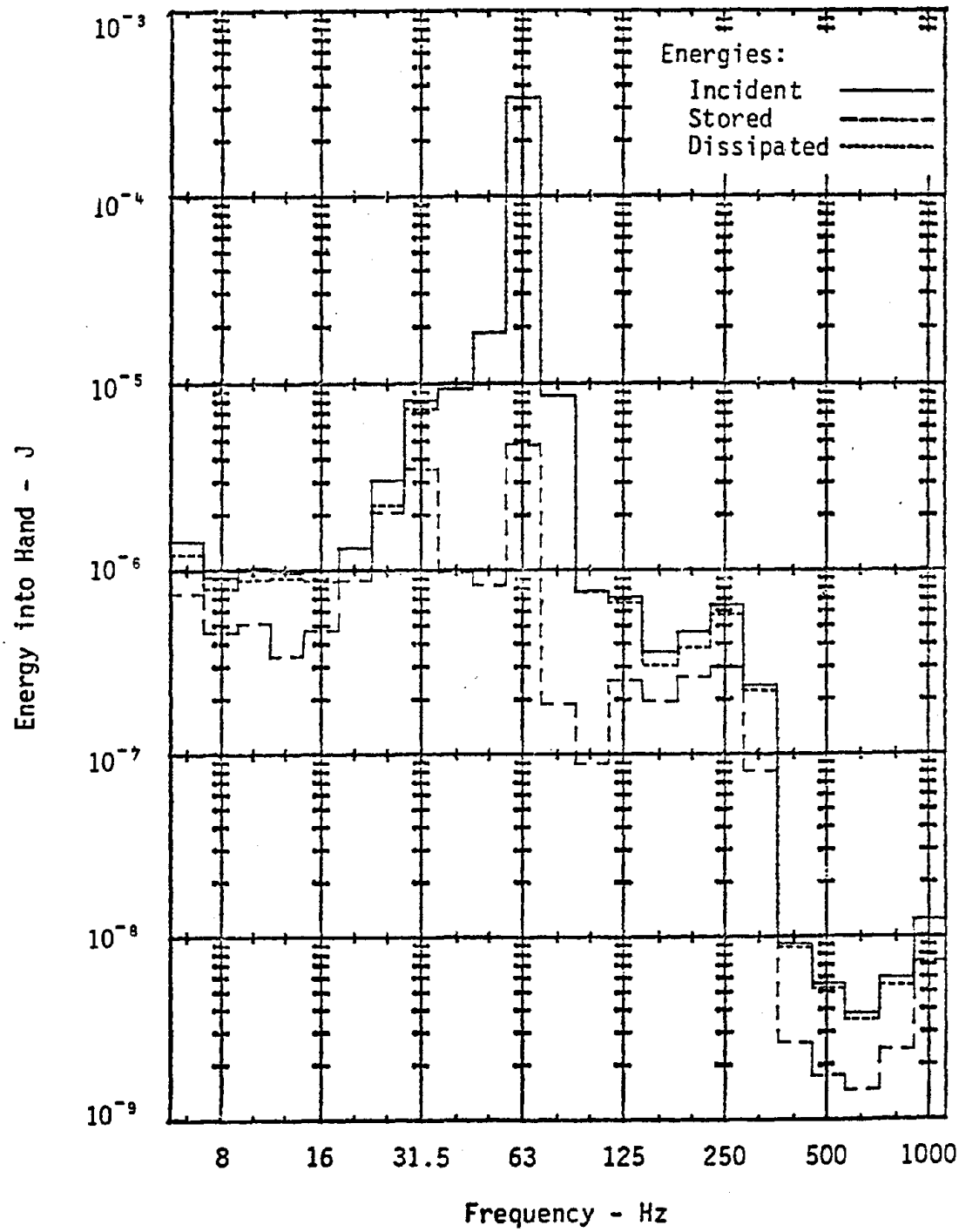

Figure 18. RMS amplitude of instantaneous energy directed into hand from horizontal grinder with coarse radial wheel. Left hand, Z-direction.

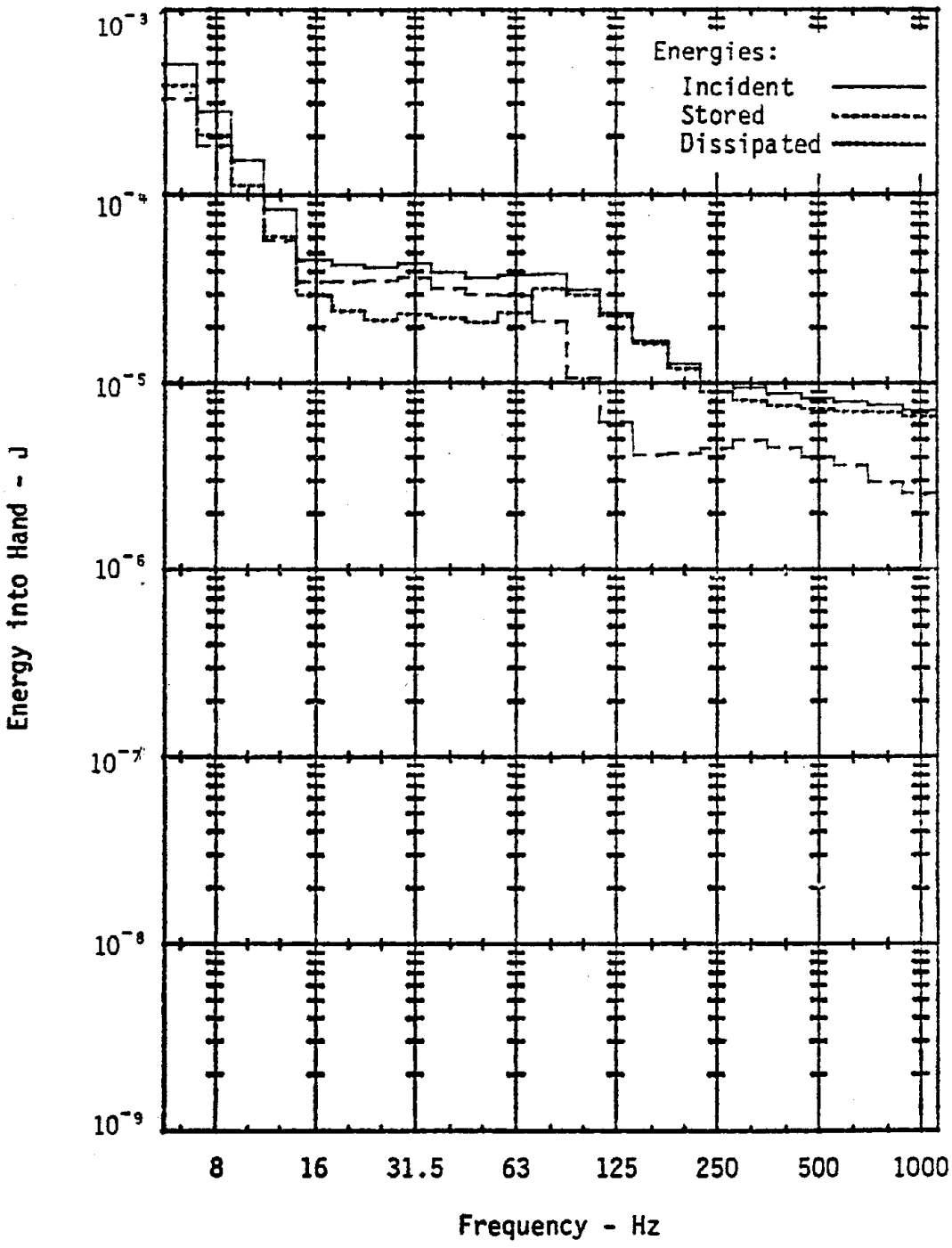

Figure 19. RMS amplitude of instantaneous energy based on proposed ISO 8 hour acceleration limits. 3.8 cm handle, X-direction.

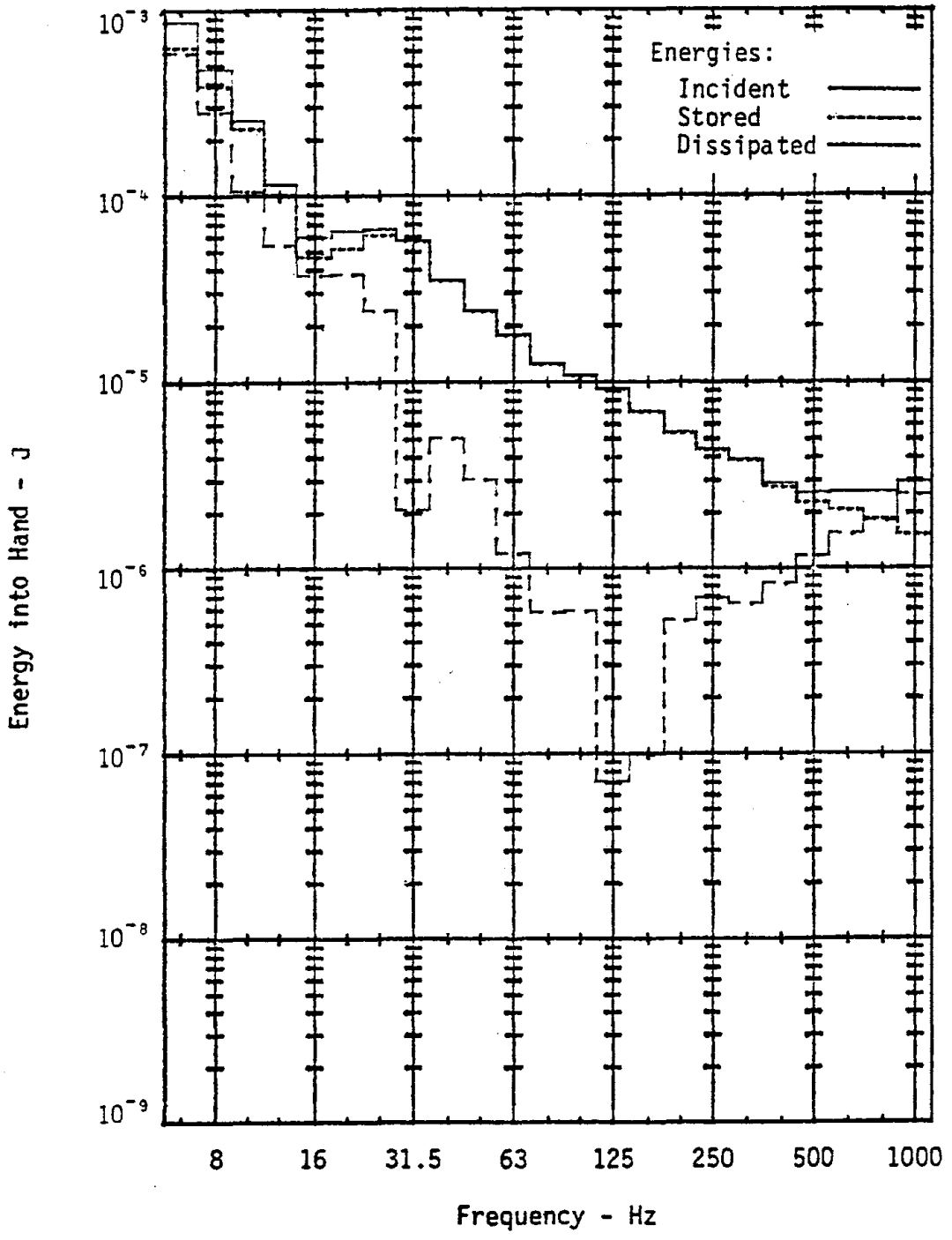

Figure 20. RMS amplitude of instantaneous energy based on proposed ISO 8 hour acceleration limits. 3.8 cm handle, Y-direction.

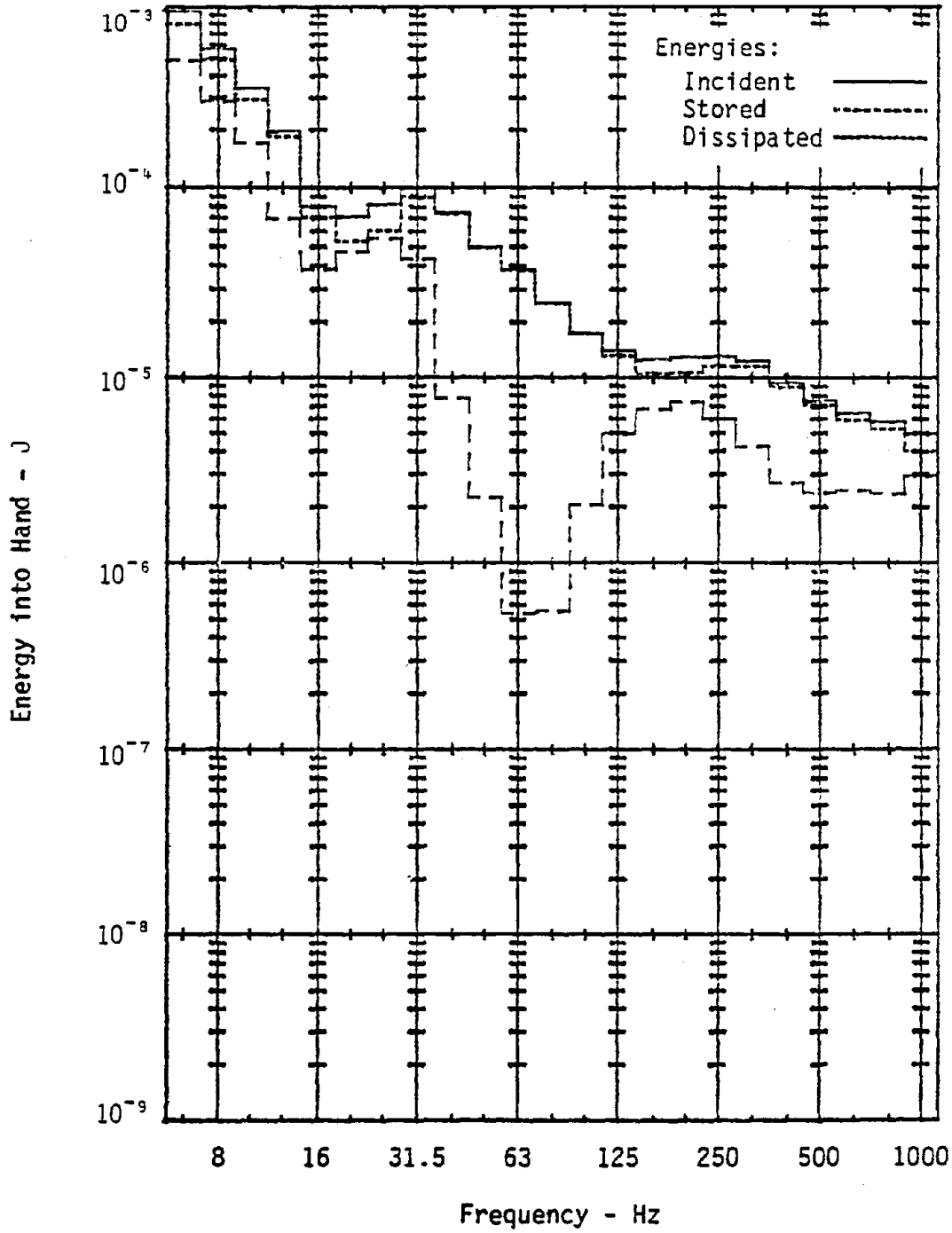

Figure 21. RMS amplitude of instantaneous energy based on proposed ISO 8 hour acceleration limits. 3.8 cm handle, Z-direction.

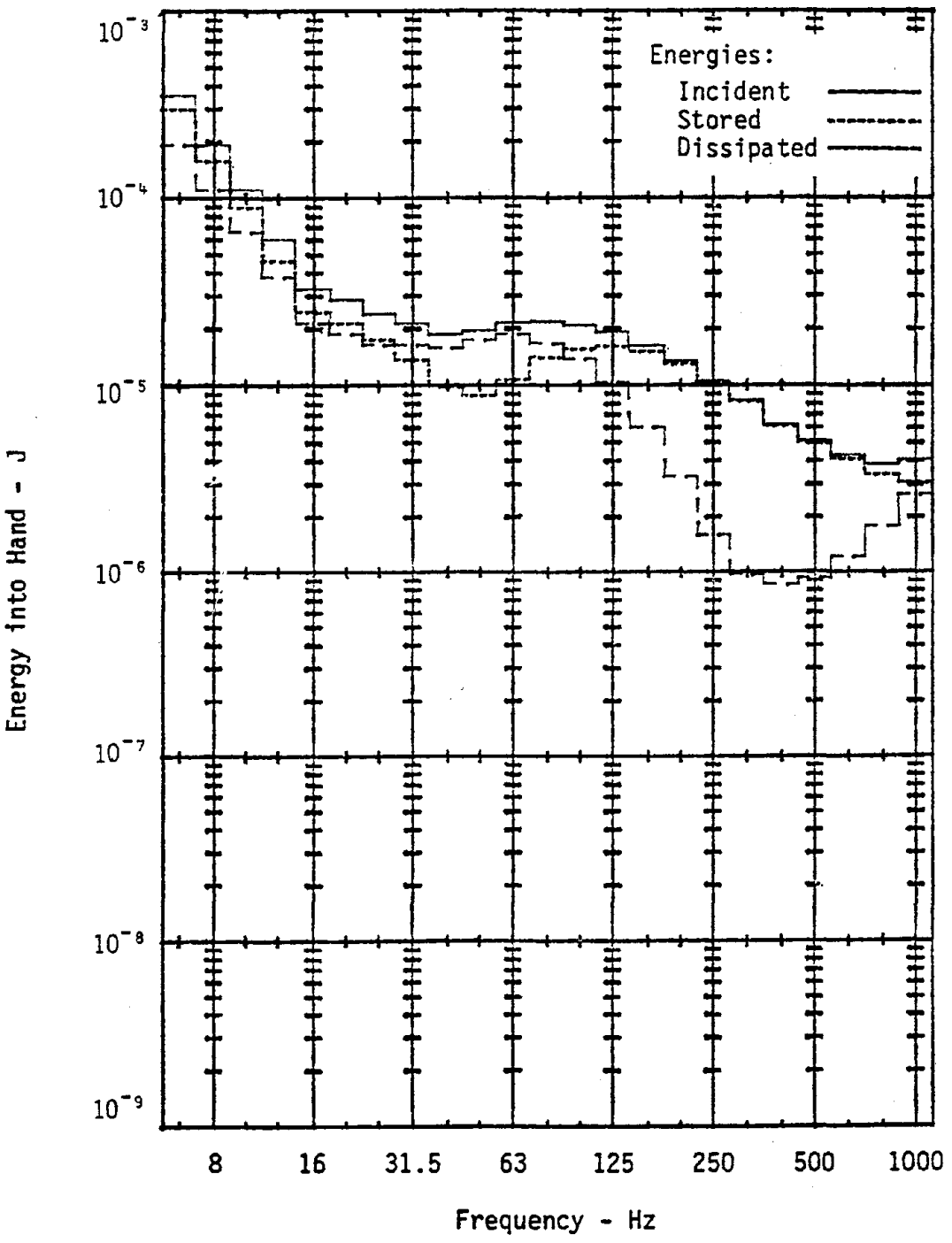

Figure 22. RMS amplitude of instantaneous energy based on proposed ISO 8 hour acceleration limits. 1.9 cm handle, X-direction.

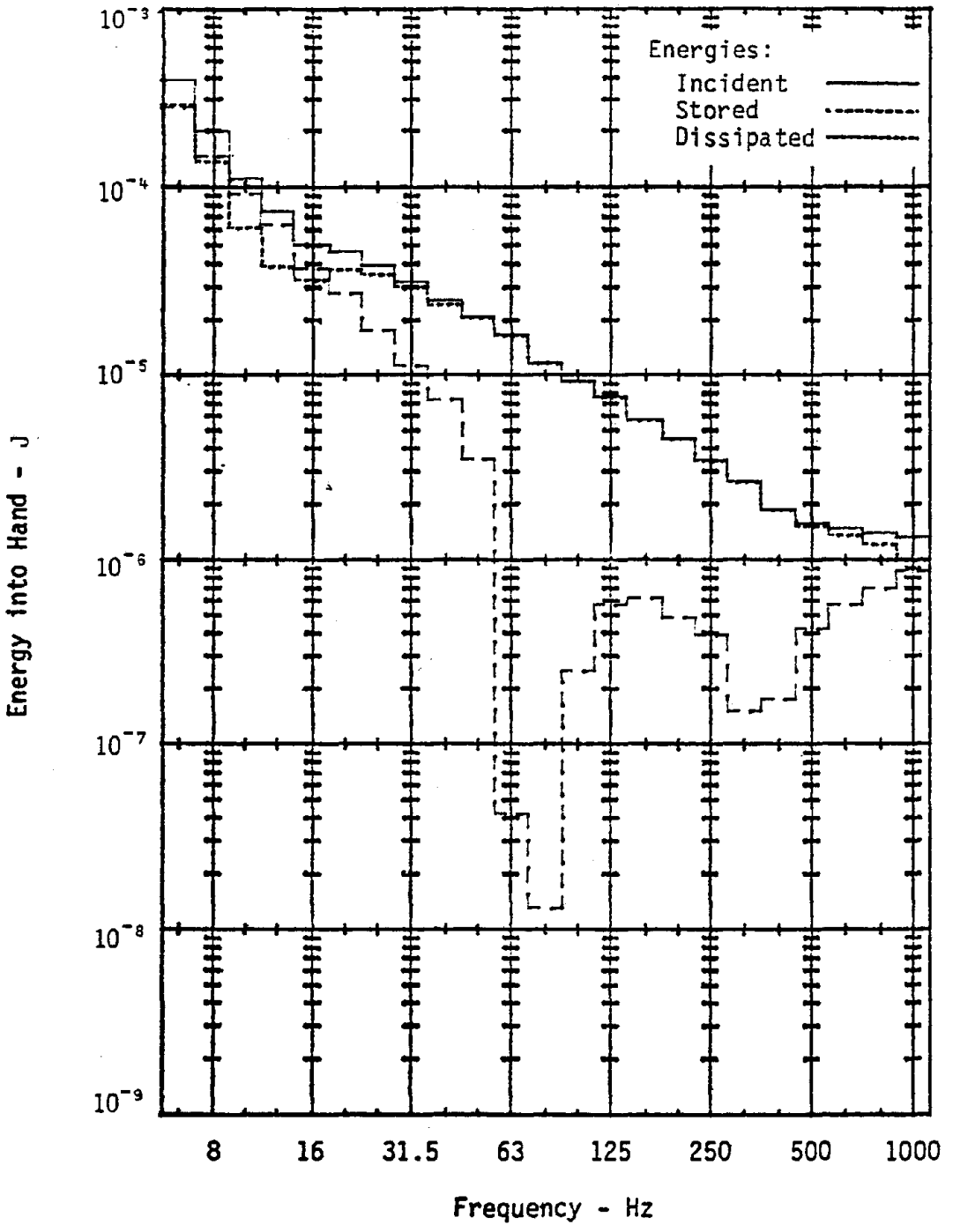

Figure 23. RMS amplitude of instantaneous energy based on proposed ISO 8 hour acceleration limits. 1.9 cm handle, Y-direction.

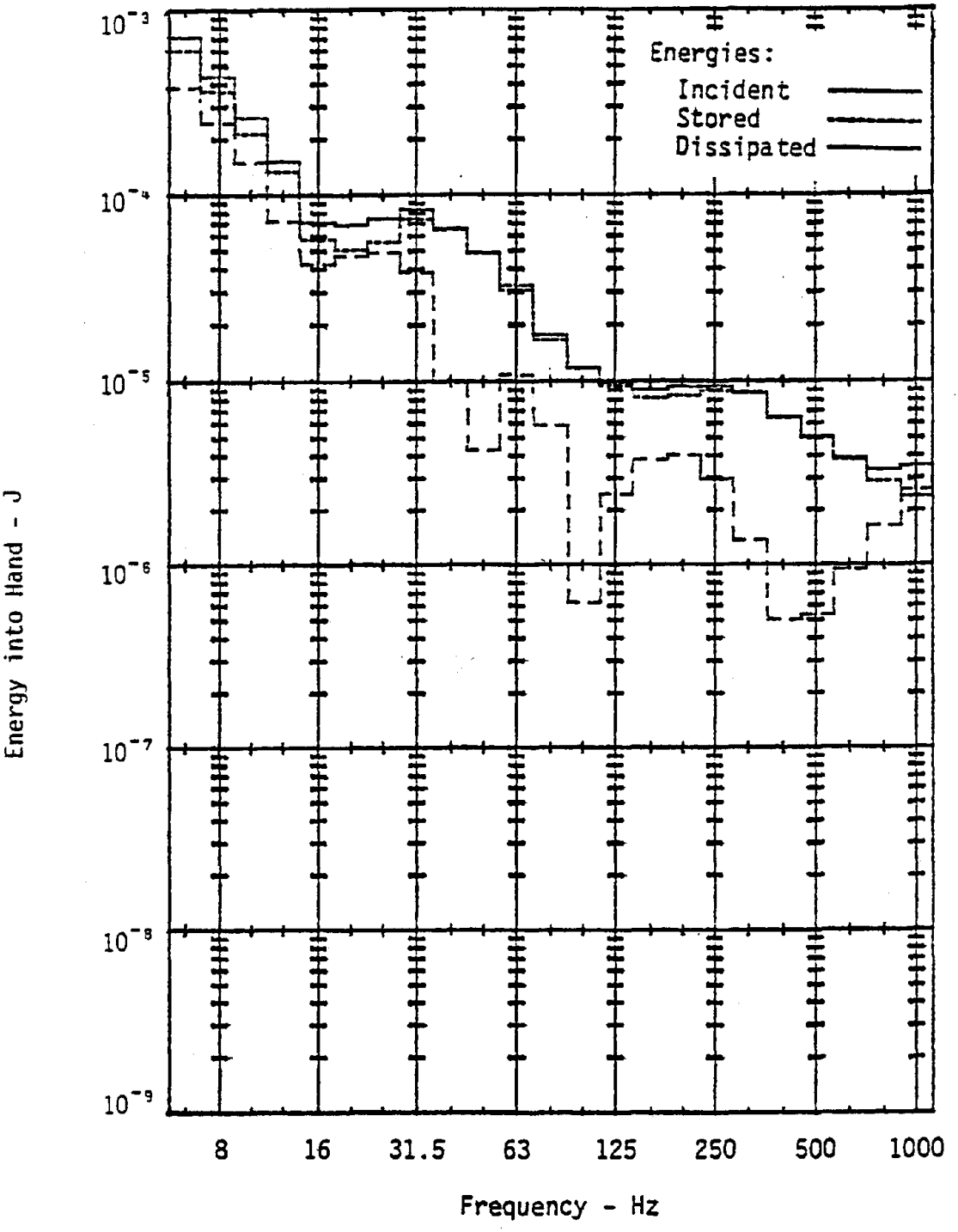

Figure 24. RMS amplitude of instantaneous energy based on proposed ISO 8 hour acceleration limits. 1.9 cm handle, Z-direction.

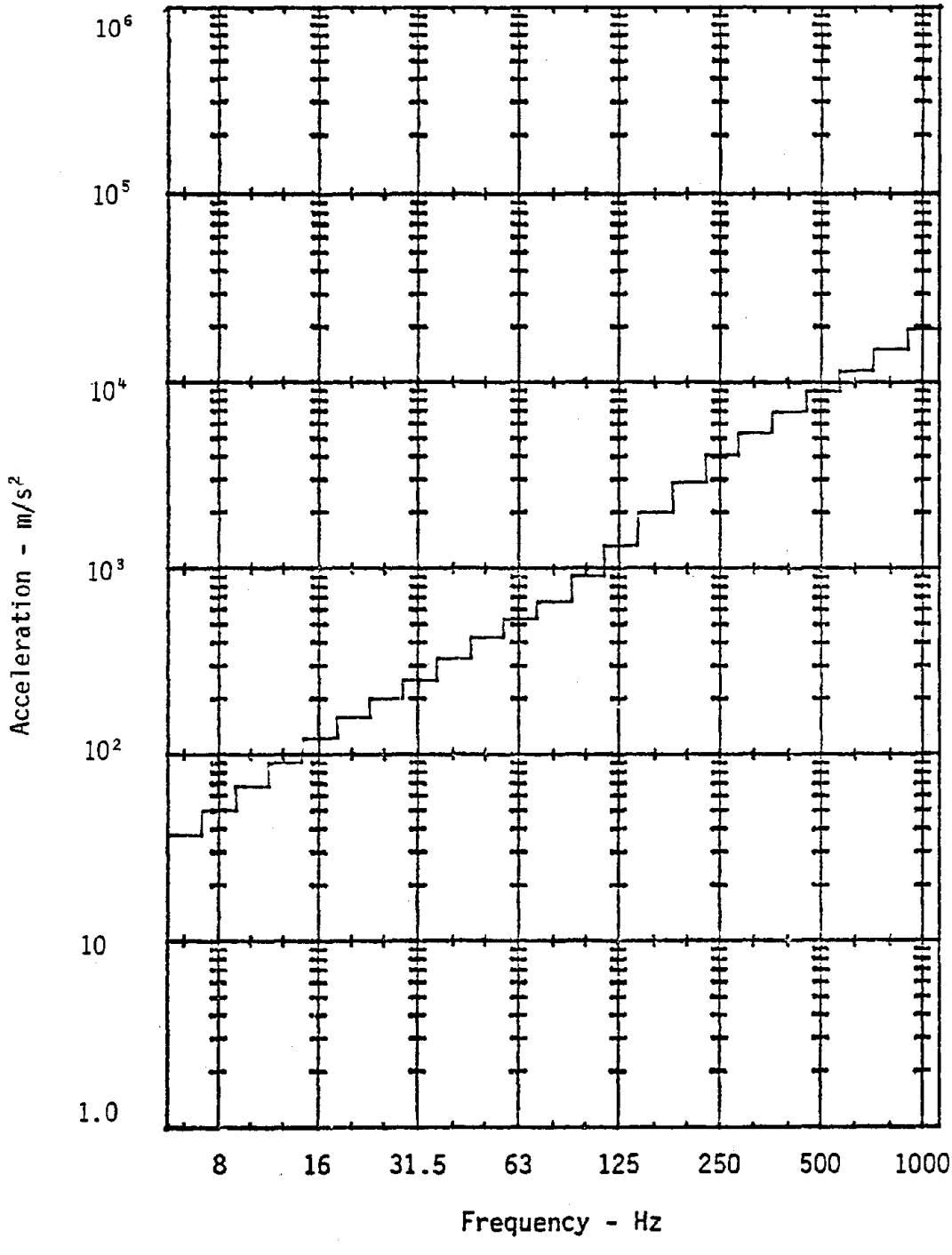

Figure 25. RMS acceleration levels which result in instantaneous energy equal to 1.0 J at center frequency. 3.8 cm diameter handle, X-direction.

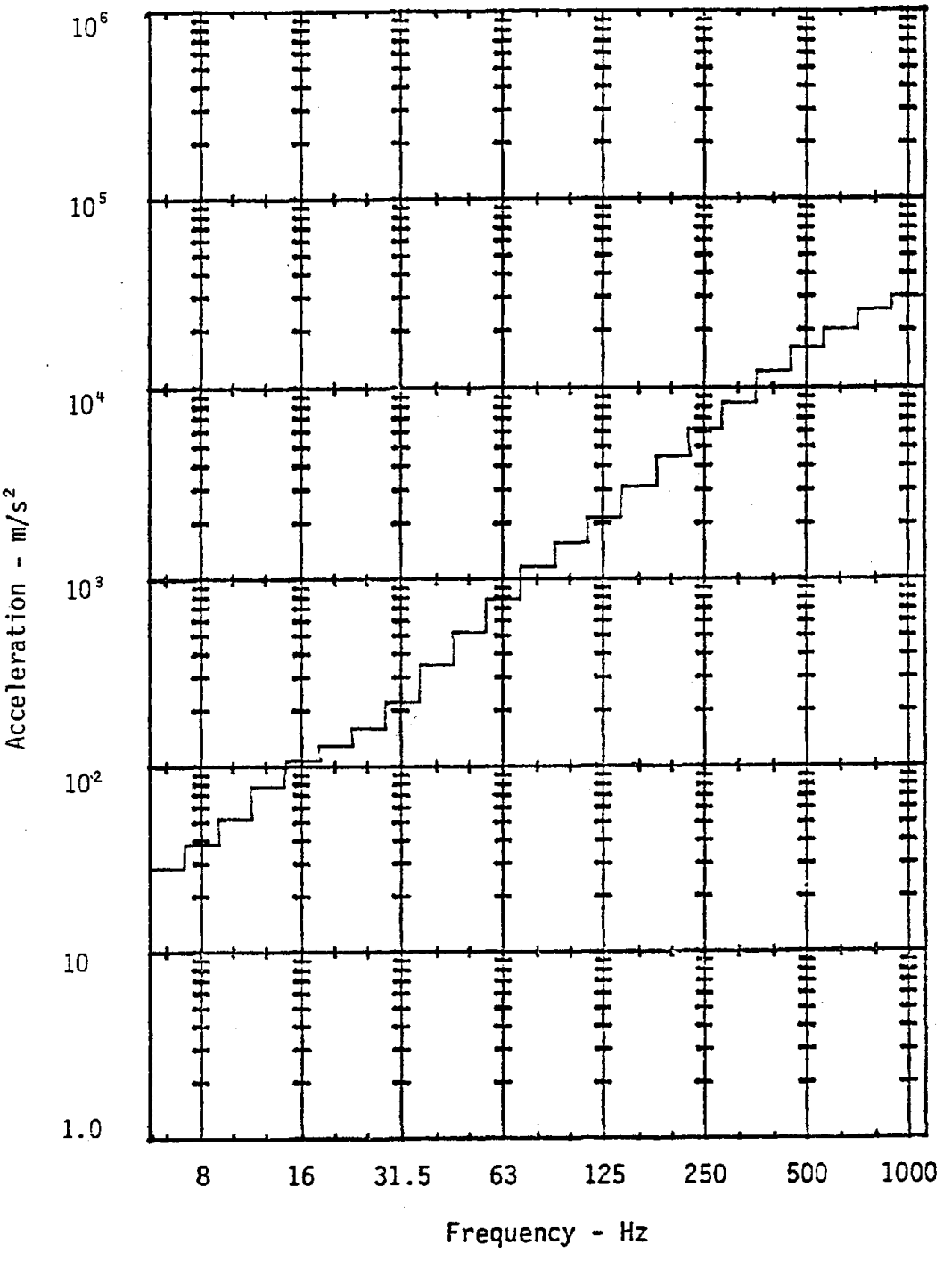

Figure 26. RMS acceleration levels which result in instantaneous energy equal to 1.0 J at each center frequency. 3.8 cm diameter handle, Y-direction.

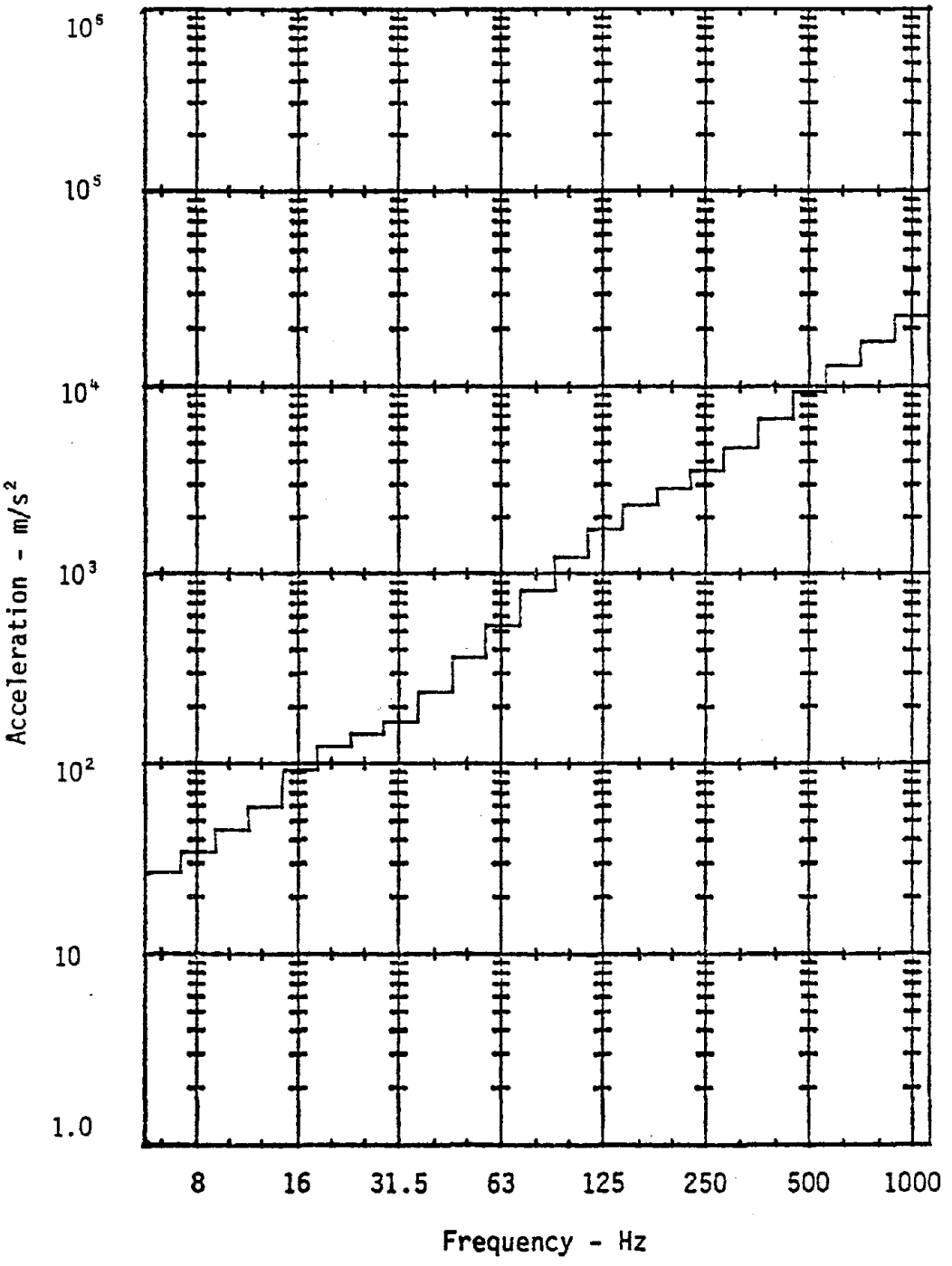

Figure 27. RMS acceleration levels which result in instantaneous energy equal to 1.0 J at each center frequency. 3.8 cm diameter handle, Z-direction.

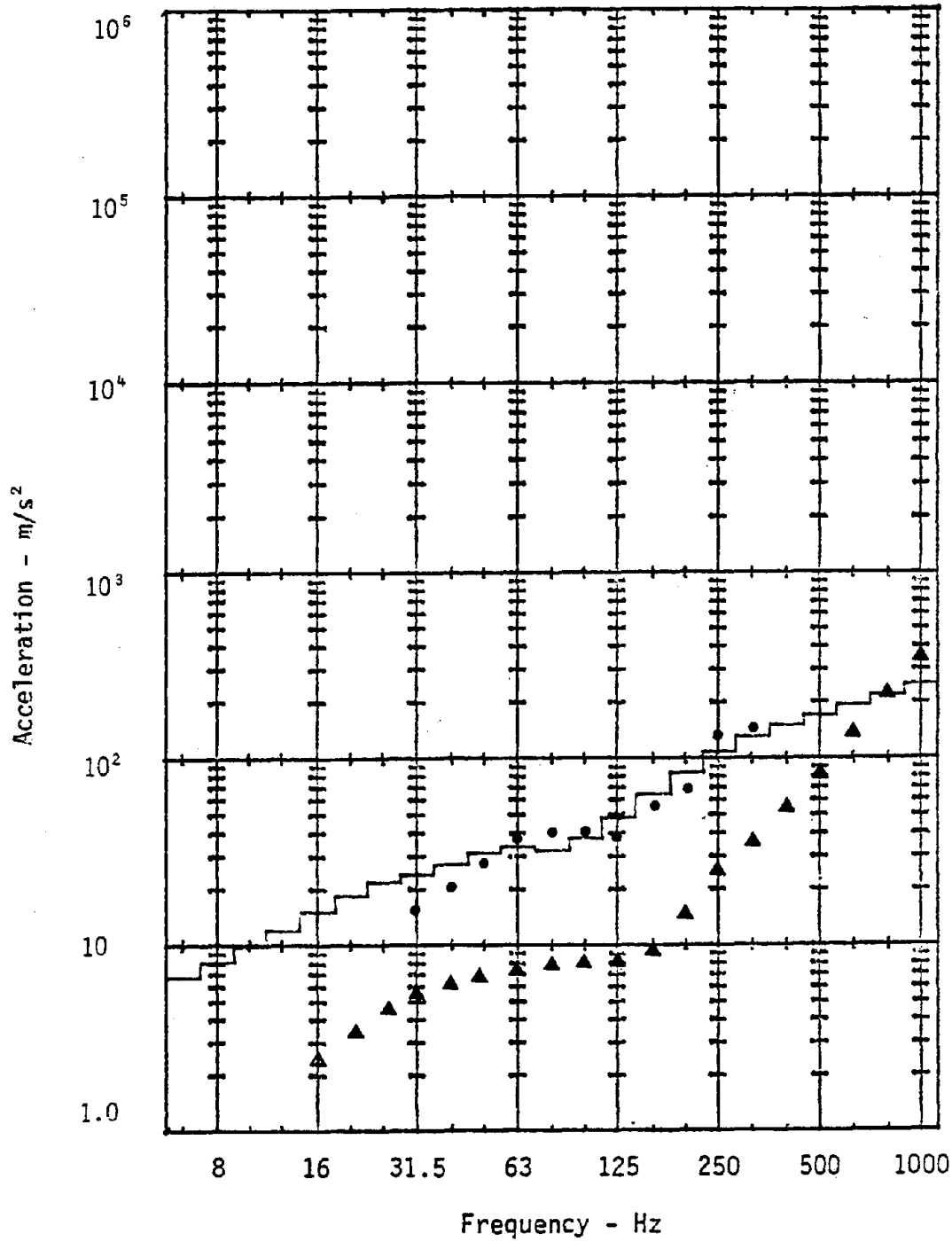

Figure 28. RMS acceleration levels which result in work per unit time equal to 1.0 J/s at each center frequency (3.8 cm diameter handle, X-direction). Compared to equal sensation data by Reynolds (•) and Suggs and Mishoe (▲).

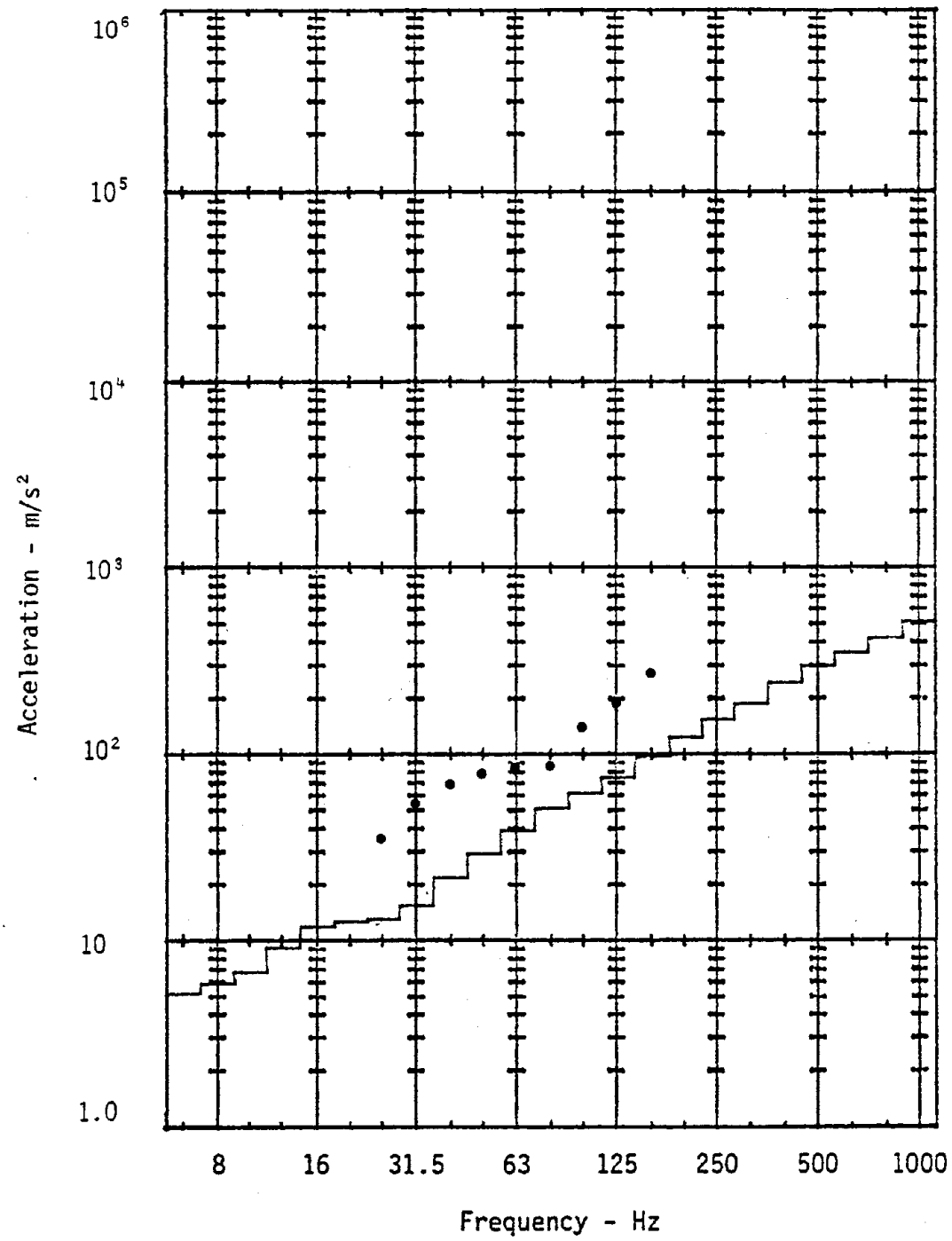

Figure 29. RMS acceleration levels which result in work per unit time equal to 1.0 J/s at each center frequency. 3.8 cm diameter handle, Y-direction. Compared to equal sensation data by Reynolds (•).

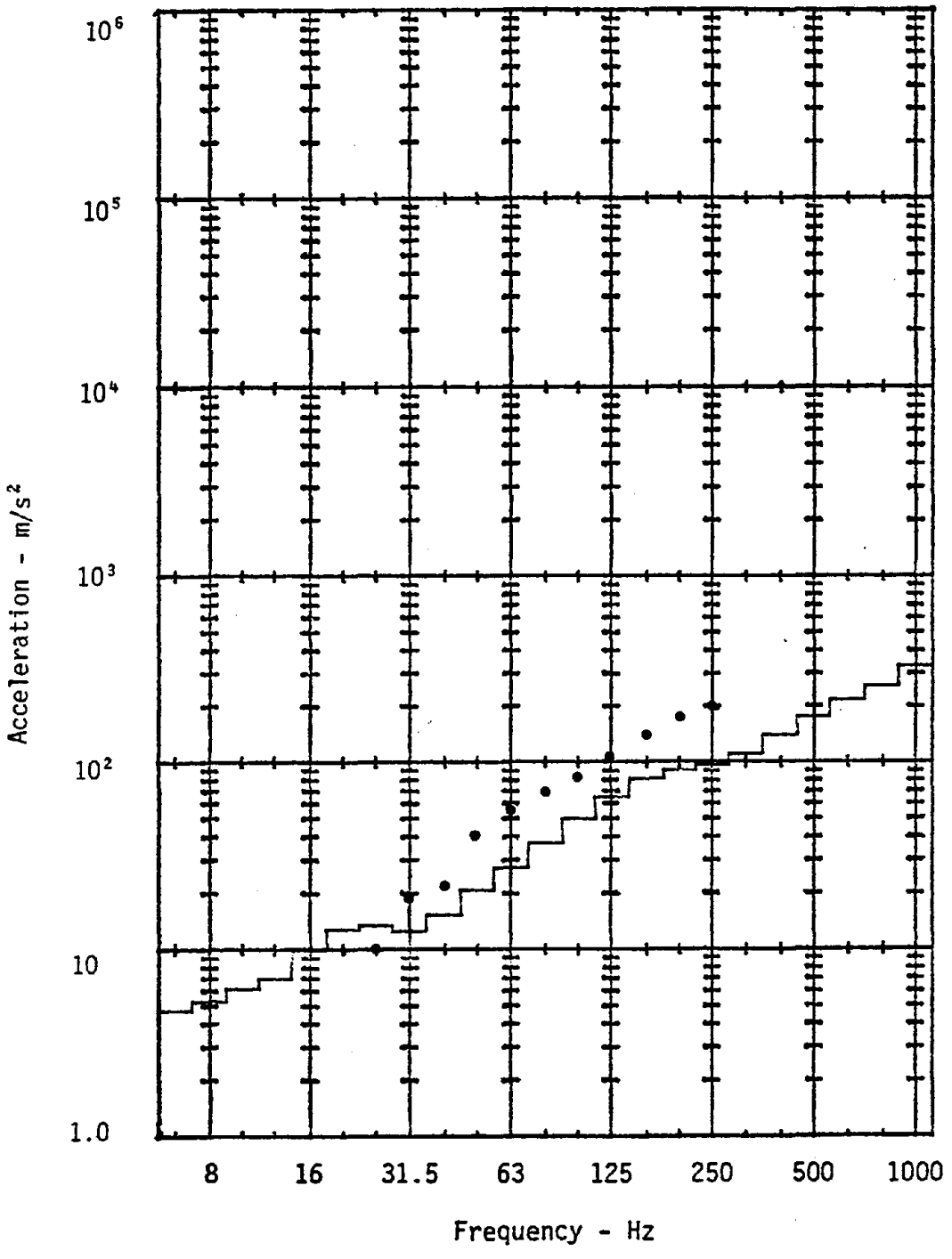

Figure 30. RMS acceleration levels which result in work per unit time equal to 1.0 J/s at each center frequency. 3.8 cm diameter handle, Z-direction. Compared to equal sensation data by Reynolds (•).

APPENDIX A

CALCULATOR PROGRAM LISTINGS

AND

PROGRAM CHRONOLOGIES DATA FILE

Appendix A: Calculator Program Listings and Program Chronologies data file.

A-1 X/F Digitization Program

The frequency, X/F and phase analog data were recorded on FM tape. Calibration data was recorded prior to each day's testing. Approximately 30 seconds of data was recorded for each of the following conditions: ω = 5Hz, X/F for .429 lb_m reference mass at 5 HZ, ϕ = 0; ω = 151 Hz, X/F for .429 lb_m reference mass at 151 Hz, ϕ 180°; and ω = 1000 Hz, X/F for .429 lb_m reference mass at 1000 Hz, ϕ = 180°. The A/D numbers for these values may be printed from the tape using this program if the following changes are made:

1. Add "PRT RX" to the end of lines 34 and 35.

2. Substitute "SPC 1; GTO 26" for line 46.

With these modifications the program will print out frequency, X/F and phase A/D numbers when the sequence "GTO 26; RUN PROGRAM" is keyed into the calculator. Representative A/D numbers must be input into the digitization program so that scale factors can be calculated for use during data play back.

Along with the other calibration data, a calibration sweep was recorded at the beginning of each test day. The calibration sweep provides values of X/F for the .429 lb_m reference mass at frequencies from 5 Hz to 1000 Hz. Before any hand-arm data was digitized, the A/D numbers chosen for data reduction were verified by digitizing the calibration sweep. The results were plotted using the spline function program and compared with the theoretical X/F versus frequency plot for a .429 lb_m mass.

Program Chronology

STEP	DISPLAY	INSTRUCTIONS
1		Enter program
2		Press "END; RUN PROGRAM." Prints "CAL 5 HZ, 0 PHASE."
3	FREQ	Enter A/D number for 5 Hz Press "RUN PROGRAM." Prints A/D number.
4	X/F	Enter A/D number for X/F at 5 Hz Press "RUN PROGRAM" Prints A/D number

STEP	DISPLAY	INSTRUCTIONS
5	PHASE	Enter A/D number for 0° phase. Press "RUN PROGRAM" Prints A/D number "1000 HZ; 180° PHASE"
6	FREQ	Enter A/D number for 1000 Hz Press "RUN PROGRAM" Prints A/D number
7	X/F	Enter A/D number for X/F at 1000 Hz Press "RUN PROGRAM" Prints A/D number
8	PHASE	Enter A/D number for 180° phase Press "RUN PROGRAM". Prints A/D number.
9	START	Begin tape playback. When frequency begins to increase Press "RUN PROGRAM".
10	FILE NUMBER	Enter the cassette tape file number to be used for data storage. Records data on cassette tape. Prints file number.
11	START	Repeat steps 9 and 10

X/F Digitization Program Listing

```
0:
FXD 0;0→R510;
SPC 2;PRT "CAL
      ";500→X⊢
1:
PRT "5 HZ,0 PHAS
E";ENT "FREQ",RX
;PRT RX;X+1→X;1+
R510→R510;GTO +2
⊢
2:
PRT "1000 HZ,180
 PHASE";ENT "FRE
Q",RX;PRT RX;X+1
→X;1+R510→R510⊢
3:
ENT "X/F",RX;
PRT RX;X+1→X⊢
4:
ENT "PHASE",RX;
PRT RX;X+1→X;IF
R510=1;GTO -2⊢
5:
6→X;0→A;0→R1000;
10→C;STP ;DSP "S
TART"⊢
6:
6→X⊢
7:
FXD 0;CMD "?U&",
"H1AJ","5F"⊢
8:
RDB 13→R0;RDB 13
→R1⊢
9:
FXD 0;CMD "?U&",
"H2AJ","5F"⊢
10:
RDB 13→R2;RDB 13
→R3⊢
11:
FXD 0;CMD "?U&",
"H4AJ","5F"⊢
12:
RDB 13→R4;RDB 13
→R5⊢
13:
0→A;1→B⊢
14:
IF RA>3;(255-RA)
*256+256-RB→RX;R
X*-1→RX;DSP RX⊢
15:
IF RA≤3;RA*256+R
B→RX;DSP RX⊢
16:
A+2→A;B+2→B;X+1→
X⊢
17:
IF A=6;GTO +2⊢
18:
GTO -4⊢
19:
6→X;FLT 5;0→Z⊢
20:
(RX-R500)((LOG 1
000-LOG 5)/(R503
-R500))+LOG 5→RC
⊢
21:
IF RC>2.5;GTO +5
⊢
22:
X+1→X;C+1→C⊢
23:
(RX-R504)(4.6020
59990/(R501-R504
))+LOG 2.2801E-5
→RC;X+1→X;C+1→C⊢
24:
(RX-R502)(180/(R
505-R502))→RC;X+
1→X;C+1→C⊢
25:
GTO 6⊢
26:
6→X⊢
```

```
27:
FXD 0;CMD "?U&",
"H1AJ","5F"⊢
28:
RDB 13→R0;RDB 13
→R1⊢
29:
FXD 0;CMD "?U&",
"H2AJ","5F"⊢
30:
RDB 13→R2;RDB 13
→R3⊢
31:
FXD 0;CMD "?U&",
"H4AJ","5F"⊢
32:
RDB 13→R4;RDB 13
→R5⊢
33:
0→A;1→B⊢
34:
IF RA>3;((255-RA
)*256+256-RB)*-1
→RX⊢
35:
IF RA≤3;RA*256+R
B→RX⊢
36:
A+2→A;B+2→B;X+1→
X⊢
37:
IF A=6;GTO +2⊢
38:
GTO -4⊢
39:
6→X;FLT 5;0→Z⊢
40:
(RX-R500)((LOG 1
000-LOG 5)/(R503
-R500))+LOG 5→RC
⊢
41:
IF RC-R(C-3)≤.00
1;GTO +5⊢
42:
X+1→X;C+1→C⊢
43:
(RX-R504)(4.6020
5999/(R501-R504)
)+LOG 2.2801E-5→
RC;X+1→X;C+1→C⊢
44:
(RX-R502)(180/(R
505-R502))→RC;X+
1→X;C+1→C⊢
45:
GTO -19⊢
46:
ENT "FILE NUMBER
",Y⊢
47:
RCF Y;R10;R(C-1)
;FXD 2;SPC 2;
PRT Y;10↑R10;10↑
R(C-3)⊢
48:
GTO 5⊢
49:
END ⊢
R1286
```

A-2 Spline Funtion Interpolation and Plotting Program

The spline function program interpolates the digitized X/F and phase data, the results and determines the values of X/F and phase at 1/3 octave band center frequencies.

STEP	DISPLAY	INSTRUCTIONS
1		Load program in calculator. Load X/F DIGITIZATION DATA tape in cassette deck. Install paper in vy plotter and set limits for X/F plot. Press "RUN PROGRAM".
2	FILE	Enter data file number Press "RUN PROGRAM". Prints file number. Reads data file, and plots X/F versus frequency.
3	STORAGE TAPES	Load 1/3 octave band data storage tape in cassette deck. Press "RUN PROGRAM".
4	FILE NUMBER	Enter 1/3 octave band data storage file number Press "RUN PROGRAM". Prints storage file number, then lists 1/3 octave band X/F levels. Change xy plotter limits to those for phase versus frequency plots. Press "RUN PROGRAM".
6	RAM DATA TAPE	Load X/F digitization cassette in tape deck. Press "RUN PROGRAM". Repeats steps 2 through 5 for phase.

Spline Function Interpolation and Plotting Program Listing

```
0:
ENT "FILE ",R752
;FXD 3;PRT "FILE
 NO.",R752⊢
1:
0→R750;801→R751;
-5→R753;-1→R754;
SPC 3⊢
2:
1224→R1225;1000→
R1201;800→R1202;
630→R1203;500→R1
204;400→R1205⊢
3:
315→R1206;250→R1
207;200→R1208;16
0→R1209;125→R121
0;100→R1211⊢
4:
80→R1212;63→R121
3;50→R1214;40→R1
215;31.5→R1216;2
5→R1217⊢
5:
20→R1218;16→R121
9;12.5→R1220;10→
R1221;8→R1222;6.
3→R1223⊢
6:
1201→C⊢
7:
LOG RC→RC;C+1→C;
IF C=1224;GTO +2
⊢
8:
GTO -1⊢
9:
FDF R752;IDF A,B
,C,Z;B/3→R1200⊢
10:
LDF R752⊢
11:
0→Y⊢
12:
RY→R(Y+800)⊢
13:
IF Y=3B-1;GTO +2
⊢
14:
Y+1→Y;GTO -2⊢
15:
.01→R0;CFG 13;
IF R(3B+799)≤3;3
.01→R(B+797)⊢
16:
800→Y;0→A⊢
17:
RY→R(1+A);IF Y=8
00+3B-3;GTO +2⊢
18:
Y+3→Y;A+2→A;GTO
-1⊢
19:
0→A⊢
20:
RR751→R(2+A);IF
R751>800+3B-3;
GTO +2⊢
21:
R751+3→R751;A+2→
A;GTO -1⊢
22:
R1200→A;0→R(4A+1
)→R(5A)→B;4(2-r3
)→C⊢
23:
(R(2(B+1→B)+2)-R
(2B))/(R(2B+1)-R
(2B-1)→R((3A+B→Z
)-A))→RZ;JMP B>1
⊢
24:
(2(RZ-R(Z-1))/(R
(Z-1-A)+R(Z-A))→
R(Z+A))3/2→R(Z+2
A)⊢
```

```
25:
IF A-1>B;GTO -2⊢
26:
0→X;2→B⊢
27:
C((((R((4A+B→Z)+
1)→Y)-R(Z-1))/(1
+R(Z-2A)/R(Z-2A-
1))-Y)/2-RZ+R(Z+
A))→Y⊢
28:
IF ⌐(YY)>X;⌐(YY)
→X⊢
29:
RZ+Y→RZ;IF (B+1→
B)≠A;GTO -2⊢
30:
IF R0≤X;GTO -4⊢
31:
0→C;1→B⊢
32:
(R((4A+B→Z)-2A)→
Y)(R(2B)+R(2B+2)
)/2-YYY(RZ+R(Z+1
))/24+C→C;JMP A=
(B+1→B)⊢
33:
1→B⊢
34:
(R((4A+B→Z)+1)-R
Z)/R(Z-2A→Z)→RZ;
JMP (B+1→B)=A⊢
35:
CFG 1;CFG 13;
LOG 5→X⊢
36:
3→C⊢
37:
(C-X)/200→R0⊢
38:
SCL X,C,R753,R75
4⊢
39:
R(1→B)→X⊢
40:
GSB +6⊢
41:
PLT X,Y;IF (X+R0
→X)≤R(2A-1);JMP
-1⊢
42:
PEN ⊢
43:
RR1225→X;700→R75
0⊢
44:
SFG 1→B;R1225-1→
R1225;R750+1→R75
0;RR1225→X;GSB +
2⊢
45:
JMP -1⊢
46:
IF B>A;RET ⊢
47:
GTO +1;IF A=B;
GTO +6;IF (X-R(2
A-1)→Z)=0;JMP 2⊢
48:
IF (0>(X-R(2B-1)
→Y))+(0≤(X-R(2B+
1)→Z));B+1→B;
JMP -2⊢
49:
R(4A+B)+YR(2A+B)
→C;IF FLG 1;FXD
3;PRT 10↑X⊢
50:
(R(4A+B)+R(4A+B+
1)+C)/6→C⊢
51:
R(2B)+YR(3A+B)+Y
ZC→Y⊢
52:
IF FLG 1;FXD 3;
PRT Y;SPC 1;Y→RR
750⊢
53:
RET ;IF R750>725
;GTO +1⊢
```

```
54:
STP ;DSP "STORAG
E TAPE"⊢
55:
ENT "FILE NUMBER
",X⊢
56:
PRT "IN FILE
    ",X;SPC 2;
RCF X,R701,R723⊢
57:
IF R751=1;GTO +3
⊢
58:
STP ;DSP "CHANGE
 LIMITS"⊢
59:
STP ;DSP "RAW DA
TA TAPE"⊢
60:
802→R751;0→R750;
0→R753;180→R754;
GTO 2;⊢
61:
END ⊢
R1226
```

A-3 X/F Sum and Sum of Squares Program

This program is used to obtain the sum and the sum of the squares of X/F and phase values at each 1/3 octave band center frequency for several sequential data files. Data is normally entered one subject at a time (12 data files).

Program Chronology

STEP	DISPLAY	INSTRUCTIONS
1		Load program in calculator. Load 1/3 octave band data tape in cassette deck. Press "RUN PROGRAM".
		Press "RUN PROGRAM". Prints first and last file numbers. Program reads in X/F and phase data files sequentially, printing out the direction and file number each time. After the last file, the program prints the number of subjects surveyed at that point.
4	STORAGE FILE	Enter storage tape file number. Press "RUN PROGRAM". Program stores data, then prints file number.

X/F Sum and Sum of Squares Program Listing

```
0:
FLT 3;ENT "FIRST
 FILE",X,"LAST F
ILE",Y;PRT "FIRS
T FILE",X,"LAST
FILE",Y;SPC 2⊢
1:
0→A;R0+1→R0⊢
2:
LDF X,R1;0→C;A+1
→A;23A→B⊢
3:
IF A≠1;GTO +2⊢
4:
SPC 1;PRT "LX X/
F",X;GTO 16⊢
5:
IF A≠3;GTO +2⊢
6:
SPC 1;PRT "LY X/
F",X;GTO 19⊢
7:
IF A≠5;GTO +2⊢
8:
SPC 1;PRT "LZ X/
F",X;GTO 19⊢
9:
IF A≠7;GTO +2⊢
10:
SPC 1;PRT "SX X/
F",X;GTO 19⊢
11:
IF A≠9;GTO +2⊢
12:
SPC 1;PRT "SY X/
F",X;GTO 19⊢
13:
IF A≠11;GTO +2⊢
14:
SPC 1;PRT "SZ X/
F",X;GTO 19⊢
15:
PRT "PHASE",X⊢
16:
B+1→B;C+1→C;RB+R
C→RB;R(B+276)+RC
↑2→R(B+276)⊢
17:
IF C≠23;GTO -1⊢
18:
GTO +3⊢
19:
B+1→B;C+1→C;LOG
(10↑RB+10↑RC)→RB
;LOG (10↑R(B+276
)+10↑RC↑2)→R(B+2
76)⊢
20:
IF C≠23;GTO -1⊢
21:
X+1→X;IF X>Y;
GTO +3⊢
22:
IF A=11;GTO 1⊢
23:
GTO 2⊢
24:
PRT "R0",R0;ENT
"STORAGE FILE",C
⊢
25:
RCF C,R0,R575;
PRT "STORAGE FIL
E",C⊢
26:
END ⊢
R1362
```

A-4 X/F Average and Confidence Limits Program

This program uses the sum and sum of squares data to find the average and confidence limits for X/F and phase at each 1/3 octave band center frequency.

Program Chronology

STEP	DISPLAY	INSTRUCTIONS
1		Load program and sum and sum of squares data tape. Press "END: RUN PROGRAM".
2	FILE	Enter file number. Press "RUN PROGRAM". Program prints file number. Reads data file, then prints the number of degrees of freedom.
3	COEFF	Enter coefficient, C, given in equation (42). Program calculates average and confidence limits and prints results of X/F or phase in one direction.
4	AVG FILE	Load storage file number for direction just printed. Press "RUN PROGRAM". Stores data in cassette file. Repeats steps 3 and 4 until all X/F and phase data is reduced.

X/F Average and Confidence Limits Program Listing

```
0:
FLT 3;ENT "FILE"
,X;PRT "FILE",X;
0→A⊢
1:
LDF X,R0;SPC 2;
PRT "DOF",R0;
ENT "COEFF, C",C
;PRT "COEFF, C",
C⊢
2:
0→Y;A+1→A⊢
3:
IF A≠1;GTO +2⊢
4:
SPC 1;PRT "LX X/
F",X;GTO 21⊢
5:
IF A≠3;GTO +2⊢
6:
SPC 1;PRT "LY X/
F",X;GTO 21⊢
7:
IF A≠5;GTO +2⊢
8:
SPC 1;PRT "LZ X/
F",X;GTO 21⊢
9:
IF A≠7;GTO +2⊢
10:
SPC 1;PRT "SX X/
F",X;GTO 21⊢
11:
IF A≠9;GTO +2⊢
12:
SPC 1;PRT "SY X/
F",X;GTO 21⊢
13:
IF A≠11;GTO +2⊢
14:
SPC 1;PRT "SZ X/
F",X;GTO 21⊢
15:
PRT "PHASE",X⊢
16:
Y+1→Y;R(23A+Y)/R
0→RY⊢
17:
C(R(23A+Y+276)-R
0RY↑2)↑.5→R(Y+57
5)⊢
18:
SPC 1;PRT RY,R(Y
+575)⊢
19:
IF Y≠23;GTO -3⊢
20:
GTO +5⊢
21:
Y+1→Y;LOG (10↑R(
23A+Y)/R0)→RY⊢
22:
LOG (C(10↑R(23A+
Y+276)-R(0)10↑RY
↑2)↑.5)→R(Y+575)
⊢
23:
SPC 1;PRT RY,R(Y
+575)⊢
24:
IF Y≠23;GTO -3⊢
25:
ENT "AVG FILE",B
;PRT "AVG FILE",
B⊢
26:
RCF B,R1,R23⊢
27:
ENT "CONF LIMIT
FILE",B;RCF B,R5
76,R598;PRT "CON
F LIMIT FILE",B⊢
28:
IF A≠12;GTO 2⊢
29:
END ⊢
R1355
```

A-5 X/F Plotting File Assembly Program

This program uses data from the average and confidence limit program to assemble data files in a format which can be accepted by the spline function program.

Program Chronology

STEP	DISPLAY	INSTRUCTIONS
1		Load Program. Load average and confidence limits cassette tapes.
2	X/F AVG FILE	Enter file number Press "RUN PROGRAM". Program prints file number and reads in data
3	CONF LIMIT	Enter confidence limit file number. Press "RUN PROGRAM". Program prints file number and reads in data. Prints direction.
4	AVG FILE	Enter storage file number for average plotting file. Press "RUN PROGRAM". Program prints file number and records data on cassette tape.
5	HIGH FILE	Enter storage file number for high confidence limit plotting file. Press "RUN PROGRAM". Program prints file number and records data on cassette tape.
6	LOW FILE	Enter file number for low confidence limit plotting file. Press "RUN PROGRAM". Program prints file number and records data on cassette tape.
7		Repeat steps 4 through 6 for all directions.

X/F Plotting File Assembly Program Listing

```
0:
FLT 5;0→A⊢
1:
A+1→A;6.3→R0;8.0
→R1;10→R2;12.5→R
3;16→R4;20→R5⊢
2:
25→R6;31.5→R7;40
→R8;50→R9;63→R10
;80→R11⊢
3:
100→R12;125→R13;
160→R14;200→R15;
250→R16;315→R17⊢
4:
400→R18;500→R19;
630→R20;800→R21;
1000→R22;43→X;-1
→Y⊢
5:
X+3→X;Y+1→Y;LOG
RY→RX→R(X+69)→R(
X+138)⊢
6:
IF Y≠22;GTO -1⊢
7:
SPC 2;ENT "X/F A
VG FILE",B;PRT "
X/F AVG FILE",B;
LDF B,R0⊢
8:
ENT "CONF LIMIT
FILE",B;PRT "CON
F LIMIT FILE",B;
LDF B,R23;44→X;-
1→Y⊢
9:
X+3→X;Y+1→Y;LOG
(10↑RY+10↑R(Y+23
))→R(X+69);LOG (
10↑RY-10↑R(Y+23)
)→R(X+138)⊢
10:
RY→RX;IF Y≠22;
GTO -1⊢
11:
ENT "PHASE AVG F
ILE",B;PRT "PHAS
E AVG FILE",B;
LDF B,R0⊢
12:
ENT "CONF LIMIT
FILE",B;PRT "CON
F LIMIT FILE",B;
LDF B,R23;45→X;-
1→Y⊢
13:
X+3→X;Y+1→Y;RY→R
X;RY+R(Y+23)→R(X
+69);RY-R(Y+23)→
R(X+138)⊢
14:
IF Y≠22;GTO -1⊢
15:
IF A≠1;GTO +2⊢
16:
SPC 2;PRT "LG X"
;GTO +10⊢
17:
IF A≠2;GTO +2⊢
18:
SPC 2;PRT "LG Y"
;GTO +8⊢
19:
IF A≠3;GTO +2⊢
20:
SPC 2;PRT "LG Z"
;GTO +6⊢
21:
IF A≠4;GTO +2⊢
22:
SPC 2;PRT "SM X"
;GTO +4⊢
```

```
23:
IF A≠5;GTO +2⊢
24:
SPC 2;PRT "SM Y"
;GTO +2⊢
25:
SPC 2;PRT "SM Z"
⊢
26:
ENT "AVG FILE",C
;PRT "AVG FILE",
C;RCF C,R46,R114
⊢
27:
ENT "HIGH FILE",
C;PRT "HIGH FILE
",C;RCF C,R115,R
183⊢
28:
ENT "LOW FILE",C
;PRT "LOW FILE",
C;RCF C,R184,R25
2⊢
29:
IF A≠6;GTO 1⊢
30:
END ⊢
R1311
```

A-6 Acceleration Digitization Program

The acceleration digitization program is used to digitize the 1/3 octave band acceleration levels which are output from the General Radio Corporation 1/3 octave band analysis system. To permit longer integration times during data playback from the FM tape recorder, the 6.3 Hz to 1000 Hz frequency range is analyzed in two parts. The first six center frequencies, 6.3 Hz through 20 Hz, are obtained while playing the FM tape recorder at 15 inches per second tape speed. Since the analog data was originally recorded at 3 3/4 inches per second, the frequencies between 6.3 Hz and 20 Hz will be read as 25 Hz through 80 Hz in the spectrum analyzer. The integration time used is 4 seconds. The FM tape is then rewound to the same starting point and the final 17 center frequencies are analyzed at 3 3/4 inches per second tape speed. The integration time used for the second playback is 16 seconds.

The data is stored on cassette tapes.

Program Chronology

STEP	DISPLAY	INSTRUCTIONS
1		Load program into calculator. Press "END; RUN PROGRAM".
2	MAX DB	Enter 120. Press "RUN PROGRAM".
3	MIN DB	Enter 60. Press "RUN PROGRAM".
4	CAL DB	Play calibration signal into 1/3 octave band analyzer and obtain db level. Enter db value into calculator and Press "RUN PROGRAM".
5	CAL G	Enter calibration signal acceleration value in g's. Press "RUN PROGRAM". Program prints values for maximum db, minimum db, calibration db, and calibration acceleration.
6	LOAD MAX DB	With the maximum band level displayed on the analyzer, Press "RUN PROGRAM". Program prints A/D number for maximum band level.

STEP	DISPLAY	INSTRUCTIONS
7	LOAD MIN DB	With the minimum band level displayed on the analyzer, Press "RUN PROGRAM". Program prints A.D number for minimum band level.
8	READY	Obtain the acceleration levels for the first six center frequencies using 4 second intergration time on the analyzer and 15 inches per second tape speed on the FM tape recorder. Turn analyzer display rate to 1/band/second. Press "RUN PROGRAM". When first db level is displayed on analyzer. Program prints first six db band levels as they are read from the analyzer.
9	READY	Repeat step 8 for the center frequencies from 25 Hz through 1000 Hz using 16 seconds as the integration time and 3 3/4 inches per second tape speed. Program prints db band levels as they are read.
10	FILE NUMBER	Enter cassette tape storage file number. Press "RUN PROGRAM".
11	TAPE NUMBER	Enter tape designator if more than one cassette tape has been used. Press "RUN PROGRAM". Program prints file numbers and tape number, then records band levels in g's on the cassette tape.

Acceleration Digitization Program Listing

```
0:
60→Z;FXD 0;ENT "
MAX DB",C,"MIN D
B",X,"CAL SIGNAL
, DB",R102⊢
1:
ENT "CAL SIGNAL,
 G,S",R103⊢
2:
PRT "MAX DB",C;
SPC 1;PRT "MIN D
B",X;SPC 1⊢
3:
PRT "CAL DB",R10
2;SPC 1;PRT "CAL
 G",R103;SPC 1⊢
4:
R(103)10↑(-R102/
20)→R100⊢
5:
STP ;DSP "LOAD M
AX DB"⊢
6:
FXD 0;CMD "?U&",
"H1AJ","5F"⊢
7:
RDB 13→A;RDB 13→
B⊢
8:
IF A>3;(255-A)*2
56+256-B→RZ;-RZ→
RZ;PRT RZ⊢
9:
IF A≤3;256A+B→RZ
;PRT RZ⊢
10:
IF Z=61;JMP 3⊢
11:
Z+1→Z;STP ;DSP "
LOAD MIN DB"⊢
12:
GTO -6⊢
13:
FXD 3;(C-X)/(R60
-R61)→R62;SPC 1;
1→Z⊢
14:
STP ;PRT "BAND L
EVELS";SPC 1;
DSP "READY"⊢
15:
FXD 0;CMD "?U&",
"H1AJ","5F"⊢
16:
RDB 13→A;RDB 13→
B⊢
17:
IF A>3;(255-A)*2
56+256-B→RZ;-RZ→
RZ;PRT RZ⊢
18:
IF A≤3;256A+B→RZ
;PRT RZ⊢
19:
FXD 3;R62(RZ-R60
)+C→RZ;SPC 1⊢
20:
R300+1→R300;R301
+1→R301;PRT RZ;
DSP RZ;R(100)10↑
(RZ/20)→RZ⊢
21:
Z+1→Z;IF Z=7;
GTO -7⊢
22:
IF Z=25;GTO +2⊢
23:
GTO -8⊢
24:
ENT "FILE NUMBER
",Y,"TAPE NUMBER
",R1000⊢
25:
PRT "FILE NUMBER
",Y;SPC 1;PRT "T
APE NO.",R1000;
SPC 8⊢
26:
RCF Y,R1,R24⊢
27:
END ⊢
R1352
```

A-7 Acceleration Plotting Program

This program plots the 1/3 octave band acceleration levels from the cassette tape data files generated by the acceleration digitization program.

Program Chronology

STEP	DISPLAY	INSTRUCTIONS
1		Load program into calculator. Load acceleration data cassette in cassette deck. Press "RUN PROGRAM".
2	FILE	Enter the number of the data file to be plotted. Press "RUN PROGRAM". Program prints file number, and plots 1/3 octave band acceleration levels.

Acceleration Plotting Program Listing

```
0:
ENT "FILE",X;
SPC 2;PRT "FILE"
,X⊢
1:
LDF X,R0⊢
2:
6.3→R50;8→R51;10
→R52;12.5→R53;16
→R54;20→R55⊢
3:
25→R56;31.5→R57;
40→R58;50→R59;63
→R60;80→R61⊢
4:
100→R62;125→R63;
160→R64;200→R65;
250→R66;315→R67⊢
5:
400→R68;500→R69;
630→R70;800→R71;
1000→R72⊢
6:
0→X;LOG 2/6→B⊢
7:
SCL LOG 6.3-B,
LOG 1250+B,LOG
03,2⊢
8:
9.81RX→A;IF .03>
A;.03→A⊢
9:
PLT LOG R(50+X)-
B,LOG A;PLT LOG
R(50+X)+B,LOG A⊢
10:
X+1→X;IF X≠23;
GTO -2⊢
11:
PEN ⊢
12:
END ⊢
R1394
```

A-8 Instantaneous Energy Calculation Program

This program uses cassette data files for displacement mobility of the hand-arm system and 1/3 octave band acceleration levels to calculate the 1/3 octave band levels for incident, stored and dissipated instantaneous energy. The program can also be used to obtain the average of two acceleration files. The results are stored on cassette tapes.

Program Chronology

Step	Display	Instructions
1		Load program into calculator. Press "RUN PROGRAM". Program prints heading.
2	X/F DATA FILE	Load cassette containing X/F files obtained from X/F plotting file assembly program into cassette deck Enter file number. Press "RUN PROGRAM". Program prints file number and reads X/F file into memory.
3	1ST ACC FILE	Load cassette containing acceleration data files obtained from acceleration digitization program into cassette deck. Enter file number of first data file to be averaged. Press "RUN PROGRAM". Program prints file number and reads data into memory.
4	2ND ACC FILE	Enter file number of second accelera-acceleration file to be averaged. Enter same number as in step 3 if only one acceleration file is to be used. Press "RUN PROGRAM". Program prints file number and reads data into memory. Program prints out frequency (Hz), and stored, dissipated and incident energy (J), in that order, for each center frequency.
5	STORAGE TAPE	Install cassette for energy data storage. Press "RUN PROGRAM".

STEP	DISPLAY	INSTRUCTIONS
6	E FILE	Enter energy storage file number. Press "RUN PROGRAM". Program prints file number and stores energy data in cassette file.
7	ACC AVG STORE IN	Enter average acceleration data storage file number. (Omit this step is no acceleration average is desired.) Press "RUN PROGRAM". Program prints file number and stores data in cassette file. Program returns to step 2.

Instantaneous Energy Calculation Program Listing

```
0:
FLT 8;0→A→C;-1→X
⊢
1:
SPC 2;PRT "FREQ.
.....HERTZ","ES
.....N-M",
"ED.....N-
M"⊢
2:
PRT "E.....
..N-M"⊢
3:
ENT "X/F DATA FI
LE",Y;SPC 2;PRT
"X/F DATA FILE",
Y;LDF Y,R0⊢
4:
ENT "1ST ACC FIL
E",B;SPC 1;PRT "
1ST ACC FILE",B;
LDF B,R69⊢
5:
ENT "2ND ACC FIL
E",Y;SPC 1;PRT "
2ND ACC FILE",Y;
LDF Y,R200⊢
6:
A+1→A⊢
7:
IF A≠1;GTO +2⊢
8:
SPC 2;PRT "RH X"
;GTO +10⊢
9:
IF A≠2;GTO +2⊢
10:
SPC 2;PRT "RH Y"
;GTO +8⊢
11:
IF A≠3;GTO +2⊢
12:
SPC 2;PRT "RH Z"
;GTO +6⊢
13:
IF A≠4;GTO +2⊢
14:
SPC 2;PRT "LH X"
;GTO +4⊢
15:
IF A≠5;GTO +2⊢
16:
SPC 2;PRT "LH Y"
;GTO +2⊢
17:
SPC 2;PRT "LH Z"
⊢
18:
X+1→X;(R(69+X)+R
(200+X))/2→C→R(3
00+X)⊢
19:
16882.7991C↑2/(2
*10↑R(3X))↑(4)10
↑R(3X+1)→R(102+3
X)⊢
20:
R(102+3X)COS R(3
X+2)→R(100+3X);R
(102+3X)SIN R(3X
+2)→R(101+3X)⊢
21:
SPC 1;PRT 10↑R(3
X),R(100+3X),R(1
01+3X),R(102+3X)
⊢
22:
IF X≠22;GTO 18⊢
```

```
23:
STP ;DSP "STORAG
E TAPE"⊢
24:
ENT "E FILE",Y;
PRT "E IN FILE",
Y;RCF Y,R100,R16
8⊢
25:
ENT "ACC AVG STO
RE IN",Y;PRT "AC
C AVG IN",Y;RCF
Y,R300,R322⊢
26:
0→C;-1→X;IF A≠6;
GTO 3⊢
27:
END ⊢
R1338
```

A-9 Energy Plotting Program

This program plots the 1/3 octave band levels of the stored, dissipated and incident instantaneous energy using the cassette data files created by the instantaneous energy using the cassette data files created by the instantaneous energy calculation program.

Program Chronology

STEP	DISPLAY	INSTRUCTIONS
1		Load a program into calculator. Press "END, RUN PROGRAM".
2	FILE	Enter the data file number. Press "RUN PROGRAM". Program prints file number.
3	MAX ENERGY	Enter the maximum value on the energy axis (J). Press "RUN PROGRAM". Program prints maximum energy value.
4	MIN ENERGY	Enter the minimum value on the energy axis (J). Press "RUN PROGRAM". Program prints minimum energy value, then plots stored, dissipated and incident energy in that order.

Energy Plotting Program Listing

```
0:
11.7→R96;16.7→R9
7;ENT "FILE",X;
SPC 2;PRT "FILE"
,X;LDF X,R0⊢
1:
ENT "MAX ENERGY"
,R93;PRT "MAX EN
ERGY",R93⊢
2:
ENT "MIN ENERGY"
,R94;PRT "MIN EN
ERGY",R94⊢
3:
6.3→R70;8→R71;10
→R72;12.5→R73;16
→R74;20→R75⊢
4:
25→R76;31.5→R77;
40→R78;50→R79;63
→R80;80→R81⊢
5:
100→R82;125→R83;
160→R84;200→R85;
250→R86;315→R87⊢
6:
400→R88;500→R89;
630→R90;800→R91;
1000→R92;0→X⊢
7:
IF 0>RX;-RX→RX⊢
8:
X+1→X;IF X≠69;
GTO -1⊢
9:
LOG 2/6→R95;SCL
LOG 6.3-R95,LOG
1000+R95,LOG R94
,LOG R93⊢
10:
2→R98;0→A;0→X⊢
11:
.5(23(2R98-1)R97
/R96+1)→R99⊢
12:
LOG 2/3(2R98-1)→
R100⊢
13:
(LOG R93-LOG R94
)/(2R99-1)→R101⊢
14:
IF R94>R(3X+A);R
94→R(3X+A)⊢
15:
IF R94>R(3X+A+3)
;R94→R(3X+A+3)⊢
16:
1→B;LOG R(70+X)-
R95→R105;LOG R(3
X+A)→R107⊢
17:
R105+R100→R106⊢
18:
PLT R105,R107;
PLT R106,R107;
PEN ⊢
19:
1+B→B;R106+R100→
R105;IF B=R98;
GTO +2⊢
20:
GTO -3⊢
21:
LOG R(70+X)+R95→
R106;PLT R105,R1
07;PLT R106,R107
⊢
22:
IF X≠22;GTO +4⊢
23:
PEN ;0→X;A+1→A;4
→R98⊢
24:
IF A=2;GTO 35⊢
25:
GTO 11⊢
```

```
26:
LOG R(3X+A+3)-R1
07→R108⁞ABS (R10
8/2R101)→R115⊢
27:
INT R115→R109⁞
IF .5≤R115-R109⁞
R109+1→R109⊢
28:
IF R109≤1⁞GTO +6
⊢
29:
1→B⁞R108/(2R109-
1)→R110⊢
30:
R107+R110→R111⊢
31:
PLT R106,R107⁞
PLT R106,R111⁞
PEN ⊢
32:
R111+R110→R107⁞B
+1→B⁞IF B=R109⁞
GTO +2⊢
33:
GTO -3⊢
34:
PLT R106,R107⁞X+
1→X⁞GTO 15⊢
35:
IF R94>R(3X+2)⁞R
94→R(3X+2)⊢
36:
PLT LOG R(70+X)-
R95,LOG R(3X+2)⊢
37:
PLT LOG R(70+X)+
R95,LOG R(3X+2)⊢
38:
IF X=22⁞GTO +4⊢
39:
IF R94>R(3X+5)⁞R
94→R(3X+5)⊢
40:
PLT LOG R(70+X)+
R95,LOG R(3X+5)⊢
41:
X+1→X⁞GTO -5⊢
42:
END ⊢
R1278
```

A-10 Work per Unit Time Program

In this program, the total work per unit time for each tool is calculated from the dissipated instantaneous energy data which was stored on cassette tape using the instantaneous energy calculation program. The program is set-up to handle sequential data files.

Program Chronology

STEP	DISPLAY	INSTRUCTIONS
1		Load program into calculator. Press "END; RUN PROGRAM".
2	FIRST FILE	Enter file number of first data file in sequence. Press "RUN PROGRAM".
3	LAST FILE	Enter file number of last data file in sequence. Press "RUN PROGRAM". The program reads in the first data file, calculates the total work per unit time, then prints the file number and the total work per unit time (J). The program repeats the procedure for all data files lying between and including the first and last files listed above.

Work per Unit Time Program Listing

```
0:
FLT 8;SPC 2⊢
1:
6.3→R0;8→R1;10→R
2;12.5→R3;16→R4;
20→R5⊢
2:
25→R6;31.5→R7;40
→R8;50→R9;63→R10
;80→R11⊢
3:
100→R12;125→R13;
160→R14;200→R15;
250→R16;315→R17⊢
4:
400→R18;500→R19;
630→R20;800→R21;
1000→R22⊢
5:
ENT "FIRST FILE"
,X,"LAST FILE",Y
;PRT "FIRST FILE
",X,"LAST FILE",
Y;SPC 2⊢
6:
LDF X,R30;0→A;0→
R25;SPC 2;PRT "F
ILE",X⊢
7:
2πRAR(3A+31)+R25
→R25⊢
8:
A+1→A;IF A≠23;
GTO -1⊢
9:
PRT "ENERGY (N-M
/SEC)",R25⊢
10:
X+1→X;IF X≤Y;
GTO -4⊢
11:
END ⊢
R1388
```

A-11 Fourier Series Programs

Fourier series coefficients were calculated for chipping hammer acceleration time histories using two cases: the decaying exponential case, and the single cycle sinusoid.

The two programs listed here calculate and list the Fourier coefficients and phase angles for given values of the parameters discussed in section 4.2.3. The results are stored on cassette tapes. The program performs a 20 point plot of the acceleration time history based on the Calculated Fourier series. Decaying Exponential Case

Program Chronology

STEP	DISPLAY	INSTRUCTIONS
1		Load program into calculator. Press "RUN PROGRAM".
2	Y	Enter amplitude, Y (m/s^2), of the exponential function. Press "RUN PROGRAM".
3	A	Enter the time constant, a, of the exponential. Press "RUN PROGRAM". Program prints input values for Y and a.
4	T	Enter the time, T_1 (s), for one cycle. Press "RUN PROGRAM". Program prints the value of T_1 and a heading. The program then calculates and lists the values of $n\omega$, a_n, b_n, c_n, and $\theta = \tan^{-1}(as_n/b_n)$) until n is greater than 1000 Hz.
5	MIN X (TIME)	Enter minimum value on time axis for data plot. Press "RUN PROGRAM".
6	MAX X	Enter maximum value on time axis for data plot. Press "RUN PROGRAM".
7	MIN Y (ACC)	Enter minimum value on acceleration axis for data plot. Press "RUN PROGRAM".

STEP	DISPLAY	INSTRUCTIONS
8	MAX Y	Enter maximum value on acceleration axis for data plot. Press "RUN PROGRAM". Program plots 20 point acceleration time history for one cycle based on the calculated Fourier series.
9	FILE	Enter cassette file number for coefficient storage. Press "RUN PROGRAM". Program prints file number, then stores values of ω_n, c_n and θ on cassette tapes.

Single Cycle Sinusoid Case

Program Chronology

STEP	DISPLAY	INSTRUCTIONS
1		Load program into calculator. Press "RUN PROGRAM".
2	Y	Enter amplitude of sinusoid (m/s^2).
3	FREQ	Enter frequency of sinusoid in radians per second. Press "RUN PROGRAM". Program prints values of amplitude and frequency.
4	T1	Enter period of sinusoid (s). Press "RUN PROGRAM".
5	T	Enter period (s) between sinusoidal cycles. Press "RUN PROGRAM". From this point the program operation is the same as for the decaying exponential case.

Fourier Series Program Listing

Decaying Expontial Case

```
0:
FLT 5;0→X;TBL 2⊢
1:
ENT "Y",R0,"A",R
1;SPC 2;PRT "Y",
R0,"A",R1⊢
2:
ENT "T",R4;PRT "
T",R4;SPC 2⊢
3:
PRT "FREQ","AN",
"BN","CN"⊢
4:
PRT "PHASE";SPC
1;1000R4→R5⊢
5:
X+1→X;2πX/R4→R6;
R6/2π→R(17+3X)⊢
6:
17+3X+3→R14;R14+
1→R15⊢
7:
2R0R1(1-EXP (-R1
R4))/R4(R1R1+R6R
6)→RR14⊢
8:
4πXR0(1-EXP (-R1
R4))/R4R4(R1R1+R
6R6)→RR15⊢
9:
RR14RR14+RR15RR1
5→R(R15-3)⊢
10:
⌐R(R15-3)→R(R15-
3);IF RR15≠0;
GTO +5⊢
11:
IF RR14=0;PRT "U
NDEFINED";STP ⊢
12:
IF RR14>0;GTO +2
⊢
13:
3π/2→R(R15-2);
GTO +11⊢
14:
π/2→R(R15-2);
GTO +10⊢
15:
ATN (RR14/RR15)→
R(R15-2)⊢
16:
IF 0≤R(R15-2);
GTO +3⊢
17:
IF RR14≤0;GTO +7
⊢
18:
R(R15-2)+π→R(R15
-2);GTO +6⊢
19:
IF RR14>0;GTO +5
⊢
20:
IF RR14=0;GTO +2
⊢
21:
R(R15-2)+π→R(R15
-2);GTO +3⊢
22:
IF RR15>0;GTO +2
⊢
23:
π→R(R15-2)⊢
24:
SPC 1;PRT R(17+3
X),RR14,RR15,R(R
15-3),R(R15-2)⊢
25:
IF X>R5;GTO +2⊢
26:
GTO 7⊢
```

```
27:
ENT "MINX (TIME)
",A,"MAX X",B;
ENT "MIN Y (ACC)
",C,"MAX Y",Y;
SCL A,B,C,Y⊢
28:
SPC 2;0→B;X-1→R1
8;PRT "T","F(T)"
;R4/20→R16;-R16→
A⊢
29:
A+R16→A;0→X;R15+
1→R17;A→RR17;R19
→R(R17+1)⊢
30:
X+1→X;17+3X→C;R(
C+1)SIN (2πARC+R
(C+2))+R(R17+1)→
R(R17+1)⊢
31:
IF X≠R18;GTO -1⊢
32:
PLT RR17,R(R17+1
);PEN ;SPC 1;
PRT RR17,R(R17+1
);IF A>R4;GTO +2
⊢
33:
GTO -4⊢
34:
ENT "FILE",A;
RCF A,R19,R(R15-
2)⊢
35:
END ⊢
R1306
```

Fourier Series Programs Listing

Single Cycle Sinusoid Case

```
0:
FLT 5;0→X;TBL 2⊢
1:
ENT "Y",R0,"FREQ
",R1;SPC 2;PRT "
Y",R0,"FREQ",R1⊢
2:
ENT "T1",R2,"T",
R4;PRT "T1",R2,"
T",R4;SPC 2⊢
3:
PRT "FREQ","AN",
"BN","CN"⊢
4:
PRT "PHASE";SPC
1;1000R4→R5⊢
5:
X+1→X;2πX/R4→R6;
R6/2π→R(17+3X)⊢
6:
17+3X+3→R14;R14+
1→R15⊢
7:
R0((COS ((R1-R6)
R2)-1)/2(R1-R6)+
(COS ((R1+R6)R2)
-1)/2(R1+R6))→RR
14⊢
8:
R0(SIN ((R1+R6)R
2)/2(R1+R6)-SIN
((R1-R6)R2)/2(R1
-R6))→RR15⊢
9:
RR14RR14+RR15RR1
5→R(R15-3)⊢
10:
┌R(R15-3)→R(R15-
3);IF RR15≠0;
GTO +5⊢
11:
IF RR14=0;PRT "U
NDEFINED";STP ⊢
12:
IF RR14>0;GTO +2
⊢
13:
3π/2→R(R15-2);
GTO +11⊢
14:
π/2→R(R15-2);
GTO +10⊢
15:
ATN (RR14/RR15)→
R(R15-2)⊢
16:
IF 0≤R(R15-2);
GTO +3⊢
17:
IF RR14≤0;GTO +7
⊢
18:
R(R15-2)+π→R(R15
-2);GTO +6⊢
19:
IF RR14>0;GTO +5
⊢
20:
IF RR14=0;GTO +2
⊢
21:
R(R15-2)+π→R(R15
-2);GTO +3⊢
22:
IF RR15>0;GTO +2
⊢
23:
π→R(R15-2)⊢
24:
SPC 1;PRT R(17+3
X),RR14,RR15,R(R
15-3),R(R15-2)⊢
25:
IF X>R5;GTO +2⊢
26:
GTO 5⊢
```

```
27:
ENT "MINX (TIME)
",A,"MAX X",B;
ENT "MIN Y (ACC)
",C,"MAX Y",Y;
SCL A,B,C,Y⊢
28:
SPC 2;0→B;X-1→R1
8;PRT "T","F(T)"
;R4/1000→R16;-R1
6→A⊢
29:
A+R16→A;0→X;R15+
1→R17;A→RR17;R19
→R(R17+1)⊢
30:
X+1→X;17+3X→C;R(
C+1)SIN (2πARC+R
(C+2))+R(R17+1)→
R(R17+1)⊢
31:
IF X≠R18;GTO -1⊢
32:
PLT RR17,R(R17+1
);PEN ;SPC 1;
PRT RR17,R(R17+1
);IF A>R4;GTO +2
⊢
33:
GTO -4⊢
34:
ENT "FILE",A;
RCF A,R19,R(R15-
2)⊢
35:
END ⊢
R1301
```

A-12 Displacement Program

This program calculates and lists the Fourier series coefficients for chipping hammer displacement using the acceleration Fourier series coefficients determined using the Fourier series program. The results are stored on cassette tapes.

Program Chronology

STEP	DISPLAY	INSTRUCTIONS
1		Load program into calculator. Press "END; RUN PROGRAM".
2	FILE	Enter file number of acceleration coefficient storage file. Press "RUN PROGRAM". Program lists frequency (Hz) C_n (m), and phase (rad).
3	FILE	Enter storage file number. Press "RUN PROGRAM". Program stores coefficients in cassette data file. The program then gives a 20 point displacement time history for one cycle.

Displacement Program Listing

```
0:
0→X;TBL 2;FLT 8⊢
1:
ENT "FILE",C;
SPC 2;PRT "FILE"
,C⊢
2:
FDF C;IDF C,Y,A,
Z;LDF C,R0;(Y-1)
/3→A⊢
3:
SPC 2;PRT "DISPL
ACEMENT","COEFFI
CIENTS";SPC 2⊢
4:
PRT "FREQ(HERTZ)
","CN (METERS)",
"PHASE (RADIANS)
"⊢
5:
X+1→X;-R(3X-1)/R
(3X-2)R(3X-2)(2π
)(2π)→R(3X-1)⊢
6:
SPC 1;PRT R(3X-2
),R(3X-1),R(3X)⊢
7:
IF A>X;GTO -2⊢
8:
ENT "FILE",C;
SPC 2;PRT "IN FI
LE",C;RCF C,R1,R
(3X)⊢
9:
SPC 2;PRT "TIME
(SEC)","X(T) (ME
TERS)"⊢
10:
1/20R1→Y;-Y→C;0→
B⊢
11:
0→X;C+Y→C;0→B⊢
12:
X+1→X;B+R(3X-1)
SIN (2πR(3X-2)C+
R(3X))→B⊢
13:
IF A>X;GTO -1⊢
14:
SPC 1;PRT C,B⊢
15:
IF C≤20Y;GTO -4⊢
16:
END ⊢
R1384
```

A-13 Acceleration and Displacement Time History Plotting Program

This program plots the acceleration or displacement time history using the Fourier series coefficients stored on cassette tape. The listing as shown plots acceleration time histories. To plot displacement time histories, line 1 must be changed from "Y/3→A" to "(Y - 1)/3→A".

Program Chronology

STEP	DISPLAY	INSTRUCTIONS
1		Load program into calculator. Pres "END; RUN PROGRAM".
2	FILE	Enter Fourier series coefficient data storage file number. Press "RUN PROGRAM".
3	Y MAX	Enter maximum value on displacement or acceleration axis of plot. Press "RUN PROGRAM". Program prints value of Y maximum.
4	Y MIN	Enter minimum value on displacement or acceleration axis of plot. Press "RUN PROGRAM". Program prints value of Y minimum. Program plots the number of displacement or acceleration cycles occuring in .03 seconds.

Acceleration and Displacement Time History Plotting Program Listing

```
0:
TBL 2;ENT "FILE"
,C;SPC 2;PRT "FI
LE",C⊢
1:
FDF C;IDF C,Y,A,
Z;LDF C,R1;Y/3→A
⊢
2:
ENT "Y MAX",X;
SPC 2;PRT "Y MAX
",X⊢
3:
ENT "Y MIN",B;
SPC 1;PRT "Y MIN
",B;1.1B→C⊢
4:
SCL -X,-B,0,.03;
PEN ;PLT -B,0;
PLT -X,0⊢
5:
PLT -X,.03;PLT -
B,.03;PLT -B,0;
PEN ⊢
6:
PLT -B-.5X,0;
PLT -B-.5X,.03;
PEN ⊢
7:
PLT 0,0;PLT 0,.0
3;PEN ;PLT -.5X,
0;PLT -.5X,.03;
PEN ⊢
8:
PLT -C,0;PLT -C,
.0004;PEN ;C+.1X
→C⊢
9:
IF X>C;GTO -1⊢
10:
0→C⊢
11:
C+.001→C;PLT -X,
C;PLT -X+X/27,C;
PEN ⊢
12:
IF .03>C;GTO -1⊢
13:
PLT -X,.01;PLT -
X+X/18,.01;PEN ⊢
14:
PLT -X,.02;PLT -
X+X/18,.02;PEN ⊢
15:
1.1B→C⊢
16:
PLT -C,.03;PLT -
C,.0296;PEN ;C+.
1X→C⊢
17:
IF X>C;GTO -1⊢
18:
0→C⊢
19:
C+.001→C;PLT -B,
C;PLT -B-X/27,C;
PEN ⊢
```

```
20:
IF .03>C;GTO -1⊢
21:
PLT -B,.01;PLT -
B-X/18,.01;PEN ⊢
22:
PLT -B,.02;PLT -
B-X/18,.02;PEN ⊢
23:
1/20R1→Y;-Y→C;0→
B⊢
24:
0→X;C+Y→C;0→B⊢
25:
X+1→X;B+R(3X-1)
SIN (2πCR(3X-2)+
R(3X))→B⊢
26:
IF A>X;GTO -1⊢
27:
PLT -B,C⊢
28:
IF C<.03;GTO -4⊢
29:
PEN ;STP ⊢
30:
-Y→C;0→B;GTO -6⊢
31:
END ⊢
R1352
```

A-14 Fourier Coefficient Plotting Program

This program plots the RMS values of the acceleration Fourier series coefficients stored on cassette tape.

Program Chronology

STEP	DISPLAY	INSTRUCTIONS
1		Load program into calculator. Press "END; RUN PROGRAM".
2	FILE	Enter acceleration Fourier series coefficient dats storage file number. Press "RUN PROGRAM".
3	MAX ACC	Enter maximum acceleration value on vertical axis of plot. Press "RUN PROGRAM". Program prints maximum acceleration.
4	MIN ACC	Enter minimum acceleration value on vertical axis of plot. Press "RUN PROGRAM". Program lists minimum acceleration, then plots acceleration coefficients at the harmonic frequencies.

Fourier Coefficient Plotting Program Listing

```
0:
ENT "FILE",X;
SPC 2;PRT "FILE"
,X⊢
1:
FDF X;IDF X,Y,A,
B;LDF X,R0⊢
2:
(Y-1)/3→Y⊢
3:
ENT "MAX ACC",A;
SPC 1;PRT "MAX A
CC",A⊢
4:
ENT "MIN ACC",B;
SPC 1;PRT "MIN A
CC",B⊢
5:
LOG 2/6→X;SCL
LOG 6.3-X,3+X,
LOG B,LOG A;0→X⊢
6:
X+1→X;PLT LOG R(
3X-2),LOG (.707
ABS R(3X-1));
PLT LOG R(3X-2),
LOG B;PEN ⊢
7:
IF Y>X;GTO -1⊢
8:
PEN ;STP ⊢
9:
END ⊢
R1413
```

A-15 Nicolet Acceleration Time History Plotting Program

This program plots acceleration time histories from the analog data contained on the FM tapes by using the Nicolet Instrument Corporation model 1090A digital storage oscilloscope and NIC-191A calculator interface. Analog data played into the oscilloscope is digitized and stored in memory within the oscilloscope. The calculator interface permits the oscilloscope digital memory to be read by the calculator, then plotted. This program was written by R. Falkenberg.

Program Chronology

STEP	DISPLAY	INSTRUCTIONS
1		Load program into calculator. Press "RUN PROGRAM".
2	VERT. SENS.	Load calibration signal into oscilloscope and adjust scale as required. Enter vertical sensitivity setting. Press "RUN PROGRAM".
3	TIME PER POINT	Enter "sweep time per point" setting. Press "RUN PROGRAM".
4	CAL. FREQ.	Enter frequency of calibration signal. Press "RUN PROGRAM".
5	CAL. ACC. (G'S)	Enter calibration acceleration level (g). Press "RUN PROGRAM".
6	LOAD CAL. SIGNAL	With calibration signal onoscilloscope display, Press "RUN PROGRAM".
7	ACC LINES (G'S)	Enter the desired interval between major acceleration divisions on coordinate axis. Press "RUN PROGRAM".
8	ACC DIV. (SEC)	Enter desired interval between time divisions on coordinate axis. Press "RUN PROGRAM".

STEP	DISPLAY	INSTRUCTIONS
9	ACC TICKS (G'S)	Enter desired interval between minor acceleration devisions on coordinate axis. Press "RUN PROGRAM". Program plots coordinate axis.
10	LOAD DATA	With desired acceleration time history displayed on the oscilloscope, Press "RUN PROGRAM". Program plots time history.

Nicolet Acceleration Time History Plotting Program Listing

```
0:
ENT "VERT. SENS.
",Y,"TIME PER PO
INT",X;0→C;Y/200
0→B;0→A⊢
1:
4095X→Z⊢
2:
ENT "CAL. FREQ",
R1100,"CAL. ACC.
 (G'S)",R1101⊢
3:
1/(X*R1100)→R110
0;STP ;DSP "LOAD
 CAL. SIGNAL"⊢
4:
FMT 1,FXD 5.0;0→
A⊢
5:
FMT "A";WRT 1⊢
6:
FMT "G";WRT 1;
RED 1.1,RA⊢
7:
IF A>R1100-1;
GTO +2⊢
8:
A+1→A;GTO -2⊢
9:
0→A;R0→R1102;R0→
R1103⊢
10:
IF RA>R1102;RA→R
1102⊢
11:
IF RA<R1103;RA→R
1103⊢
12:
IF A>R1100-1;
GTO +2⊢
13:
A+1→A;GTO -3⊢
14:
(R1102+R1103)/2→
R1104;(R1102-R11
03)/2→R1108⊢
15:
PLT 0,0;PLT 0,1;
PLT 1,1;PLT 1,0;
PLT 0,0;PLT ⊢
16:
PLT 0,(R1104*B-Y
)/2Y;PLT 1,(R110
4*B+Y)/2Y;PLT ⊢
17:
ENT "ACC LINES(G
'S)",R1105,"TIME
 DIV.(SEC)",R110
6;1→R1107⊢
18:
ENT "ACC TICKS(G
'S)",R1120;0→R11
22;1→R1121⊢
19:
(R1107*R1105*B*R
1108/R1101+R1104
*B+Y)/2Y→R1109⊢
20:
(R1104*B-R1107*R
1105*B*R1108/R11
01+Y)/2Y→R1110⊢
21:
PLT 0,R1109;PLT
R1121,R1109;PLT
;PLT .99,R1109;
PLT 1,R1109;PLT
⊢
22:
PLT 0,R1110;PLT
R1121,R1110;PLT
;PLT .99,R1110;
PLT 1,R1110;PLT
⊢
23:
R1107+1→R1107⊢
```

```
24:
IF R1109<1;GTO -
5⊢
25:
IF R1110>0;GTO -
6⊢
26:
R1120→R1105;.01→
R1121;R1122+1→R1
122;1→R1107;IF R
1122>1;GTO +2⊢
27:
GTO 19⊢
28:
R1106→R1111;(R11
04*B+Y)/2Y→R1112
⊢
29:
IF R1111>Z;GTO +
5⊢
30:
R1111/Z→R1130;
PLT R1130,0;PLT
R1130,.01;PLT ⊢
31:
PLT R1130,R1112-
.01;PLT R1130,R1
112+.01;PLT ⊢
32:
PLT R1130,.99;
PLT R1130,1;PLT
⊢
33:
R1111+R1106→R111
1;GTO -4⊢
34:
0→C;STP ;DSP "LO
AD DATA"⊢
35:
FMT 1;FXD 5.0;0→
A⊢
36:
FMT "A";WRT 1⊢
37:
FMT "G";WRT 1;
RED 1.1,RA⊢
38:
IF A=1023;GTO +2
⊢
39:
A+1→A;GTO -2⊢
40:
IF C>0;GTO +2⊢
41:
0→A;0→C;GTO +2⊢
42:
0→A;C+X→C⊢
43:
PLT C/Z,(RA*B+Y)
/2Y;IF A=1023;
GTO +3⊢
44:
A+1→A;C+X→C⊢
45:
GTO -2⊢
46:
PLT ;IF C=Z;GTO
+2⊢
47:
GTO 35⊢
48:
END ⊢
R1272
```

A-16 Work per Unit Time Plotting Program

This program calculates, then plots, the 1/3 octave band RMS levels of work per unit time. The levels are calculated from the instantaneous dissipated energy levels stored on cassette tape.

Program Chronology

STEP	DISPLAY	INSTRUCTIONS
1		Load program into calculator. Press "RUN PROGRAM".
2	FILE	Enter instantaneous energy file number. Press "RUN PROGRAM". Program prints file number, heading, loads data into calculator, then calculates and lists work per unit time levels.
3	MAX W/T	Enter maximum value of work per unit time on plot axis. Press "RUN PROGRAM".
4	MIN W/T	Enter minimum value of work per unit time on plot axis. Press "RUN PROGRAM". Program plots work per unit time versus frequency.

Work per Unit Time Plotting Program Listing

```
0:
FLT 8;SPC 2⊢
1:
6.3→R0;8→R1;10→R
2;12.5→R3;16→R4;
20→R5⊢
2:
25→R6;31.5→R7;40
→R8;50→R9;63→R10
;80→R11⊢
3:
100→R12;125→R13;
160→R14;200→R15;
250→R16;315→R17⊢
4:
400→R18;500→R19;
630→R20;800→R21;
1000→R22⊢
5:
ENT "FILE",X;
PRT "FILE",X,"W/
T.....J/S";SPC
2⊢
6:
LDF X,R30;0→A;0→
R25⊢
7:
2πRAR(3A+31)→R(A
+200);PRT R(A+20
0)⊢
8:
A+1→A;IF A≠23;
GTO -1⊢
9:
ENT "MAX W/T",R3
00,"MIN W/T",R30
1⊢
10:
PRT "MAX W/T",R3
00,"MIN W/T",R30
1⊢
11:
LOG 2/6→B;SCL
LOG 6.3-B,3+B,
LOG R301,LOG R30
0⊢
12:
0→X⊢
13:
PLT LOG RX-B,
LOG R(200+X);
PLT LOG RX+B,
LOG R(200+X)⊢
14:
1+X→X;IF X≠23;
GTO -1⊢
15:
END ⊢
R1377
```

APPENDIX B

HAND-ARM SYSTEM DYNAMIC COMPLIANCE AND PHASE DATA PLOTS

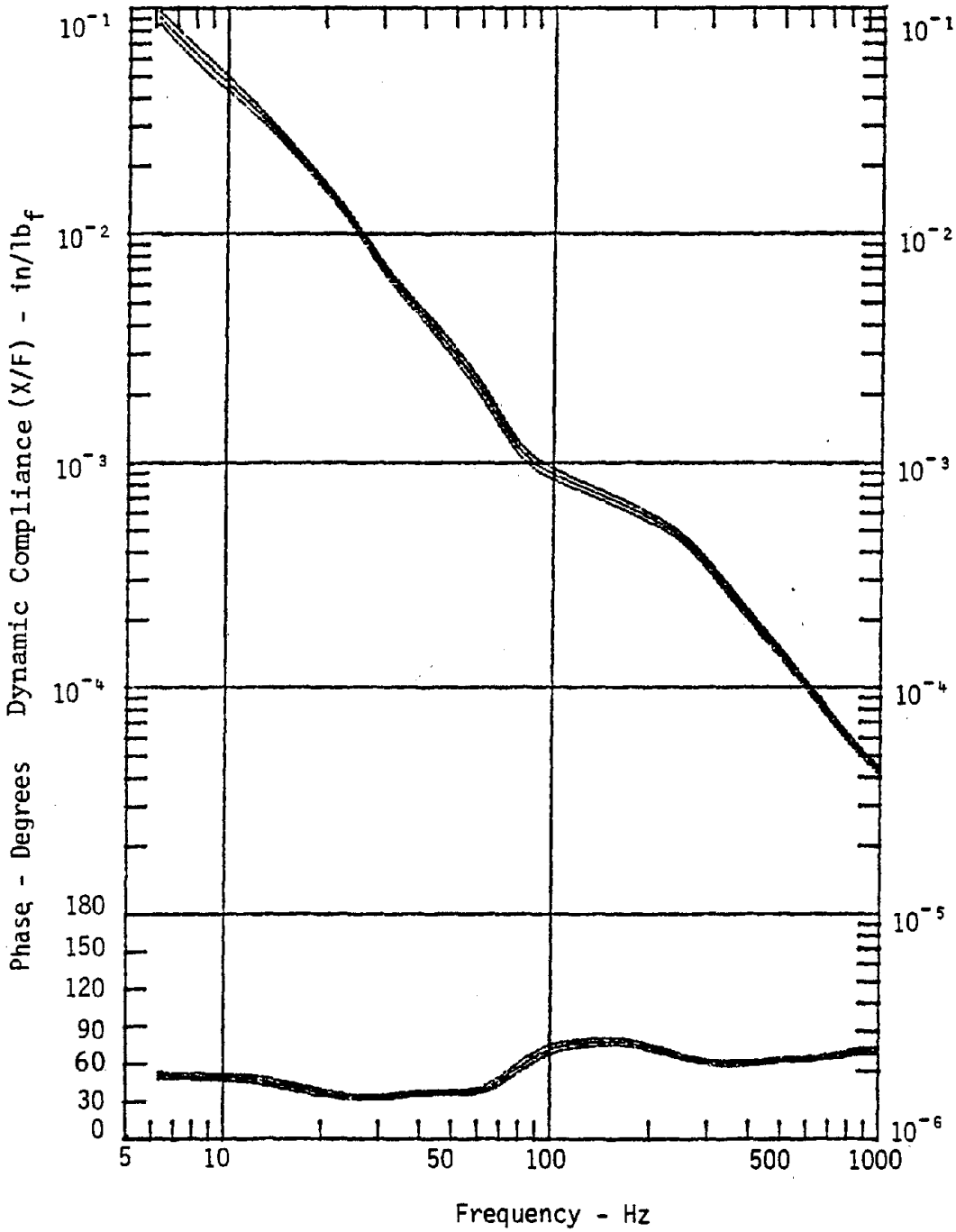

Figure B-1. Average and 90% confidence limit values of dynamic compliance and phase for the hand-arm system associated with 75 foundry workers. X-direction, 3.8 cm diameter handle, 5.7 pound grip force.

Preceding page blank

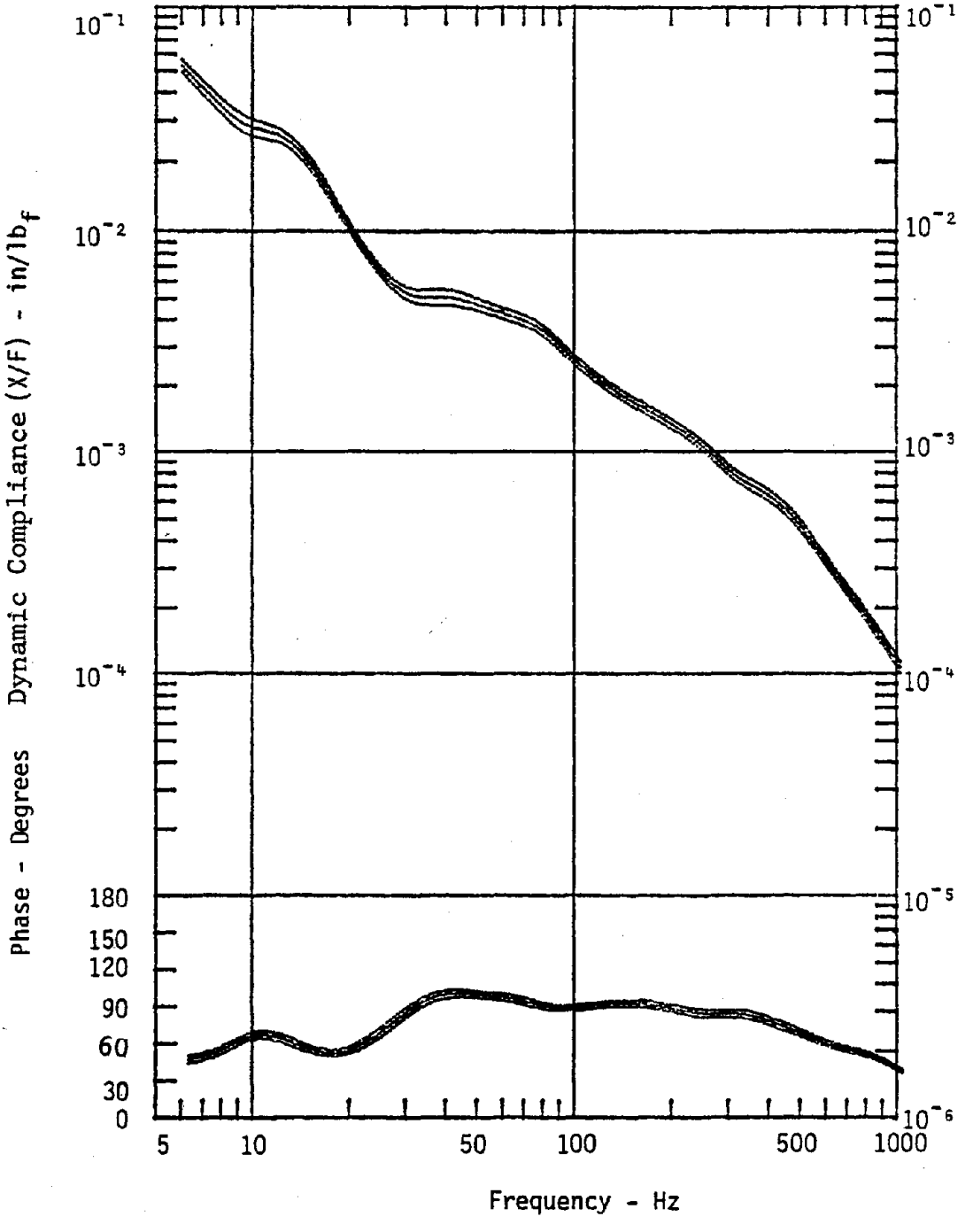

Figure B-2. Average and 90% confidence limit values of dynamic compliance and phase for the hand-arm system associated with 75 foundry workers. Y-direction, 3.8 cm diameter handle, 5.7 pound grip force.

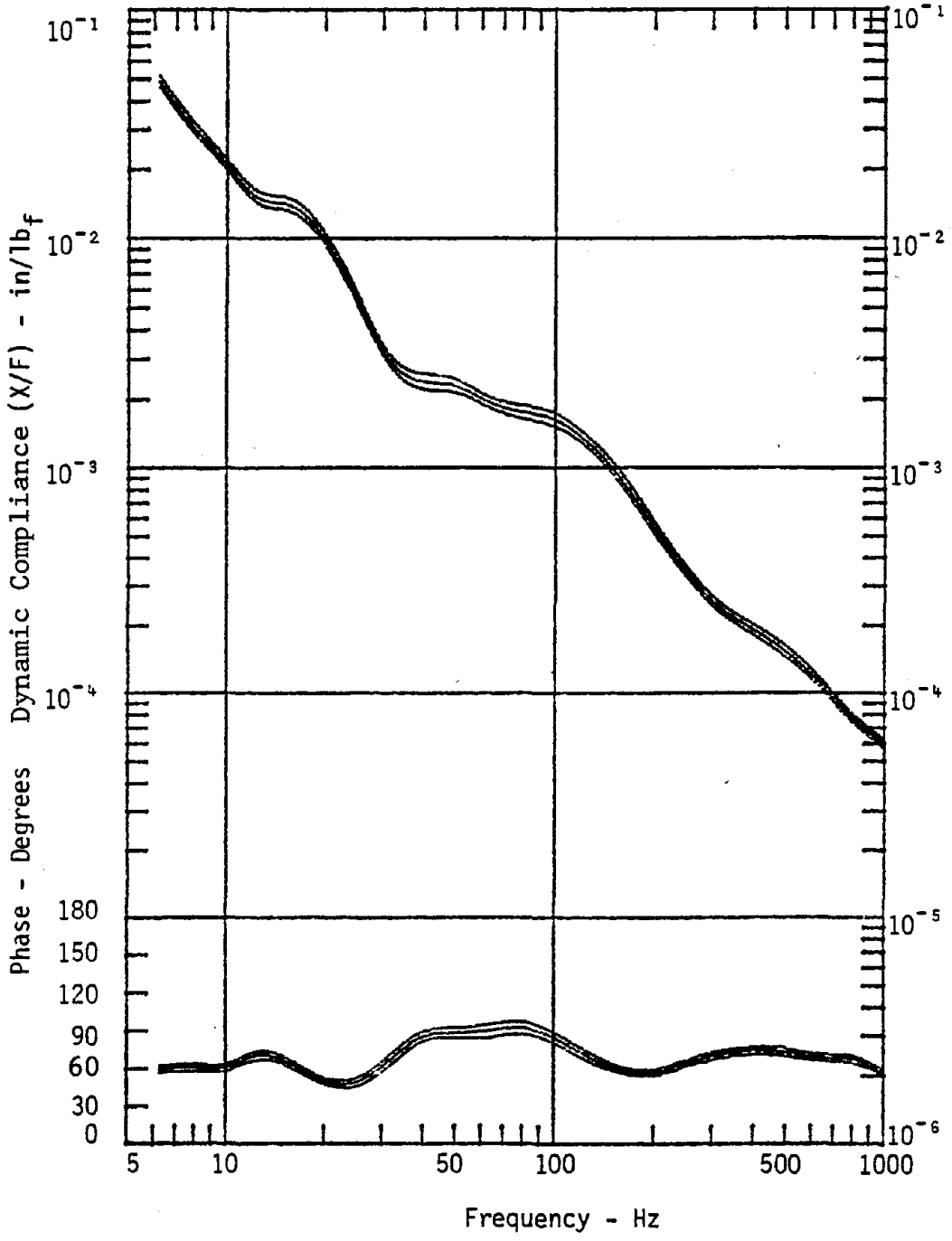

Figure B-3. Average and 90% confidence limit values of dynamic compliance and phase for the hand-arm system associated with 75 foundry workers. Z-direction, 3.8 cm diameter handle, 5.7 pound grip force.

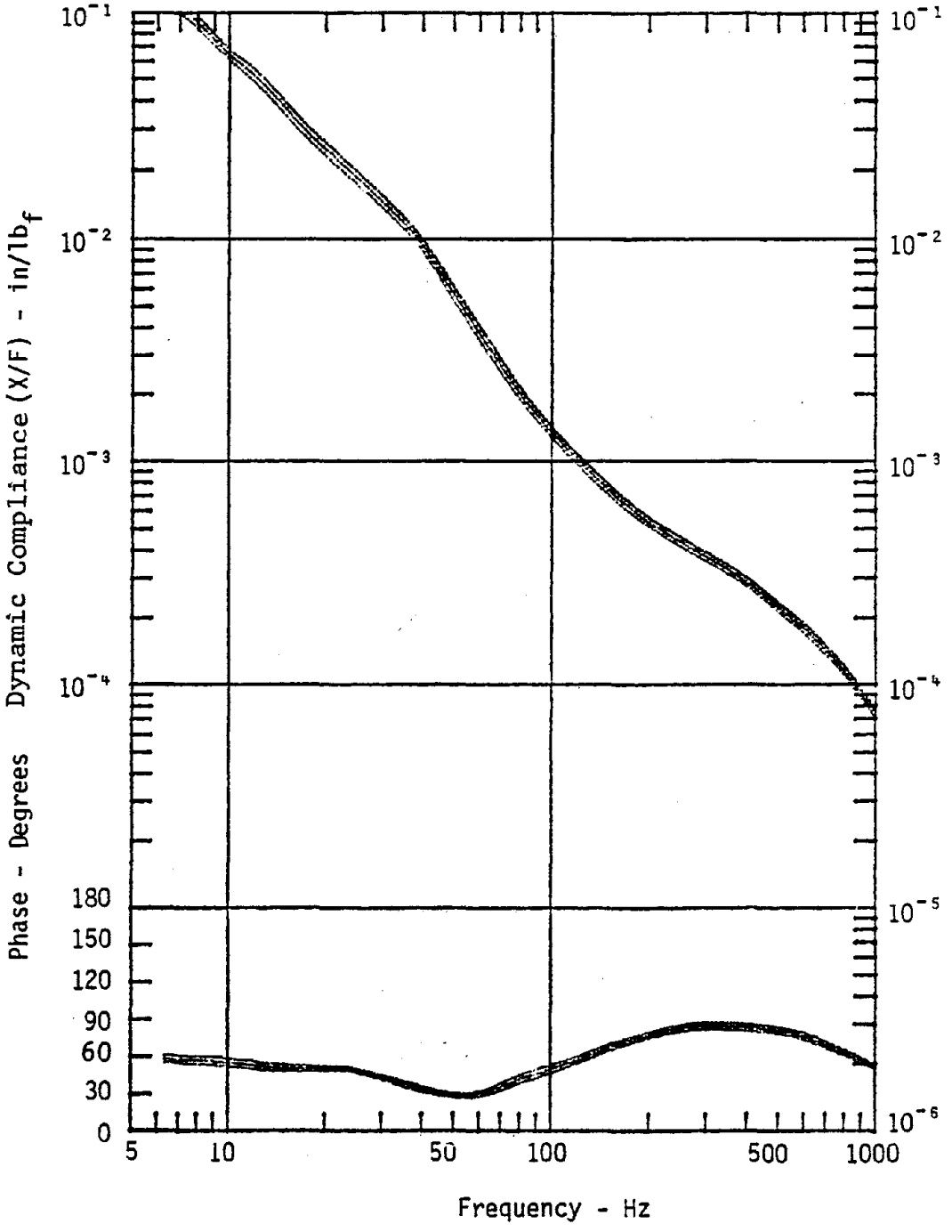

Figure B-4. Average and 90% confidence limit values of dynamic compliance and phase for the hand-arm system associated with 75 foundry workers. X-direction, 1.9 cm diameter handle, 5.7 pound grip force.

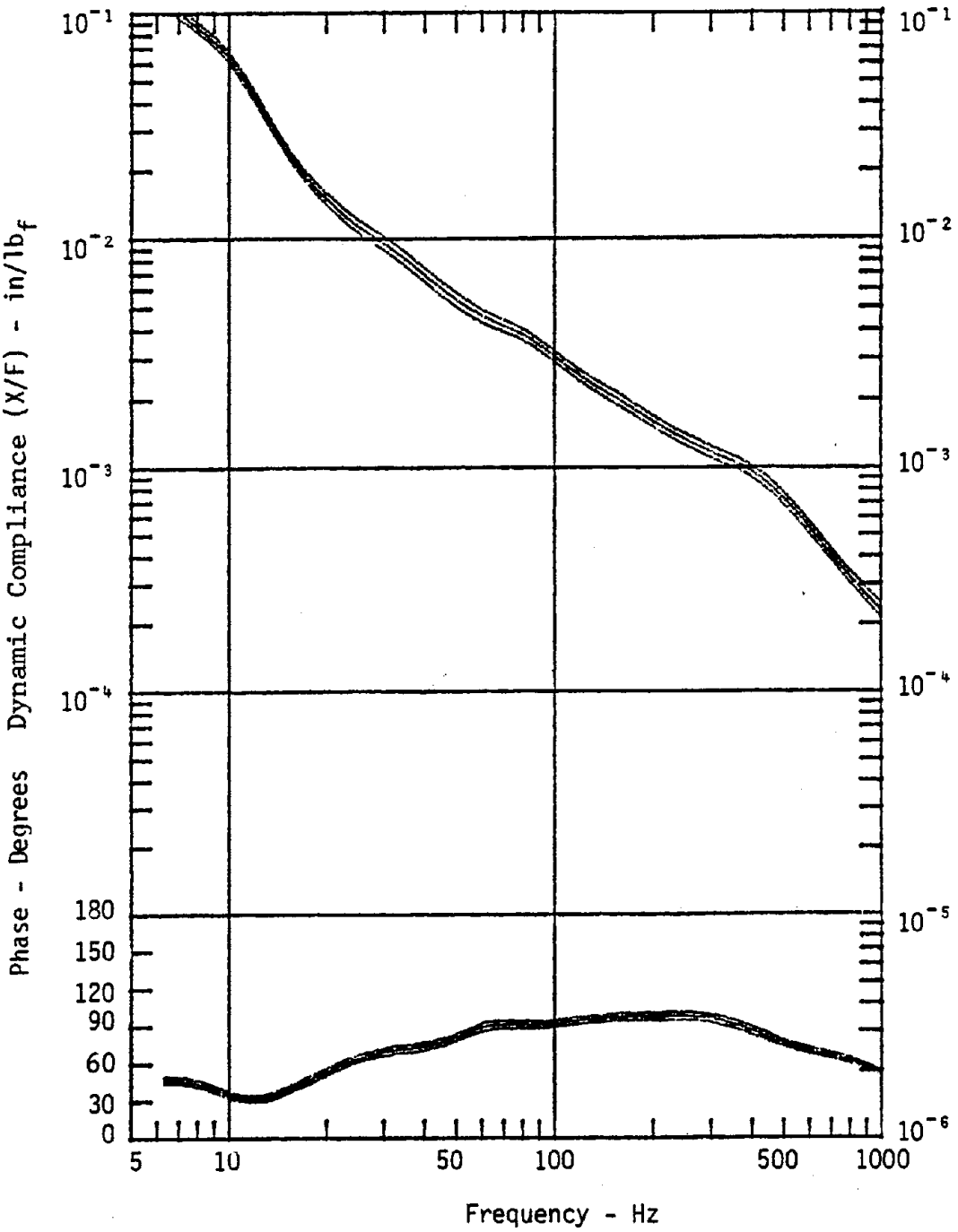

Figure B-5. Average and 90% confidence limit values of dynamic compliance and phase for the hand-arm system associated with 75 foundry workers. Y-direction, 1.9 cm diameter handle, 5.7 pound grip force.

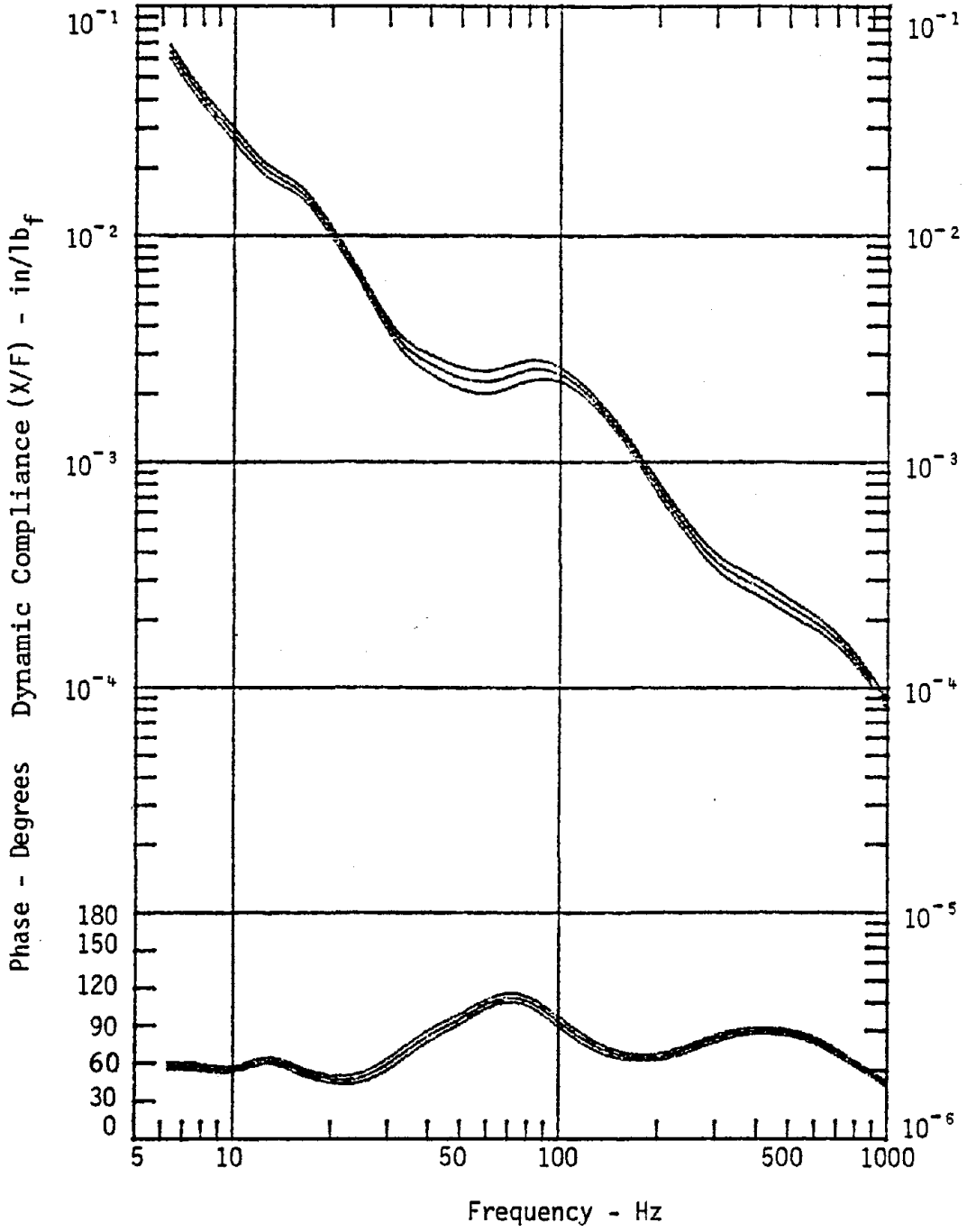

Figure B-6. Average and 90% confidence limit values of dynamic compliance and phase for the hand-arm system associated with 75 foundry workers. Z-direction, 1.9 cm diameter handle, 5.7 pound grip force.

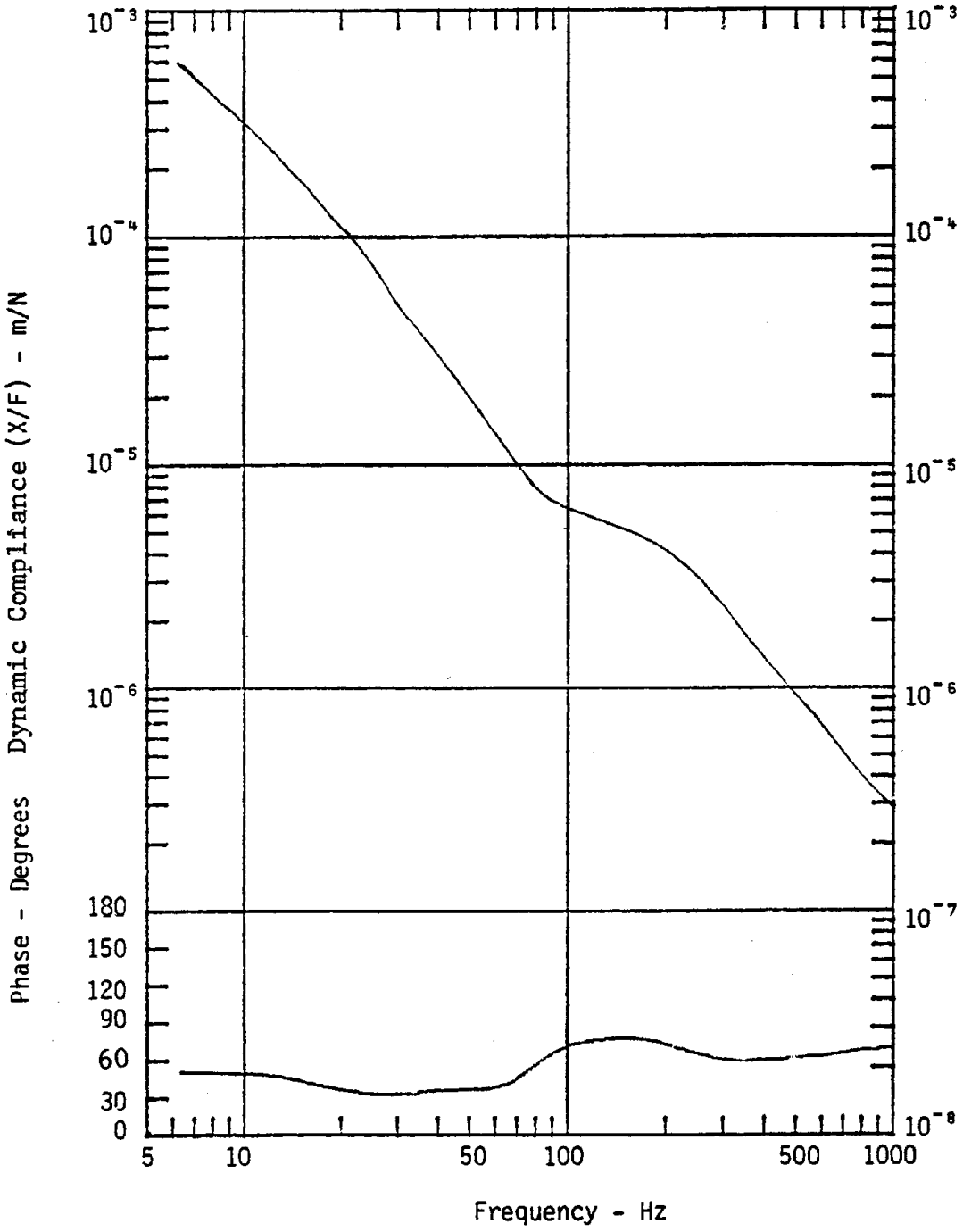

Figure B-7. Average values of dynamic compliance and phase in metric units. X-direction, 3.8 cm diameter handle.

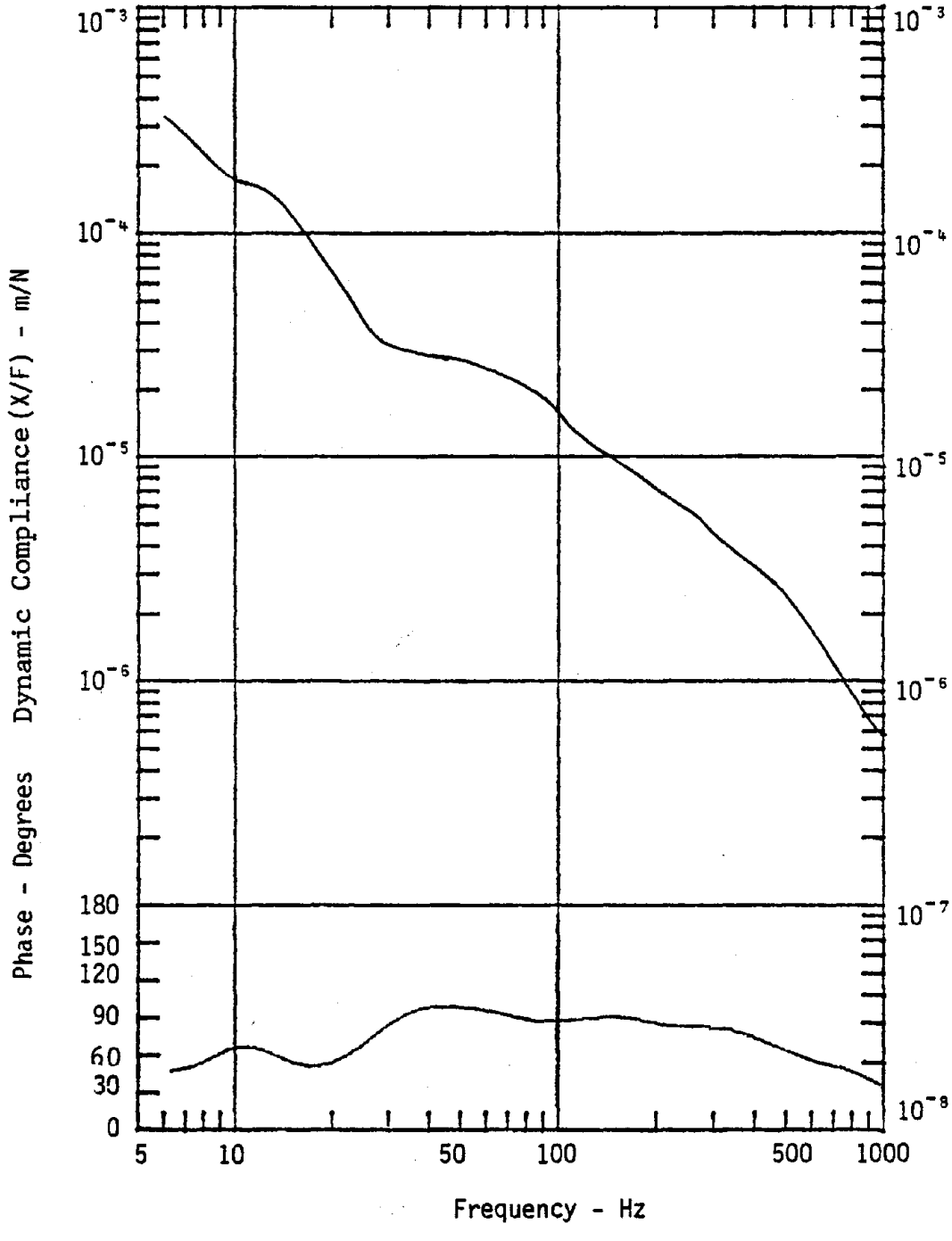

Figure B-8. Average values of dynamic compliance and phase in metric units. Y-direction, 3.8 cm diameter handle.

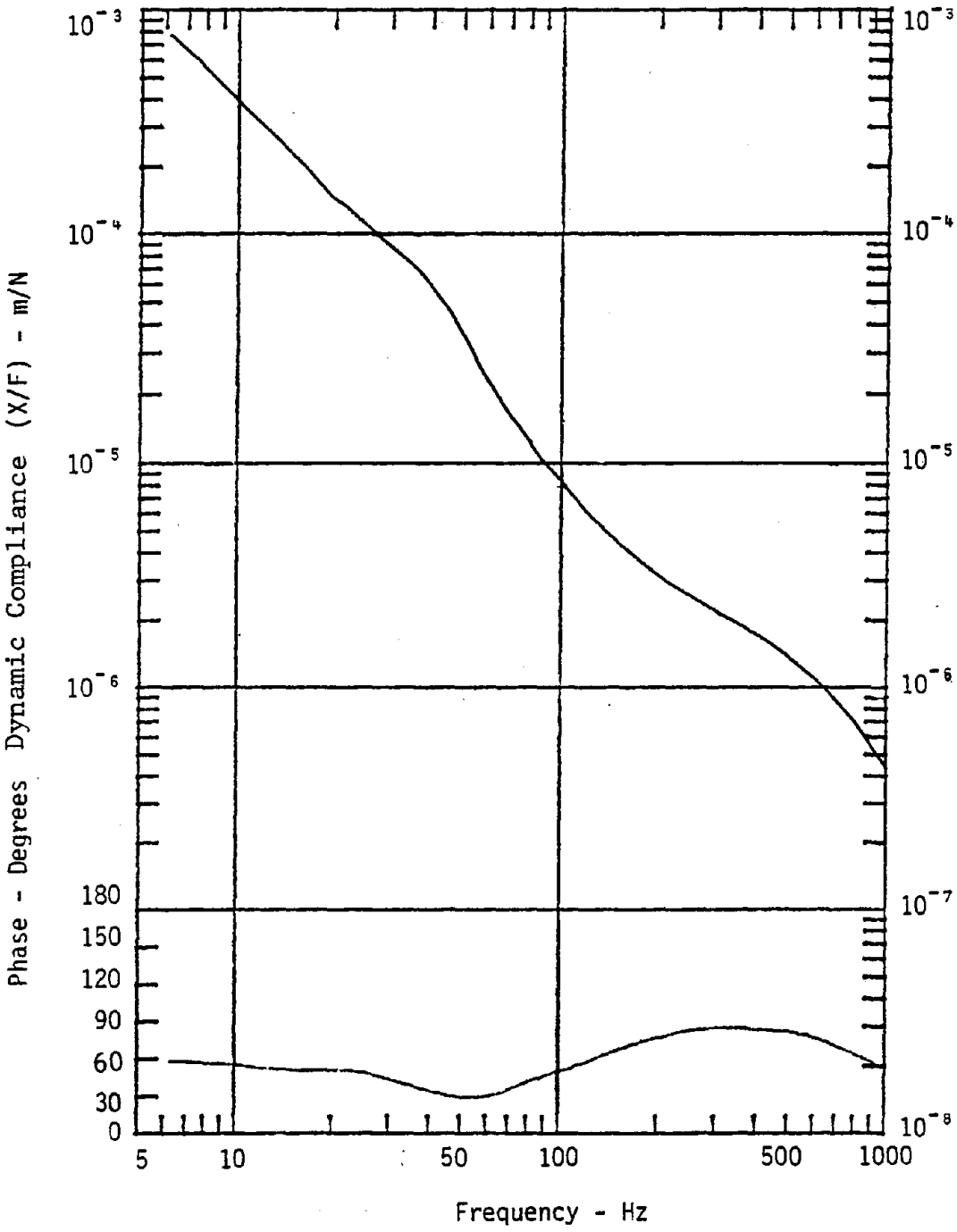

Figure B-10. Average values of dynamic compliance and phase in metric units. X-direction, 1.9 cm diameter handle.

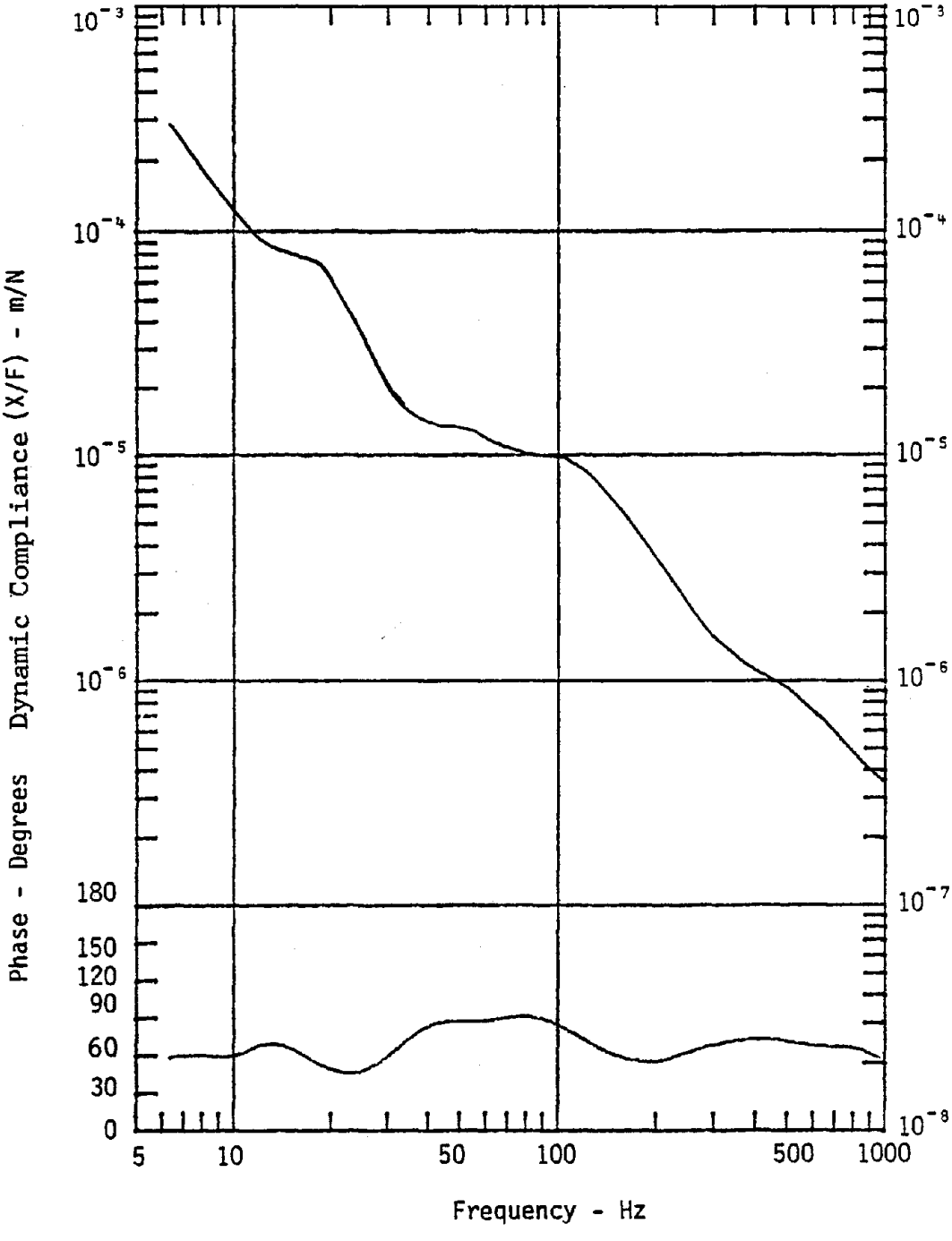

Figure B-9. Average values of dynamic compliance and phase in metric units. Z-direction, 3.8 cm diameter handle.

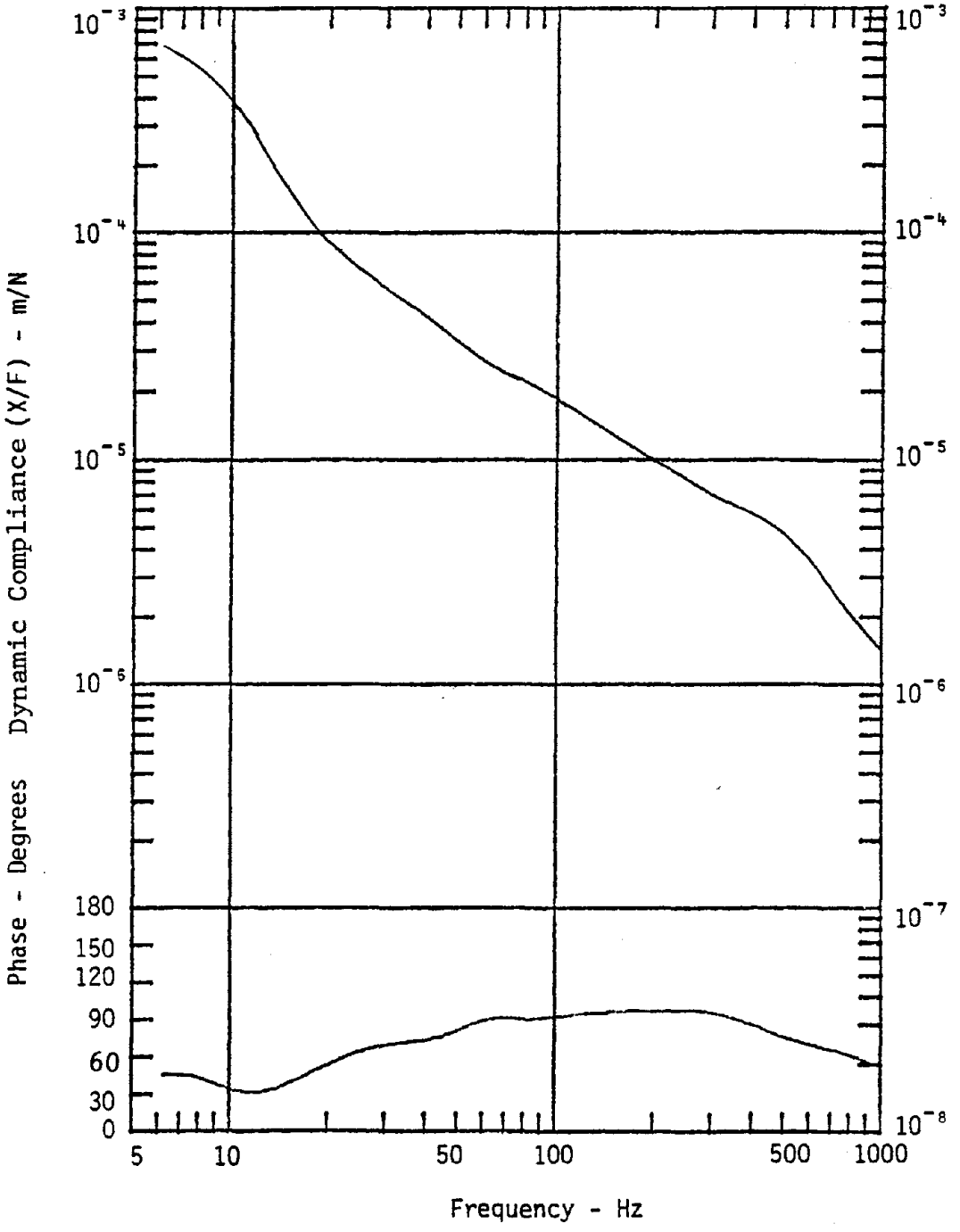

Figure B-11. Average values of dynamic compliance and phase in metric units. Y-direction, 1.9 cm diameter handle.

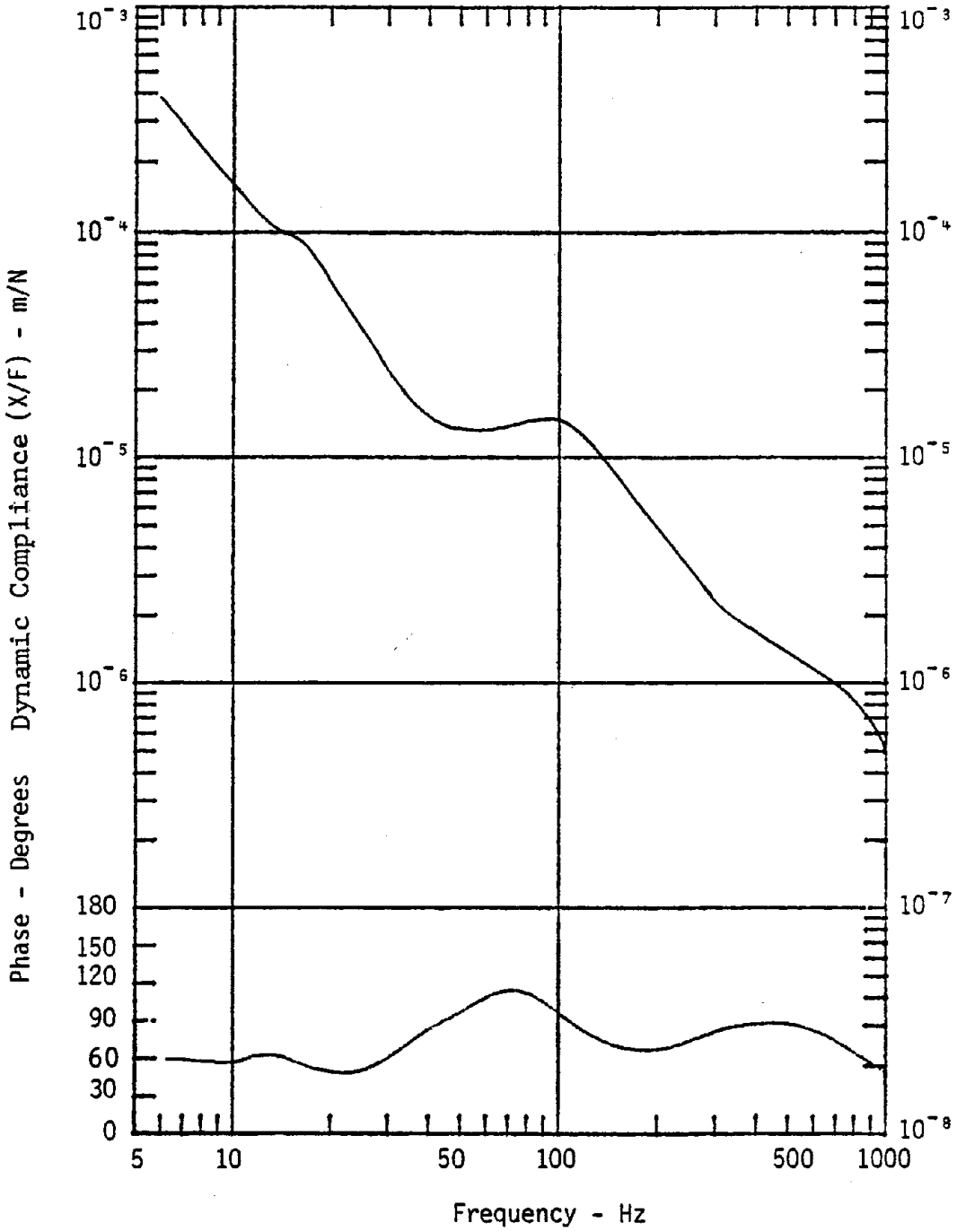

Figure B-12. Average values of dynamic compliance and phase in metric units. Z-direction, 1.9 cm diameter handle.

TABLE B-1

X/F and Phase Data, Metric Units					
Center Frequencies	6.3	8.0	10	12.5	16
Large Handles					
X-Direction					
X/F (m/N)	5.3293×10^{-4}	3.7555×10^{-4}	2.7648×10^{-4}	2.0308×10^{-4}	1.3825×10^{-4}
Phase (Degrees)	50.011	48.708	48.206	46.291	40.366
Y-Direction					
X/F (m/N)	3.1165×10^{-4}	2.1611×10^{-4}	1.6737×10^{-4}	1.5089×10^{-4}	1.0781×10^{-4}
Phase (Degrees)	46.880	54.185	65.459	62.036	51.466
Z-Direction					
X/F (m/N)	2.7776×10^{-4}	1.7566×10^{-4}	1.2209×10^{-4}	8.6630×10^{-5}	7.9007×10^{-5}
Phase (Degrees)	58.522	59.962	59.885	69.340	61.664
Small Handles					
X-Direction					
X/F (m/N)	7.4074×10^{-4}	5.2926×10^{-4}	3.7641×10^{-4}	2.8554×10^{-4}	1.9483×10^{-4}
Phase (Degrees)	57.281	55.034	53.538	50.669	48.953
Y-Direction					
X/F (m/N)	6.8181×10^{-4}	5.1247×10^{-4}	3.7902×10^{-4}	2.3156×10^{-4}	1.2813×10^{-4}
Phase (Degrees)	46.027	43.127	33.686	31.346	41.079
Z-Direction					
X/F (m/N)	3.6954×10^{-4}	2.3263×10^{-4}	1.5983×10^{-4}	1.1315×10^{-4}	9.0088×10^{-5}
Phase (Degrees)	57.916	56.045	55.131	61.788	53.600

TABLE B-1
(continued)

Center Frequencies	20	25	31.5	40	50
Large Handles					
X-Direction					
X/F (m/N)	9.4769×10^{-5}	6.2182×10^{-5}	3.8341×10^{-5}	2.5684×10^{-5}	1.7525×10^{-5}
Phase (Degrees)	35.041	31.745	32.543	34.930	35.510
Y-Direction					
X/F (m/N)	6.4219×10^{-5}	4.0056×10^{-5}	2.9969×10^{-5}	2.9152×10^{-5}	2.7081×10^{-5}
Phase (Degrees)	54.007	68.522	87.885	98.352	97.275
Z-Direction					
X/F (m/N)	5.6973×10^{-5}	3.1818×10^{-5}	1.7009×10^{-5}	1.3573×10^{-5}	1.3022×10^{-5}
Phase (Degrees)	48.582	47.707	64.283	84.025	87.414
Small Handles					
X-Direction					
X/F (m/N)	1.4278×10^{-4}	1.0881×10^{-4}	7.9555×10^{-5}	5.4660×10^{-5}	3.3471×10^{-5}
Phase (Degrees)	48.905	46.905	39.795	31.887	26.972
Y-Direction					
X/F (m/N)	8.8240×10^{-5}	6.6629×10^{-5}	5.2926×10^{-5}	4.0334×10^{-5}	3.1381×10^{-5}
Phase (Degrees)	52.975	63.396	69.498	73.112	80.407
Z-Direction					
X/F (m/N)	5.9795×10^{-5}	3.5536×10^{-5}	2.0496×10^{-5}	1.5584×10^{-5}	1.3479×10^{-5}
Phase (Degrees)	46.988	48.782	62.628	81.374	95. 031

TABLE B-1
(continued)

Center Frequencies	63	80	100	125	160
Large Handles					
X-Direction					
X/F (m/N)	1.1058×10^{-5}	6.5263×10^{-6}	5.1129×10^{-6}	4.4225×10^{-6}	3.7641×10^{-6}
Phase (Degrees)	39.070	56.219	70.444	75.048	75.930
Y-Direction					
X/F (m/N)	2.3970×10^{-5}	2.0496×10^{-6}	1.5124×10^{-5}	1.1473×10^{-5}	9.1131×10^{-6}
Phase (Degrees)	93.908	87.349	86.877	89.559	89.187
Z-Direction					
X/F (m/N)	1.1083×10^{-5}	9.9923×10^{-6}	9.2612×10^{-6}	7.5105×10^{-6}	5.0894×10^{-6}
Phase (Degrees)	89.194	91.248	83.323	69.417	57.422
Small Handles					
X-Direction					
X/F (m/N)	1.9846×10^{-5}	1.1740×10^{-5}	7.8825×10^{-6}	5.5548×10^{-6}	3.9597×10^{-6}
Phase (Degrees)	29.788	40.176	48.540	57.426	68.326
Y-Direction					
X/F (m/N)	2.5566×10^{-5}	2.2012×10^{-5}	1.7647×10^{-5}	1.3953×10^{-5}	1.1212×10^{-5}
Phase (Degrees)	89.857	89.937	91.518	94.232	96.188
Z-Direction					
X/F (m/N)	1.3172×10^{-5}	1.4678×10^{-5}	1.3985×10^{-5}	1.0982×10^{-5}	7.1724×10^{-6}
Phase (Degrees)	109.45	109.44	93.010	75.510	65.209

TABLE B-1
(continued)

Center Frequencies	200	250	315	400	500
Large Handles					
X-Direction					
X/F (m/N)	3.2038×10^{-6}	2.5862×10^{-6}	1.7810×10^{-6}	1.1552×10^{-6}	7.8103×10^{-7}
Phase (Degrees)	70.847	63.696	58.502	59.298	61.296
Y-Direction					
X/F (m/N)	7.5105×10^{-6}	5.9111×10^{-6}	4.3518×10^{-6}	3.5210×10^{-6}	2.5390×10^{-6}
Phase (Degrees)	84.479	80.982	80.471	73.354	62.843
Z-Direction					
X/F (m/N)	3.1453×10^{-6}	1.9983×10^{-6}	1.3793×10^{-6}	1.0906×10^{-6}	8.7030×10^{-7}
Phase (Degrees)	55.272	62.693	69.906	73.282	71.525
Small Handles					
X-Direction					
X/F (m/N)	3.0667×10^{-6}	2.4984×10^{-6}	2.0543×10^{-6}	1.6660×10^{-6}	1.2932×10^{-6}
Phase (Degrees)	75.792	81.288	83.367	82.090	79.575
Y-Direction					
X/F (m/N)	9.1552×10^{-6}	7.6501×10^{-6}	6.5113×10^{-6}	5.5038×10^{-6}	4.1944×10^{-6}
Phase (Degrees)	96.173	96.468	93.250	84.670	74.565
Z-Direction					
X/F (m/N)	4.4225×10^{-6}	2.8292×10^{-6}	1.9709×10^{-6}	1.6168×10^{-6}	1.3264×10^{-6}
Phase (Degrees)	64.554	71.631	81.077	85.513	83.928

TABLE B-1
(continued)

Center Frequencies	630	800	1000
Large Handles			
X-Direction			
X/F (m/N)	5.1483×10^{-7}	3.3394×10^{-7}	2.9694×10^{-7}
Phase (Degrees)	62.873	67.241	68.883
Y-Direction			
X/F (m/N)	1.5800×10^{-6}	9.7424×10^{-7}	5.8166×10^{-7}
Phase (Degrees)	53.355	45.739	31.359
Z-Direction			
X/F (m/N)	6.4219×10^{-7}	4.4123×10^{-7}	3.3703×10^{-7}
Phase (Degrees)	67.530	65.987	53.735
Small Handles			
X-Direction			
X/F (m/N)	9.7424×10^{-7}	6.7401×10^{-7}	4.2921×10^{-7}
Phase (Degrees)	73.562	62.307	49.263
Y-Direction			
X/F (m/N)	2.8227×10^{-6}	1.8436×10^{-6}	1.2962×10^{-6}
Phase (Degrees)	67.269	60.063	48.917
Z-Direction			
X/F (m/N)	1.0781×10^{-6}	7.8103×10^{-7}	4.9621×10^{-7}
Phase (Degrees)	76.015	60.414	42.559

TABLE B-2

X/F and Phase Data, English Units					
Center Frequencies	6.3	8.0	10	12.5	16
Large Handles					
X-Direction					
X/F (in/lbs)	9.3316×10^{-2}	6.5759×10^{-2}	4.8412×10^{-2}	3.5559×10^{-2}	2.4208×10^{-2}
Phase (Degrees)	50.011	48.708	48.206	46.291	40.366
Y-Direction					
X/F (in/lbs)	5.4570×10^{-2}	3.7841×10^{-2}	2.9306×10^{-2}	2.6421×10^{-2}	1.8878×10^{-2}
Phase (Degrees)	46.880	54.185	65.459	62.036	51.466
Z-Direction					
X/F (in/lbs)	4.8636×10^{-2}	3.0758×10^{-2}	2.1378×10^{-2}	1.5169×10^{-2}	1.3834×10^{-2}
Phase (Degrees)	58.522	59.962	59.885	69.340	61.664
Small Handles					
X-Direction					
X/F (in/lbs)	1.2970×10^{-1}	9.2673×10^{-2}	6.5909×10^{-2}	4.9998×10^{-2}	3.4115×10^{-2}
Phase (Degrees)	57.281	55.034	53.538	50.669	48.953
Y-Direction					
X/F (in/lbs)	1.1938×10^{-1}	8.9733×10^{-2}	6.6366×10^{-2}	4.0546×10^{-2}	2.2436×10^{-2}
Phase (Degrees)	46.027	43.127	33.686	31.346	41.079
Z-Direction					
X/F (in/lbs)	6.4706×10^{-2}	4.0734×10^{-2}	2.7986×10^{-2}	1.9813×10^{-2}	1.5774×10^{-2}
Phase (Degrees)	57.916	56.045	55.131	61.788	53.600

TABLE B-2
(continued)

Center Frequencies	20	25	31.5	40	50
Large Handles					
X-Direction					
X/F (in/lbs)	1.6594×10^{-2}	1.0888×10^{-2}	6.7135×10^{-3}	4.4973×10^{-3}	3.0686×10^{-3}
Phase (Degrees)	35.041	31.745	32.543	34.930	35.510
Y-Direction					
X/F (in/lbs)	1.1245×10^{-2}	7.0138×10^{-3}	5.2476×10^{-3}	5.1045×10^{-3}	4.7419×10^{-3}
Phase (Degrees)	54.007	68.522	87.885	98.352	97.275
Z-Direction					
X/F (in/lbs)	9.9760×10^{-3}	5.5713×10^{-3}	2.9783×10^{-3}	2.3766×10^{-3}	2.2802×10^{-3}
Phase (Degrees)	48.582	47.707	64.283	84.025	87.414
Small Handles					
X-Direction					
X/F (in/lbs)	2.5001×10^{-2}	1.9053×10^{-2}	1.3930×10^{-2}	9.5710×10^{-3}	5.8608×10^{-3}
Phase (Degrees)	48.905	46.905	39.795	31.887	26.972
Y-Direction					
X/F (in/lbs)	1.5451×10^{-2}	1.1667×10^{-2}	9.2673×10^{-3}	7.0625×10^{-3}	5.4948×10^{-3}
Phase (Degrees)	52.975	63.396	69.498	73.112	80.407
Z-Direction					
X/F (in/lbs)	1.0470×10^{-2}	6.2224×10^{-3}	3.5888×10^{-3}	2.7288×10^{-3}	2.3602×10^{-3}
Phase (Degrees)	46.988	48.782	62.628	81.374	95. 031

TABLE B-2
(continued)

Center Frequencies	63	80	100	125	160
Large Handles					
X-Direction					
X/F (in/lbs)	1.9363×10^{-3}	1.1428×10^{-3}	8.9527×10^{-4}	7.7438×10^{-4}	6.5909×10^{-4}
Phase (Degrees)	39.070	56.219	70.444	75.048	75.930
Y-Direction					
X/F (in/lbs)	4.1971×10^{-3}	3.5888×10^{-4}	2.6482×10^{-3}	2.0089×10^{-3}	1.5957×10^{-3}
Phase (Degrees)	93.908	87.349	86.877	89.559	89.187
Z-Direction					
X/F (in/lbs)	1.9406×10^{-3}	1.7497×10^{-3}	1.6216×10^{-3}	1.3151×10^{-3}	8.9115×10^{-4}
Phase (Degrees)	89.194	91.248	83.323	69.417	57.422
Small Handles					
X-Direction					
X/F (in/lbs)	3.4750×10^{-3}	2.0557×10^{-3}	1.3802×10^{-3}	9.7265×10^{-4}	6.9334×10^{-4}
Phase (Degrees)	29.788	40.176	48.540	57.426	68.326
Y-Direction					
X/F (in/lbs)	4.4766×10^{-3}	3.8543×10^{-3}	3.0900×10^{-3}	2.4432×10^{-3}	1.9632×10^{-3}
Phase (Degrees)	89.857	89.937	91.518	94.232	96.188
Z-Direction					
X/F (in/lbs)	2.3064×10^{-3}	2.5701×10^{-3}	2.4488×10^{-3}	1.9229×10^{-3}	1.2559×10^{-3}
Phase (Degrees)	109.45	109.44	93.010	75.510	65.209

TABLE B-2
(continued)

Center Frequencies	200	250	315	400	500
Large Handles					
X-Direction					
X/F (in/lbs)	5.6099×10^{-4}	4.5284×10^{-4}	3.1185×10^{-4}	2.0228×10^{-4}	1.3676×10^{-4}
Phase (Degrees)	70.847	63.696	58.502	59.298	61.296
Y-Direction					
X/F (in/lbs)	1.3151×10^{-3}	1.0350×10^{-3}	7.6200×10^{-4}	6.1653×10^{-4}	4.4458×10^{-4}
Phase (Degrees)	84.479	80.982	80.471	73.354	62.843
Z-Direction					
X/F (in/lbs)	5.5074×10^{-4}	3.4990×10^{-4}	2.4152×10^{-4}	1.9096×10^{-4}	1.5239×10^{-4}
Phase (Degrees)	55.272	62.693	69.906	73.282	71.525
Small Handles					
X-Direction					
X/F (in/lbs)	5.3698×10^{-4}	4.3747×10^{-4}	3.5971×10^{-4}	2.9172×10^{-4}	2.2644×10^{-4}
Phase (Degrees)	75.792	81.288	83.367	82.090	79.575
Y-Direction					
X/F (in/lbs)	1.6031×10^{-3}	1.3395×10^{-3}	1.1401×10^{-3}	9.6372×10^{-4}	7.3444×10^{-4}
Phase (Degrees)	96.173	96.468	93.250	84.670	74.565
Z-Direction					
X/F (in/lbs)	7.7438×10^{-4}	4.9539×10^{-4}	3.4510×10^{-4}	2.8310×10^{-4}	2.3225×10^{-4}
Phase (Degrees)	64.554	71.631	81.077	85.513	83.928

TABLE B-2
(continued)

Center Frequencies	630	800	1000
Large Handles			
X-Direction			
X/F (in/lbs)	9.0147×10^{-5}	5.8473×10^{-5}	5.1994×10^{-5}
Phase (Degrees)	62.873	67.241	68.883
Y-Direction			
X/F (in/lbs)	2.7666×10^{-4}	1.7059×10^{-4}	1.0185×10^{-4}
Phase (Degrees)	53.355	45.739	31.359
Z-Direction			
X/F (in/lbs)	1.1245×10^{-4}	7.7259×10^{-5}	5.9014×10^{-5}
Phase (Degrees)	67.530	65.987	53.735
Small Handles			
X-Direction			
X/F (in/lbs)	1.7059×10^{-4}	1.1802×10^{-4}	7.5155×10^{-5}
Phase (Degrees)	73.562	62.307	49.263
Y-Direction			
X/F (in/lbs)	4.9425×10^{-4}	3.2281×10^{-4}	2.2696×10^{-4}
Phase (Degrees)	67.269	60.063	48.917
Z-Direction			
X/F (in/lbs)	1.8878×10^{-4}	1.3676×10^{-4}	8.6886×10^{-5}
Phase (Degrees)	76.015	60.414	42.559

APPENDIX C

CHIPPING HAMMER AND GRINDER ACCELERATION DATA PLOTS

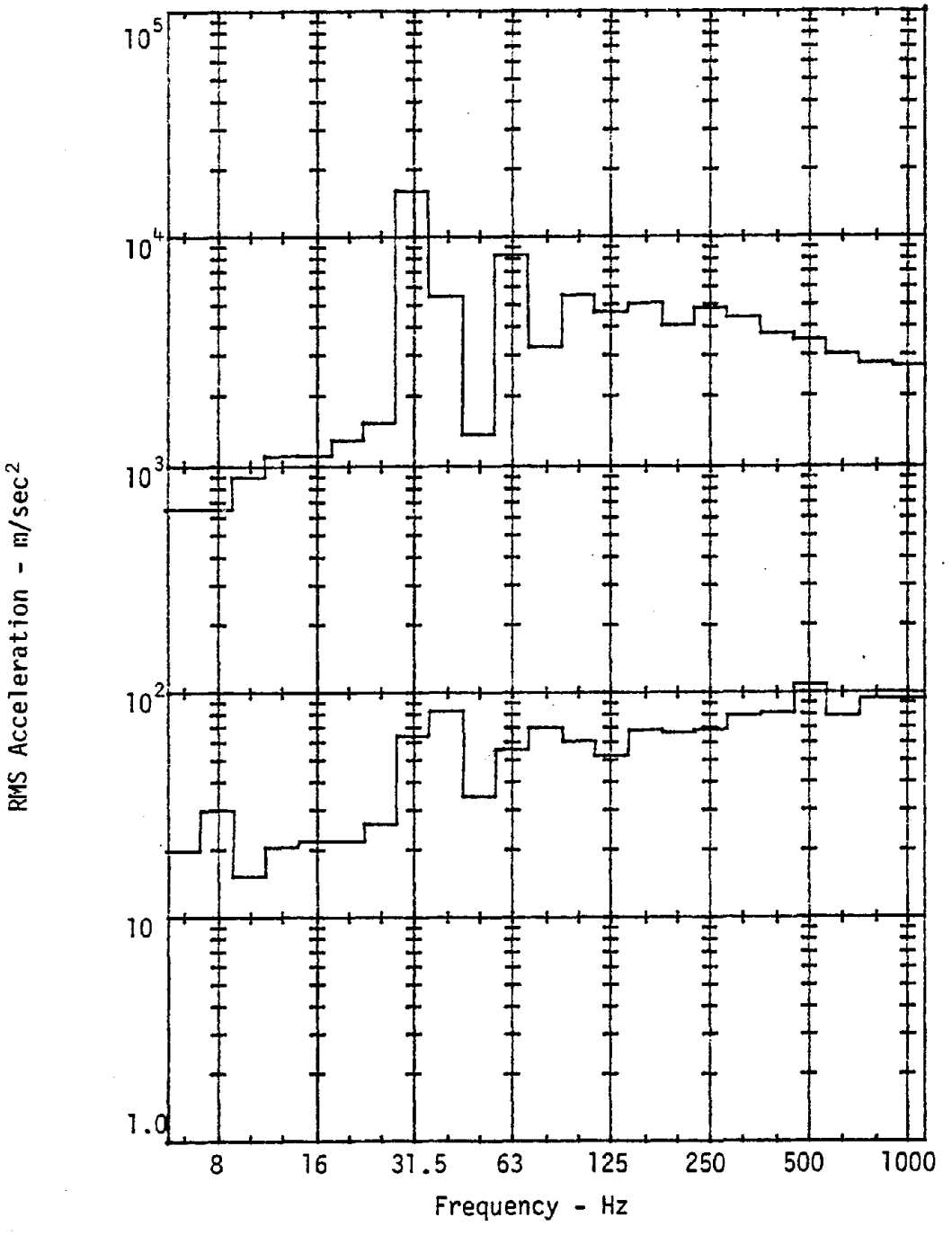

Figure C-1. RMS acceleration levels for chipping hammer A used to clean castings. Slot chipping on nodular cast iron. Top - chisel. Bottom - handle. Chipping hammer operated at full throttle.

Preceding page blank

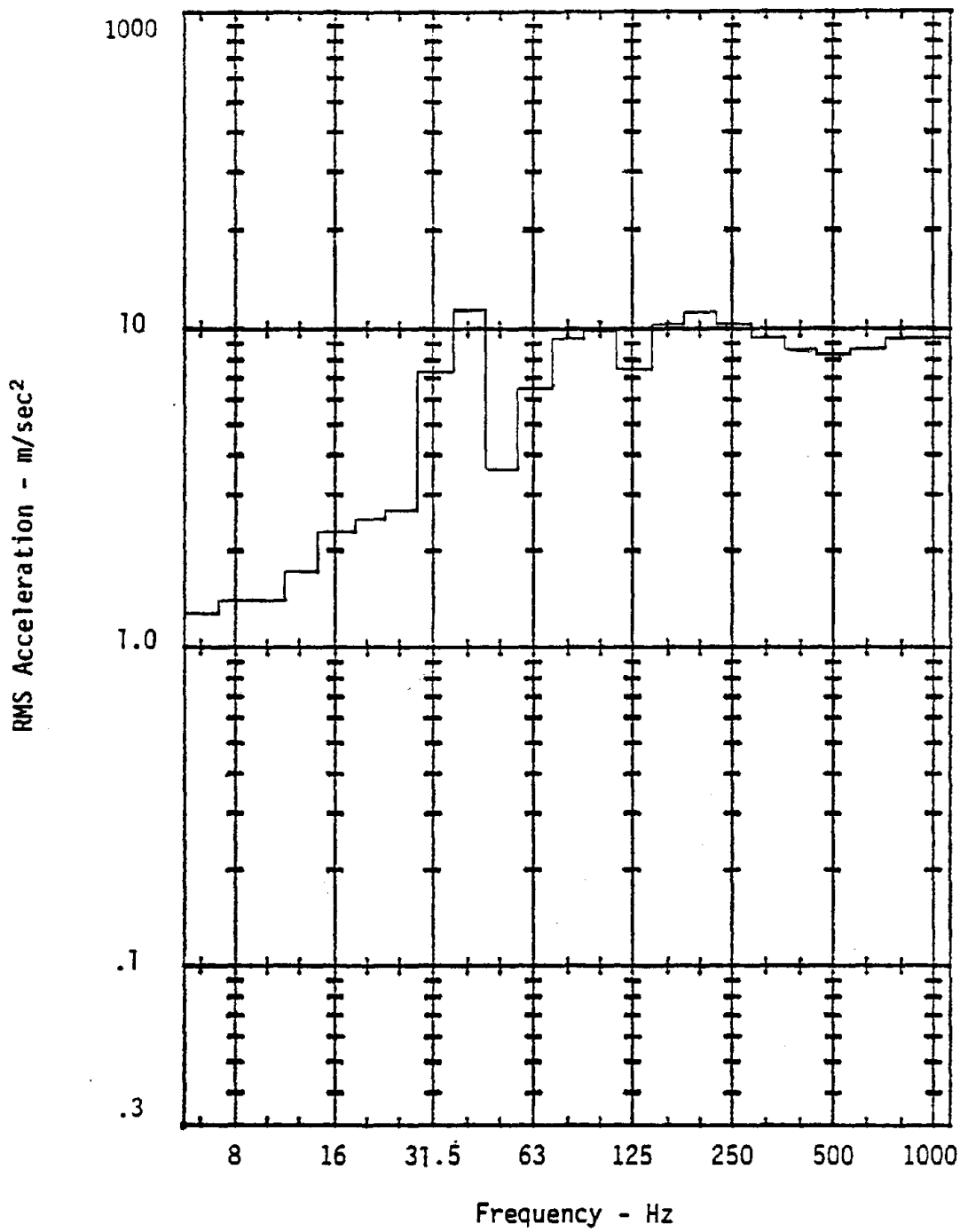

Figure C-2. RMS acceleration levels for handle of chipping hammer B used to clean castings. Slot chipping on nodular cast iron. Chipping hammer operated at full throttle.

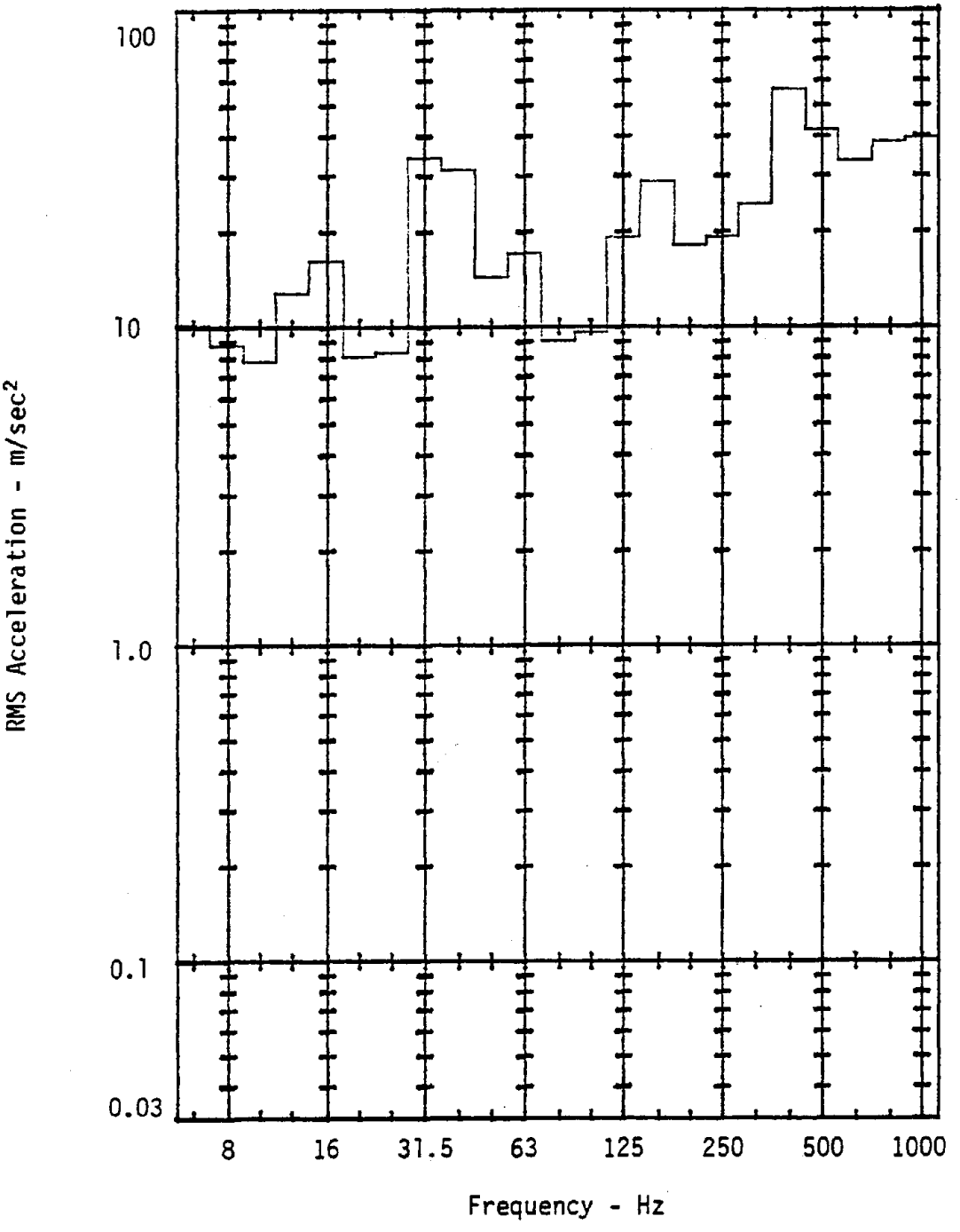

Figure C-3. RMS acceleration levels on handle of chipping hammer C used to clean castings. Slot chipping on nodular cast iron. Chipping hammer operated at full throttle.

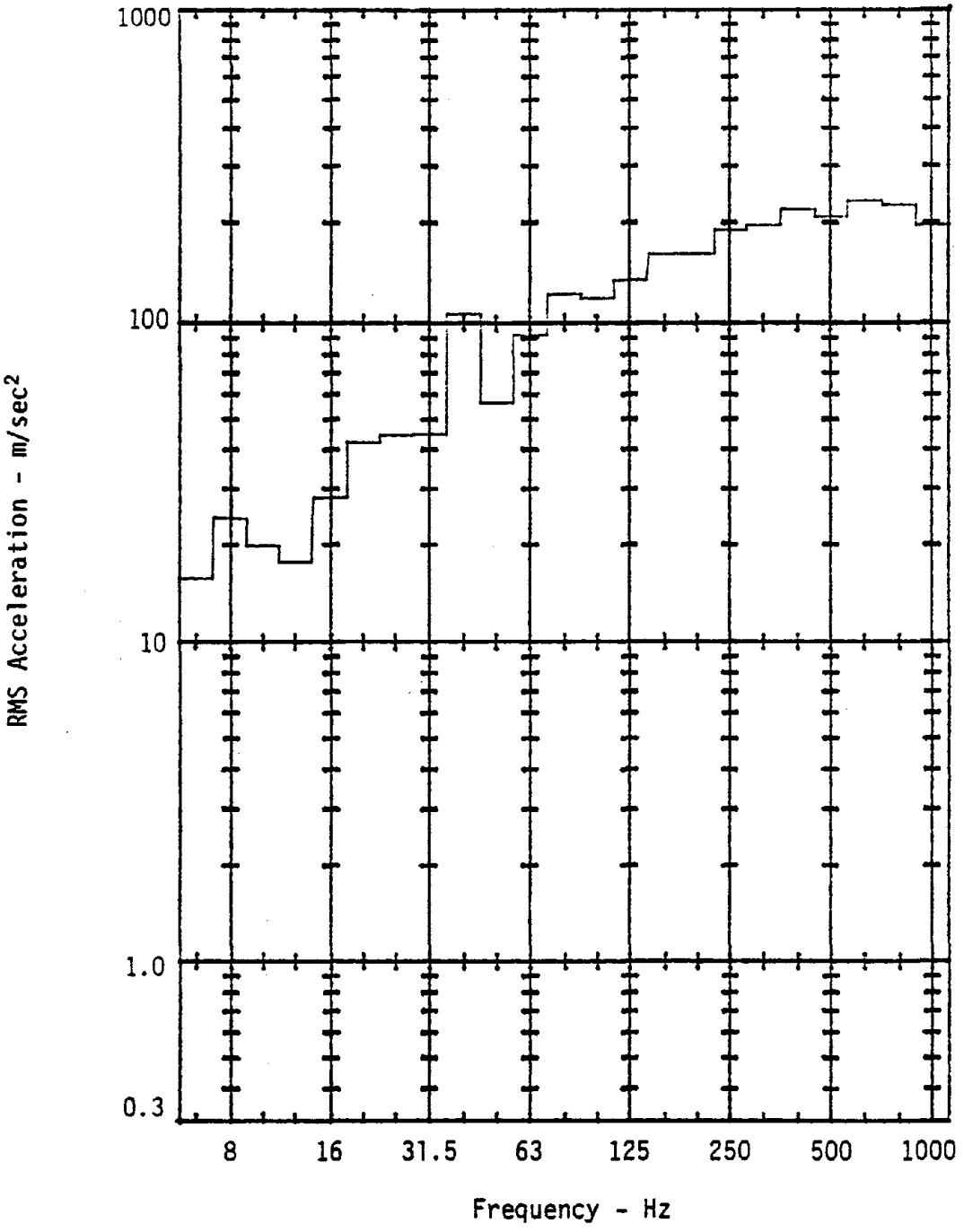

Figure C-4. RMS acceleration levels on handle of chipping hammer D used to shape propeller blades. Slot chipping on cast iron. Chipping hammer operated at full throttle.

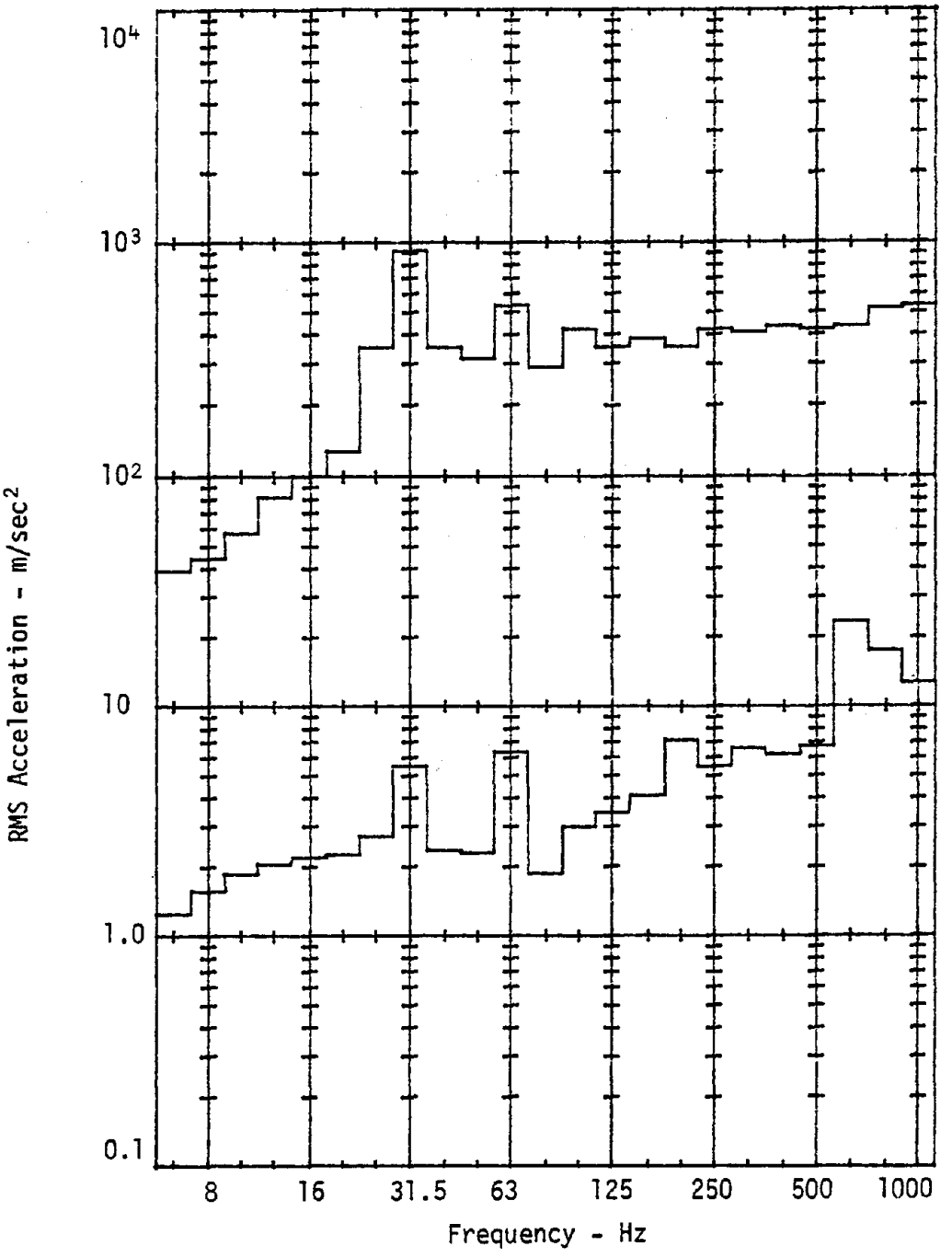

Figure C-5. RMS acceleration levels for chipping hammer D used to shape propeller blades. Chipping on Ni-Al-Br. Top - chisel. Bottom - handle. Chipping hammer operated at 1/2-3/4 throttle.

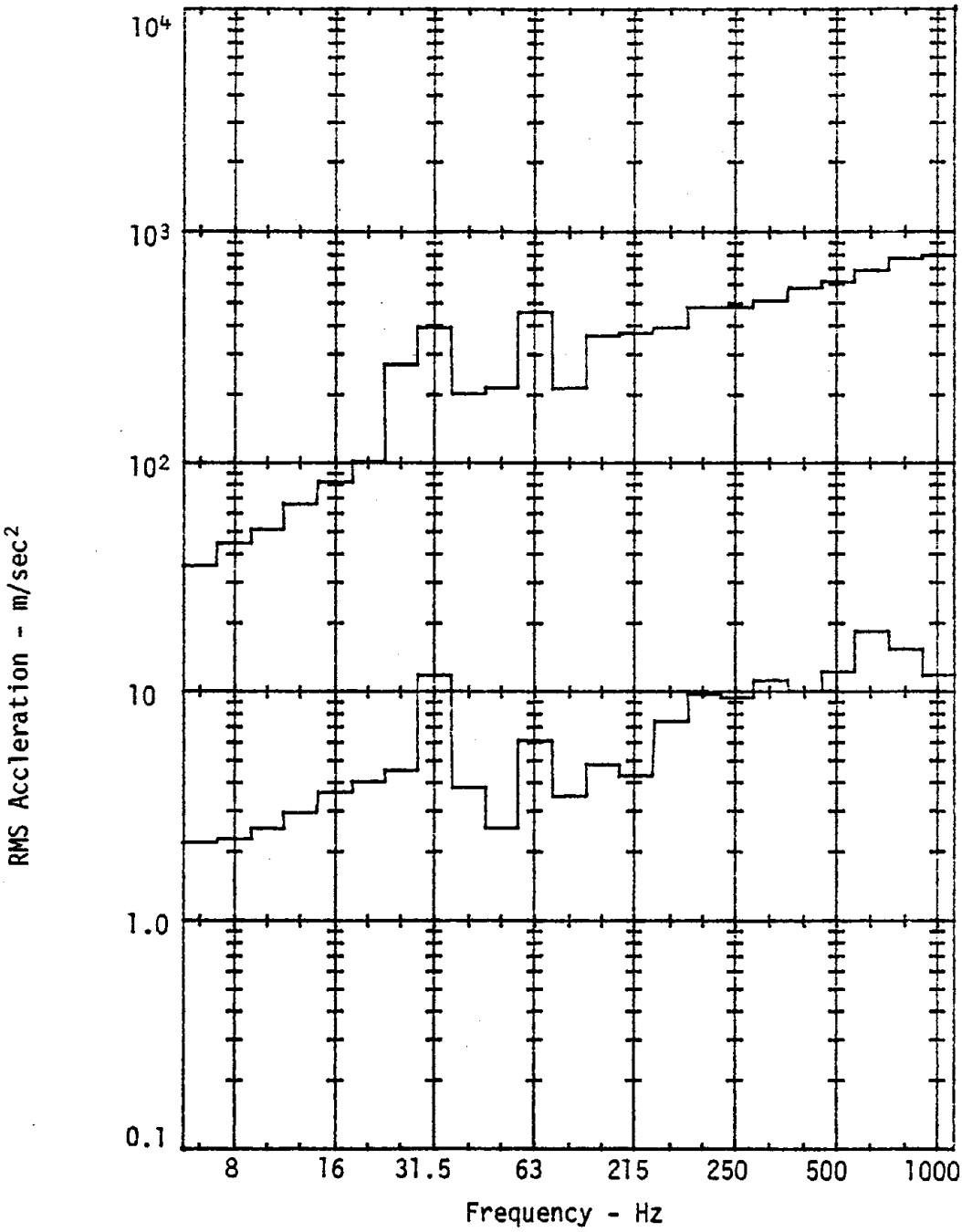

Figure C-6. RMS acceleration levels for chipping hammer D used to shape propeller blades. Chipping on mild B steel. Top - chisel. Bottom - handle. Chipping hammer operated at 1/2-3/4 throttle.

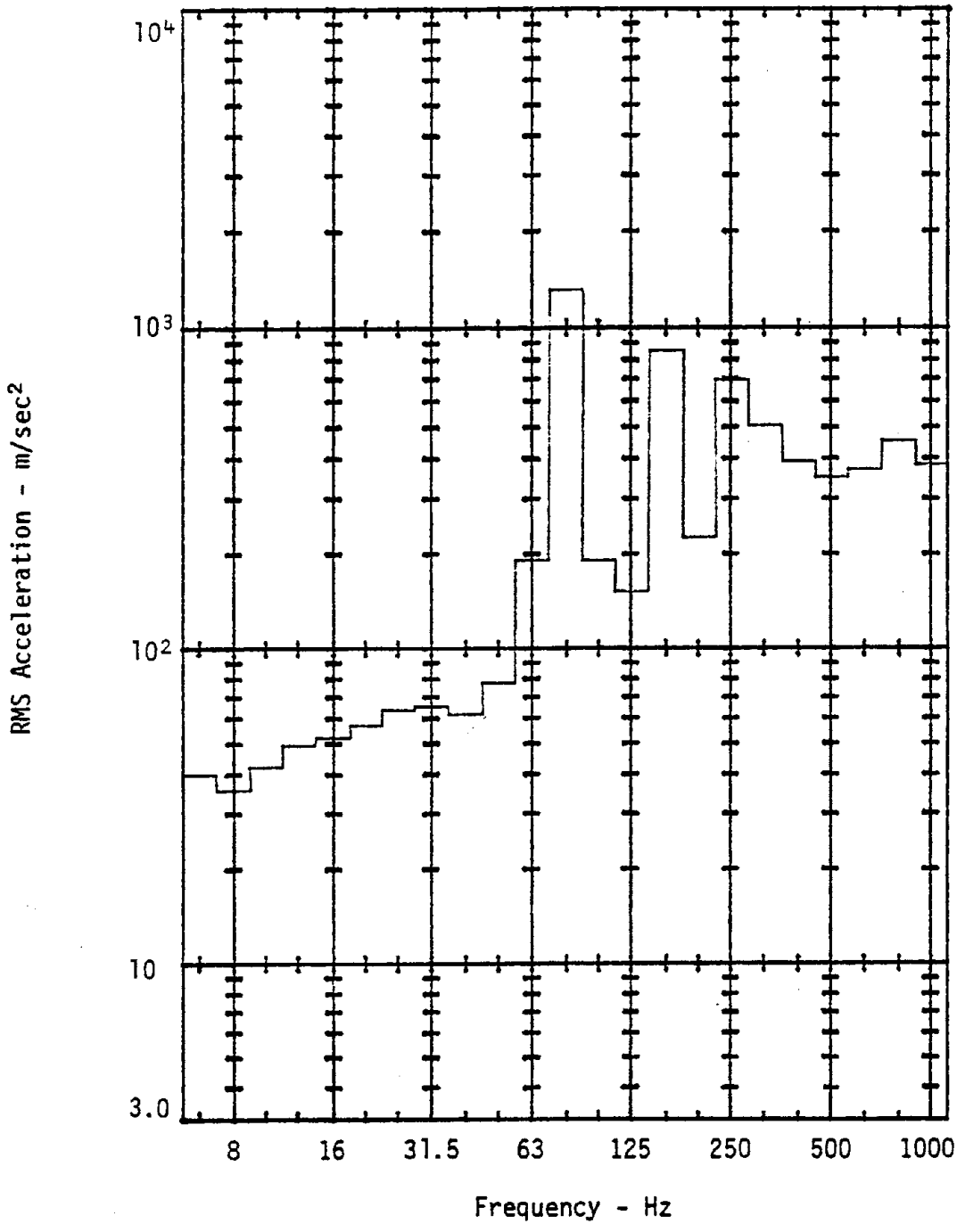

Figure C-7. RMS acceleration levels on barrel of small chipping hammer used to carve limestone. Chipping hammer operated at full throttle.

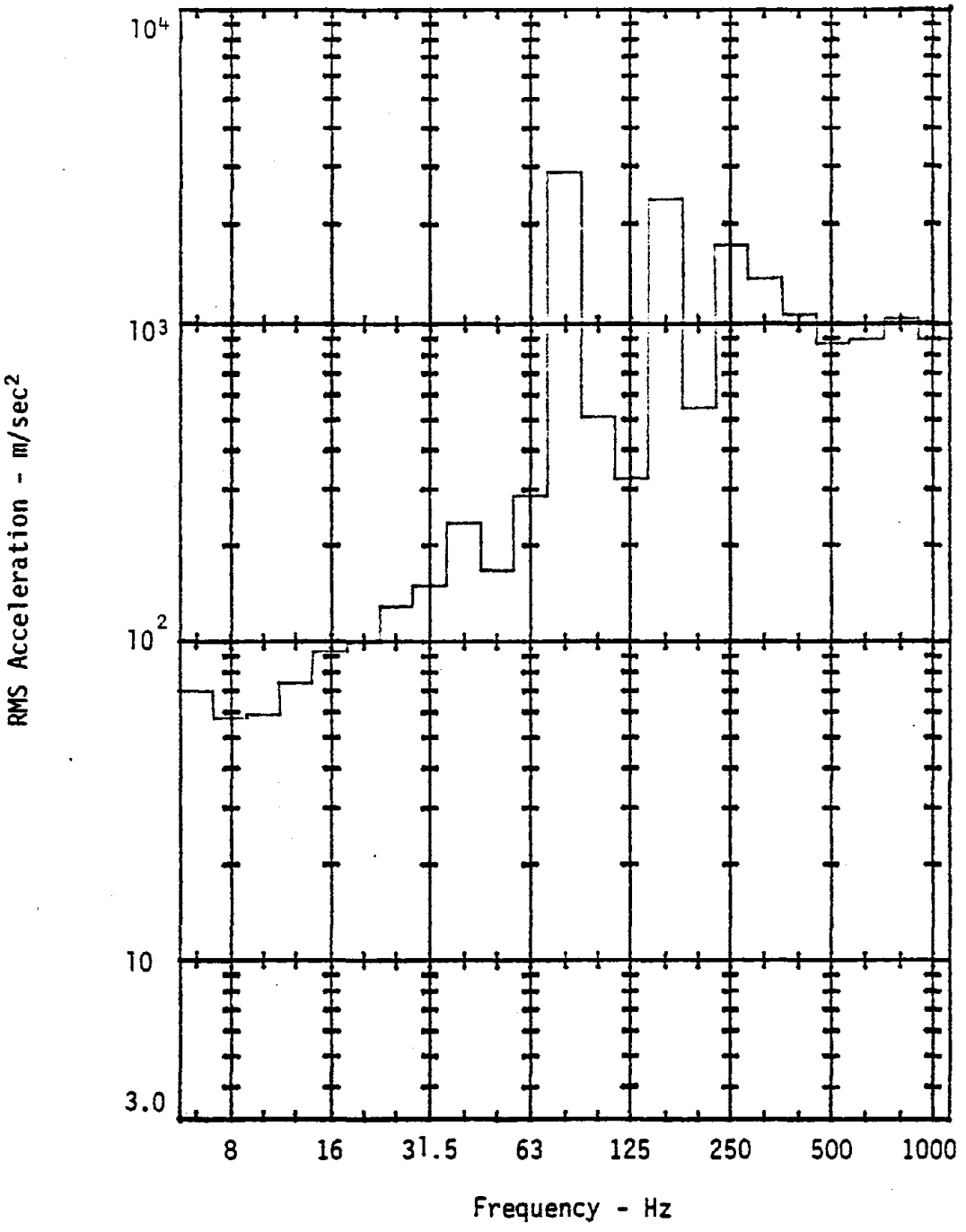

Figure C-8. RMS acceleration levels on chisel of small chipping hammer used to carve limestone. Chipping hammer operated at full throttle.

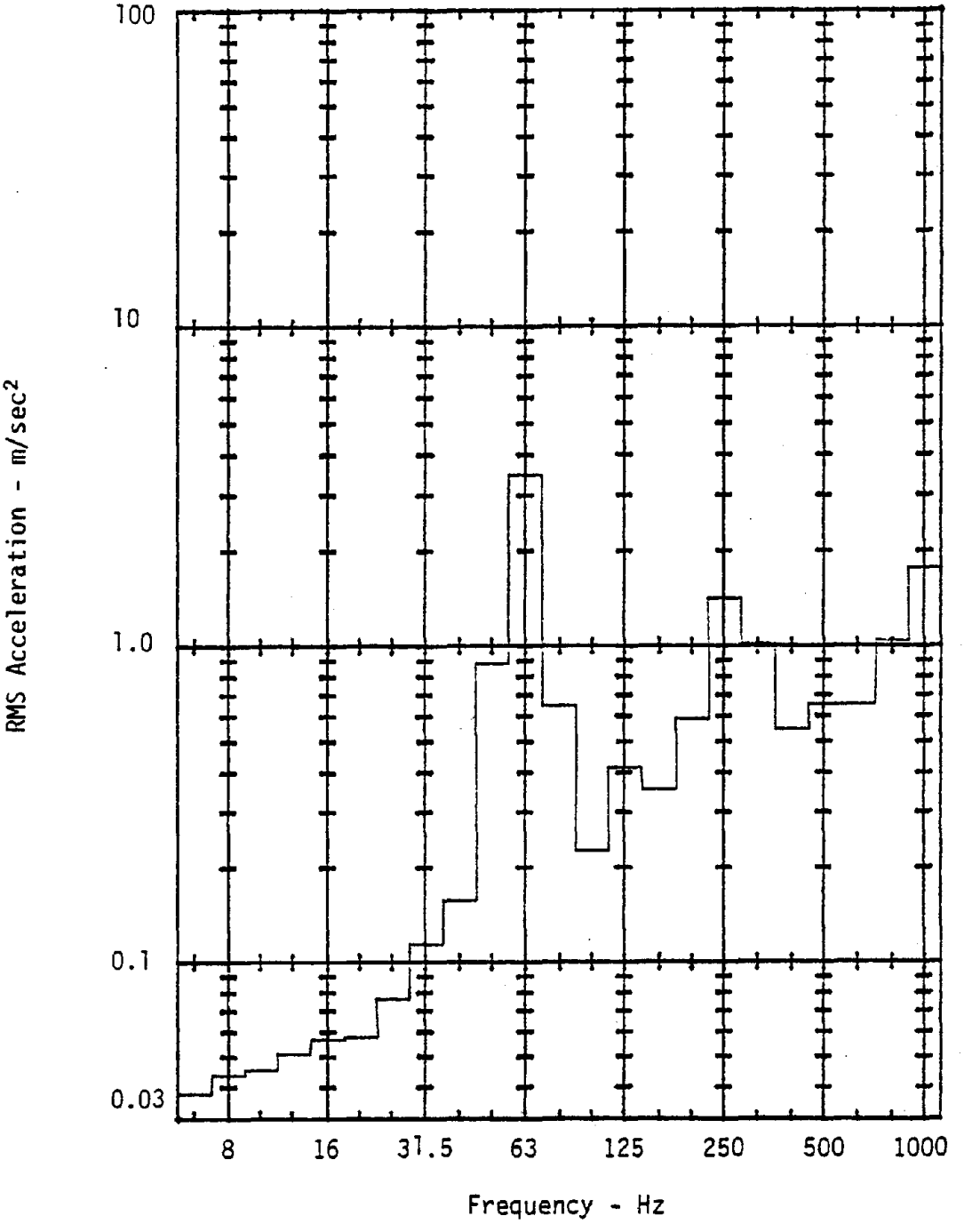

Figure C-9. RMS acceleration levels for horizontal grinder with coarse radial wheel. Right hand, X-direction.

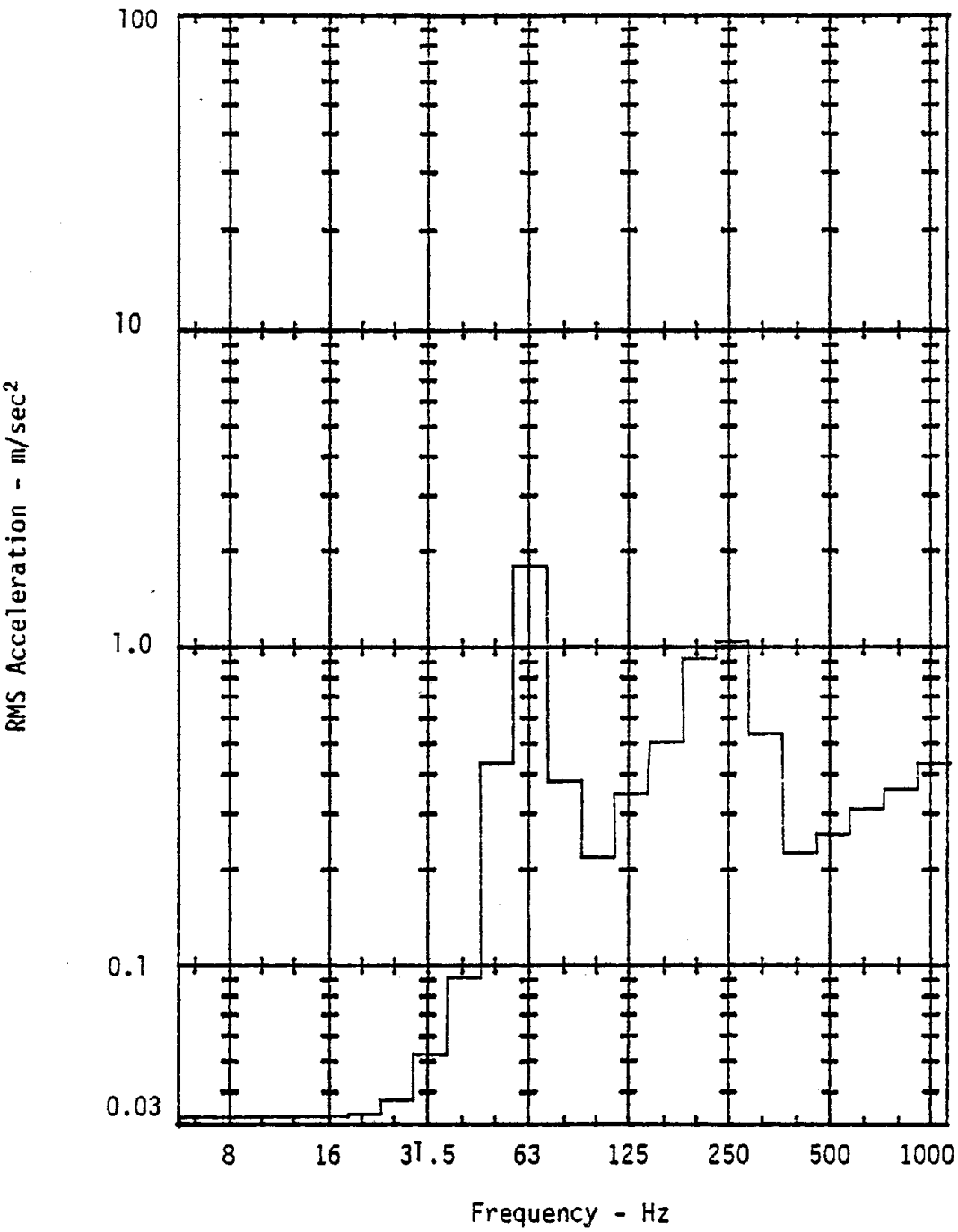

Figure C-10. RMS acceleration levels for horizontal grinder with coarse radial wheel. Right hand, Y-direction.

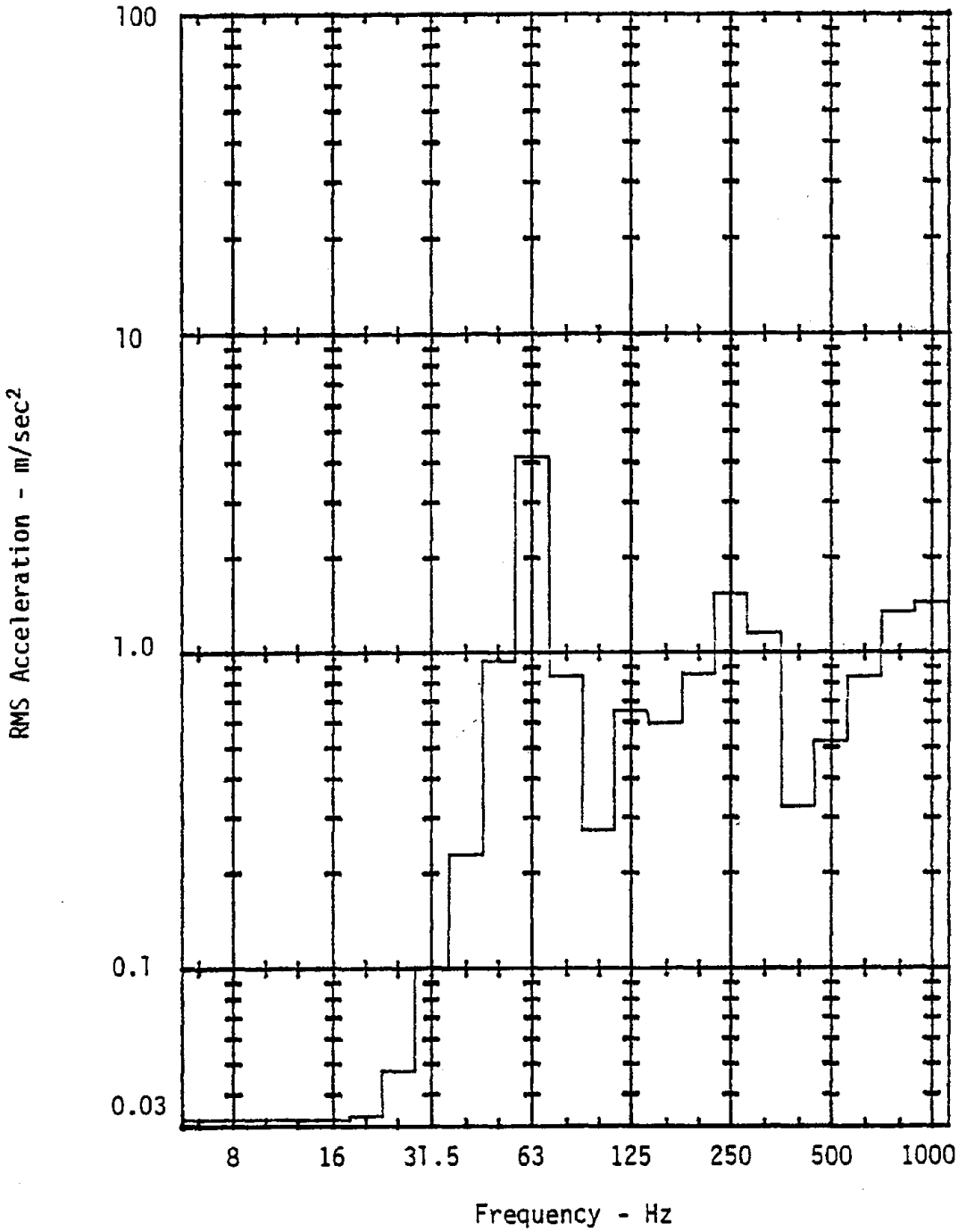

Figure C-11. RMS acceleration levels for horizontal grinder with coarse radial wheel. Right hand, Z-direction.

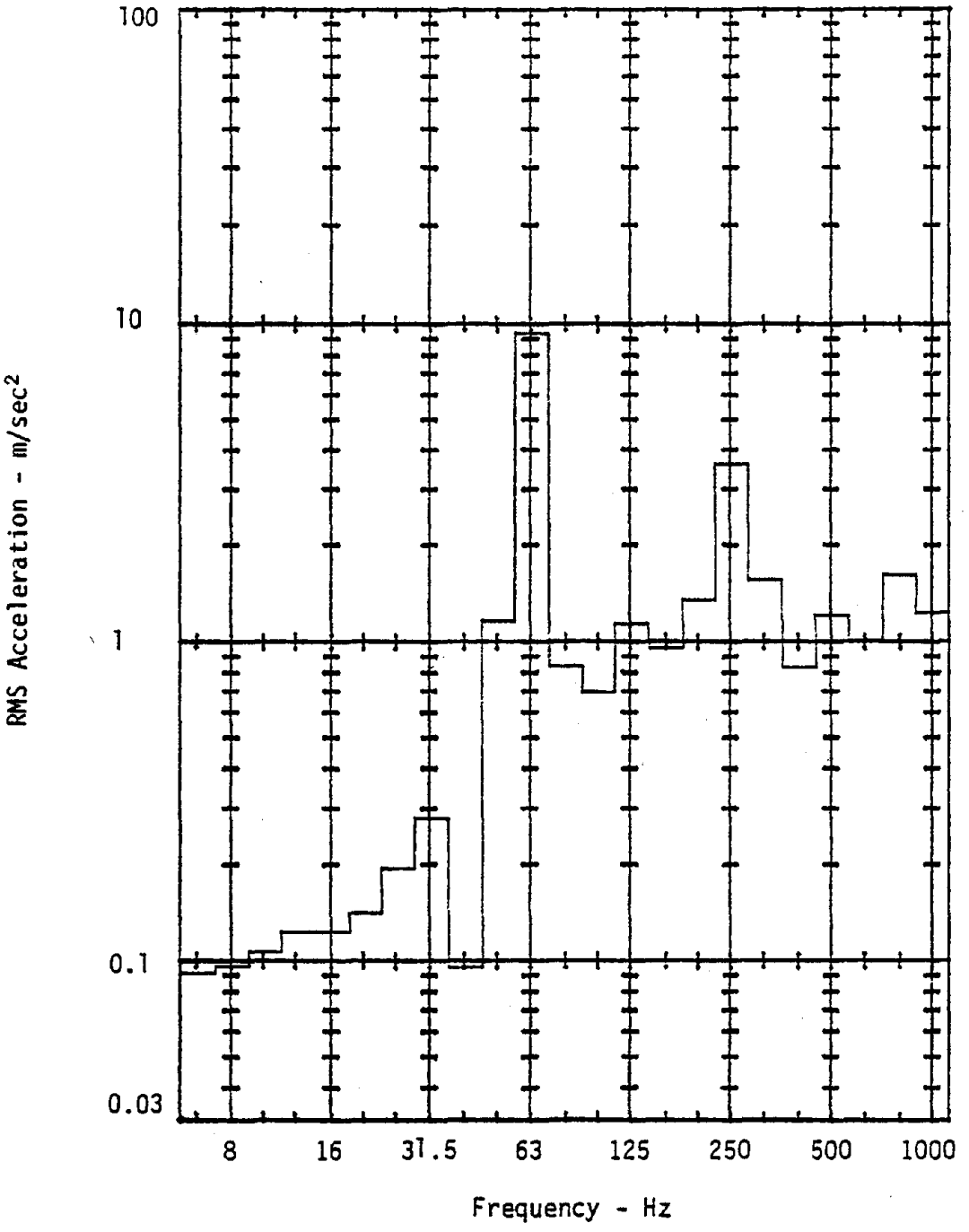

Figure C-12. RMS acceleration levels for horizontal grinder with coarse radial wheel. Left hand, X-direction.

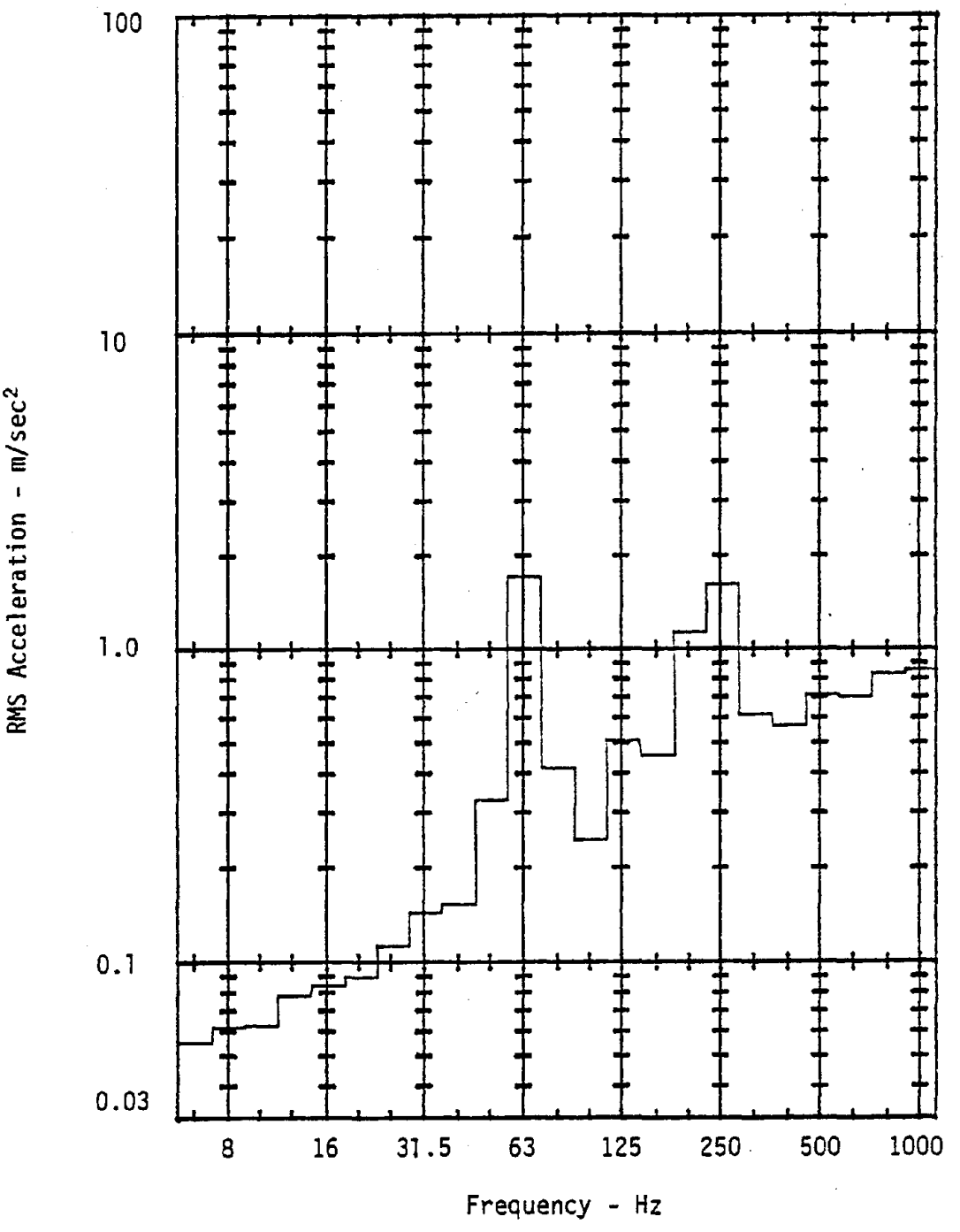

Figure C-13. RMS acceleration levels for horizontal grinder with coarse radial wheel. Left hand, Y-direction.

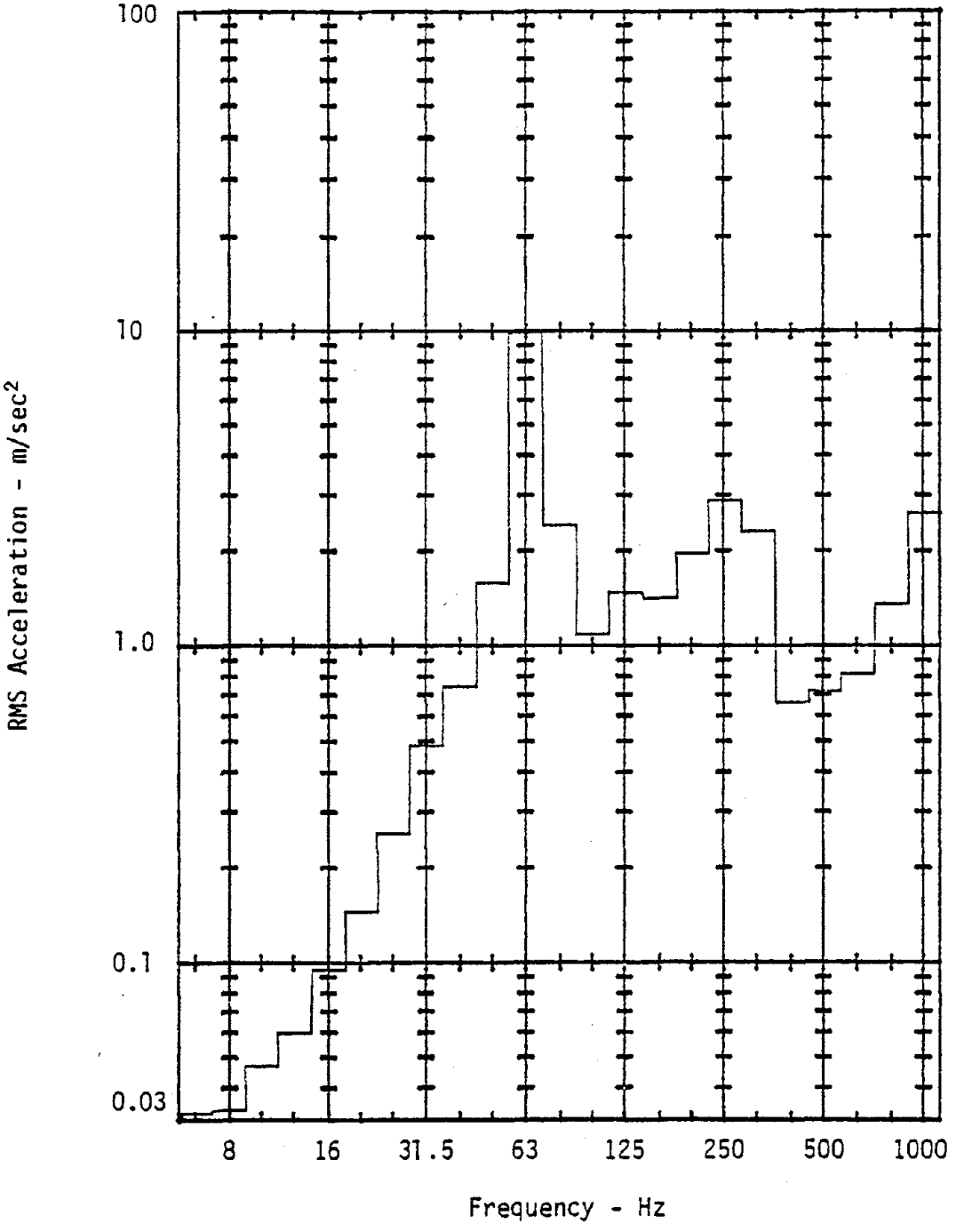

Figure C-14. RMS acceleration levels for horizontal grinder with coarse radial wheel. Left hand, Z-direction.

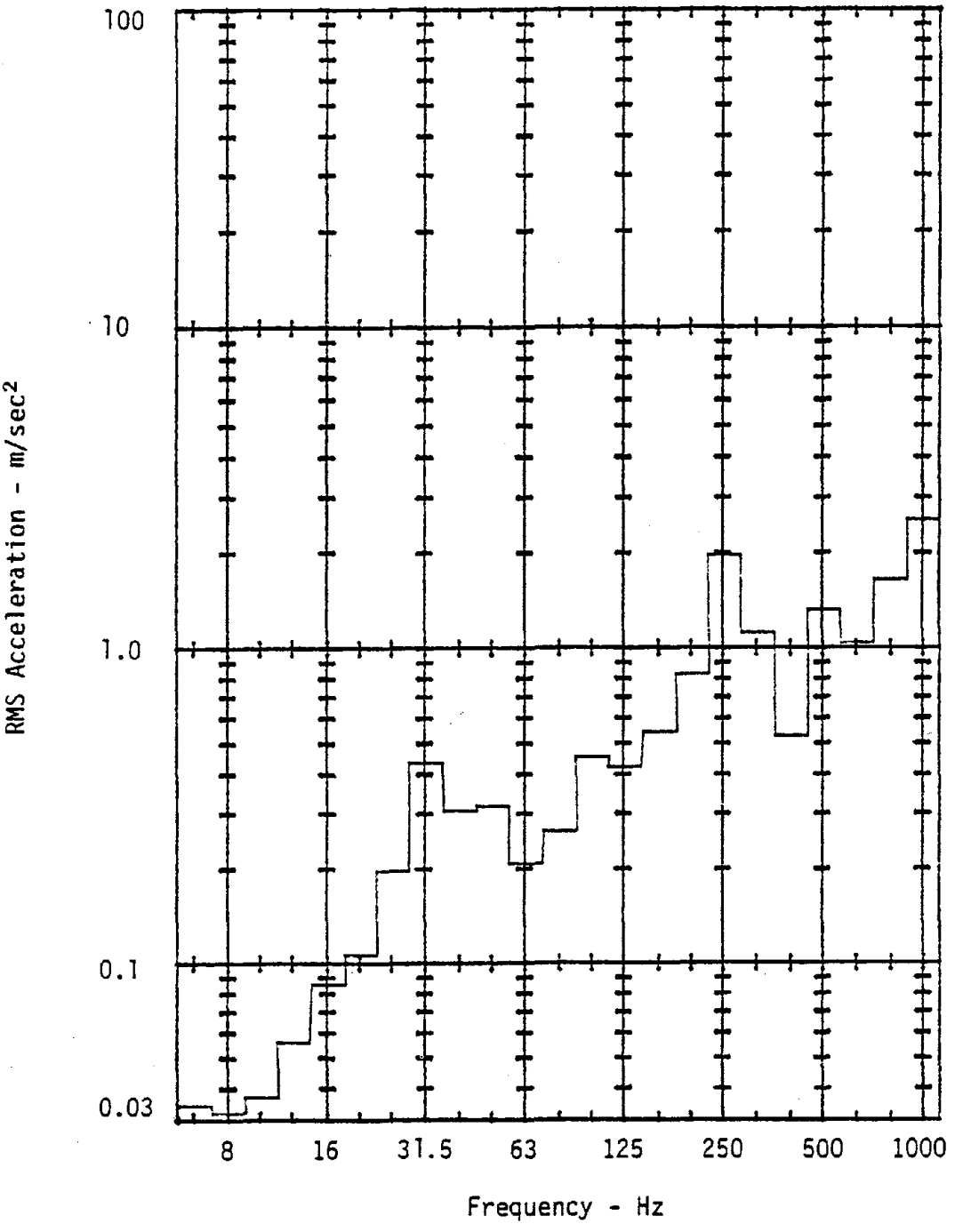

Figure C-15. RMS acceleration levels for horizontal grinder with fine radial wheel. Right hand, X-direction.

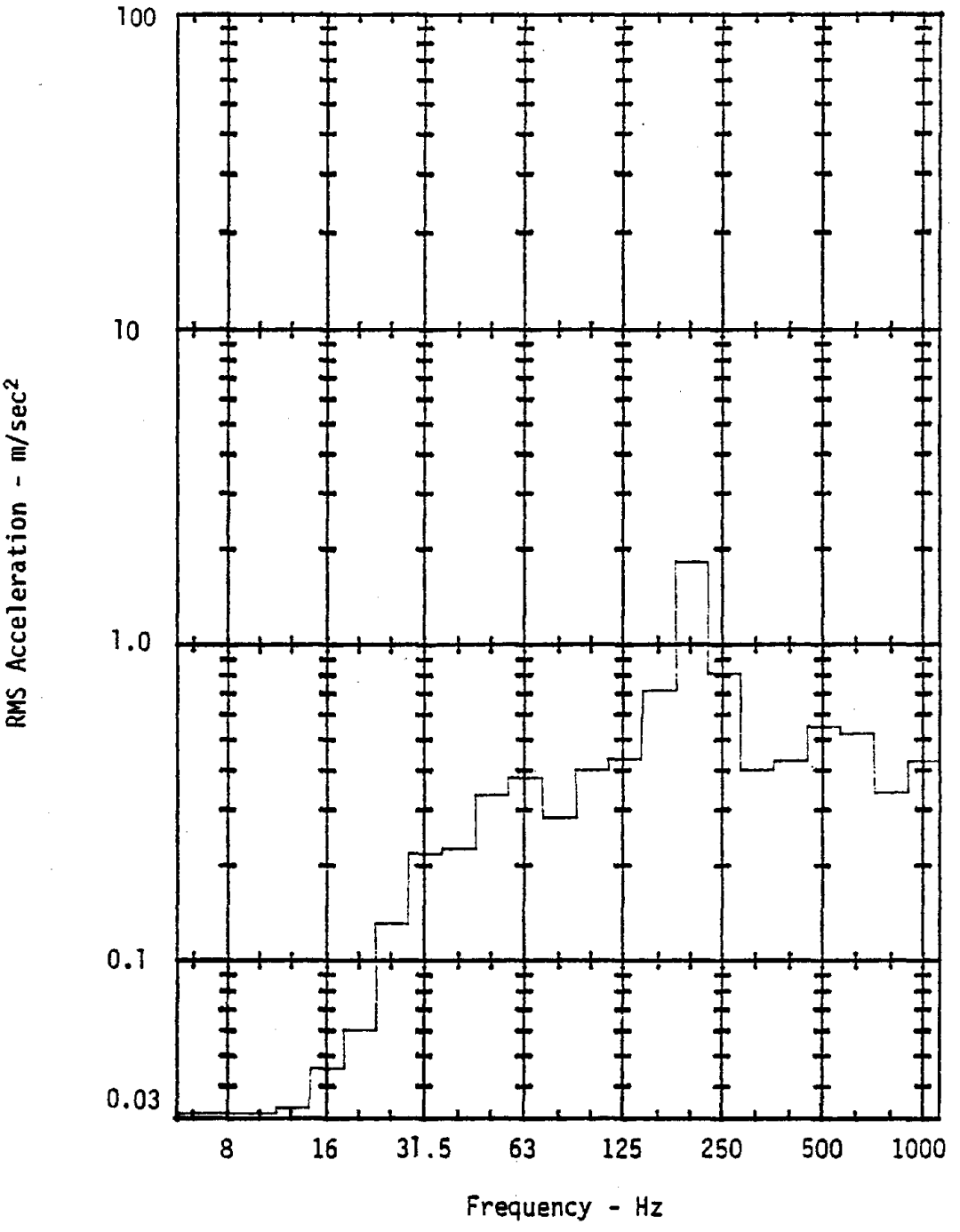

Figure C-16. RMS acceleration levels for horizontal grinder with fine radial wheel. Right hand, Y-direction.

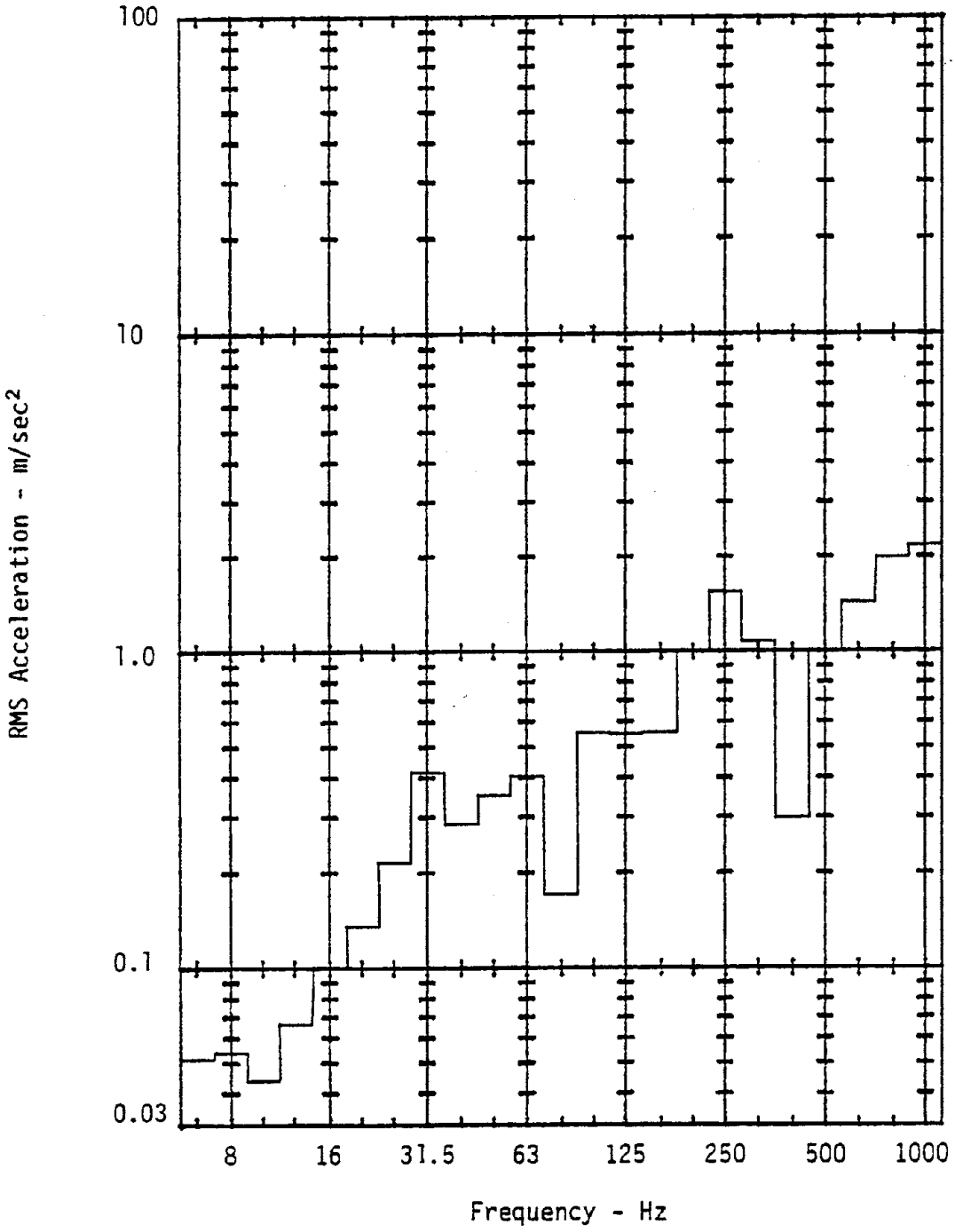

Figure C-17. RMS acceleration levels for horizontal grinder with fine radial wheel. Right hand, Z-direction.

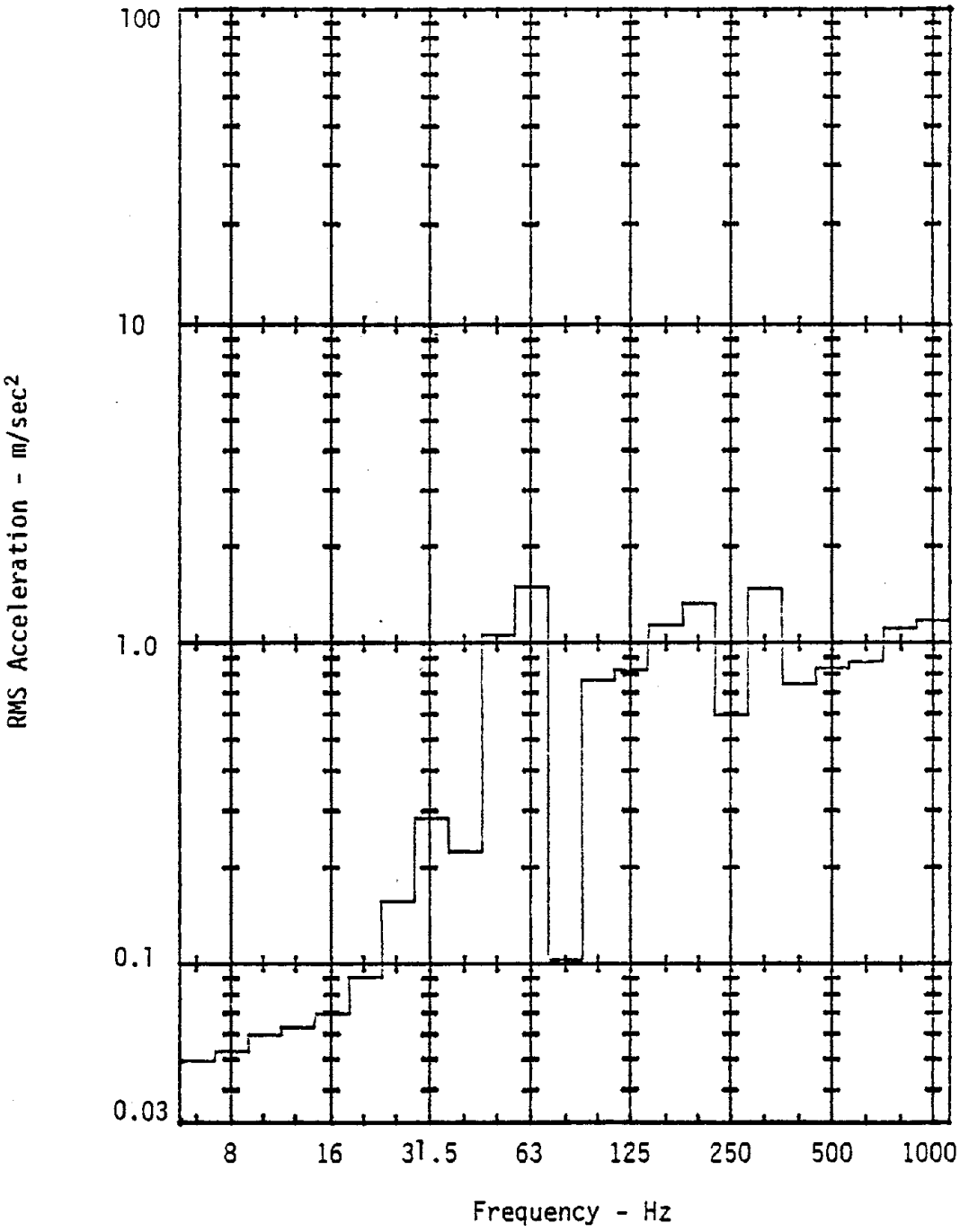

Figure C-18. RMS acceleration levels for horizontal grinder with fine radial wheel. Left hand, X-direction.

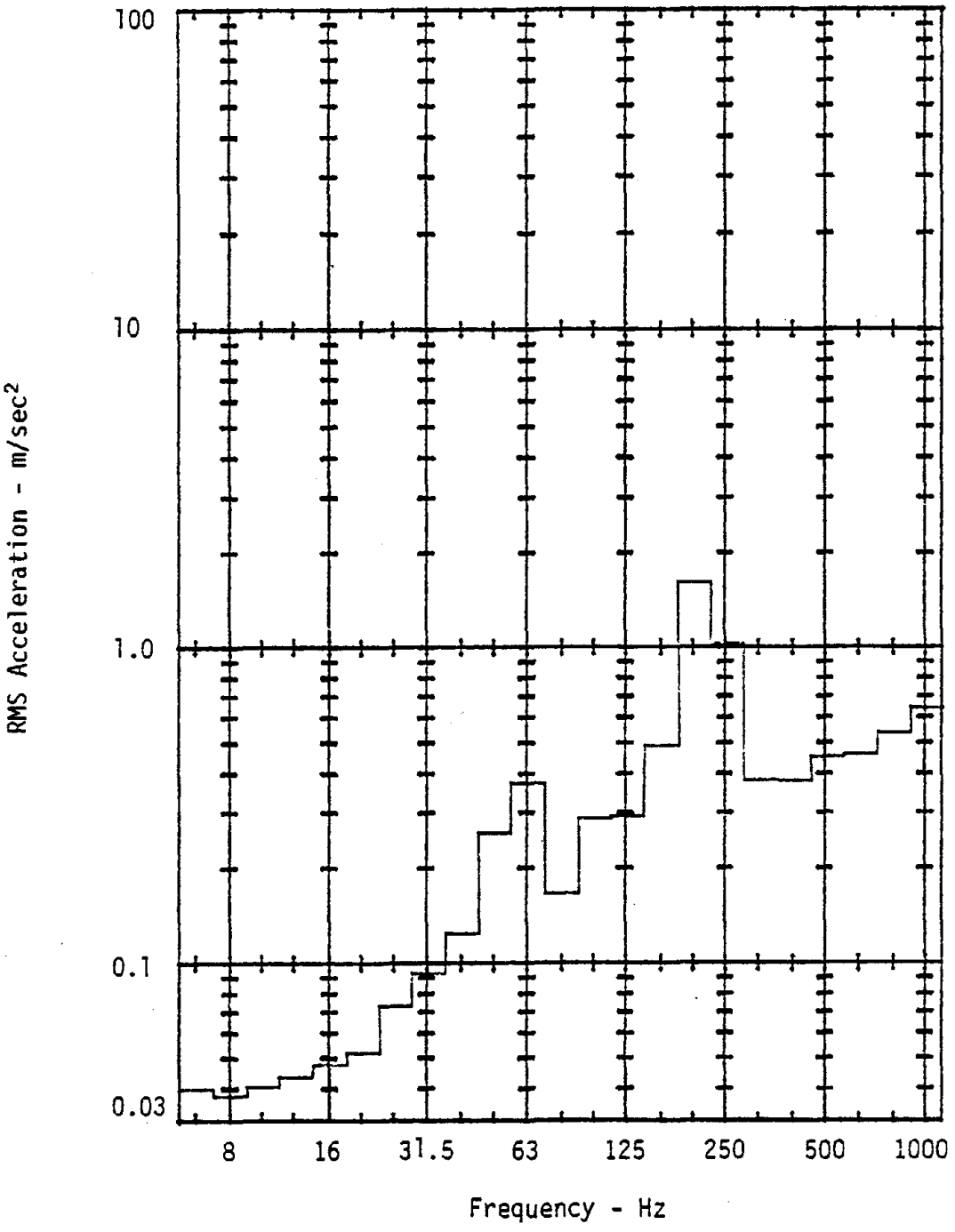

Figure C-19. RMS acceleration levels for horizontal grinder with fine radial wheel. Left hand, Y-direction.

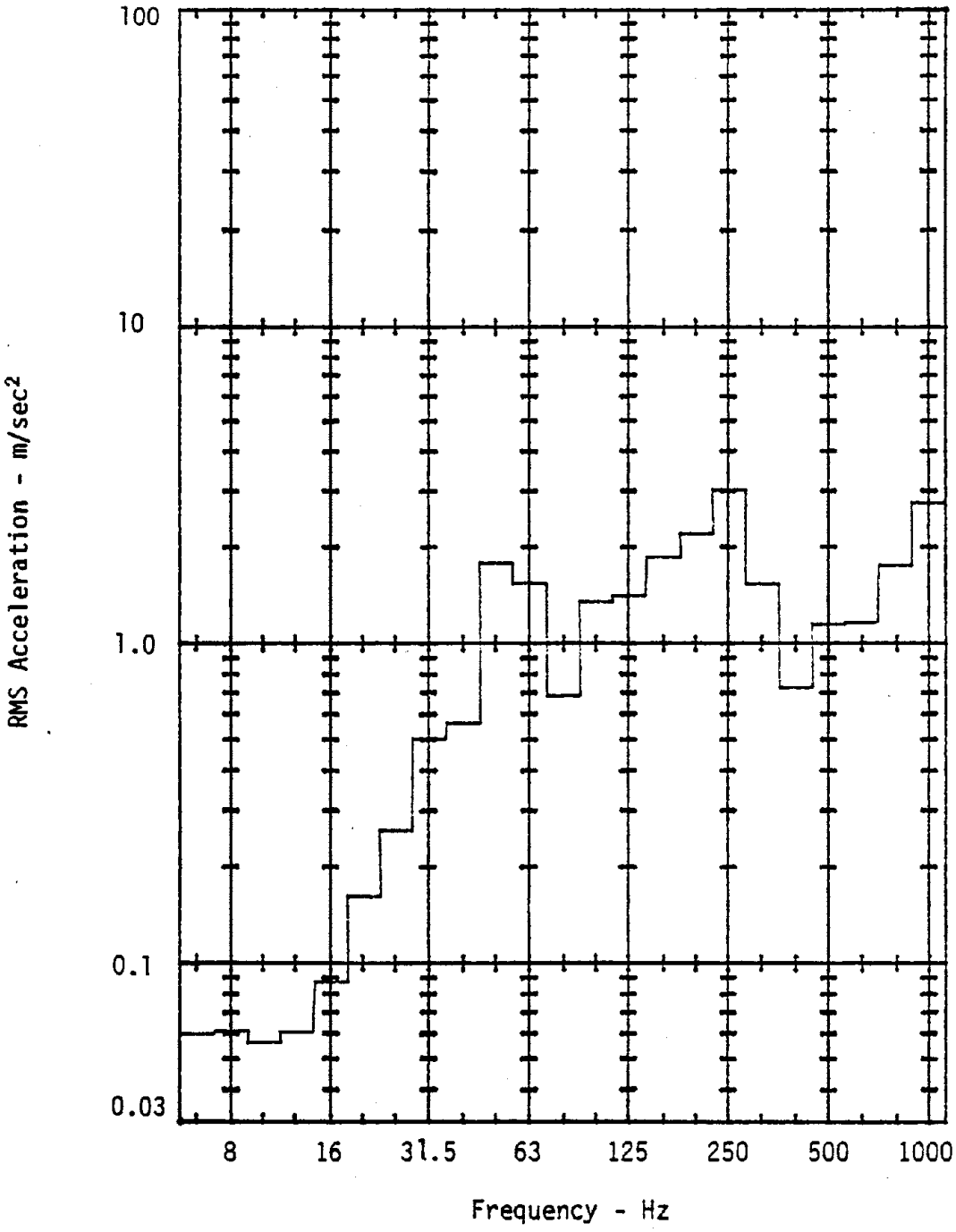

Figure C-20. RMS acceleration levels for horizontal grinder with fine radial wheel. Left hand, Z-direction.

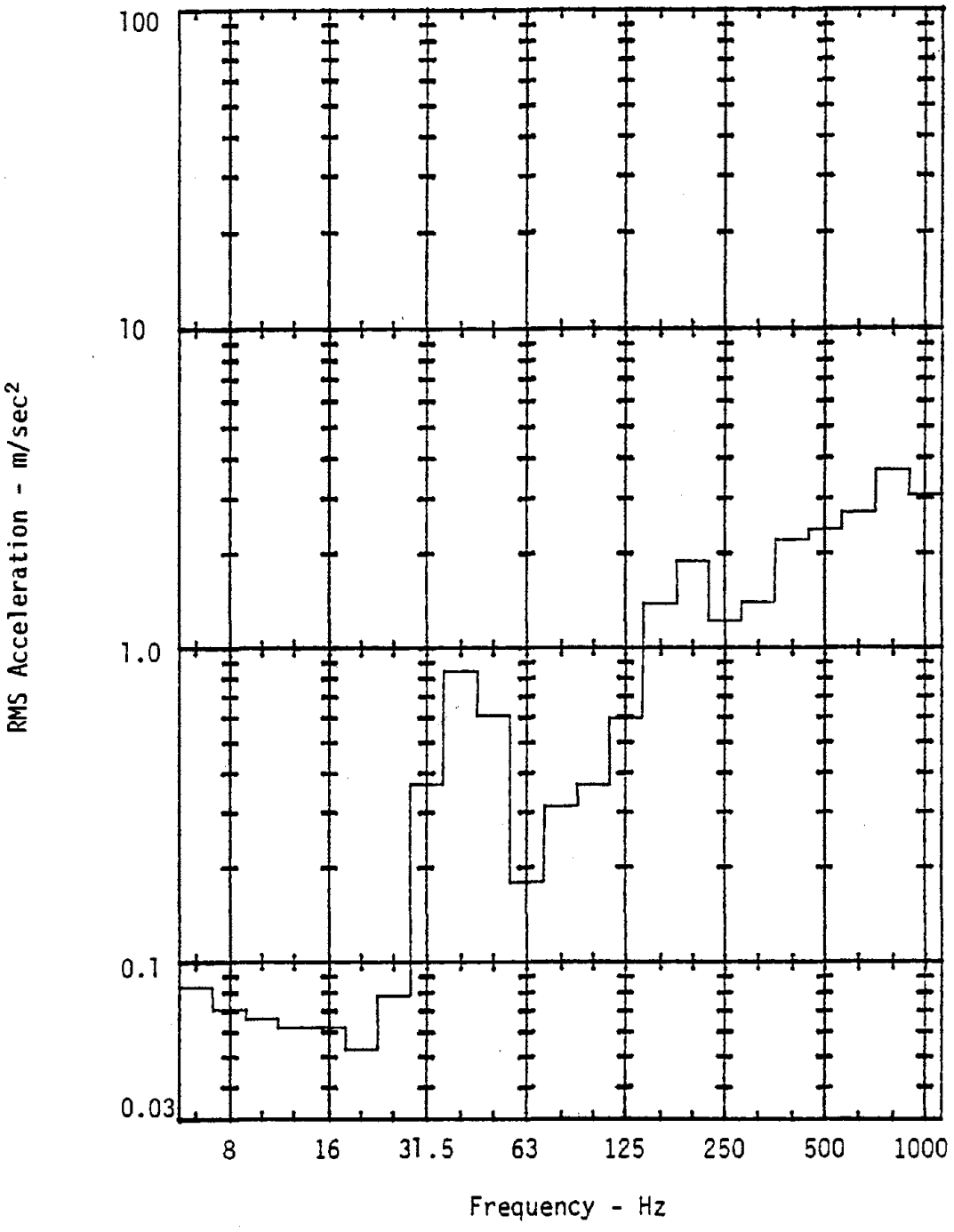

Figure C-21. RMS acceleration levels for horizontal grinder with coarse flared cup wheel. Right hand, X-direction.

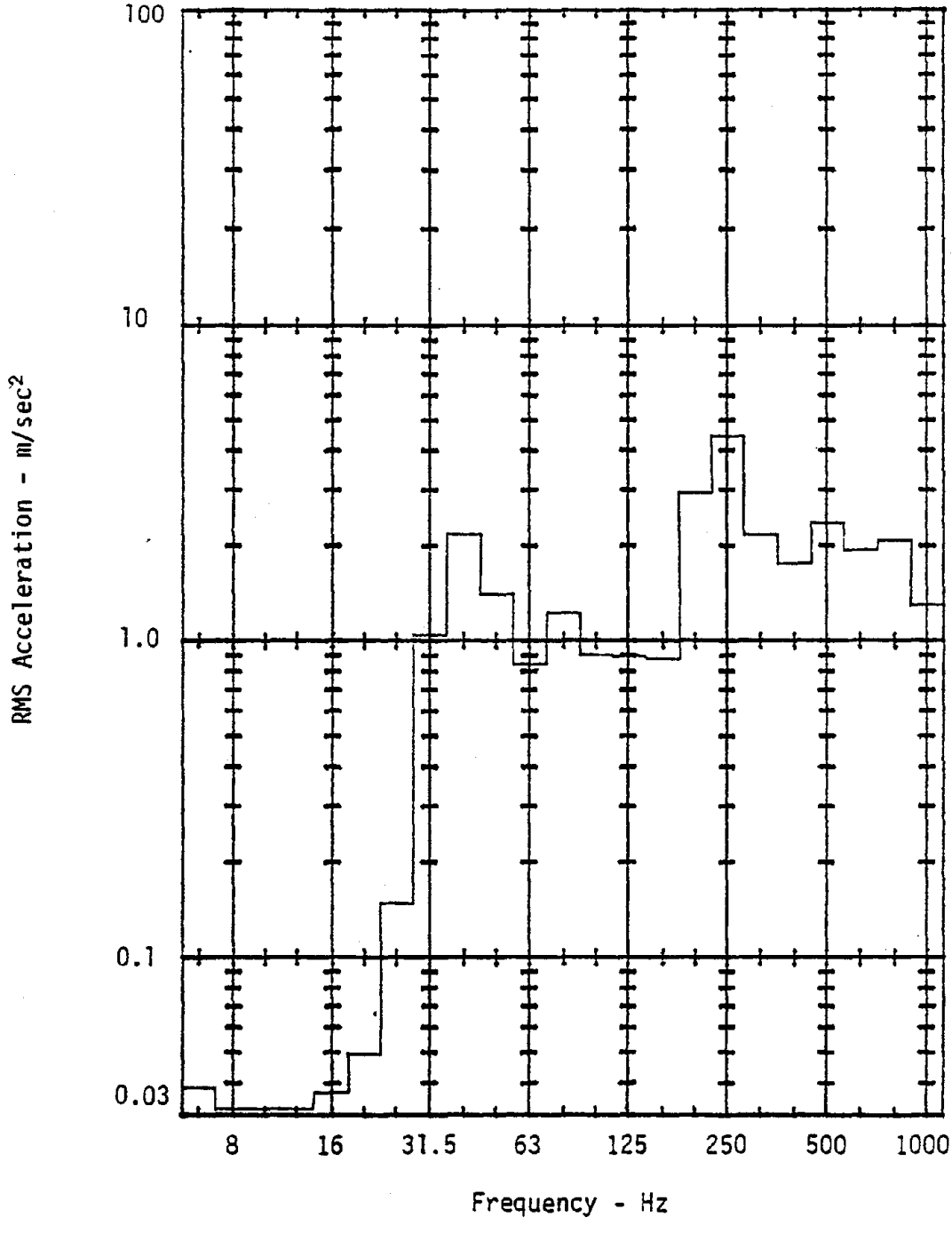

Figure C-22. RMS acceleration levels for horizontal grinder with coarse flared cup wheel. Right hand, Y-direction.

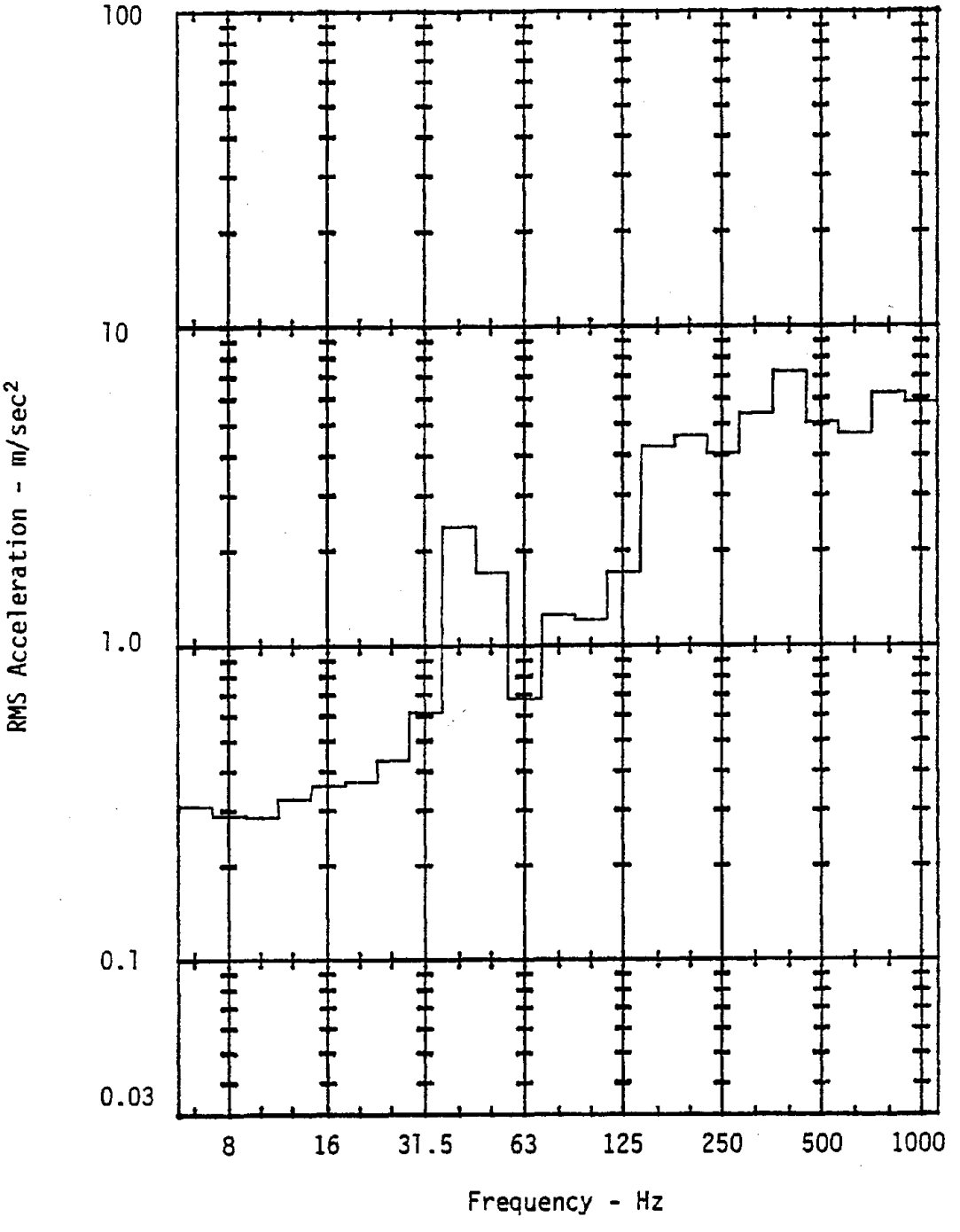

Figure C-23. RMS acceleration levels for horizontal grinder with coarse flared cup wheel. Right hand, Z-direction.

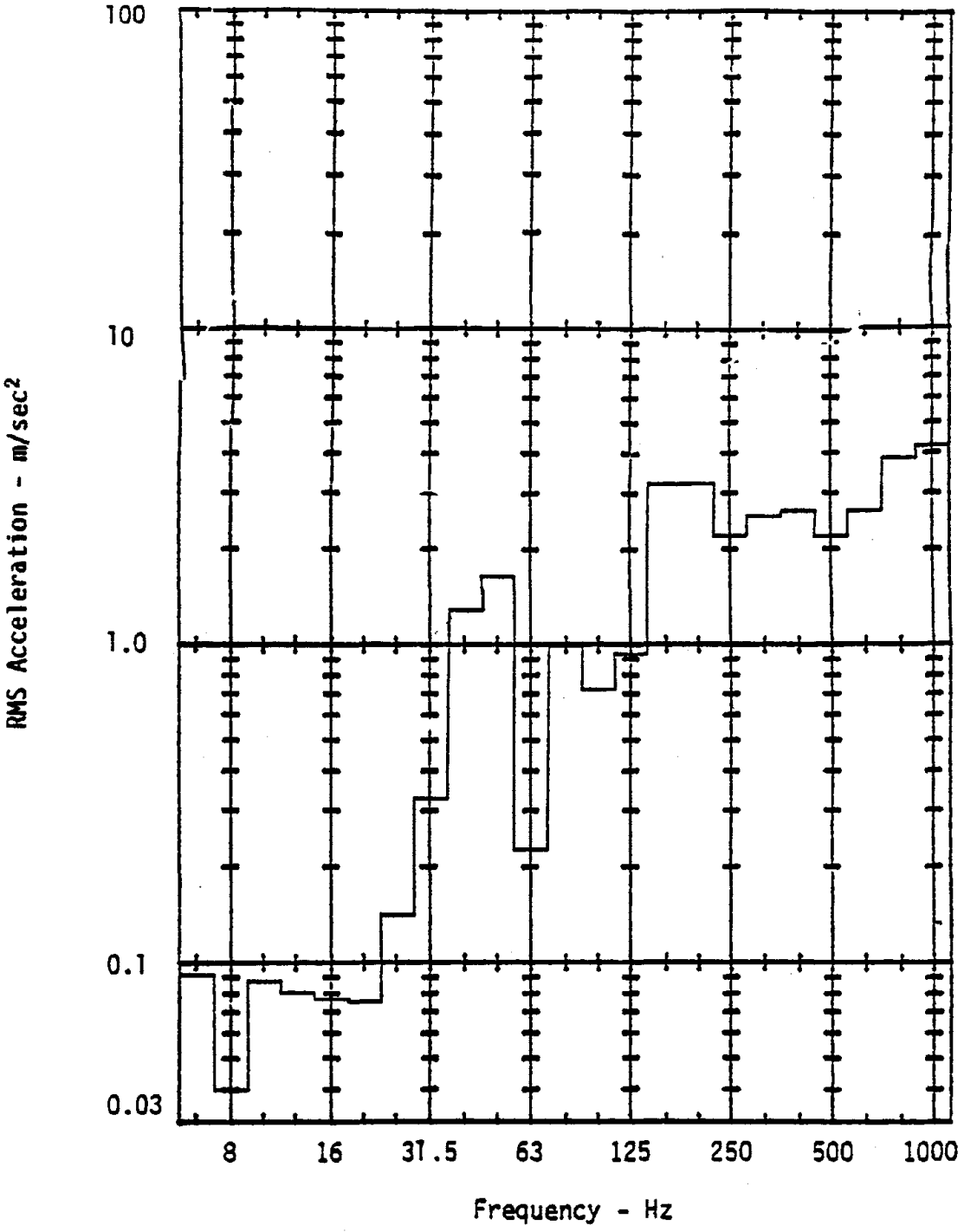

Figure C-24. RMS acceleration levels for horizontal grinder with coarse flared cup wheel. Left hand, X-direction.

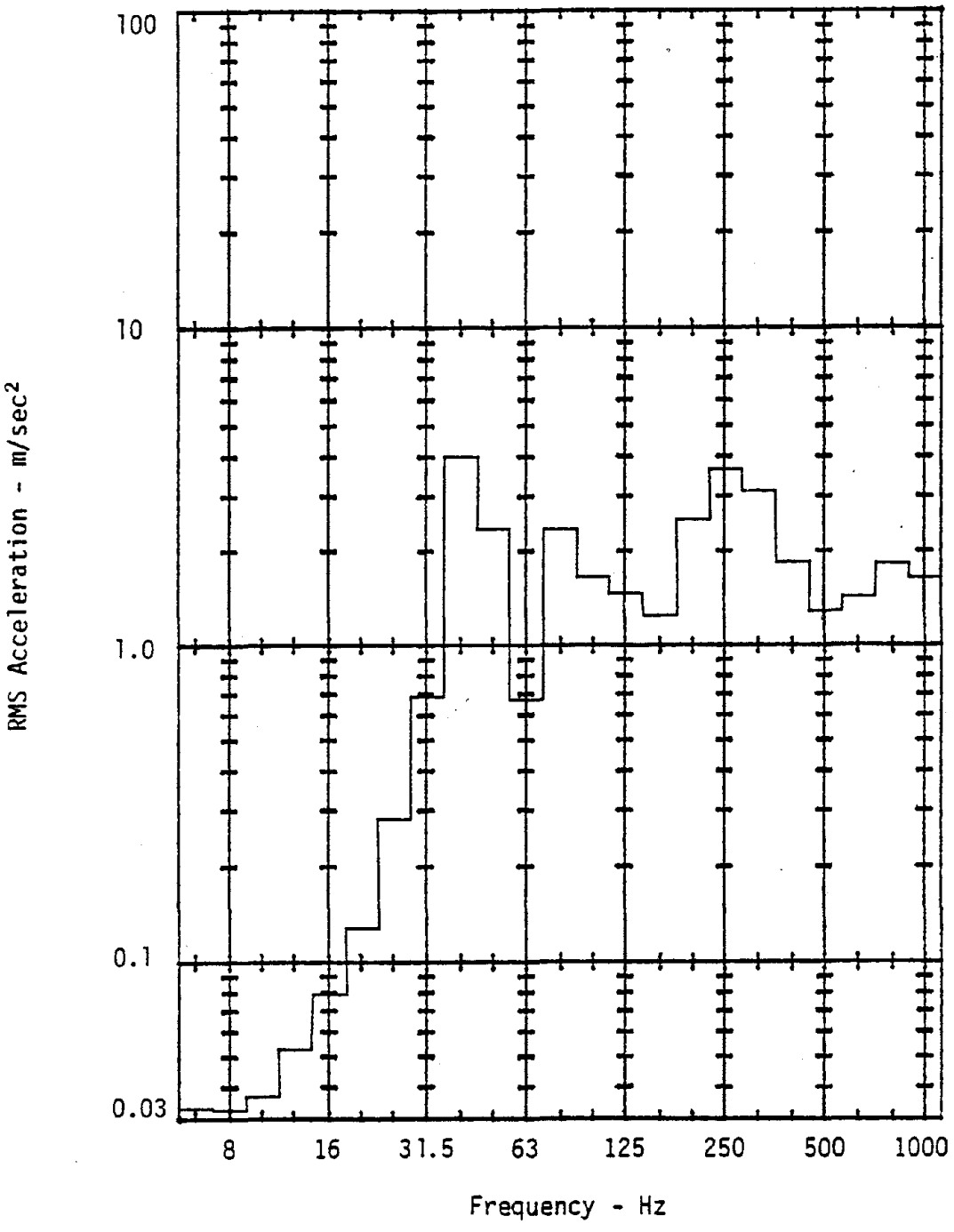

Figure C-25. RMS acceleration levels for horizontal grinder with coarse flared cup wheel. Left hand, Y-direction.

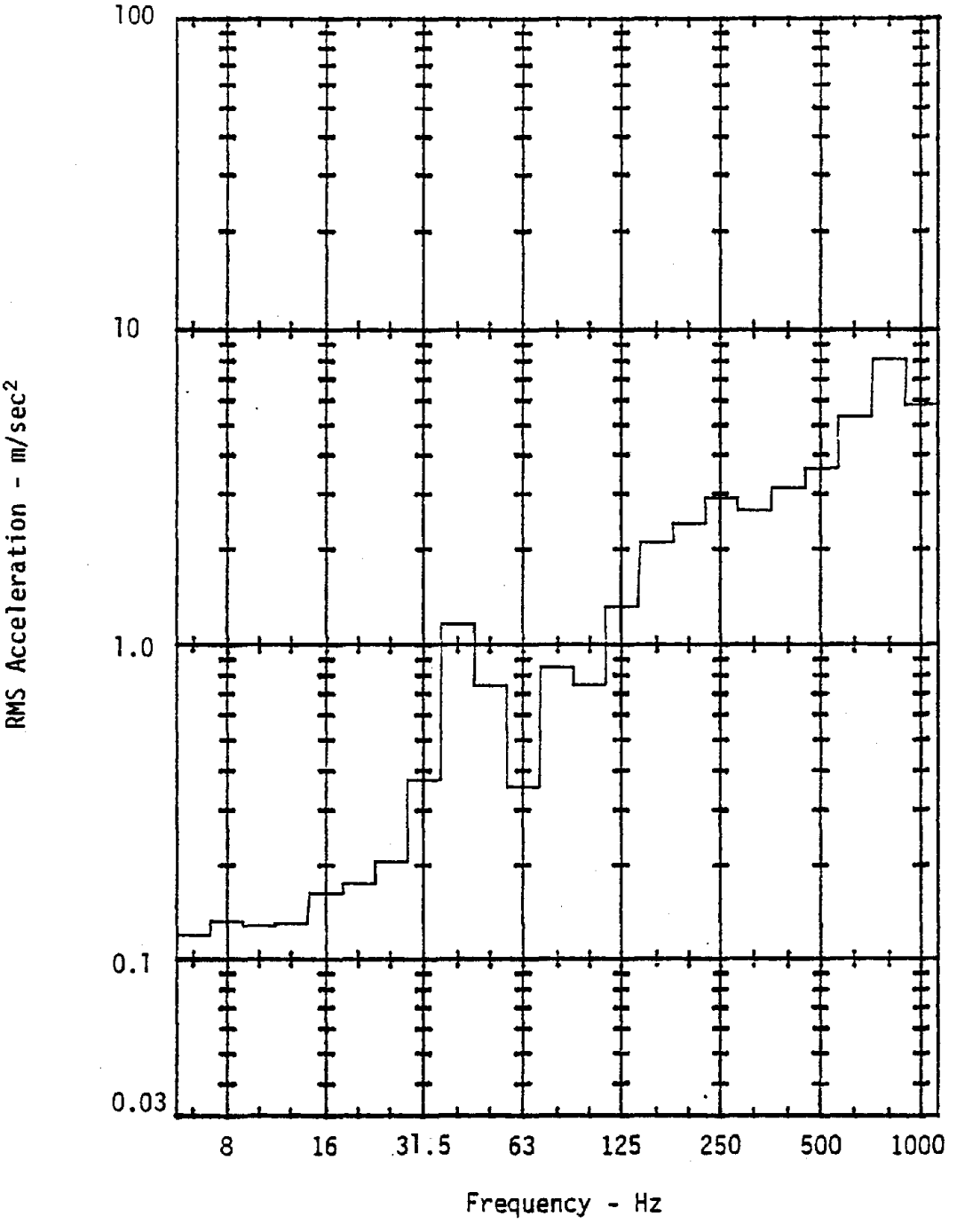

Figure C-26. RMS acceleration levels for horizontal grinder with coarse flared cup wheel. Left hand, Z-direction.

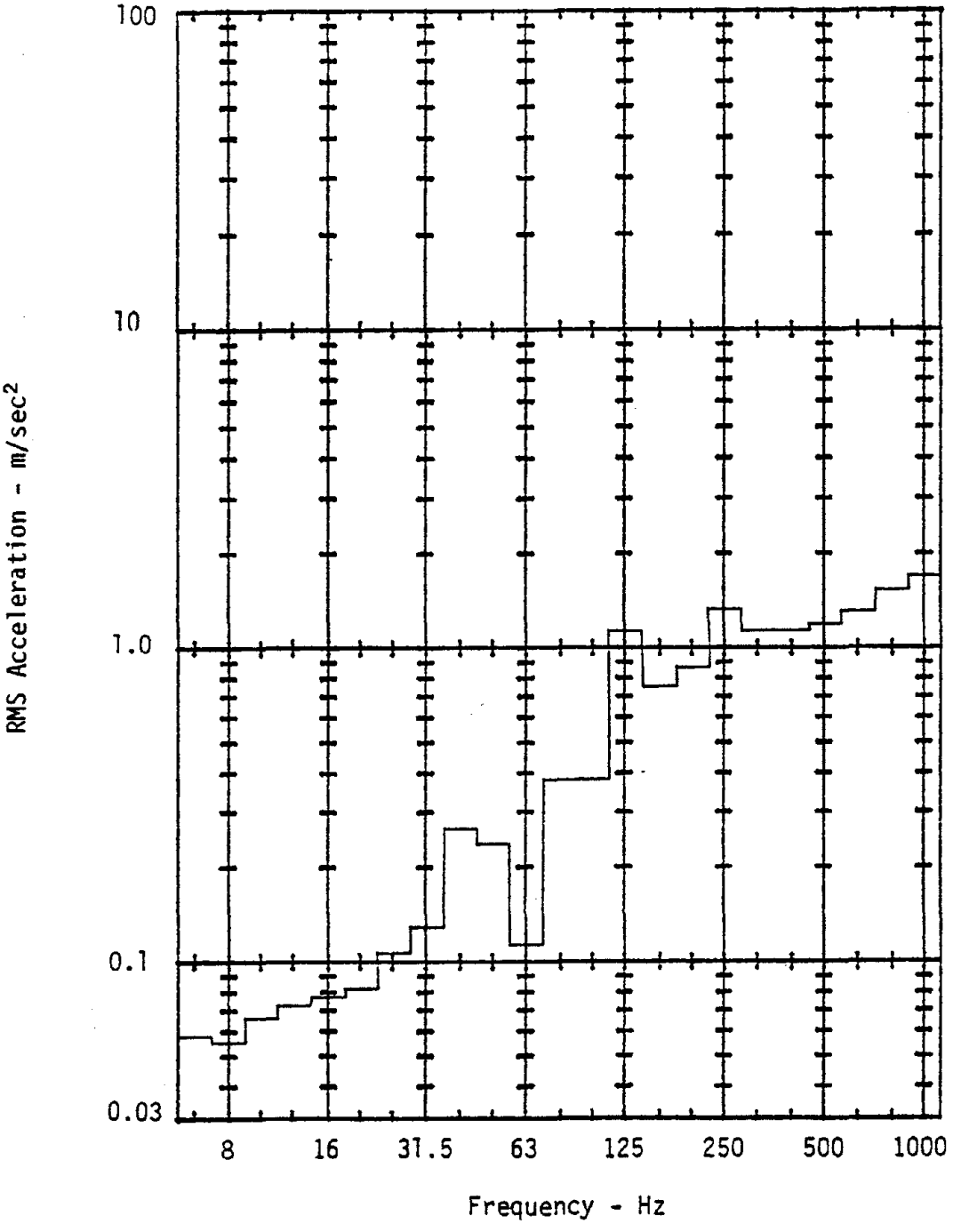

Figure C-27. RMS acceleration levels for vertical grinder with sanding pad, medium paper. Right hand, X-direction.

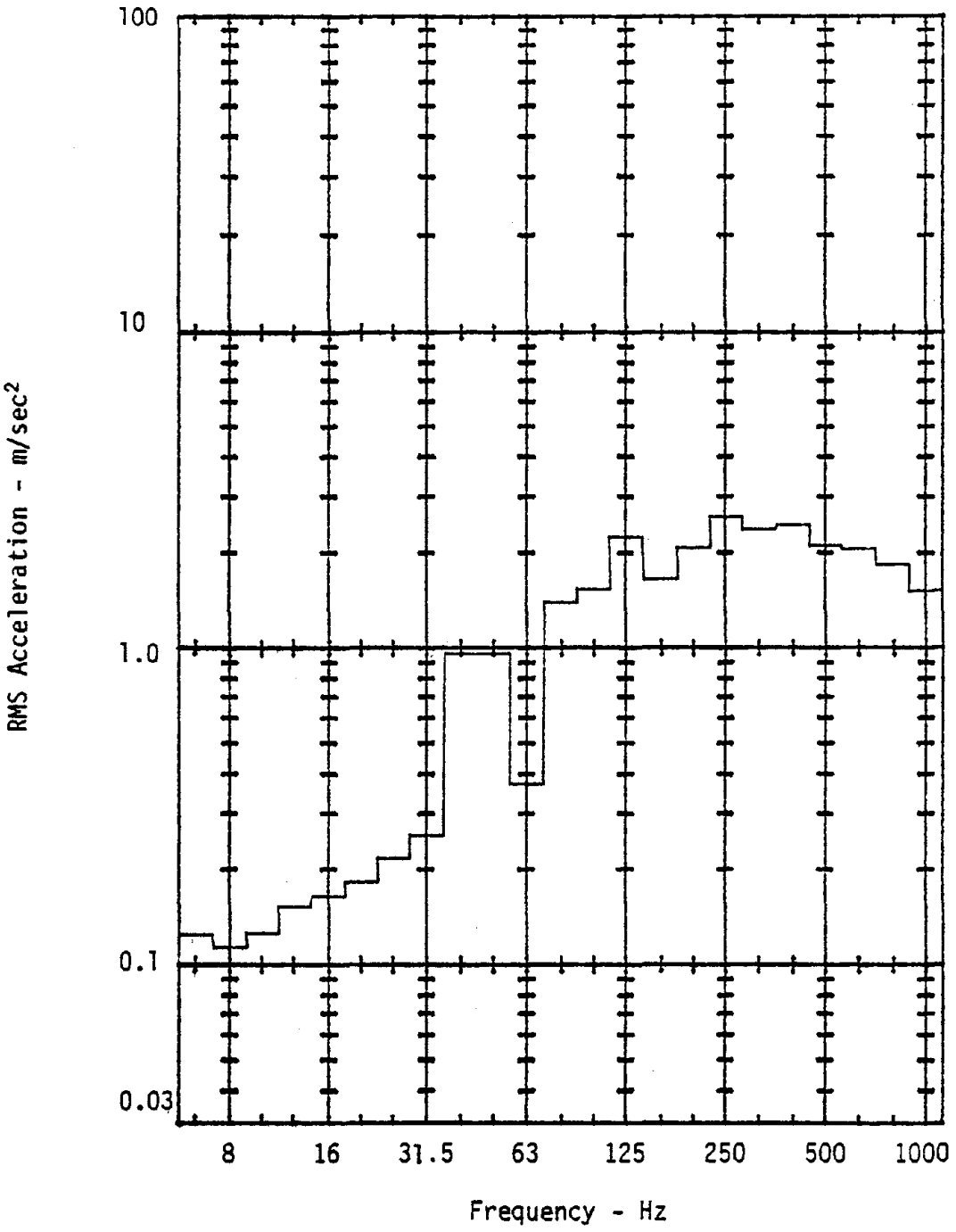

Figure C-28. RMS acceleration levels for vertical grinder with sanding pad, medium paper. Right hand, Y-direction.

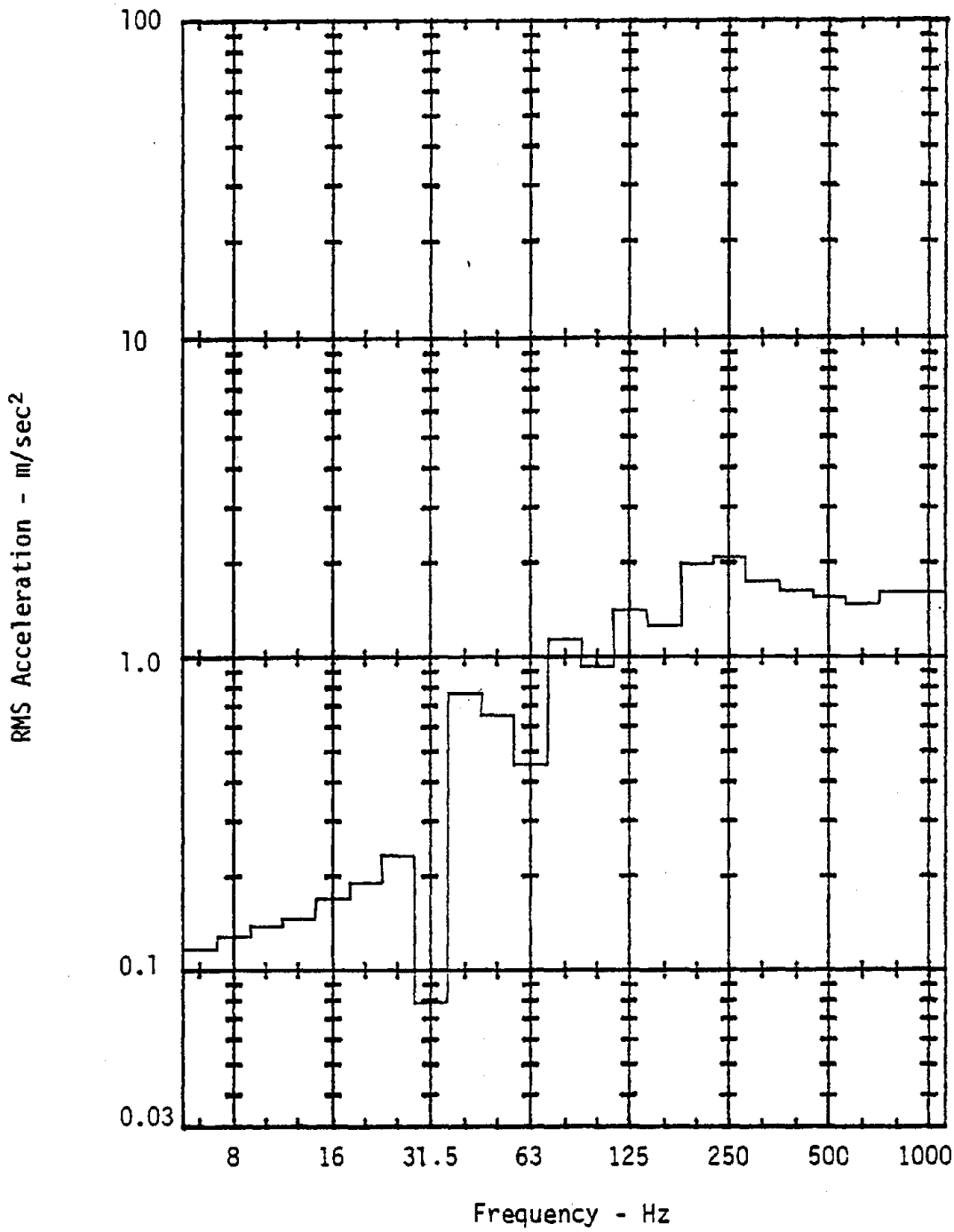

Figure C-29. RMS accelration levels for vertical grinder with sanding pad, medium paper. Right hand, Z-direction.

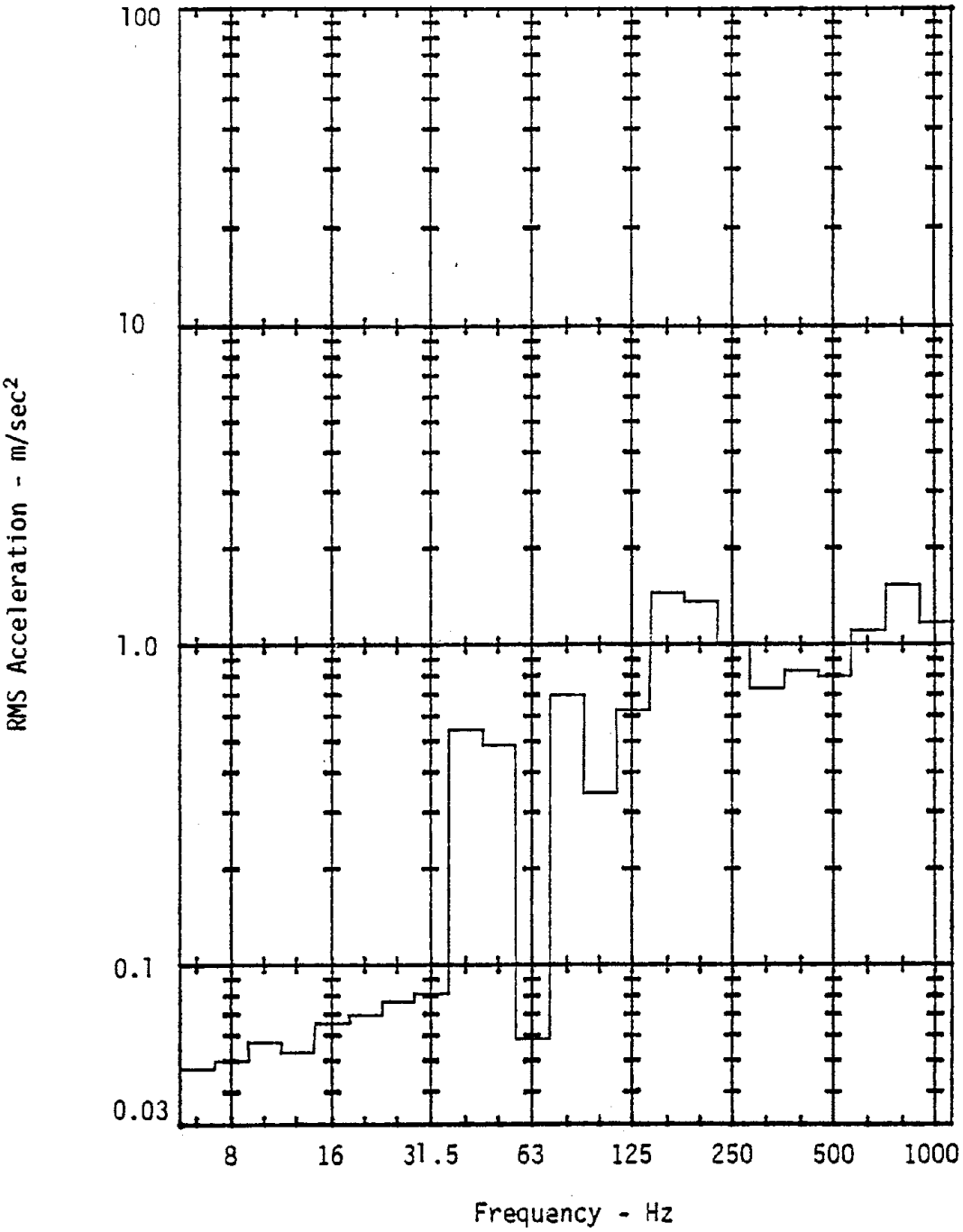

Figure C-30. RMS acceleration levels for vertical grinder with sanding pad, medium paper. Left hand, X-direction.

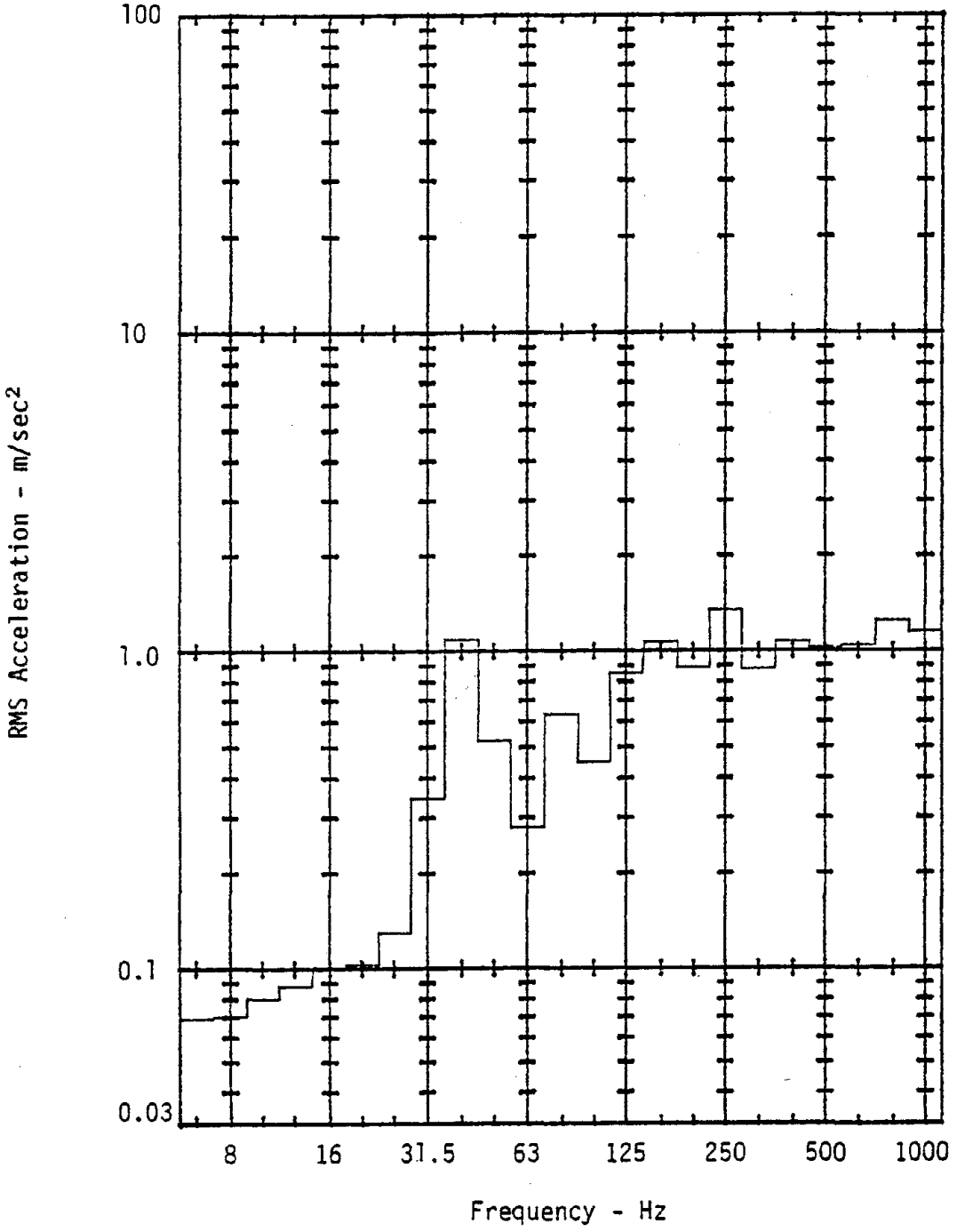

Figure C-31. RMS acceleration levels for vertical grinder with sanding pad, medium paper. Left hand, Y-direction.

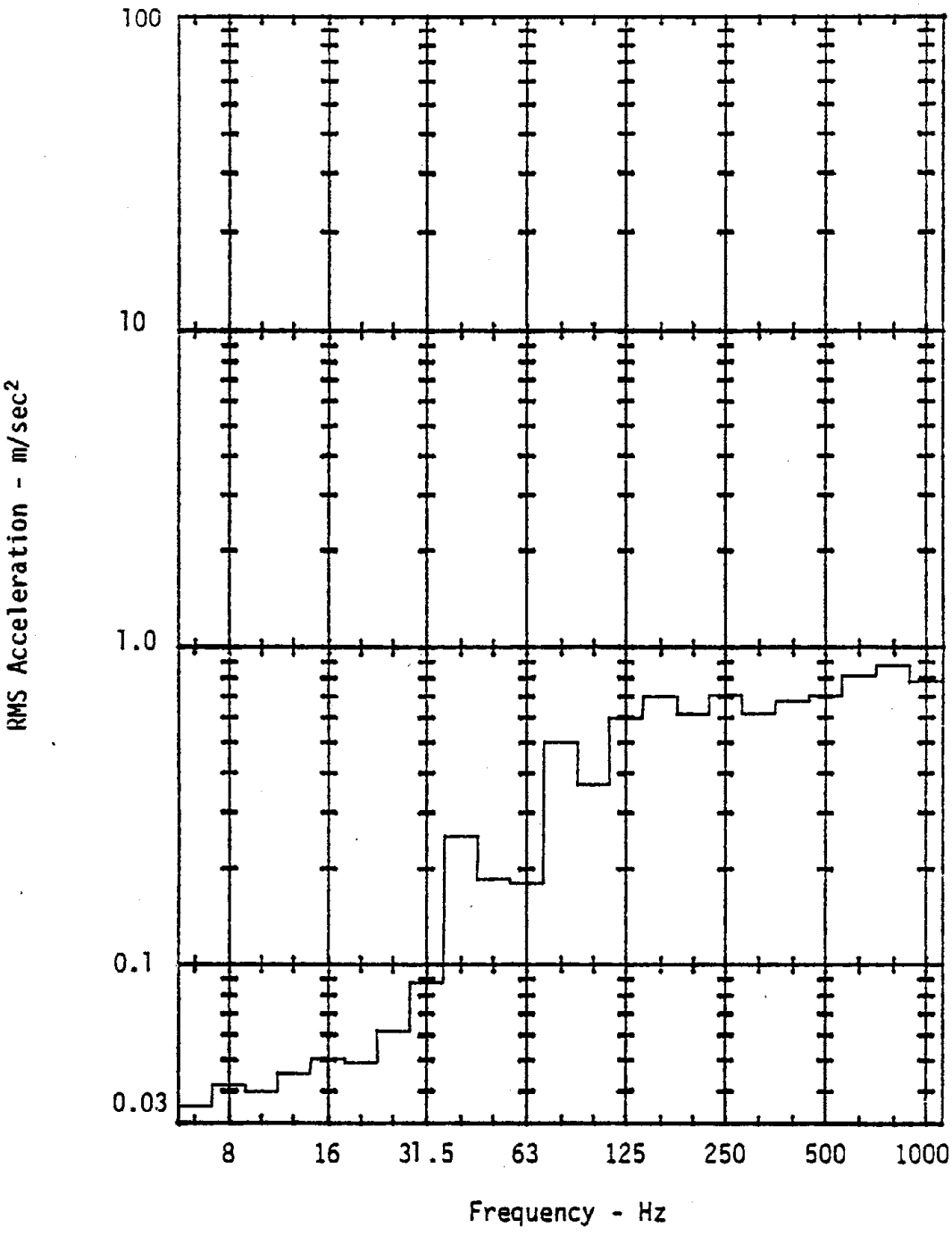

Figure C-32. RMS acceleration levels for vertical grinder with sanding pad, medium paper. Left hand, Z-direction.

APPENDIX D

INSTANTANEOUS ENERGY DATA PLOTS

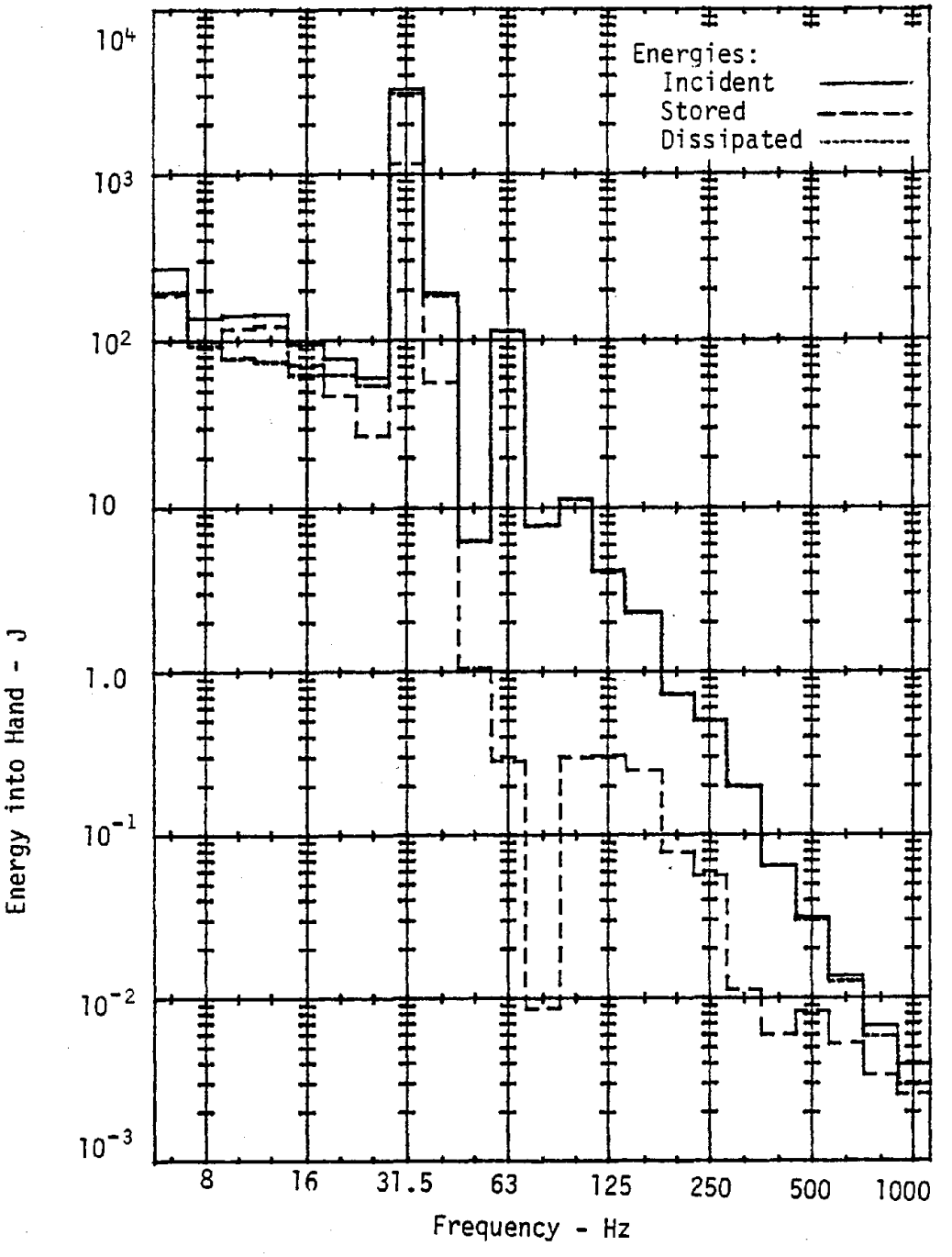

Figure D-1. RMS amplitude of instantaneous energy directed into hand from the chisel of chipping hammer A used to clean castings. Slot chipping on nodular cast iron. Chipping hammer operated at full throttle.

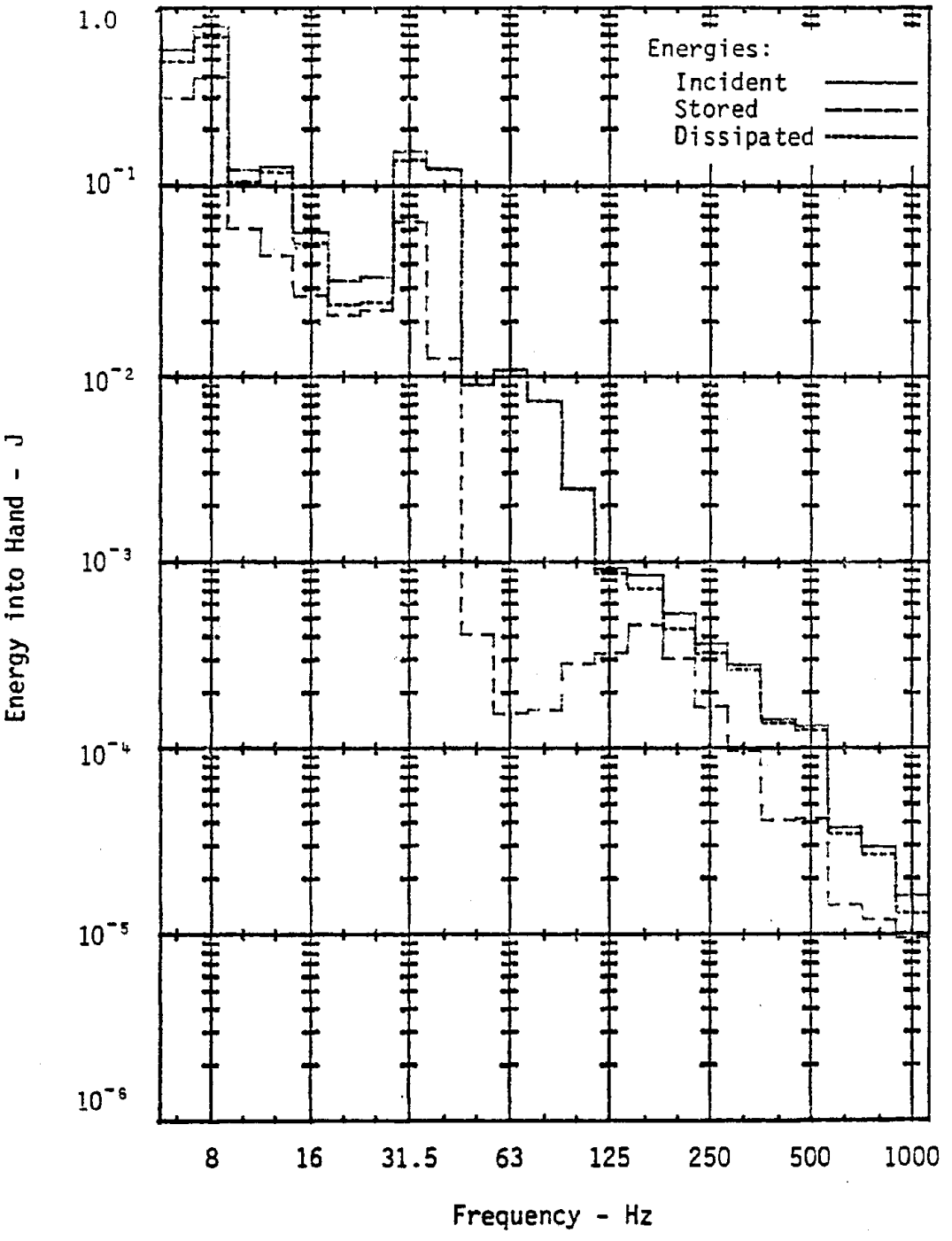

Figure D-2. RMS amplitude of instantaneous energy directed into hand from the handle of chipping hammer A used to clean castings. Slot chipping on nodular cast iron. Chipping hammer operated at full throttle.

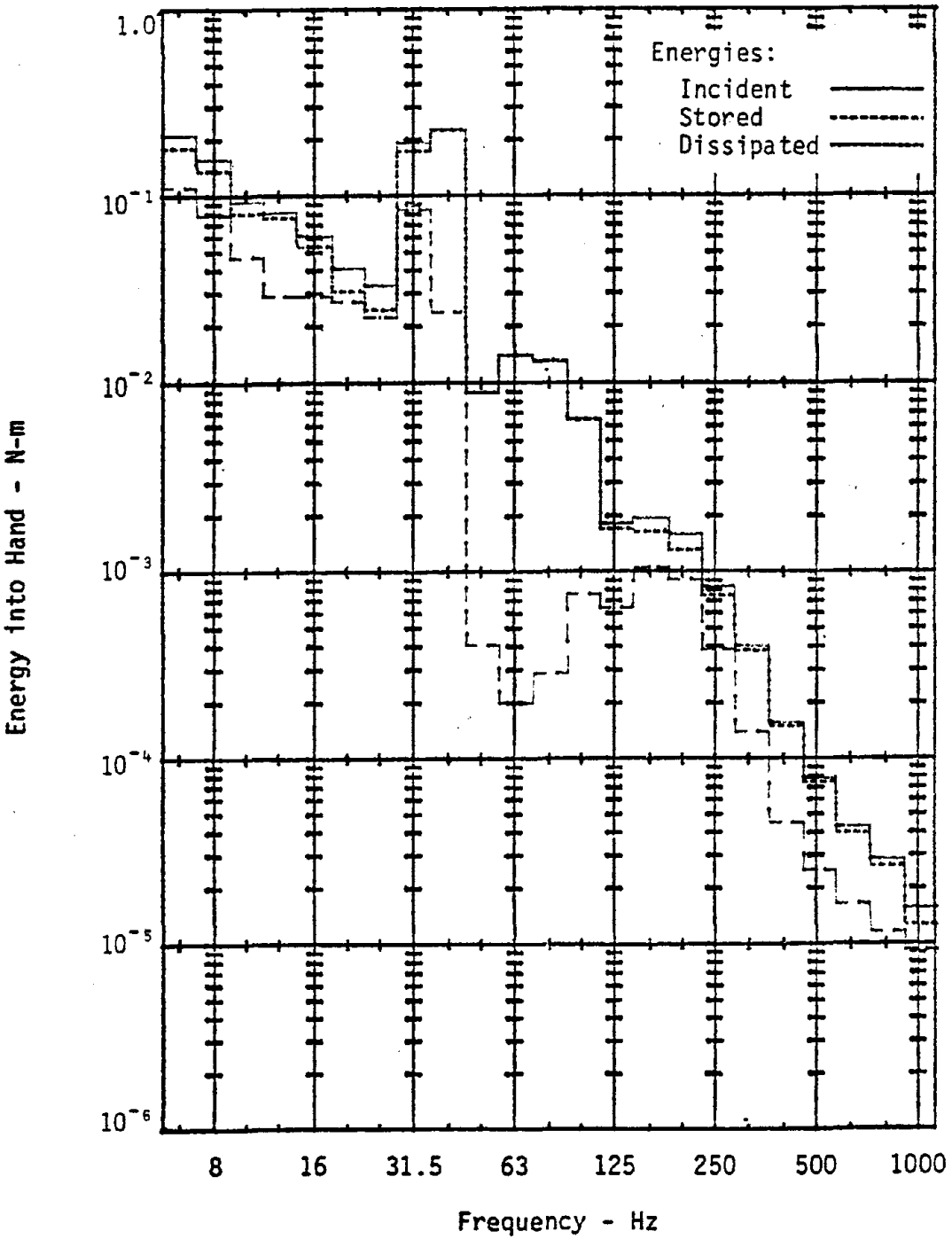

Figure D-3. RMS amplitude of instantaneous energy into the hand from the handle of chipping hammer B used to clean castings. Slot chipping on nodular cast iron. Chipping hammer operated at full throttle.

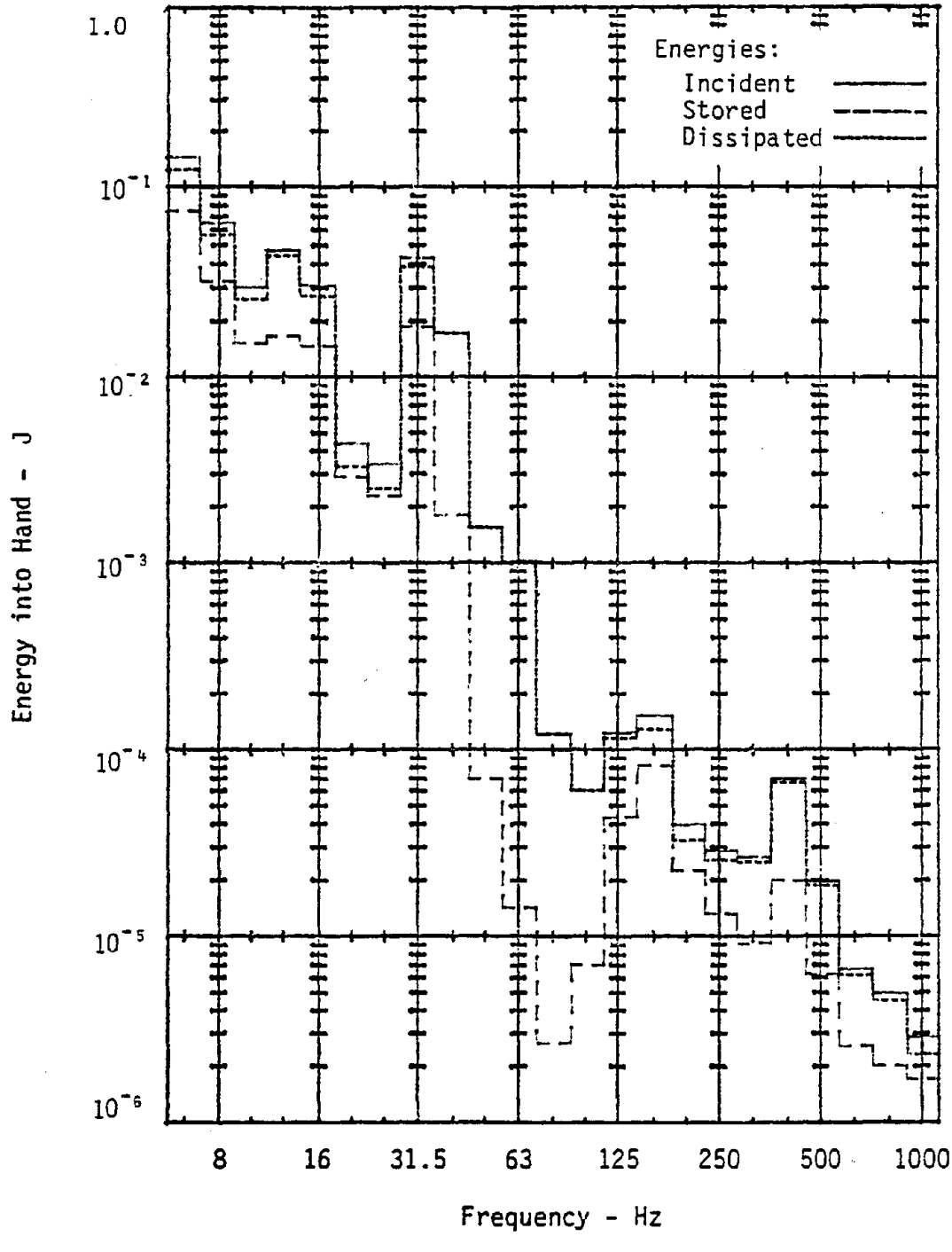

Figure D-4. RMS amplitude of instantaneous energy into the hand from the handle of chipping hammer C used to clean castings. Slot chipping on nodular cast iron. Chipping hammer operated at full throttle.

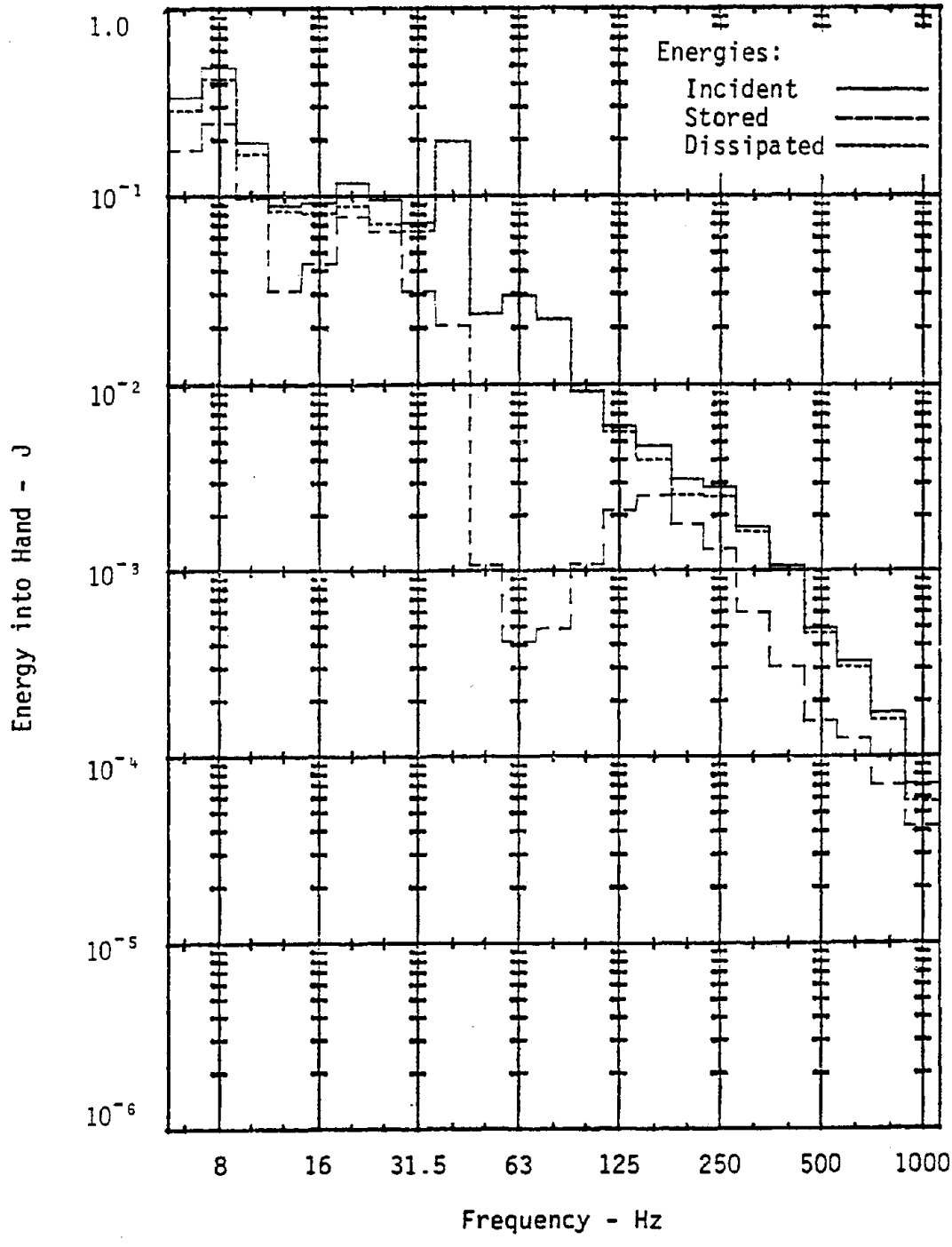

Figure D-5. RMS amplitude of instantaneous energy directed into hand from the handle of chipping hammer D used to shape propeller blades. Slot chipping on cast iron. Chipping hammer operated at full throttle.

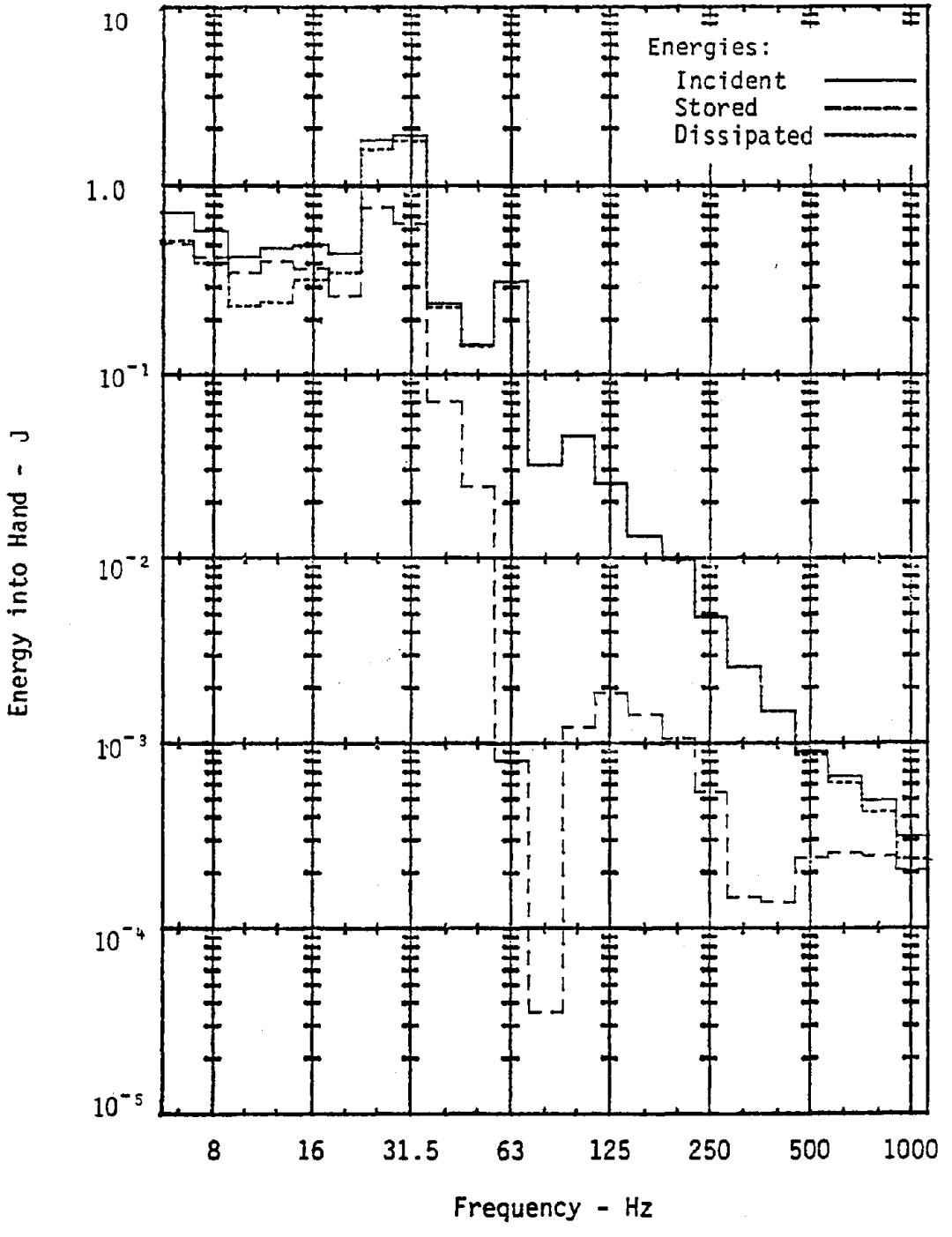

Figure D-6. RMS amplitude of instantaneous energy directed into hand from the chisel of chipping hammer D used to shape propeller blades. Chipping on mild B steel. Chipping hammer operated at 1/2-3/4 throttle.

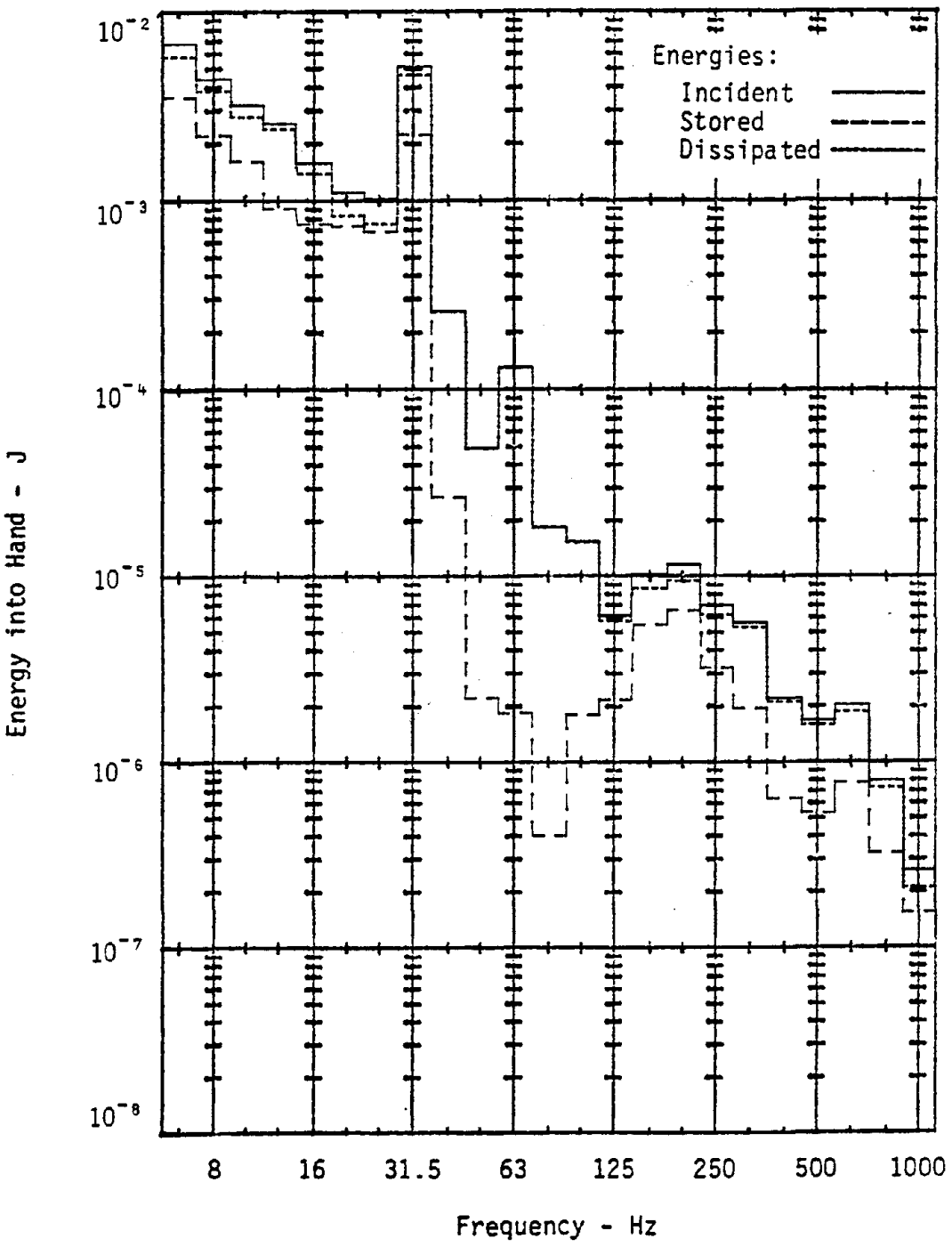

Figure D-7. RMS amplitude of instantaneous energy directed into hand from the handle of chipping hammer D used to shape propeller blades. Chipping on mild B steel. Chipping hammer operated at 1/2-3/4 throttle.

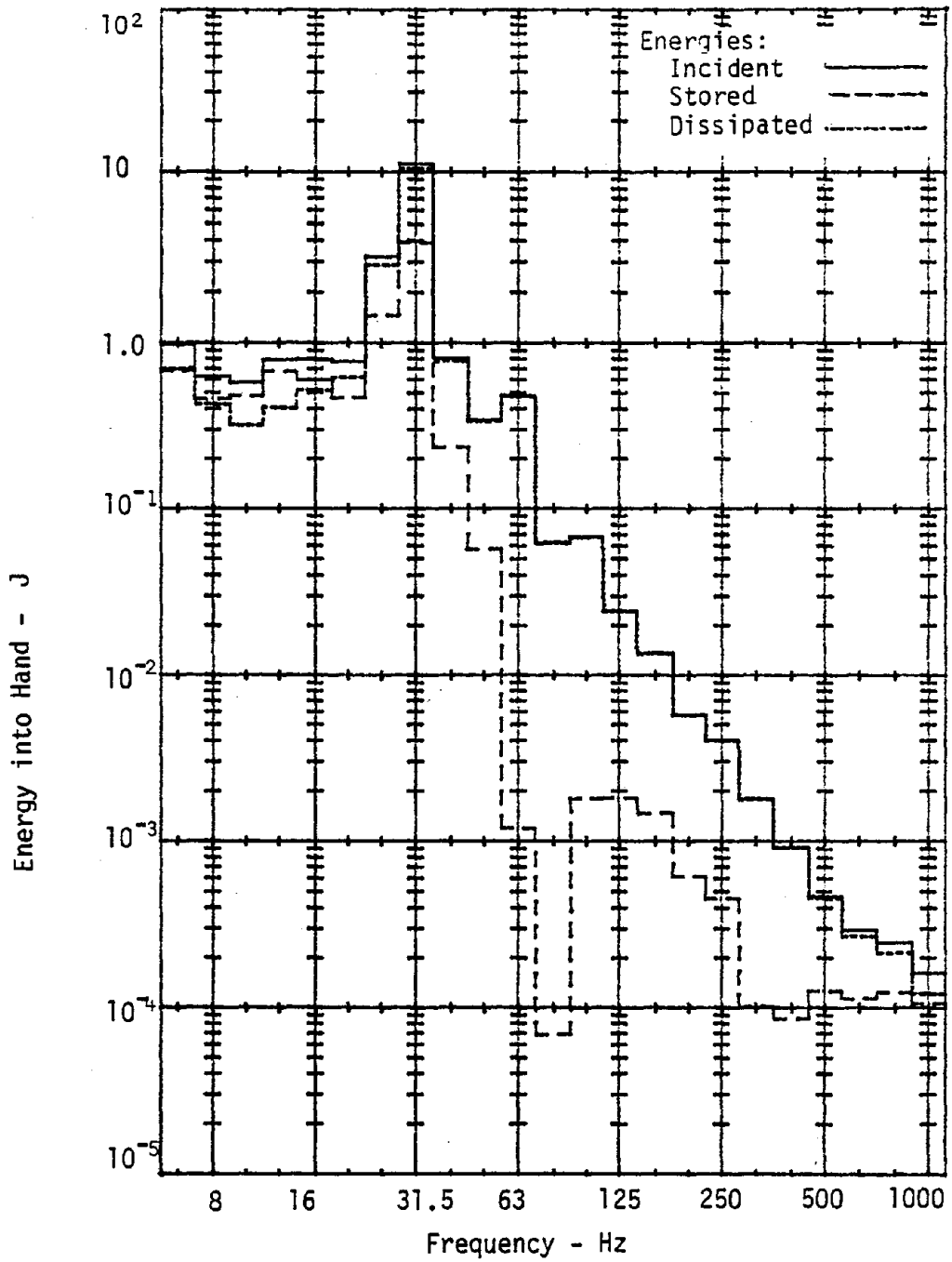

Figure D-8. RMS amplitude of instantaneous energy directed into hand from the chisel of chipping hammer D used to shape propeller blades. Chipping on Ni-Al-Br. Chipping hammer operated at 1/2-3/4 throttle.

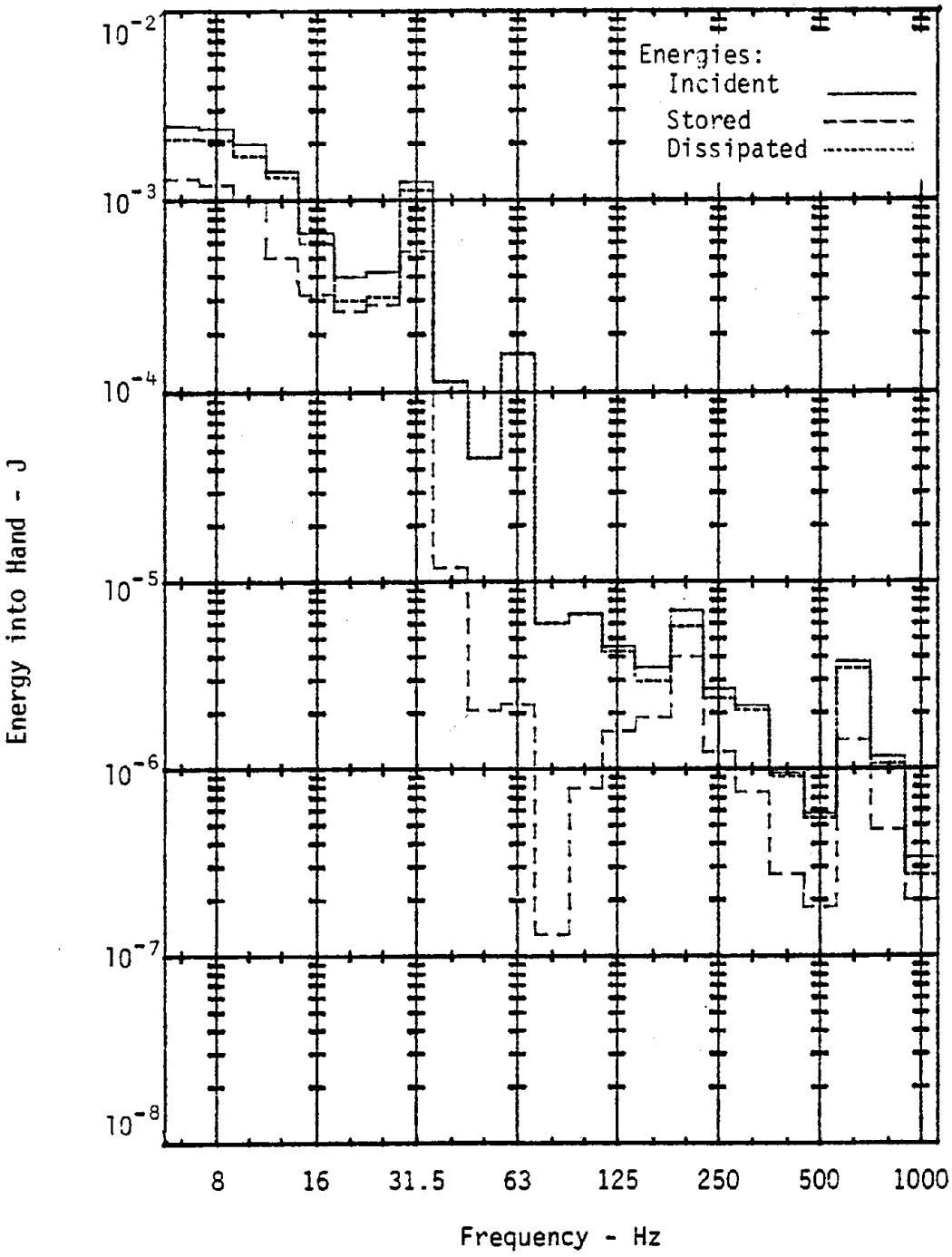

Figure D-9. RMS amplitude of instantaneous energy directed into hand from the handle of chipping hammer D used to shape propeller blades. Chipping on Ni-Al-Br. Chipping hammer operated at 1/2-3/4 throttle.

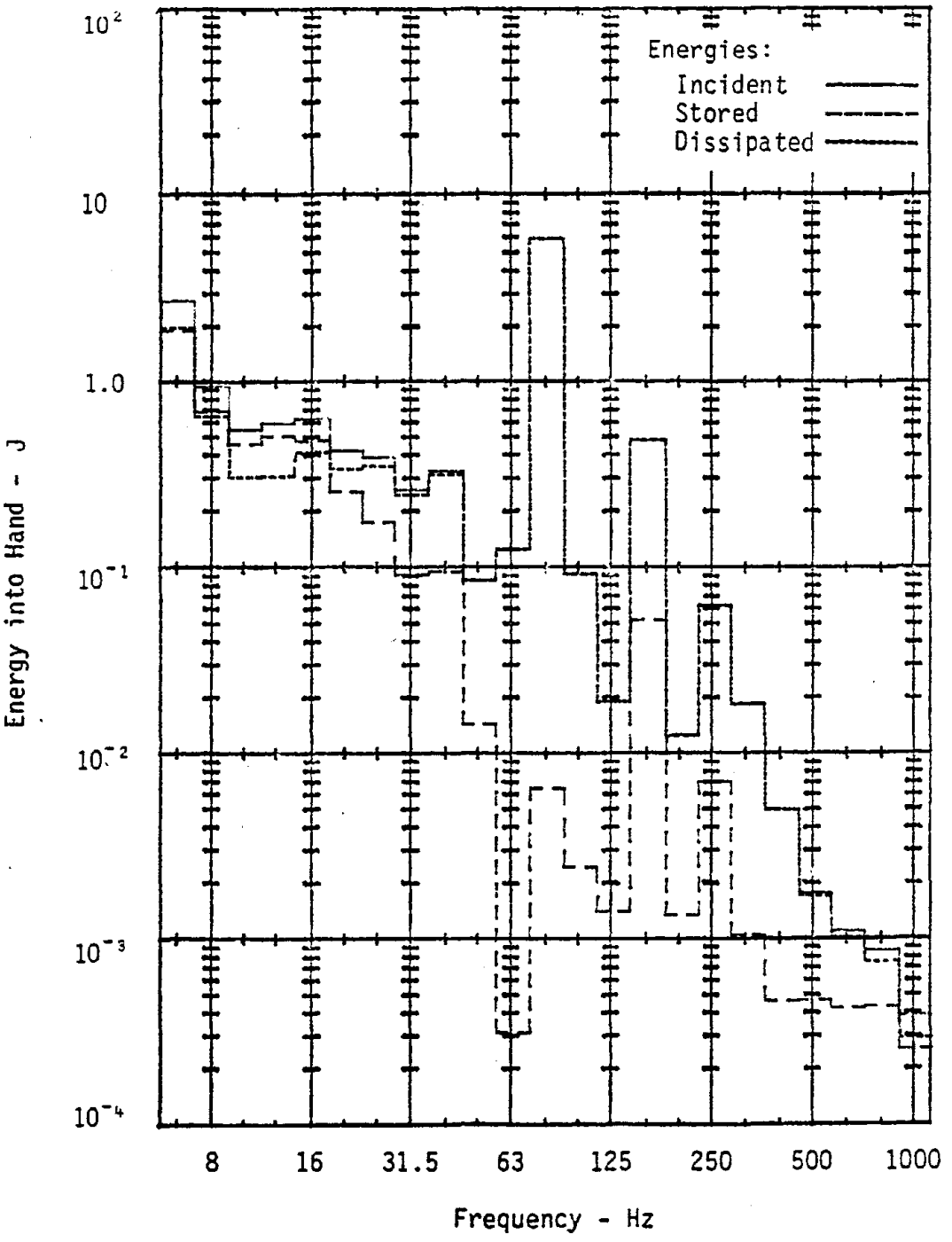

Figure D-10. RMS amplitude of instantaneous energy directed into hand from the chisel of small chipping hammer used to carve limestone. Chipping hammer operated at full throttle.

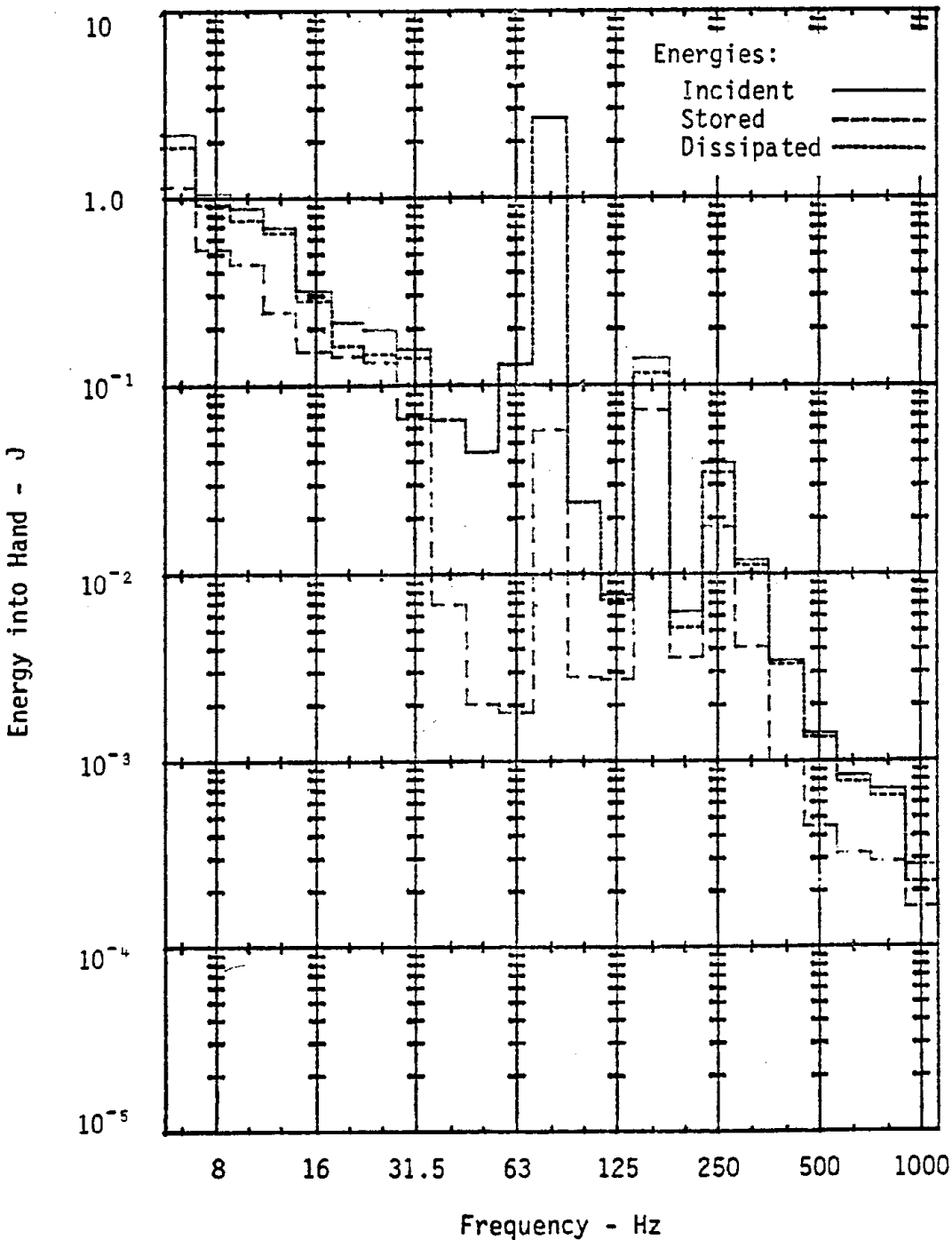

Figure D-11. RMS amplitude of instantaneous energy directed into hand from the handle of small chipping hammer used to carve limestone. Chipping hammer operated at full throttle.

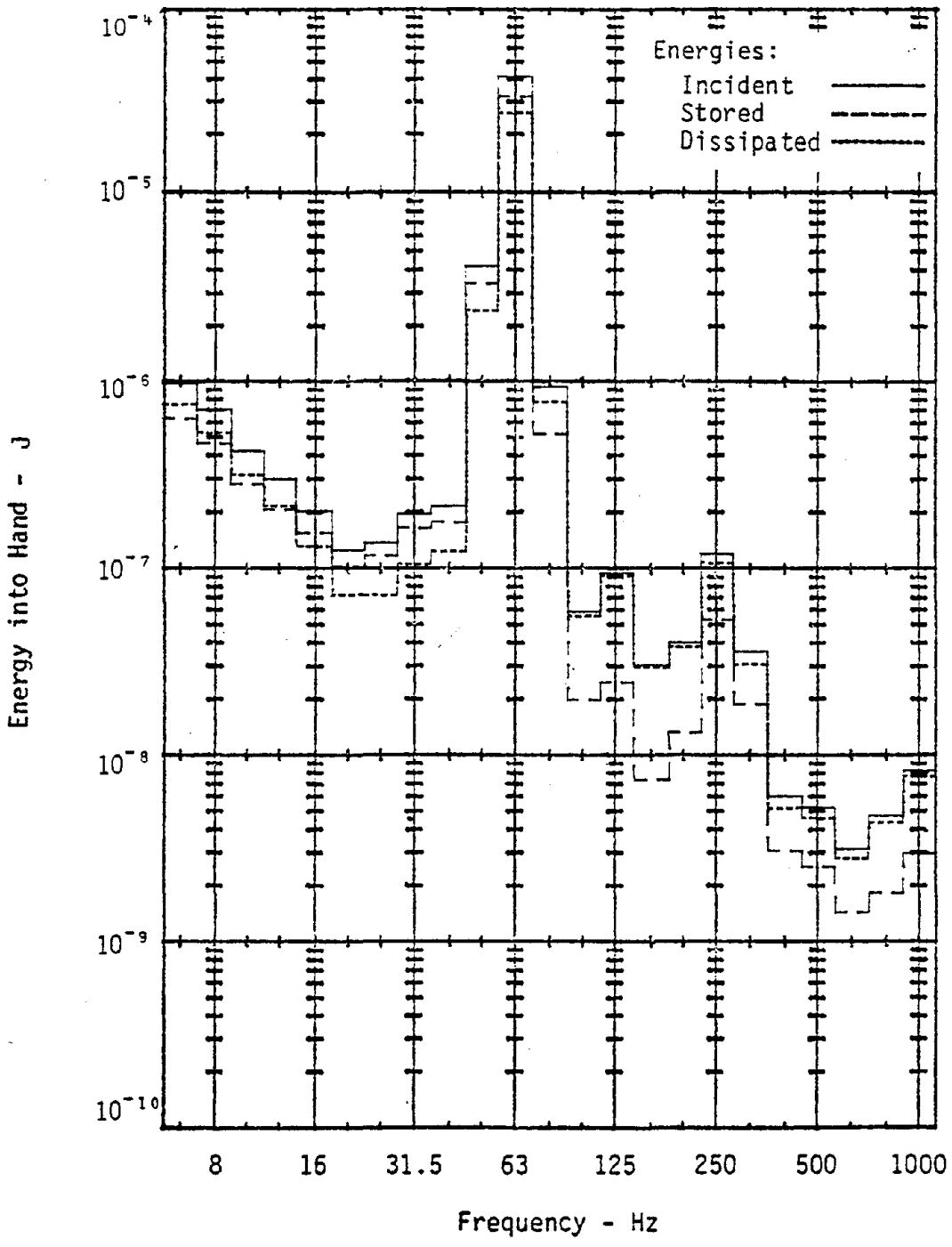

Figure D-12. RMS amplitude of instantaneous energy directed into hand from horizontal grinder with coarse radial wheel. Right hand, X-direction.

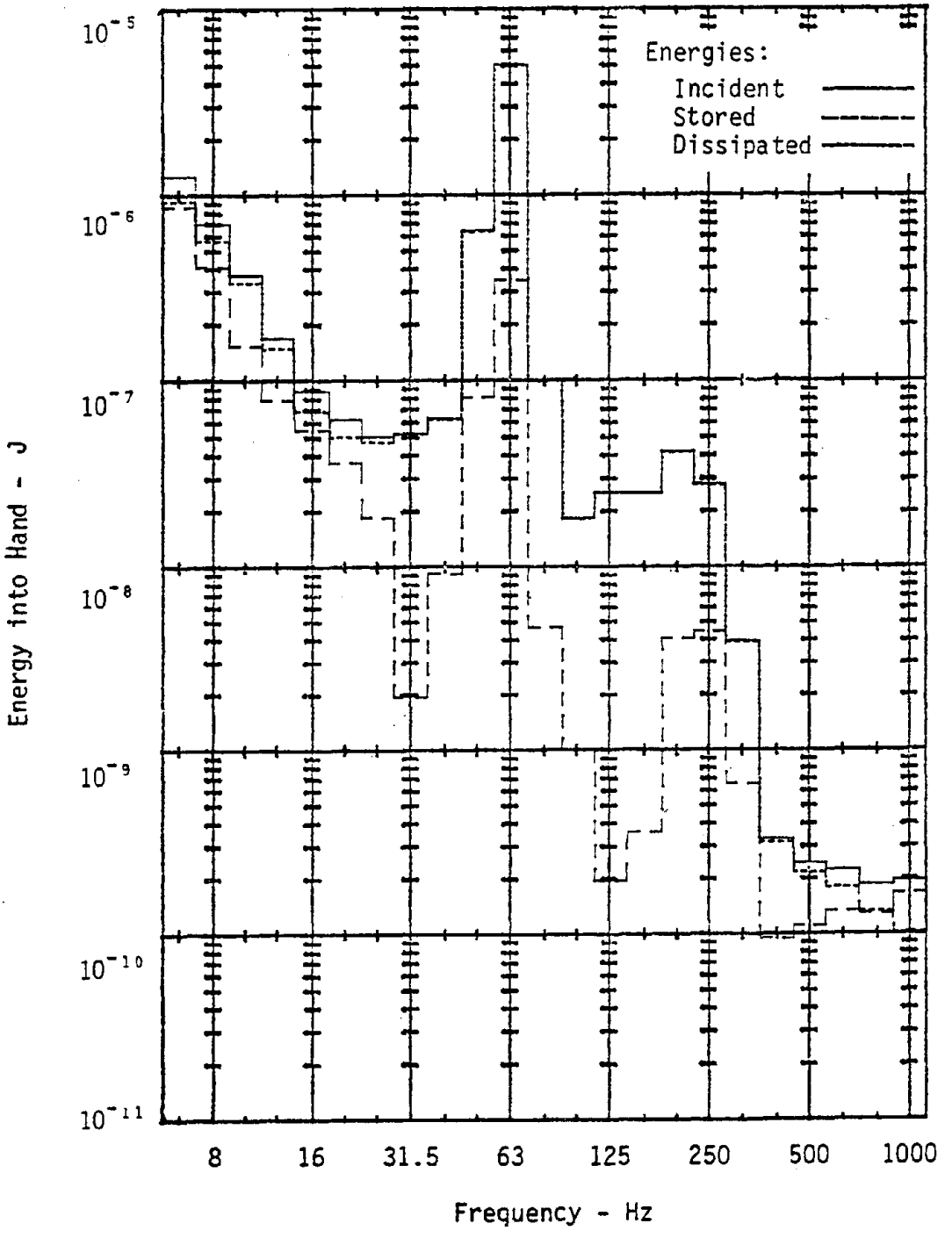

Figure D-13. RMS amplitude of instantaneous energy directed into hand from horizontal grinder with coarse radial wheel. Right hand, Y-direction.

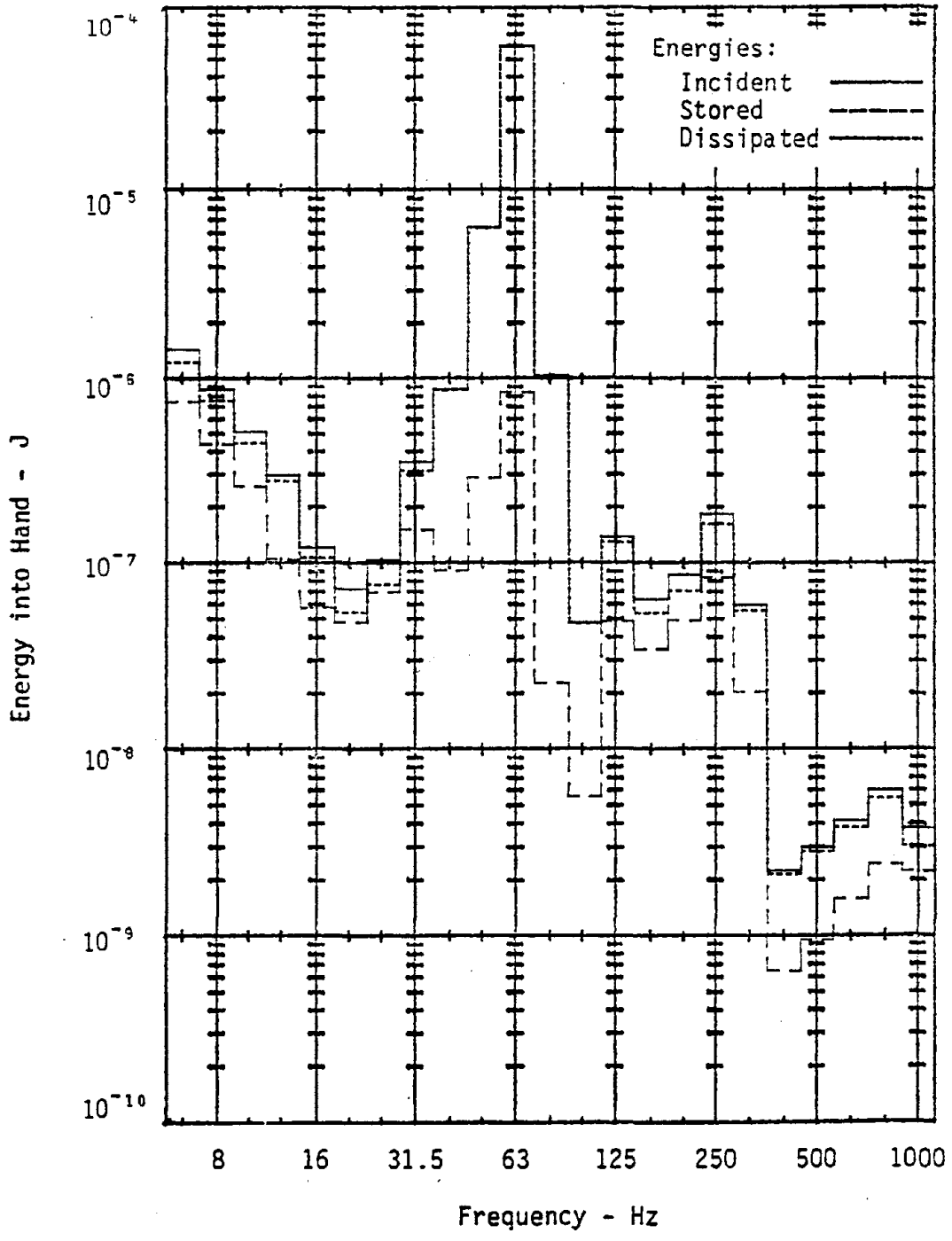

Figure D-14. RMS amplitude of instantaneous energy directed into hand from horizontal grinder with coarse radial wheel. Right hand, Z-direction.

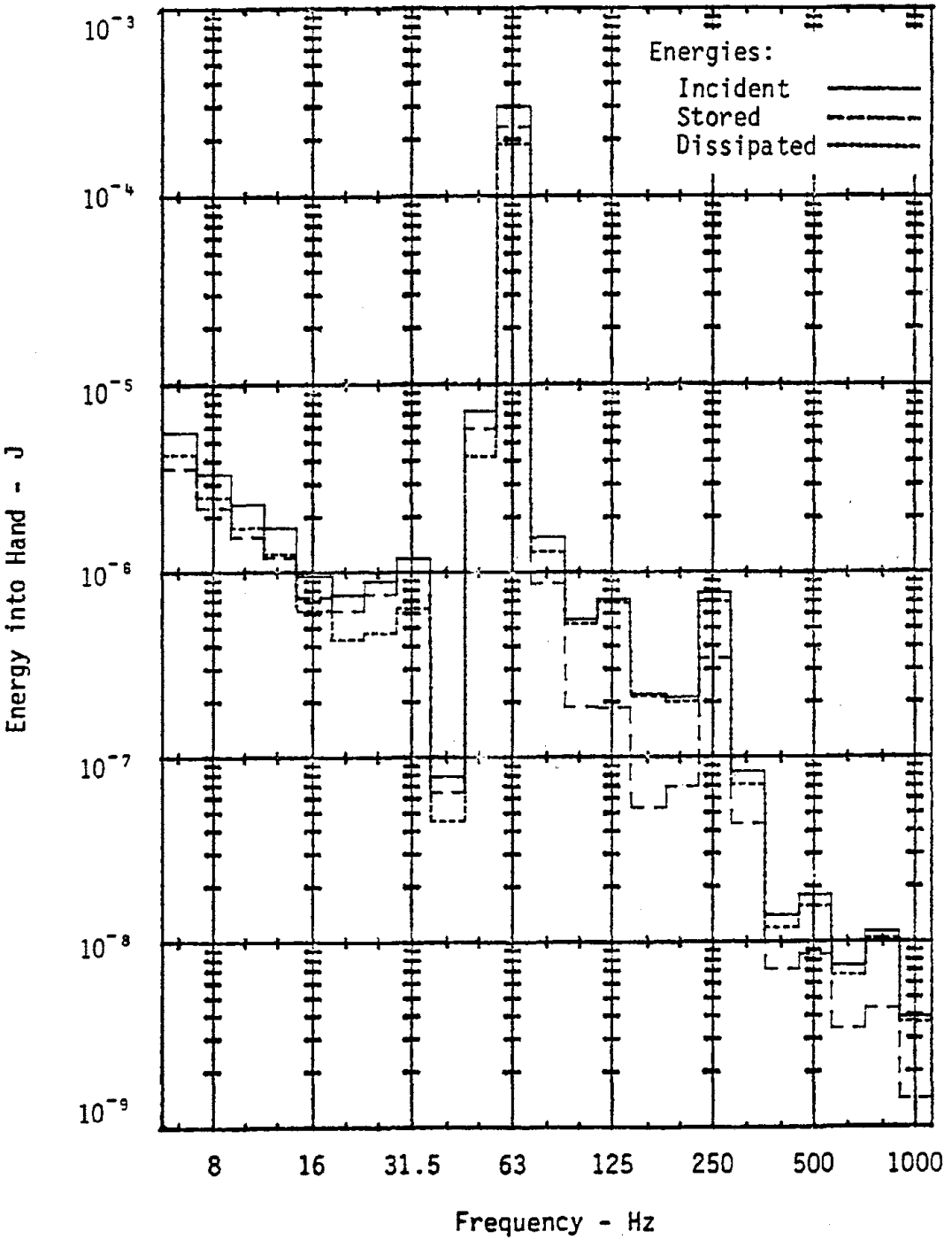

Figure D-15. RMS amplitude of instantaneous energy directed into hand from horizontal grinder with coarse radial wheel. Left hand, X-direction.

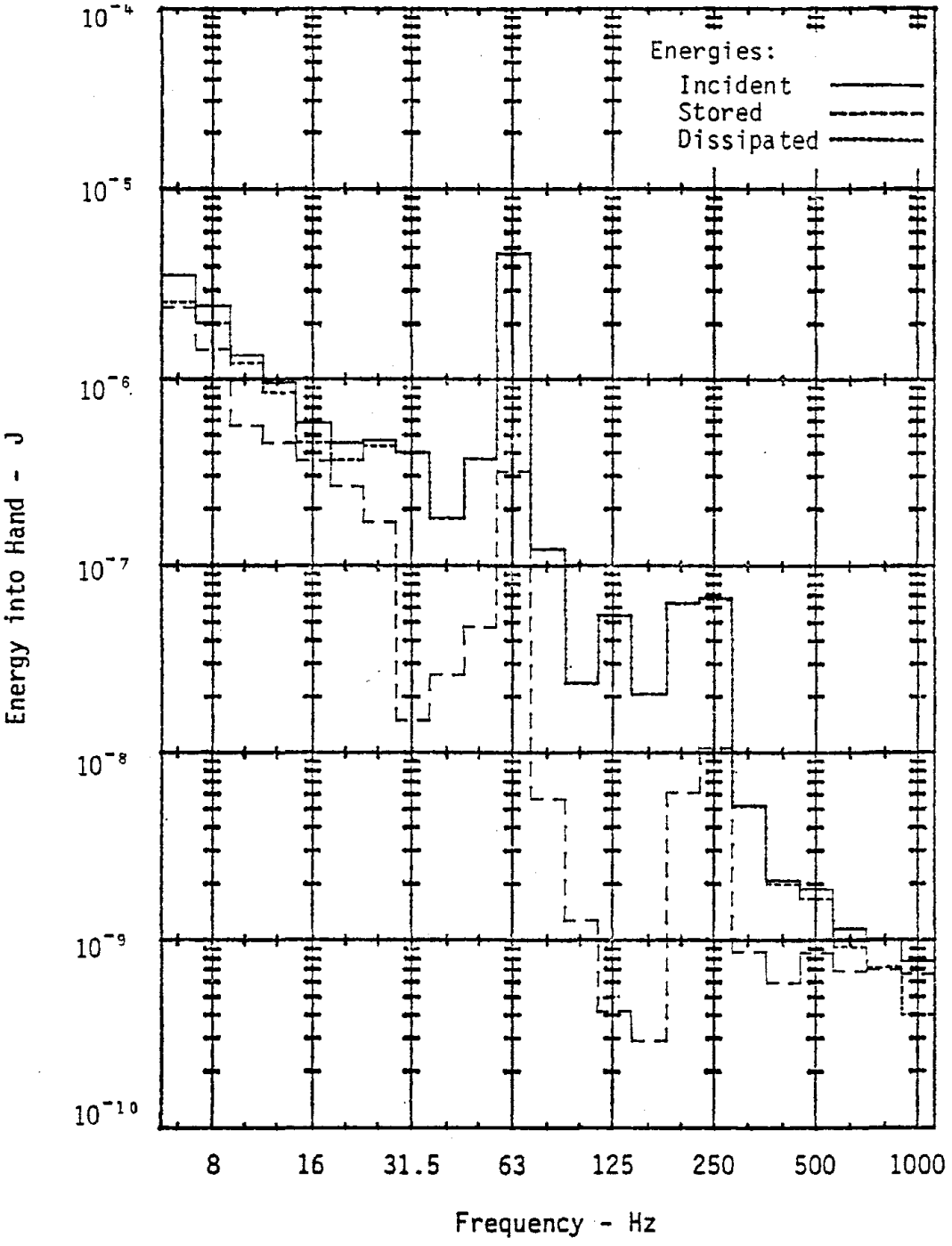

Figure D-16. RMS amplitude of instantaneous energy directed into hand from horizontal grinder with coarse radial wheel. Left hand, Y-direction.

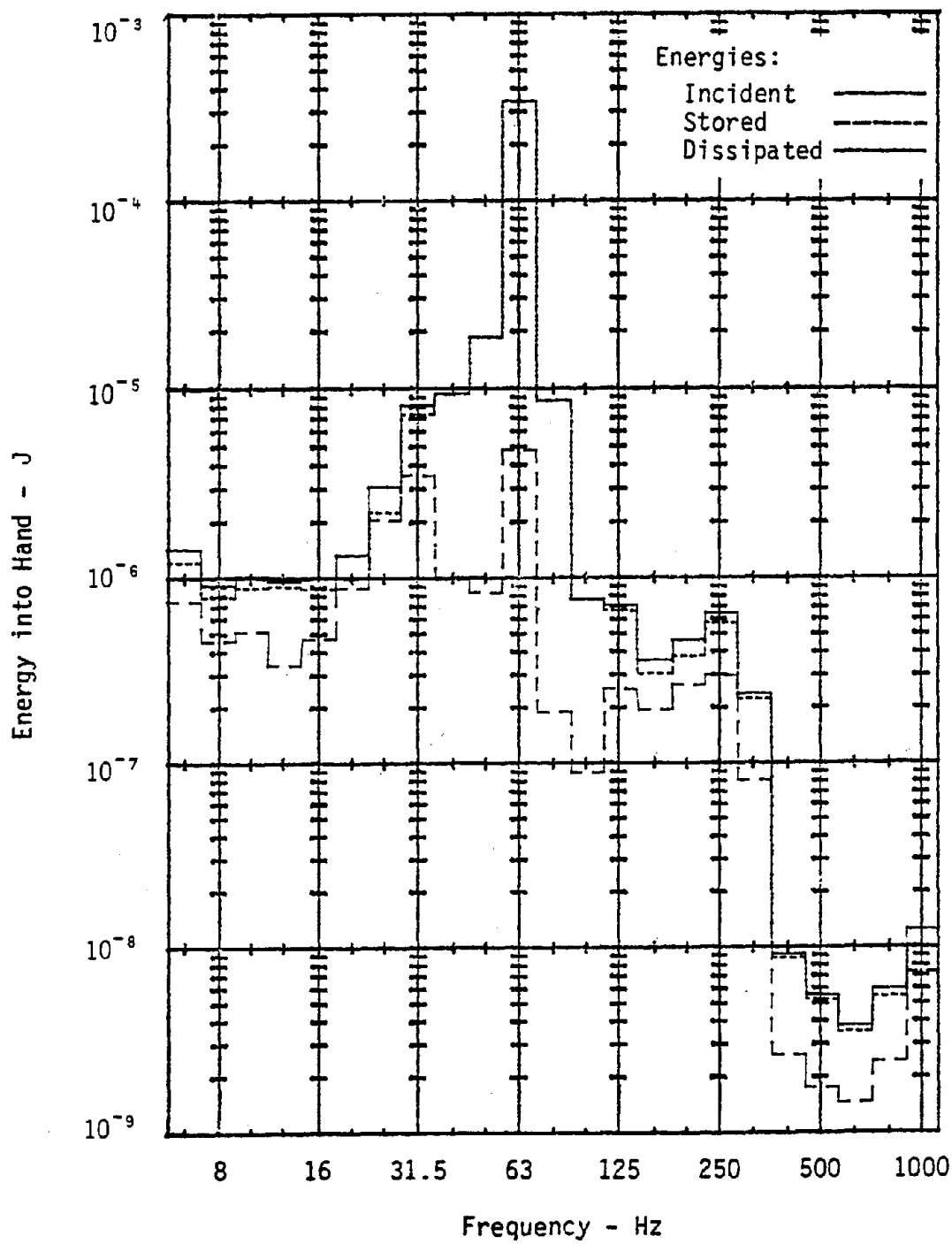

Figure D-17. RMS amplitude of instantaneous energy directed into hand from horizontal grinder with coarse radial wheel. Left hand, Z-direction.

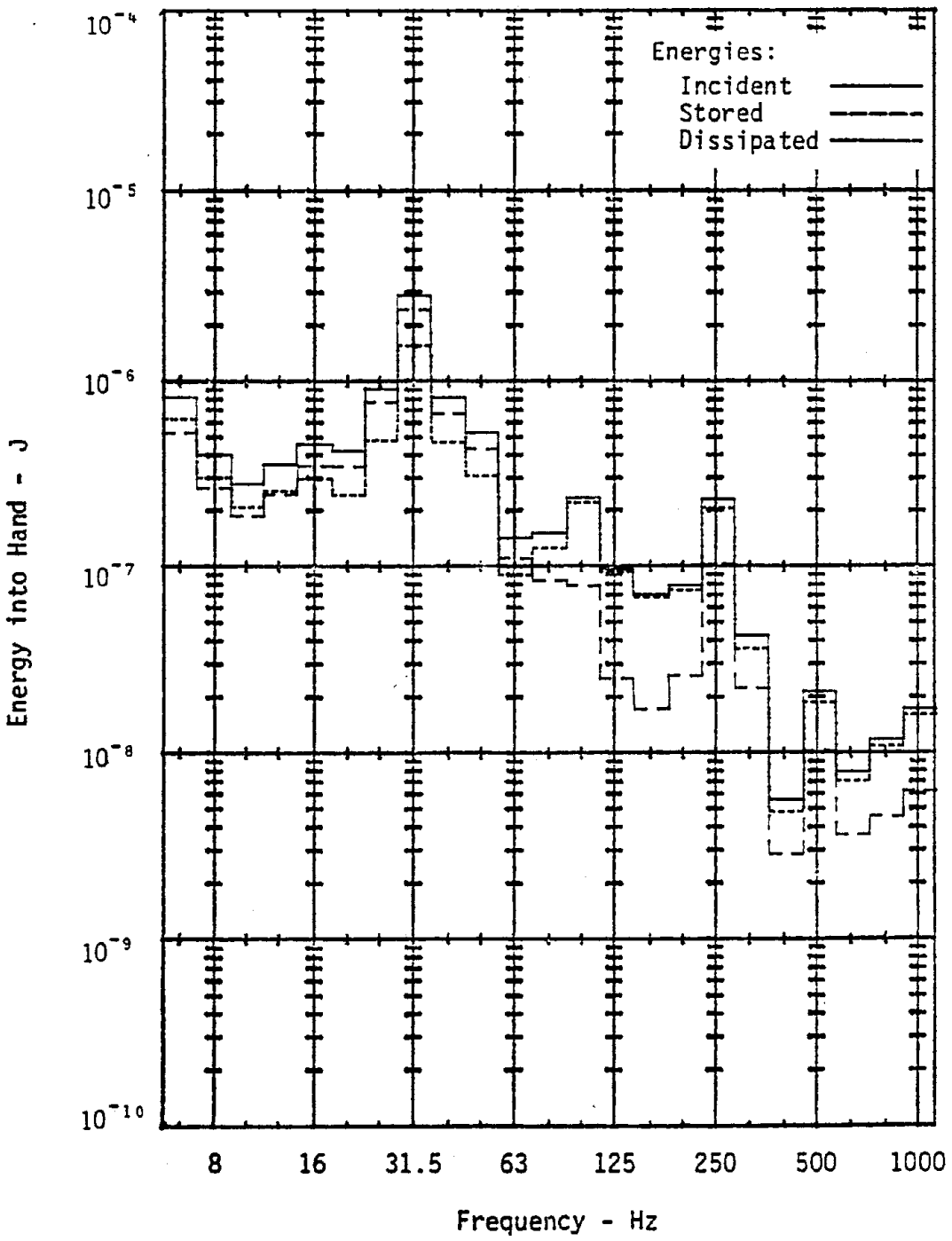

Figure D-18. RMS amplitude of instantaneous energy directed into hand from horizontal grinder with fine radial wheel. Right hand, X-direction.

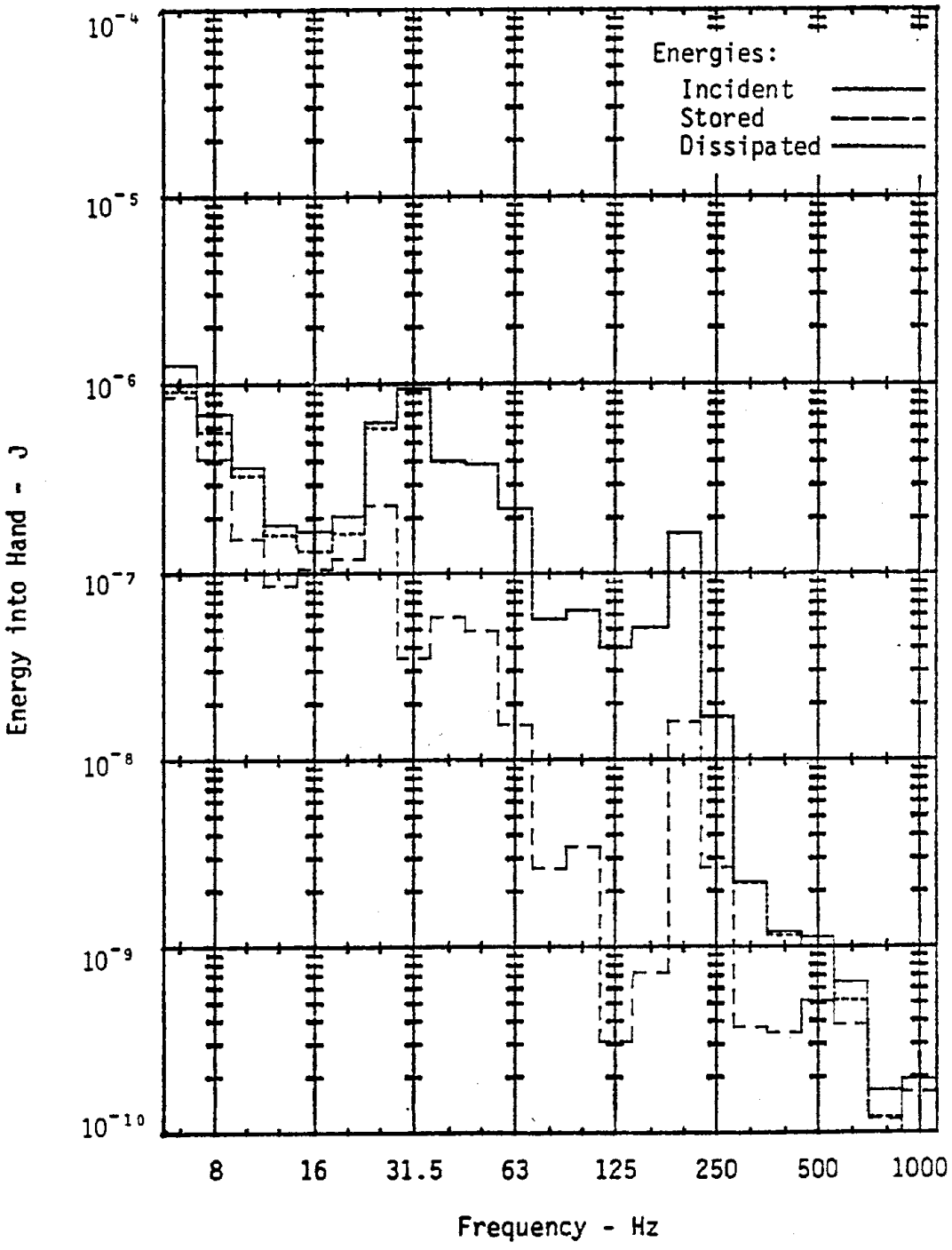

Figure D-19. RMS amplitude of instantaneous energy directed into hand from horizontal grinder with fine radial wheel. Right hand, Y-direction.

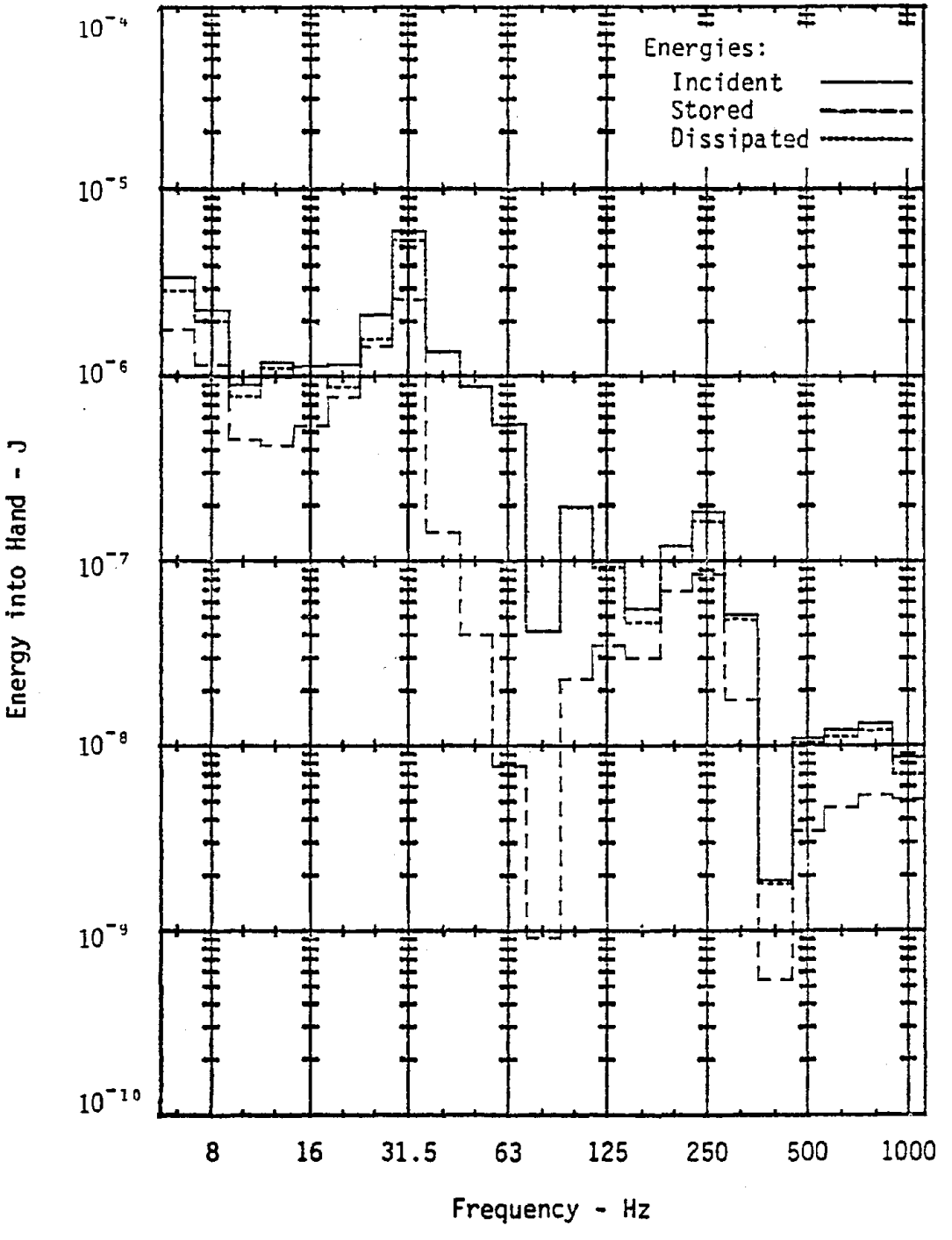

Figure D-20. RMS amplitude of instantaneous energy directed into hand from horizontal grinder with fine radial wheel. Right hand, Z-direction.

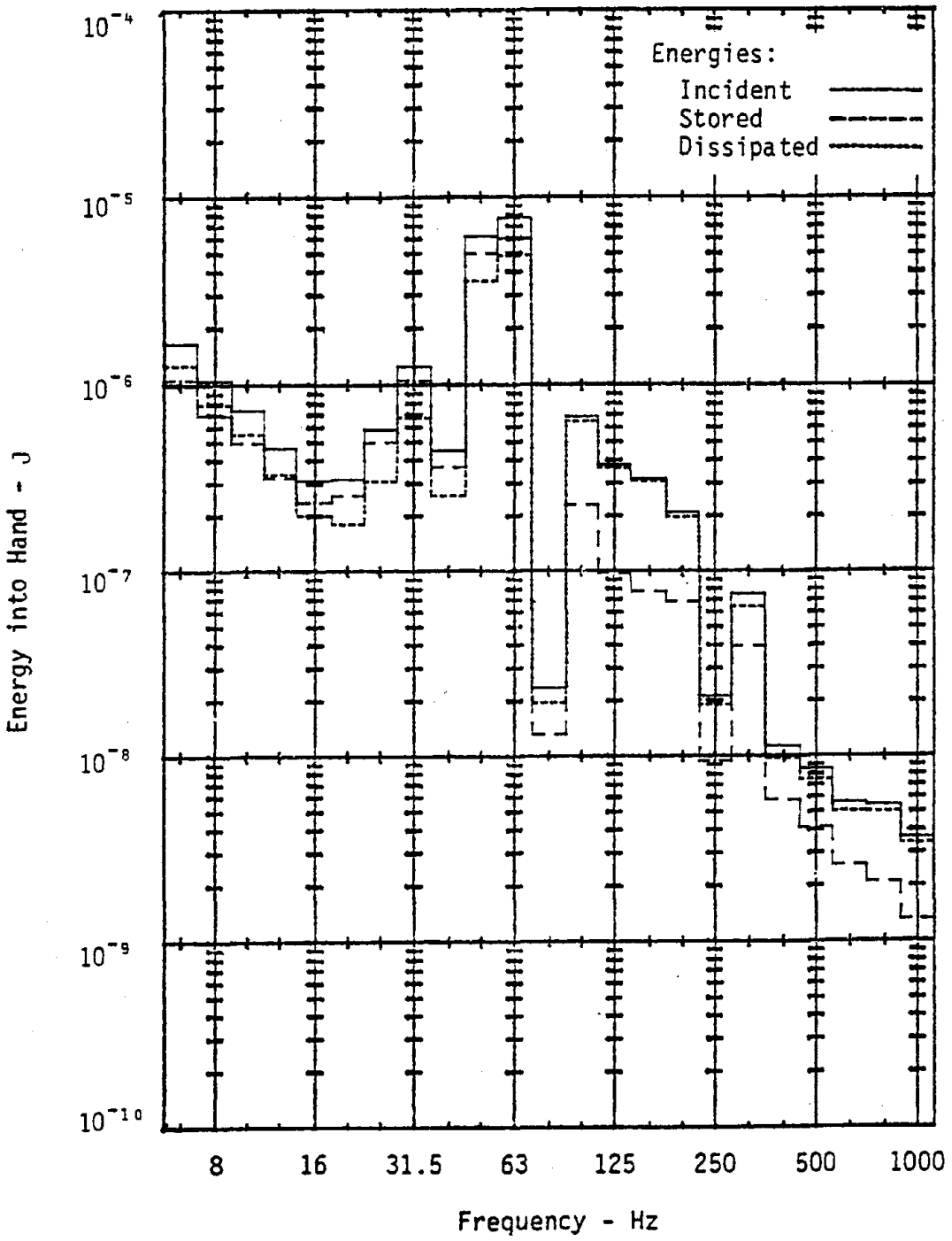

Figure D-21. RMS amplitude of instantaneous energy directed into hand from horizontal grinder with fine radial wheel. Left hand, X-direction.

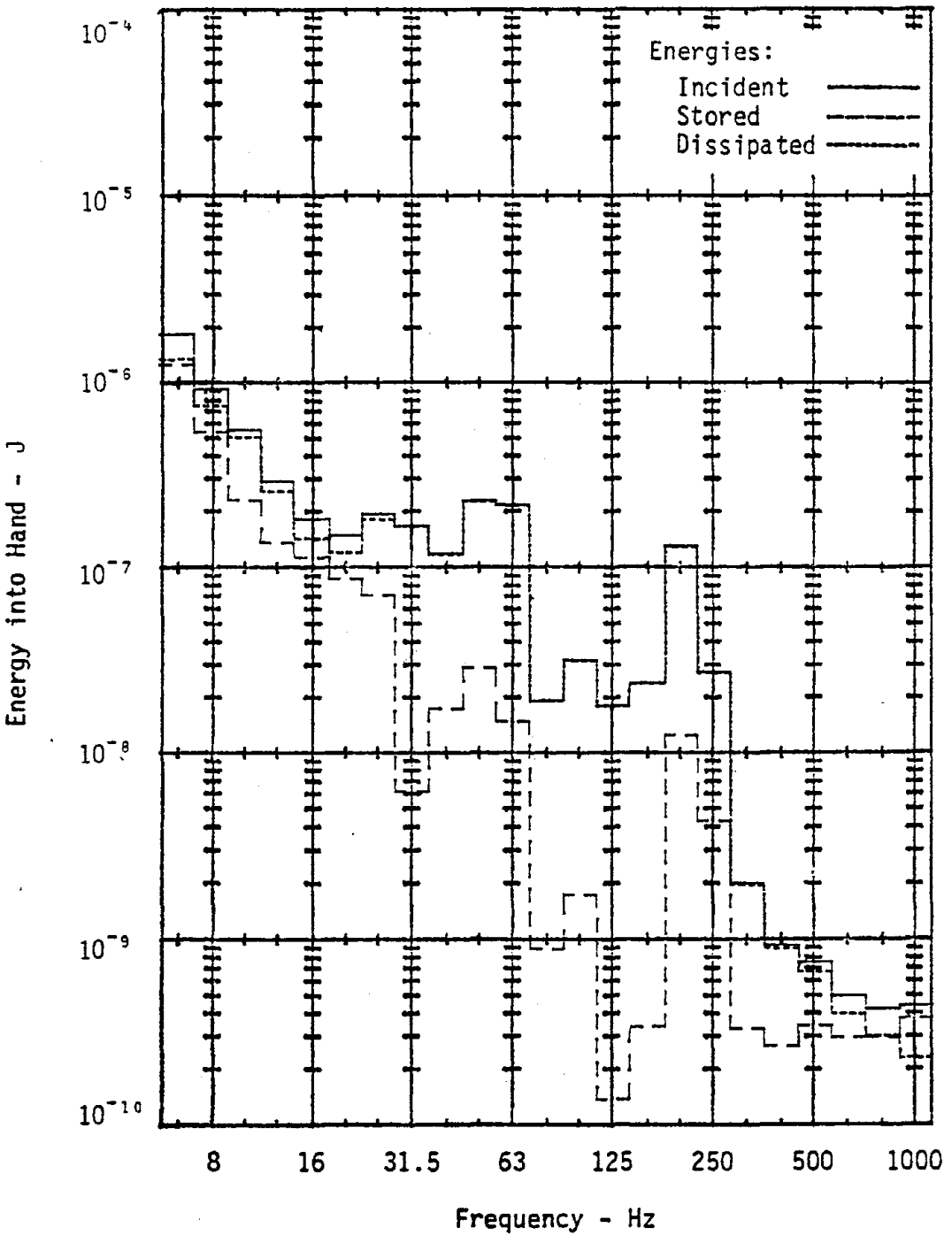

Figure D-22. RMS amplitude of instantaneous energy directed into hand from horizontal grinder with fine radial wheel. Left hand, Y-direction.

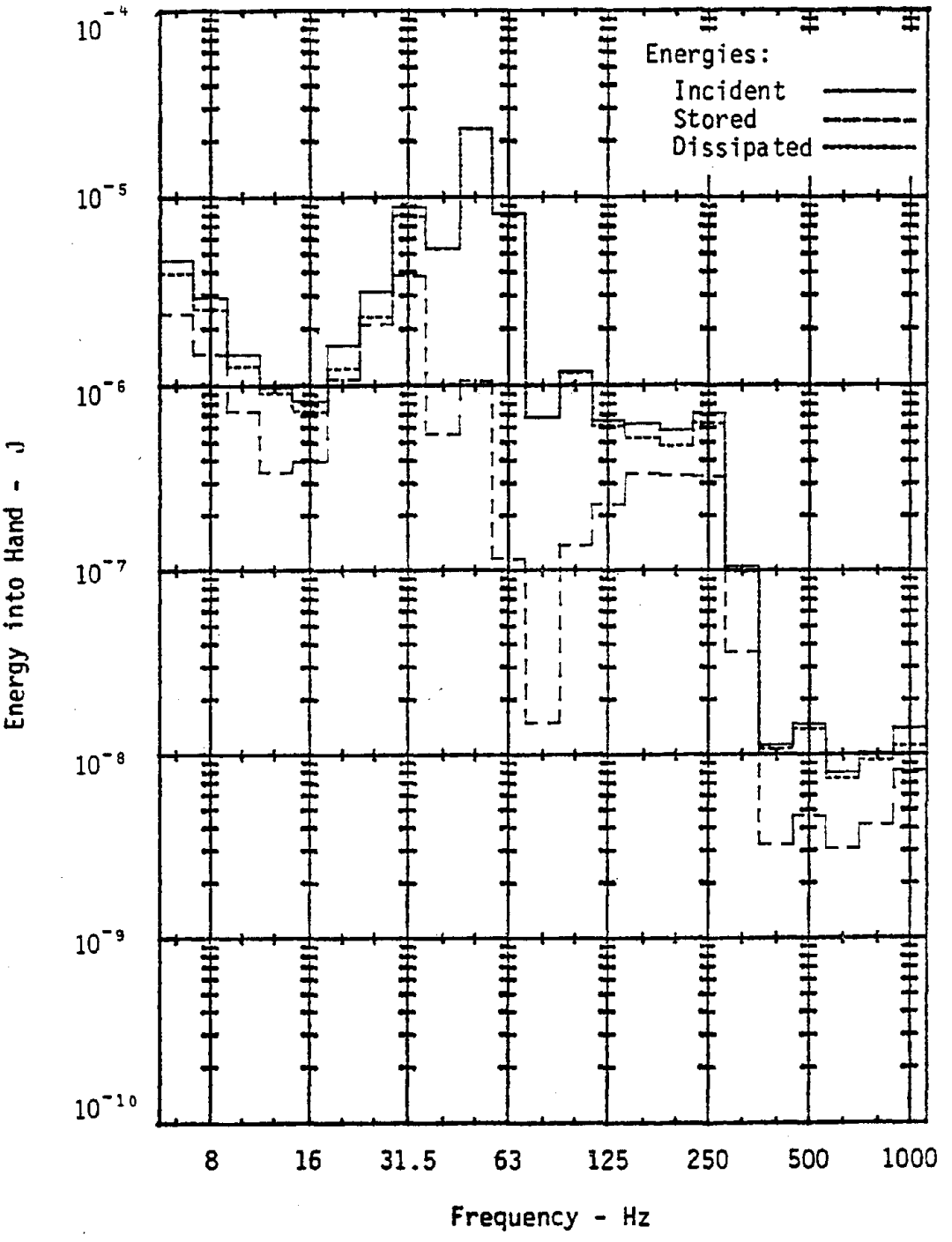

Figure D-23. RMS amplitude of instantaneous energy directed into hand from horizontal grinder with fine radial wheel. Left hand, Z-direction.

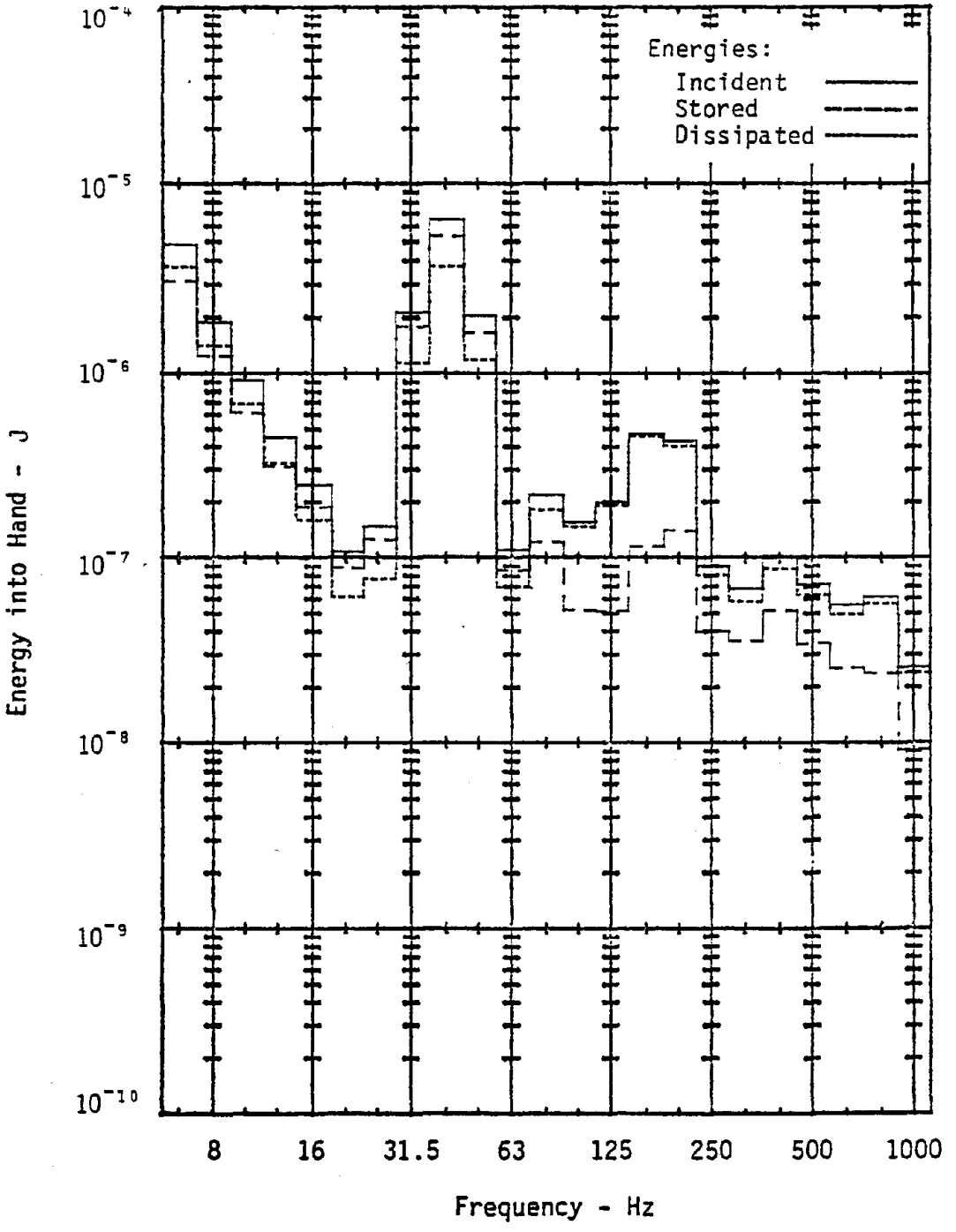

Figure D-24. RMS amplitude of instantaneous energy directed into hand from horizontal grinder with coarse flared cup wheel. Right hand, X-direction.

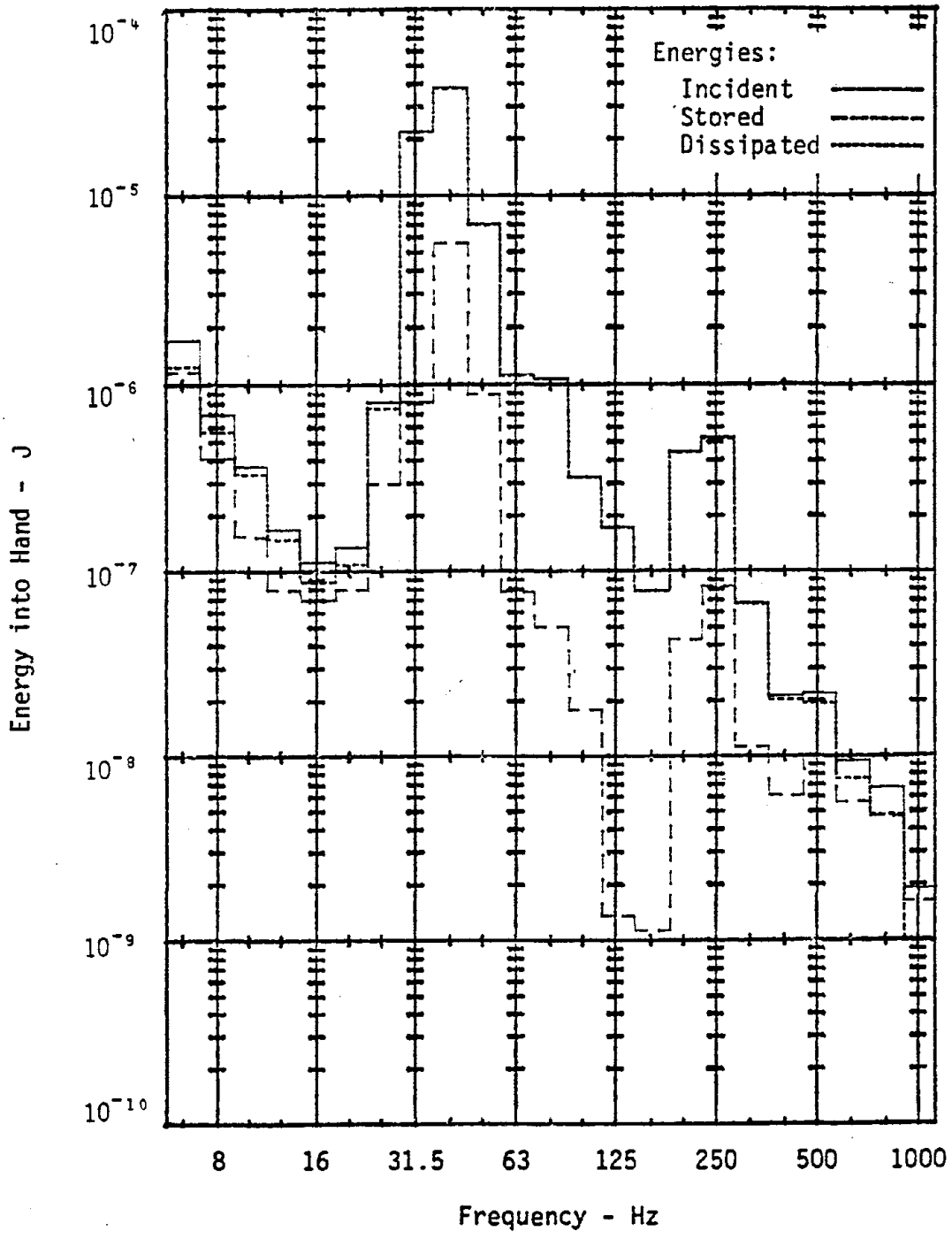

Figure D-25. RMS amplitude of instantaneous energy directed into hand from horizontal grinder with coarse flared cup wheel. Right hand, Y-direction.

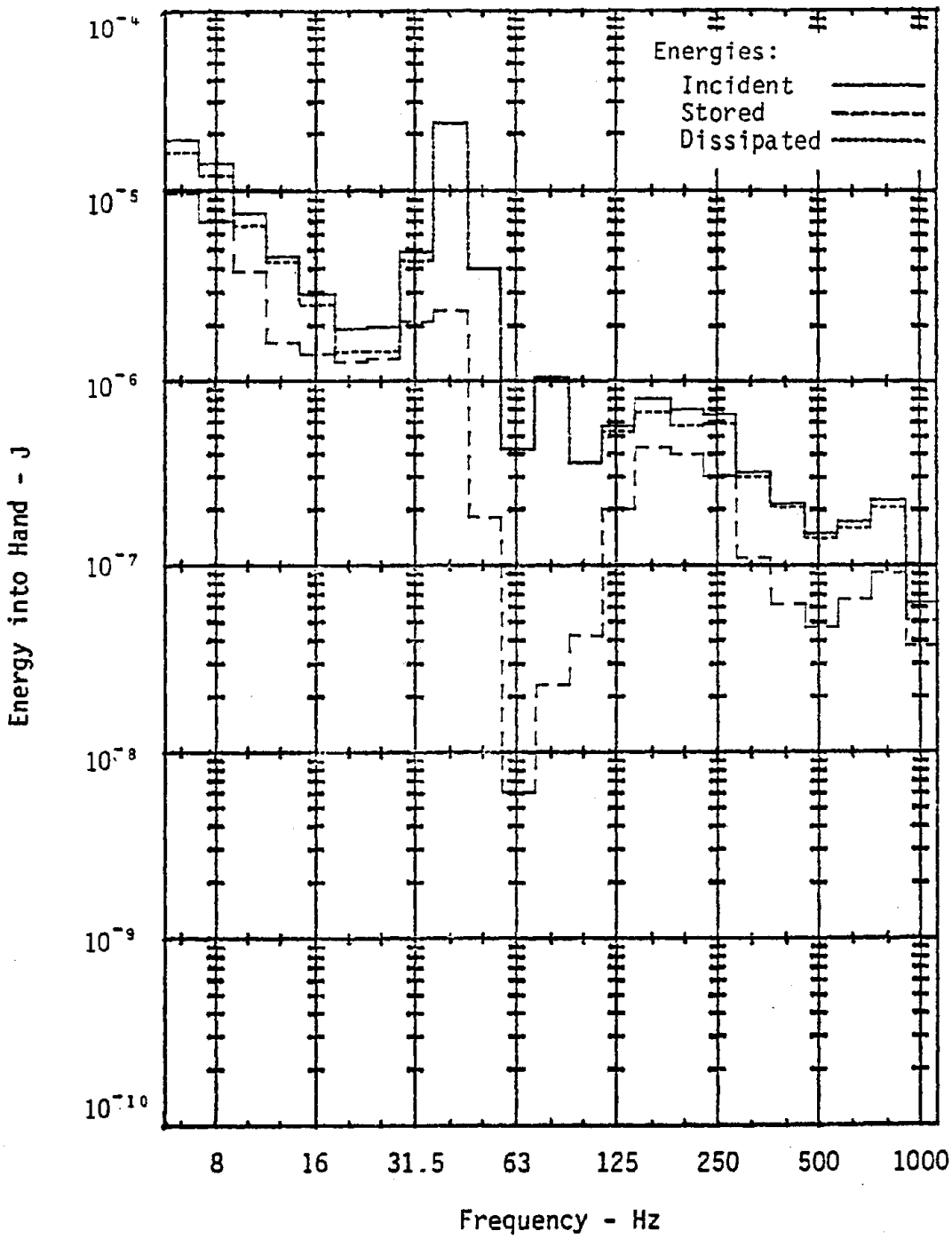

Figure D-26. RMS amplitude of instantaneous energy directed into hand from horizontal grinder with coarse flared cup wheel. Right hand, Z-direction.

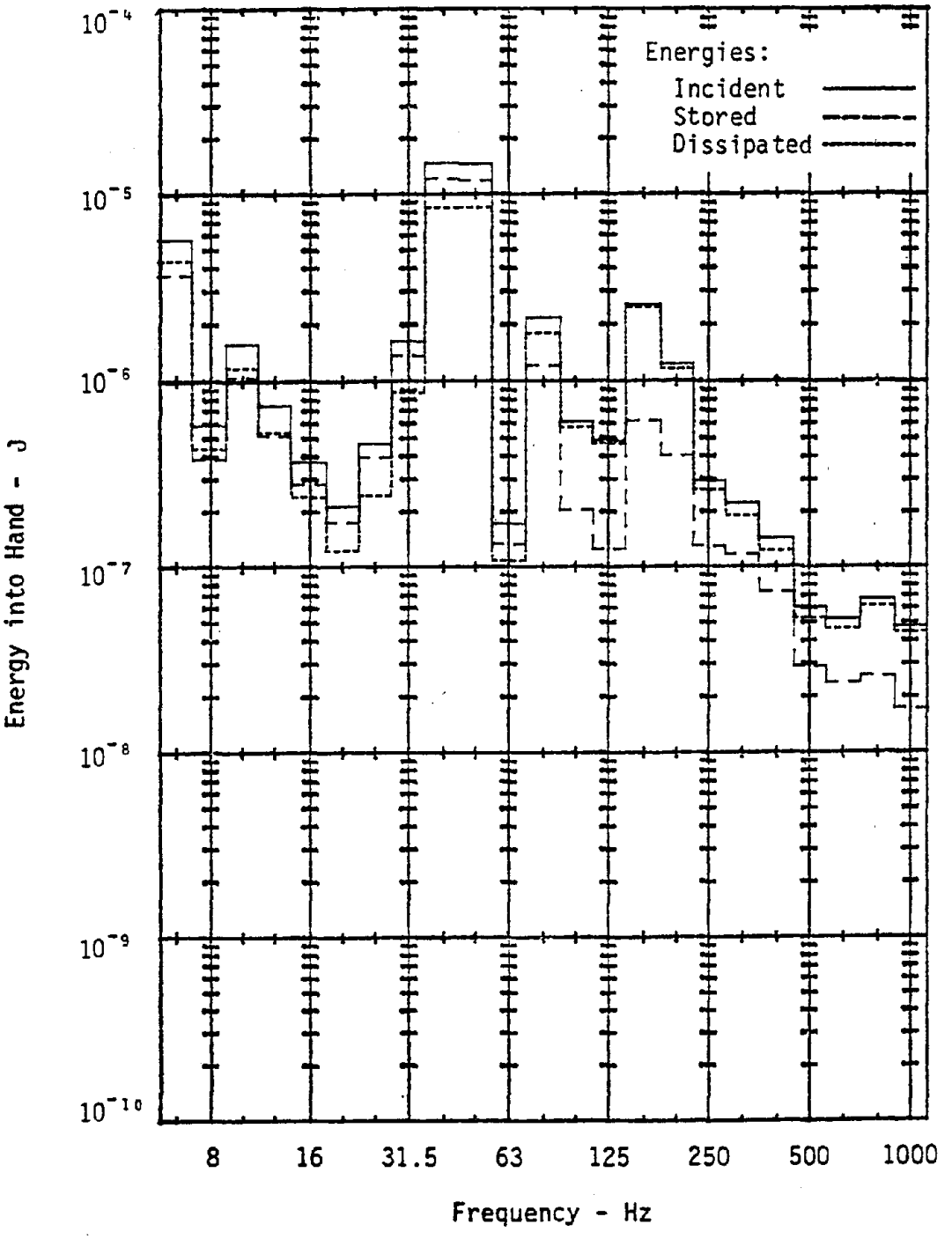

Figure D-27. RMS amplitude of instantaneous energy directed into hand from horizontal grinder with coarse flared cup wheel. Left hand, X-direction.

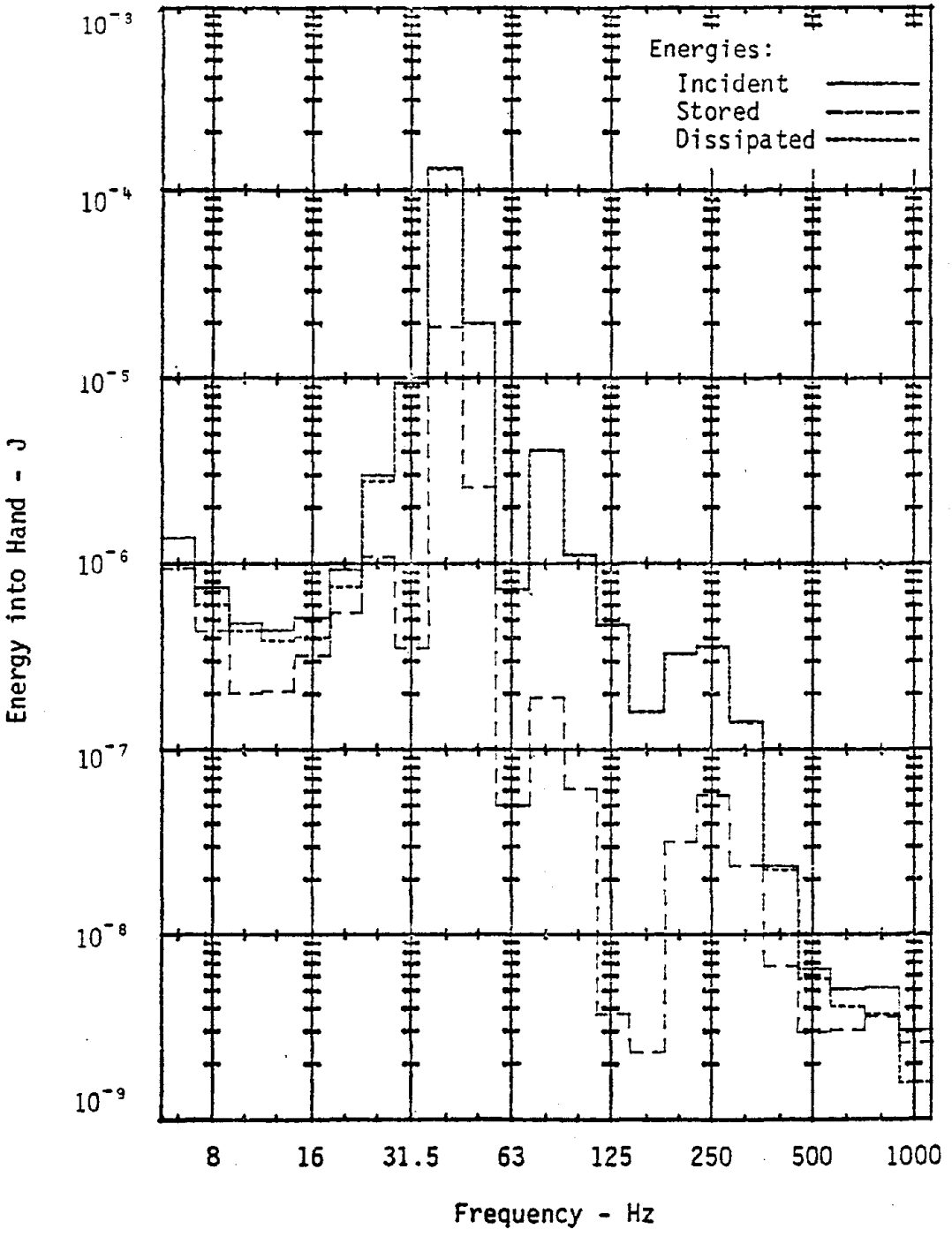

Figure D-28. RMS amplitude of instantaneous energy directed into hand from horizontal grinder with coarse flared cup wheel. Left hand, Y-direction.

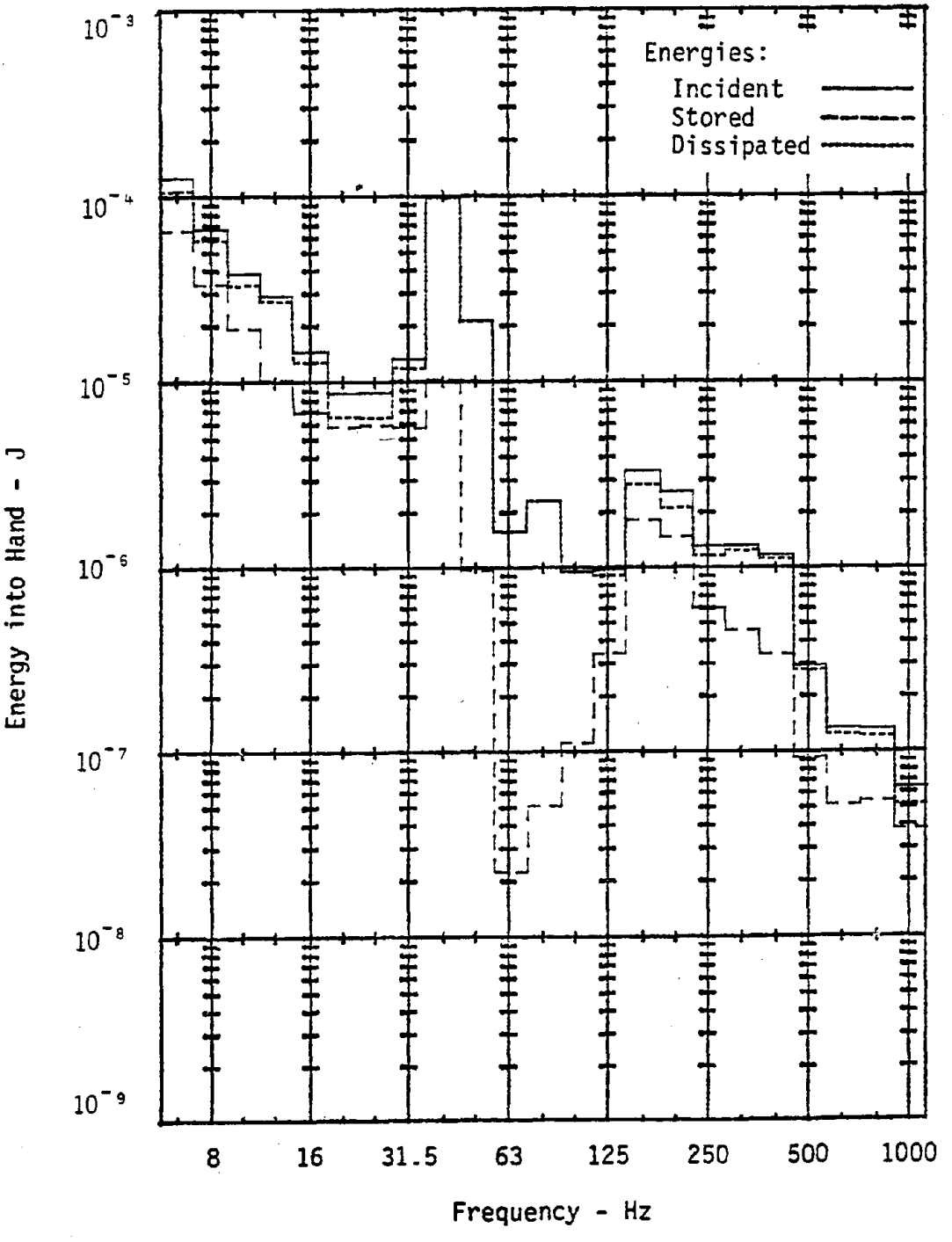

Figure D-29. RMS amplitude of instantaneous energy directed into hand from horizontal grinder with coarse flared cup wheel. Left hand, Z-direction.

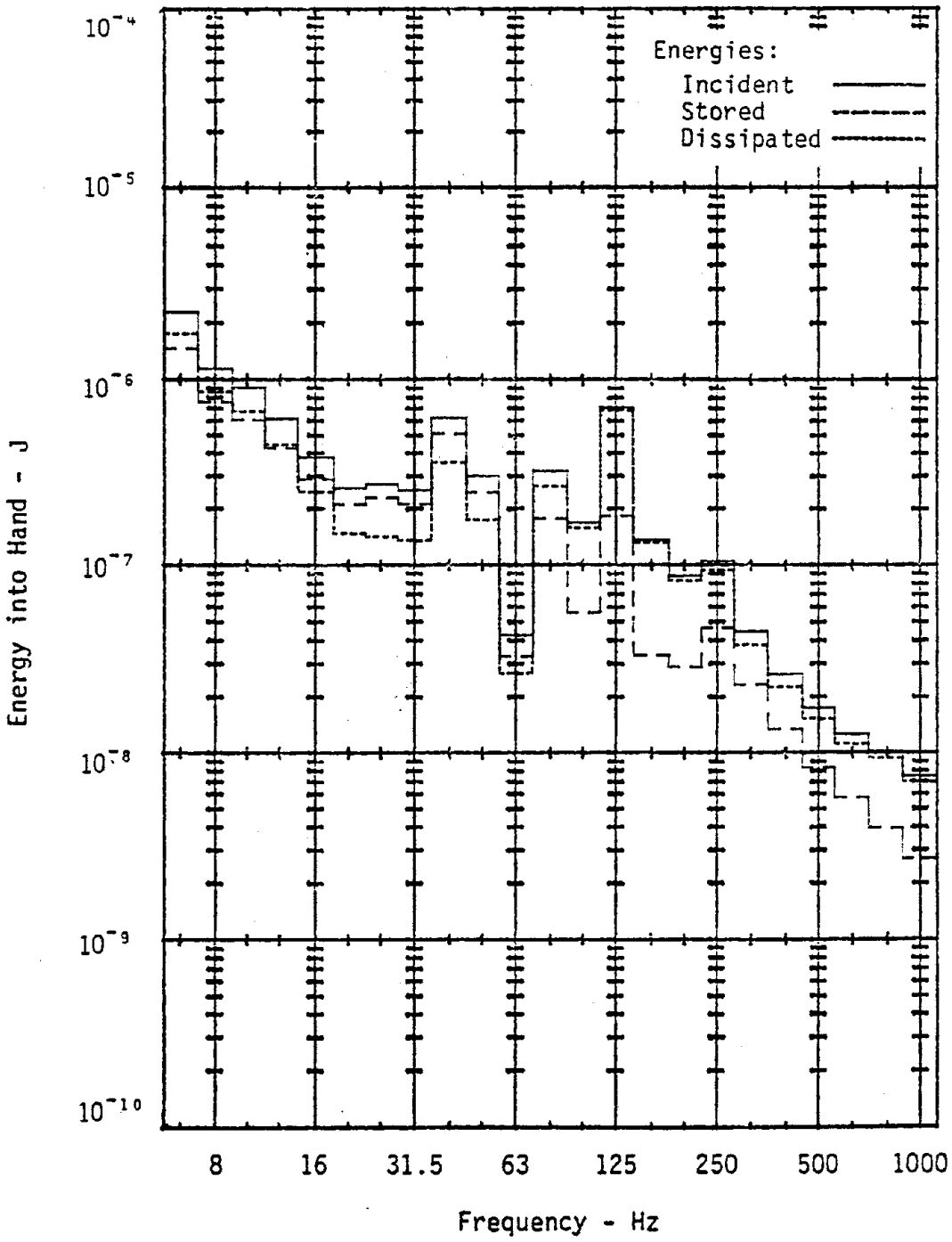

Figure D-30. RMS amplitude of instantaneous energy directed into hand from vertical grinder with sanding pad, medium paper. Right hand, X-direction.

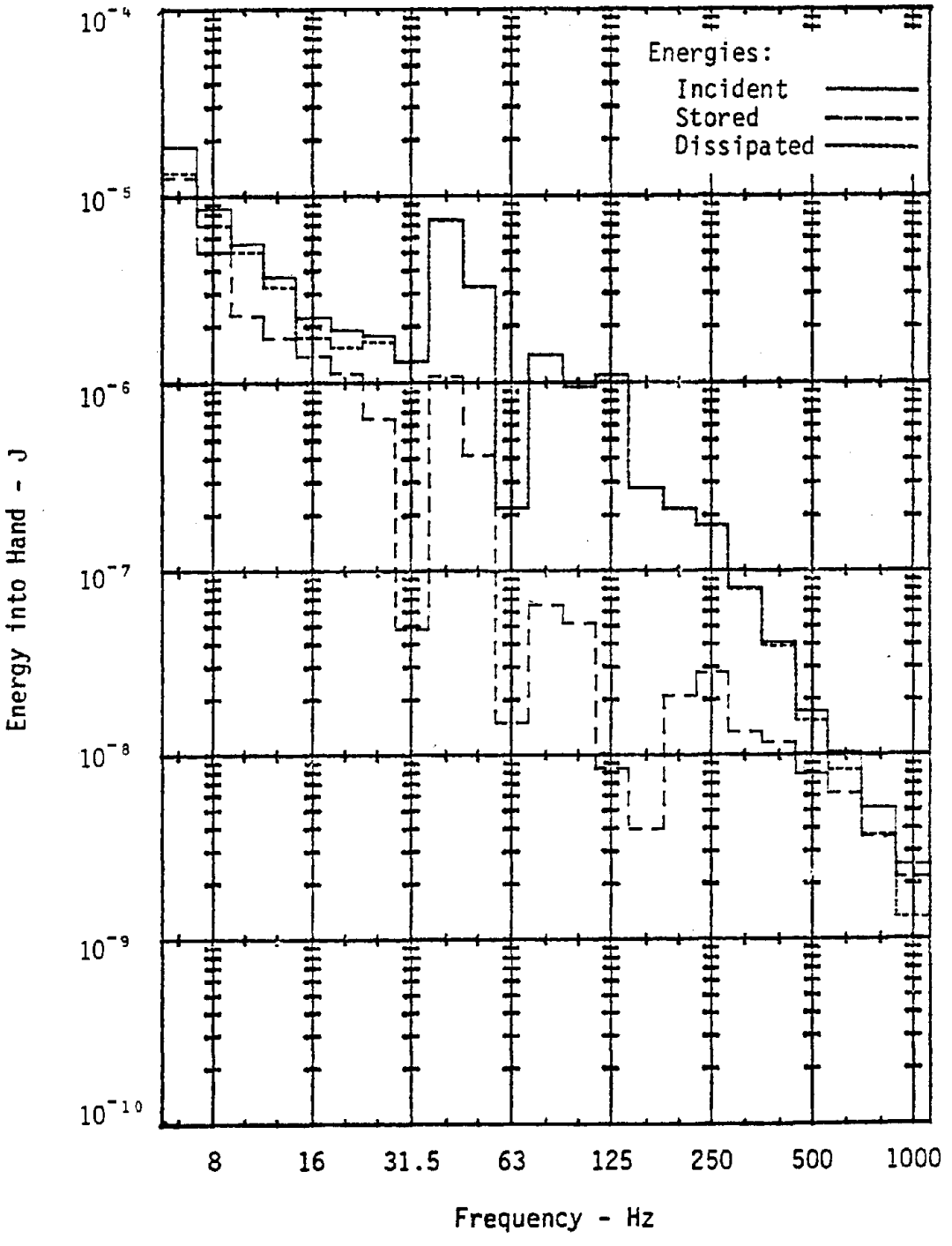

Figure D-31. RMS amplitude of instantaneous energy directed into hand from vertical grinder with sanding pad, medium paper. Right hand, Y-direction.

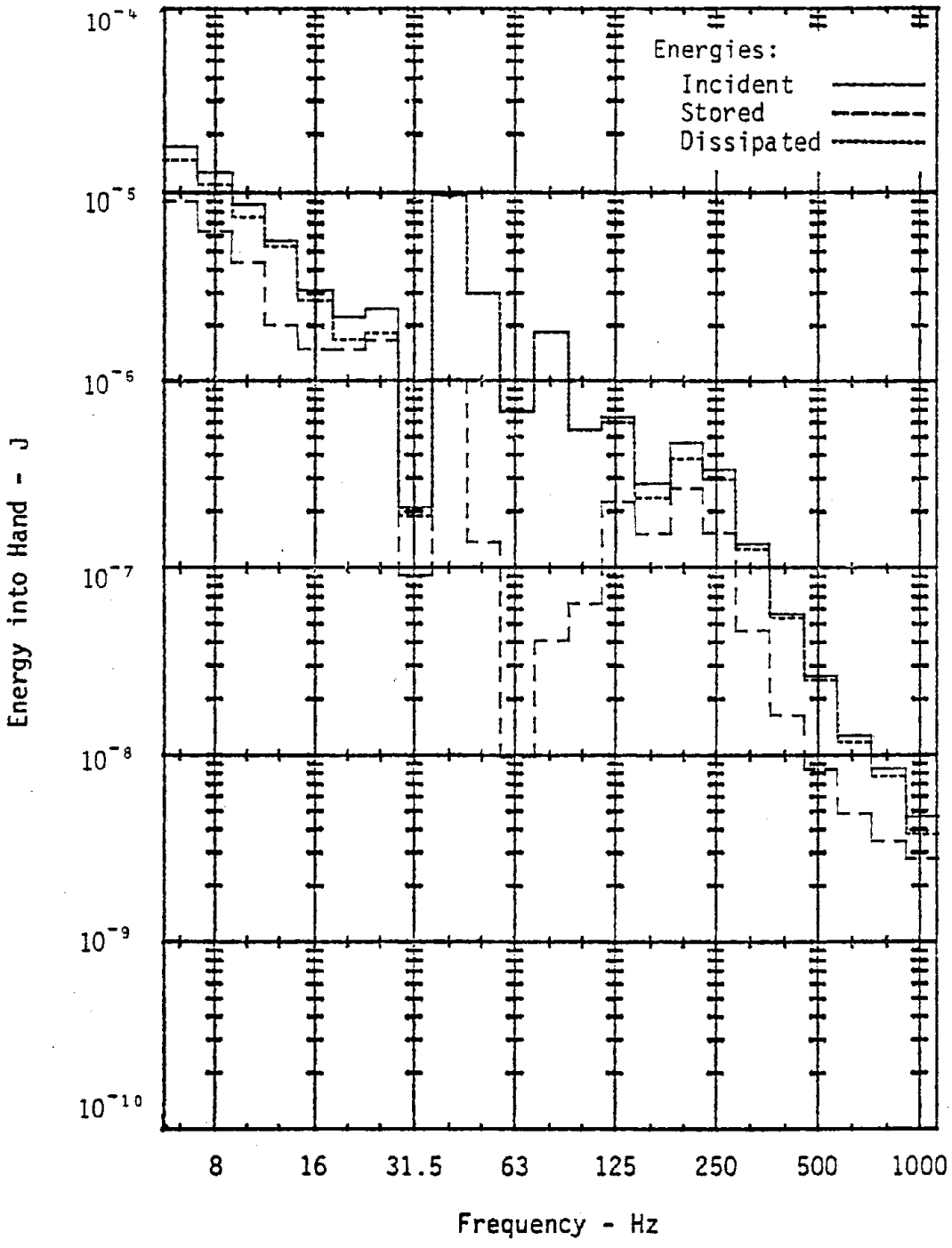

Figure D-32. RMS amplitude of instantaneous energy directed into hand from vertical grinder with sanding pad, medium paper. Right hand, Z-direction.

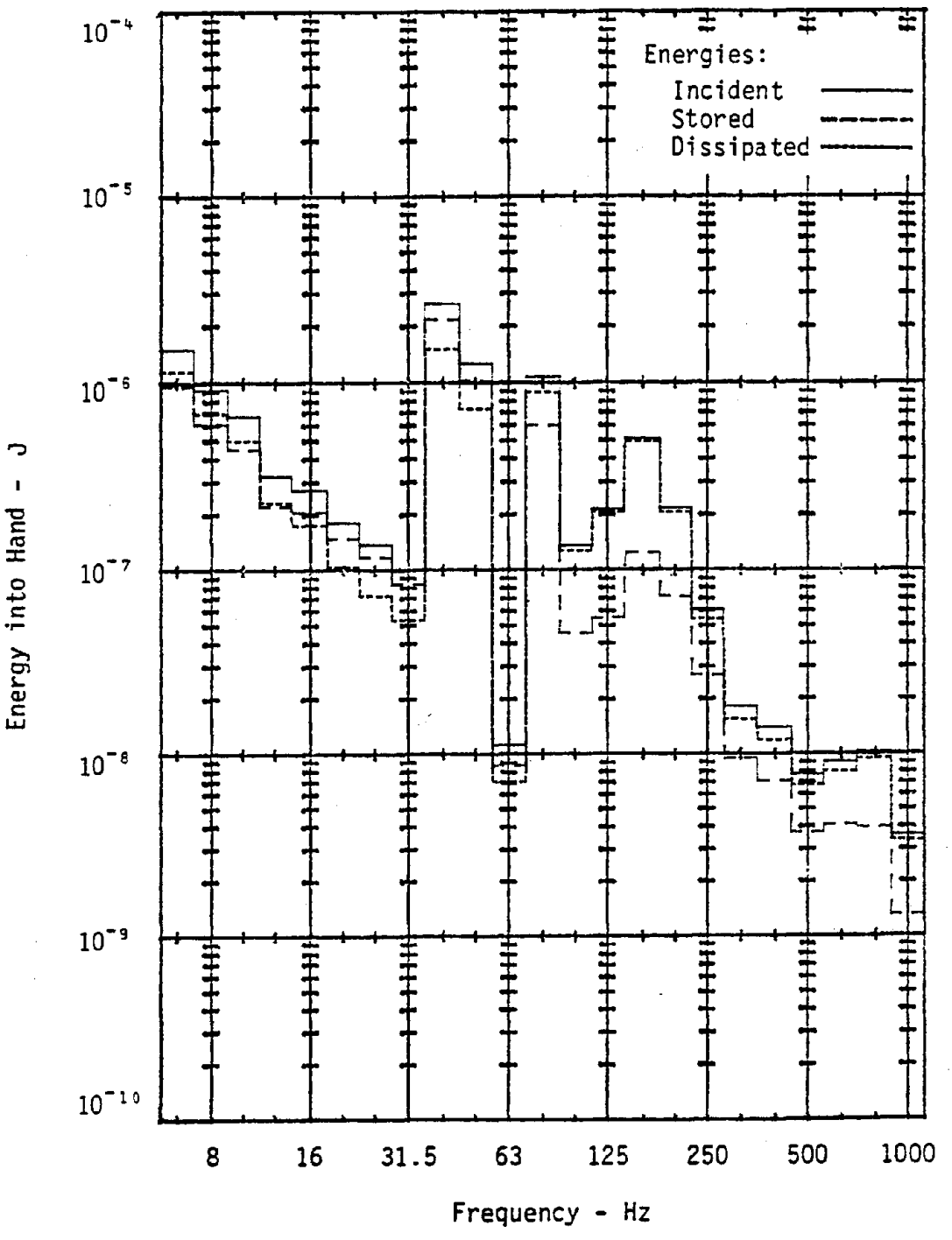

Figure D-33. RMS amplitude of instantaneous energy directed into hand from vertical grinder with sanding pad, medium paper. Left hand, X-direction.

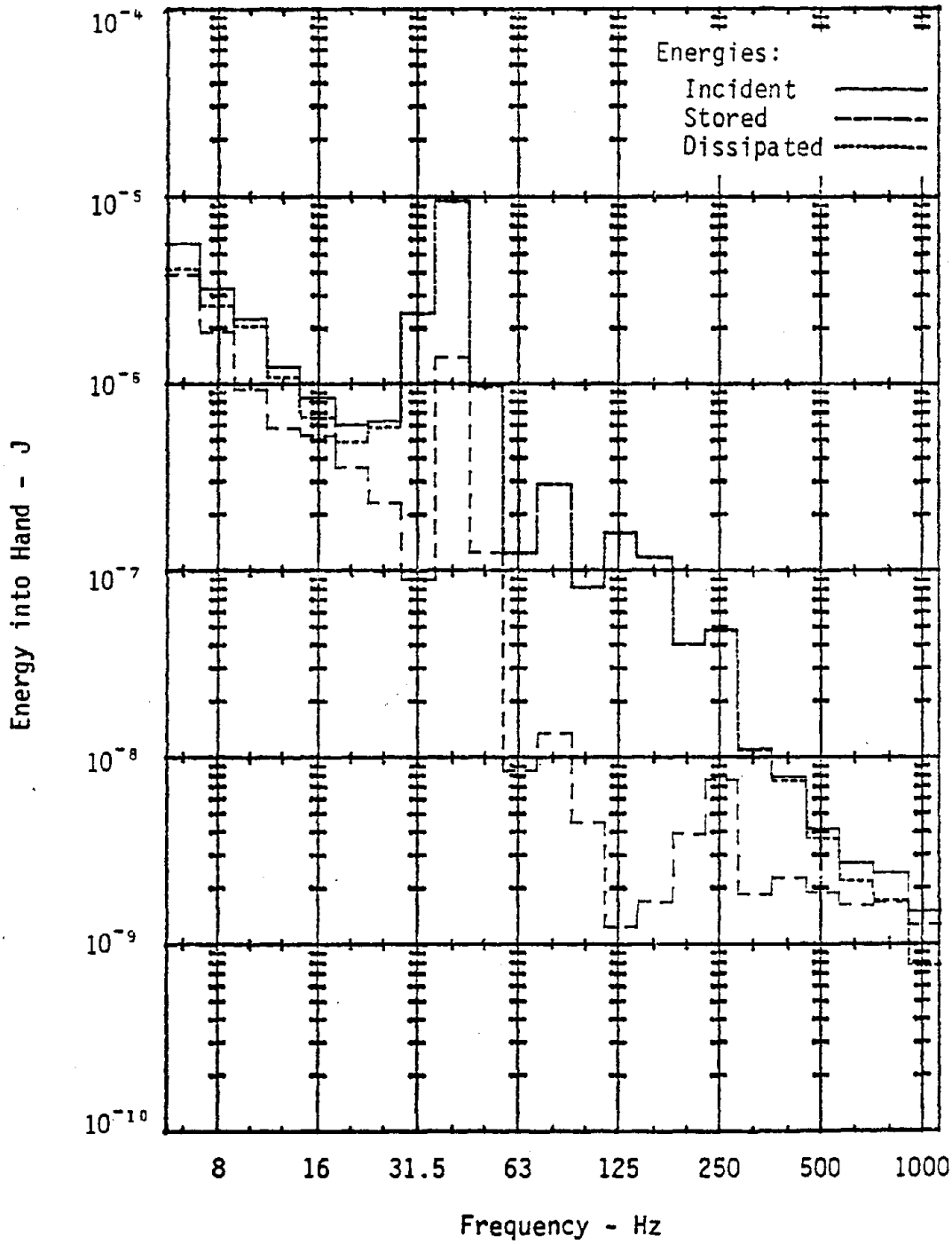

Figure D-34. RMS amplitude of instantaneous energy directed into hand from vertical grinder with sanding pad, medium paper. Left hand, Y-direction.

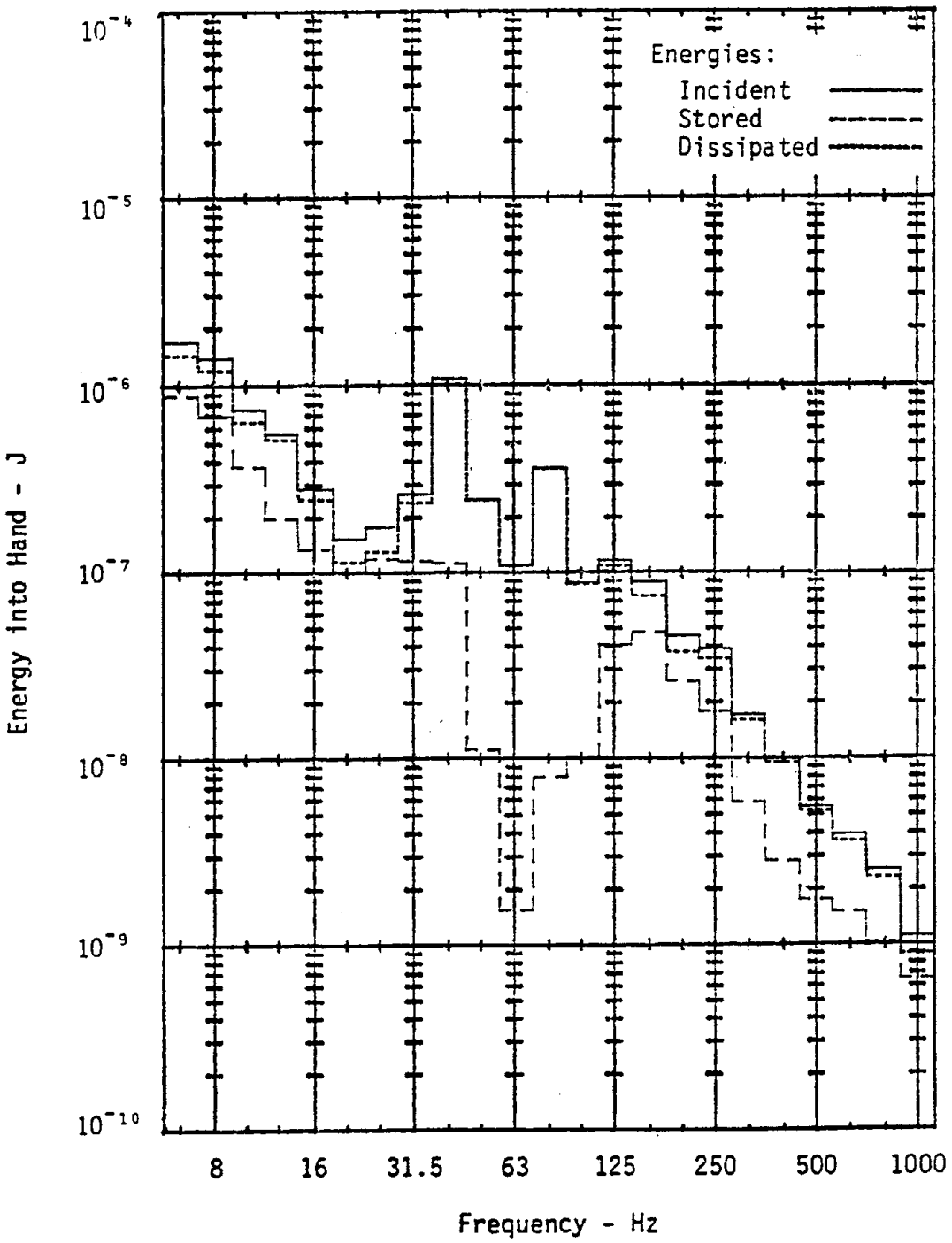

Figure D-35. RMS amplitude of instantaneous energy directed into hand from vertical grinder with sanding pad, medium paper. Left hand, Z-direction.

APPENDIX E

ACCELERATION TIME HISTORIES AND FOURIER SERIES DATA

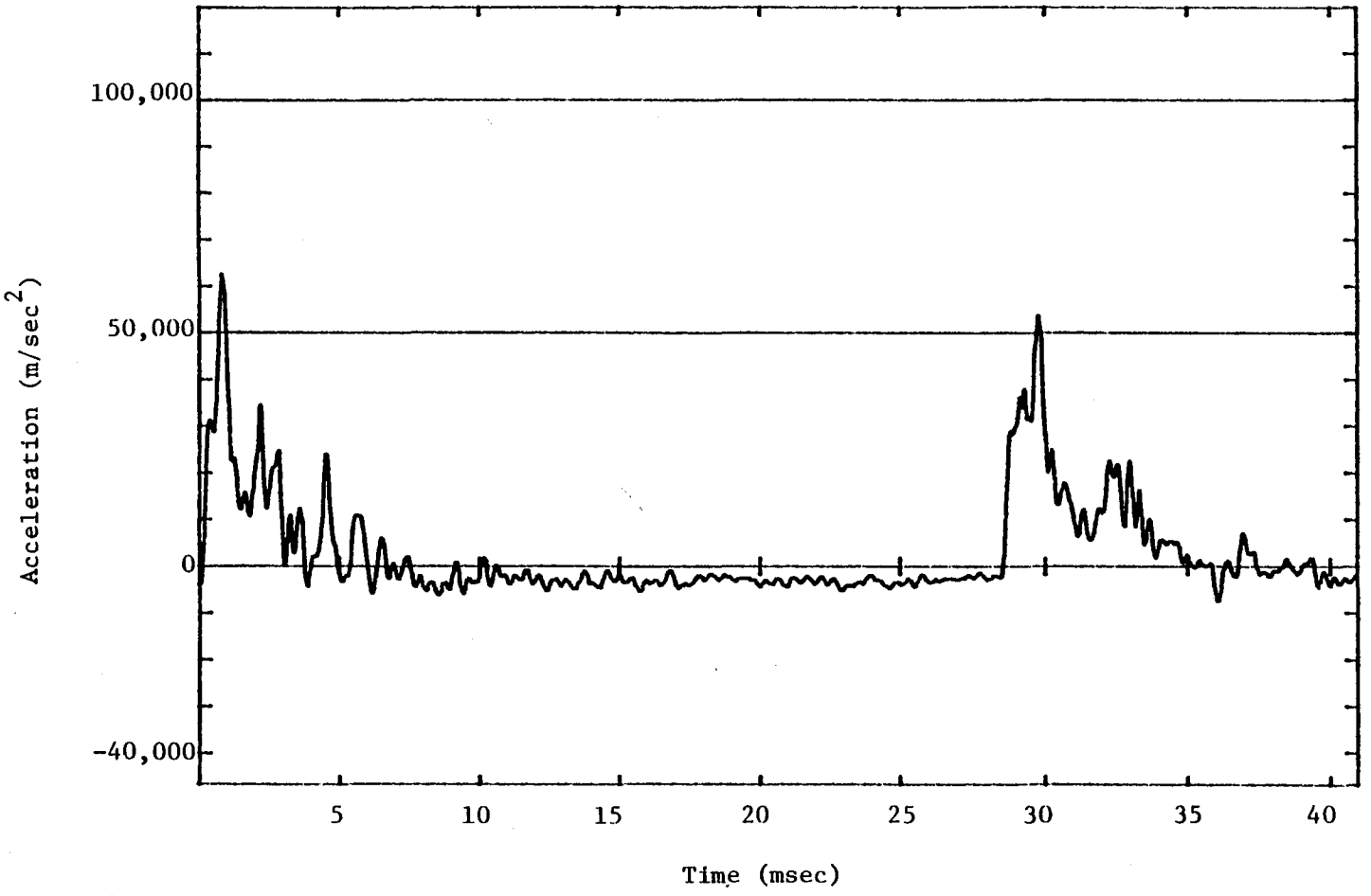

Figure E-1. Acceleration time history for chisel of chipping hammer A used to clean castings. Slot chipping on nodular cast iron. Chipping hammer operated at full throttle.

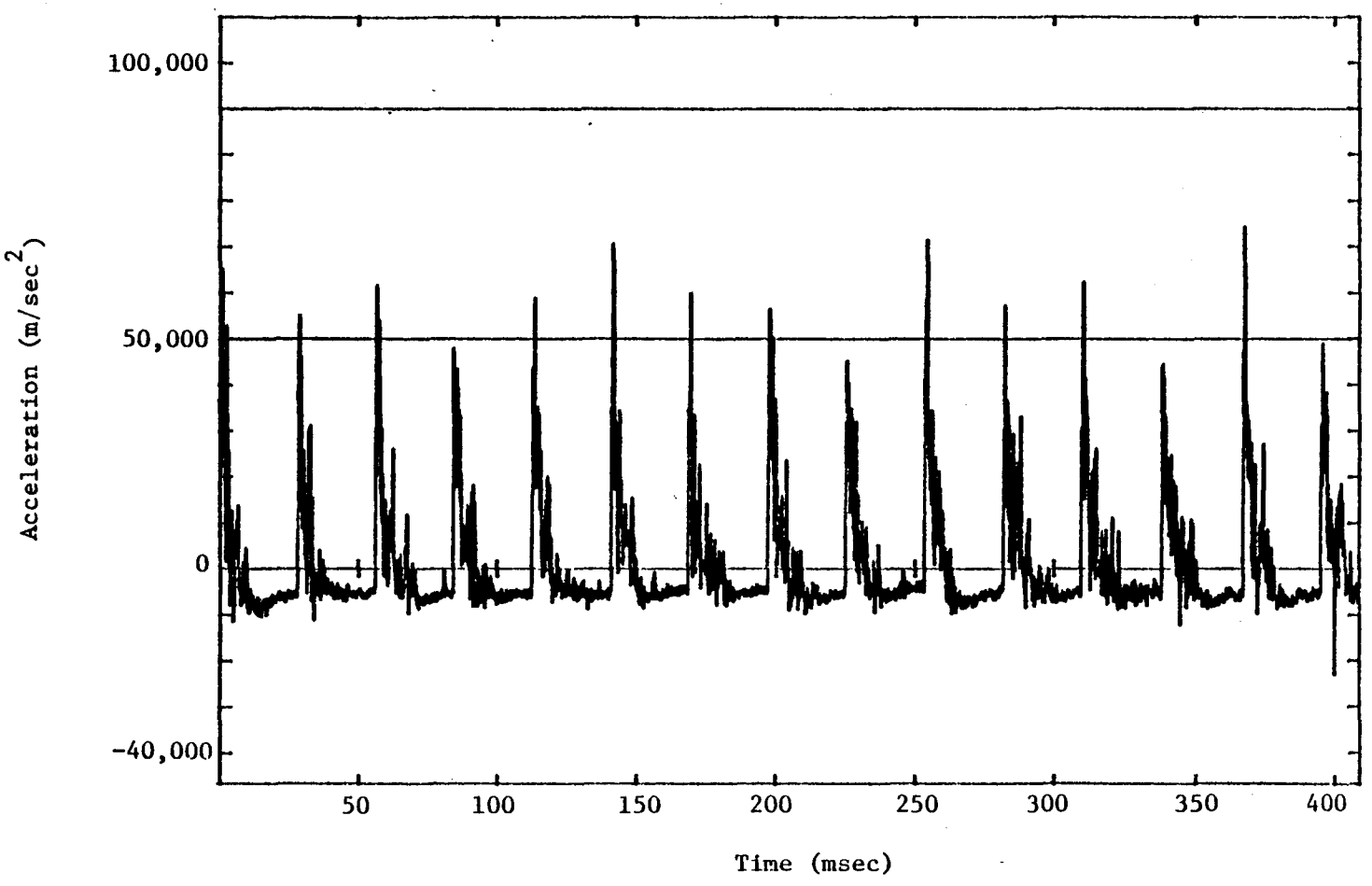

Figure E-2. Condensed time scale acceleration time history for chisel of chipping hammer A used to clean castings. Slot chipping on nodular cast iron. Chipping hammer operated at full throttle.

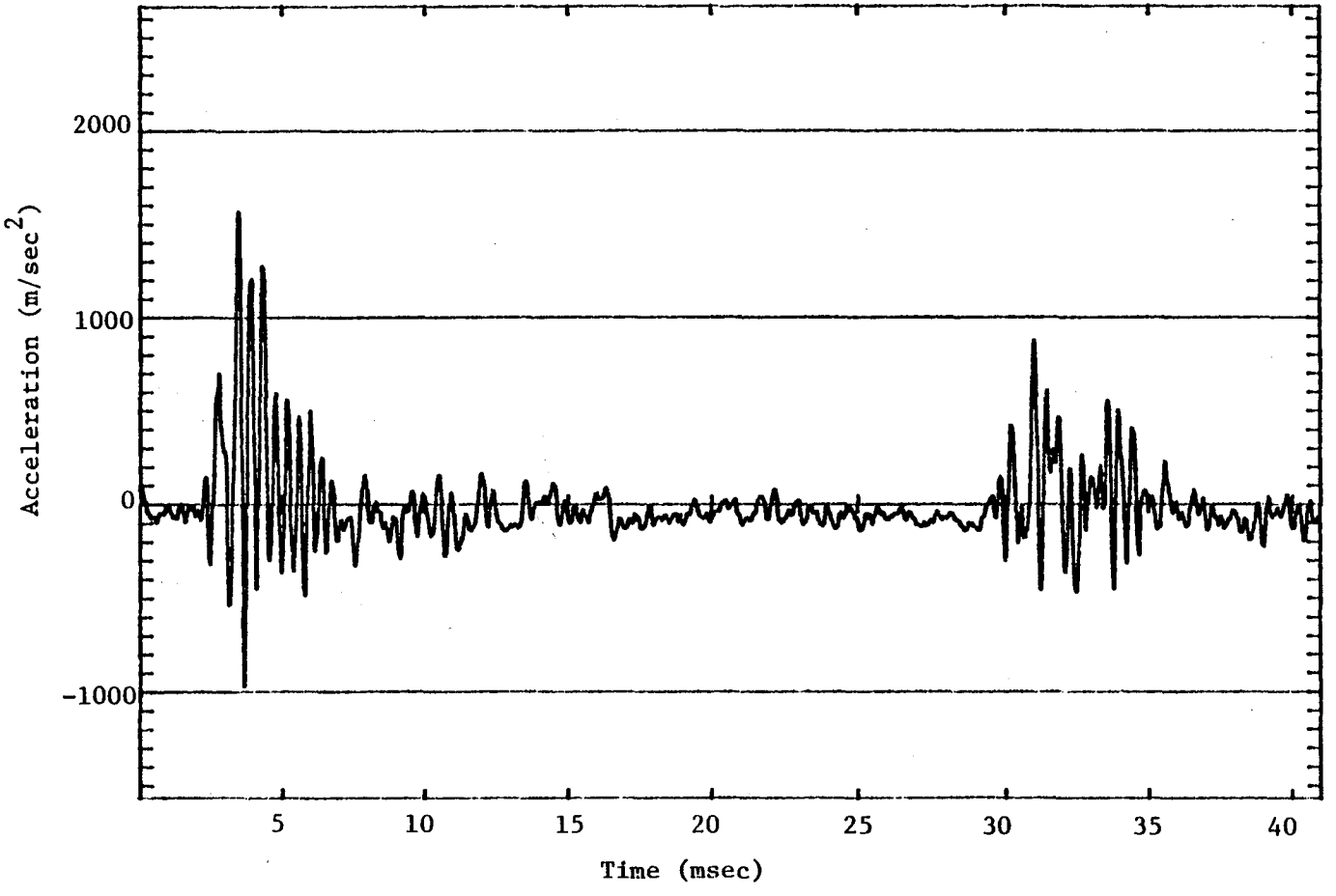

Figure E-3. Acceleration time history for handle of chipping hammer A used to clean castings. Slot chipping on nodular cast iron. Chipping hammer operated at full throttle.

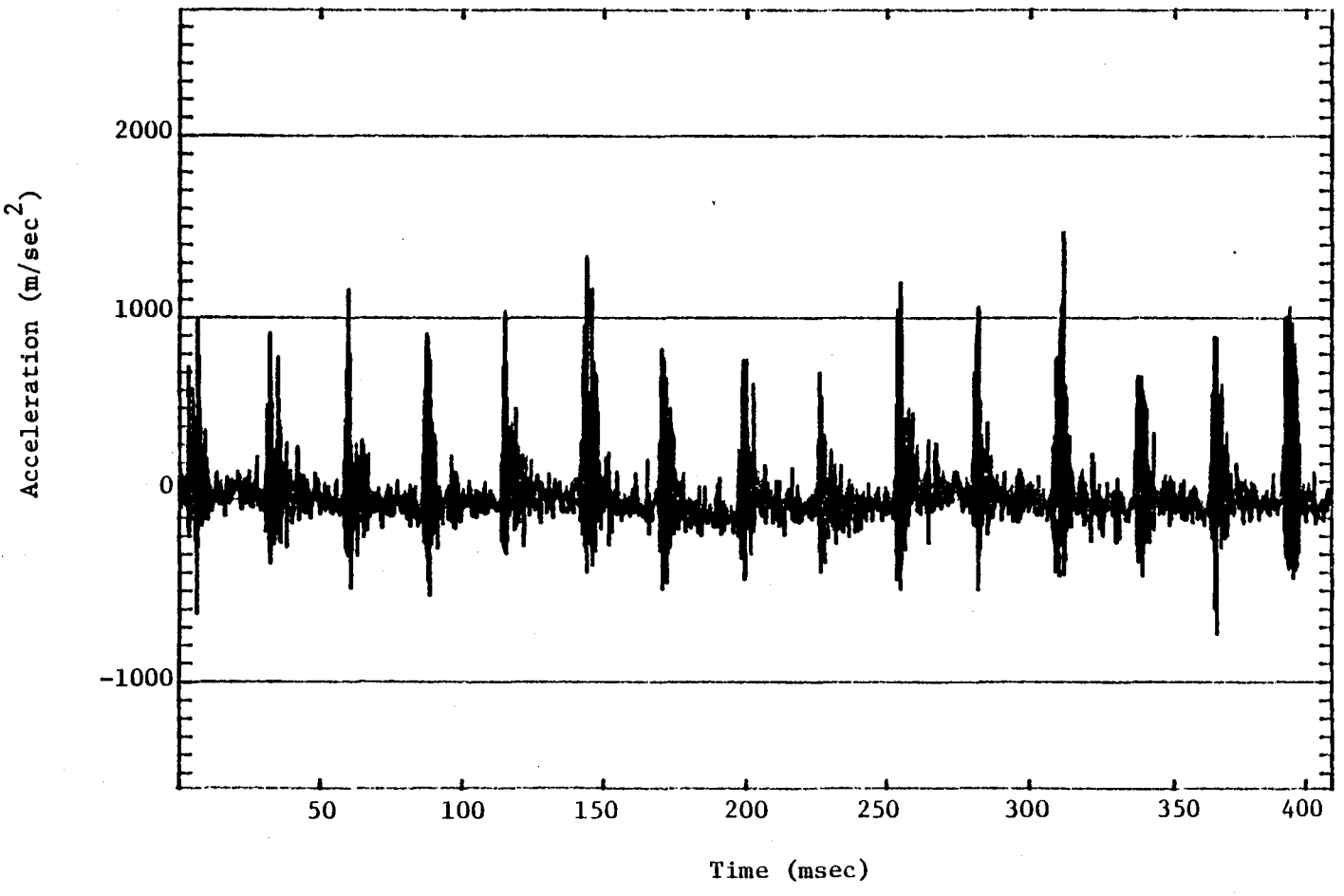

Figure E-4. Condensed time scale acceleration time history for handle of chipping hammer A used to clean castings. Slot chipping on nodular cast iron. Chipping hammer operated at full throttle.

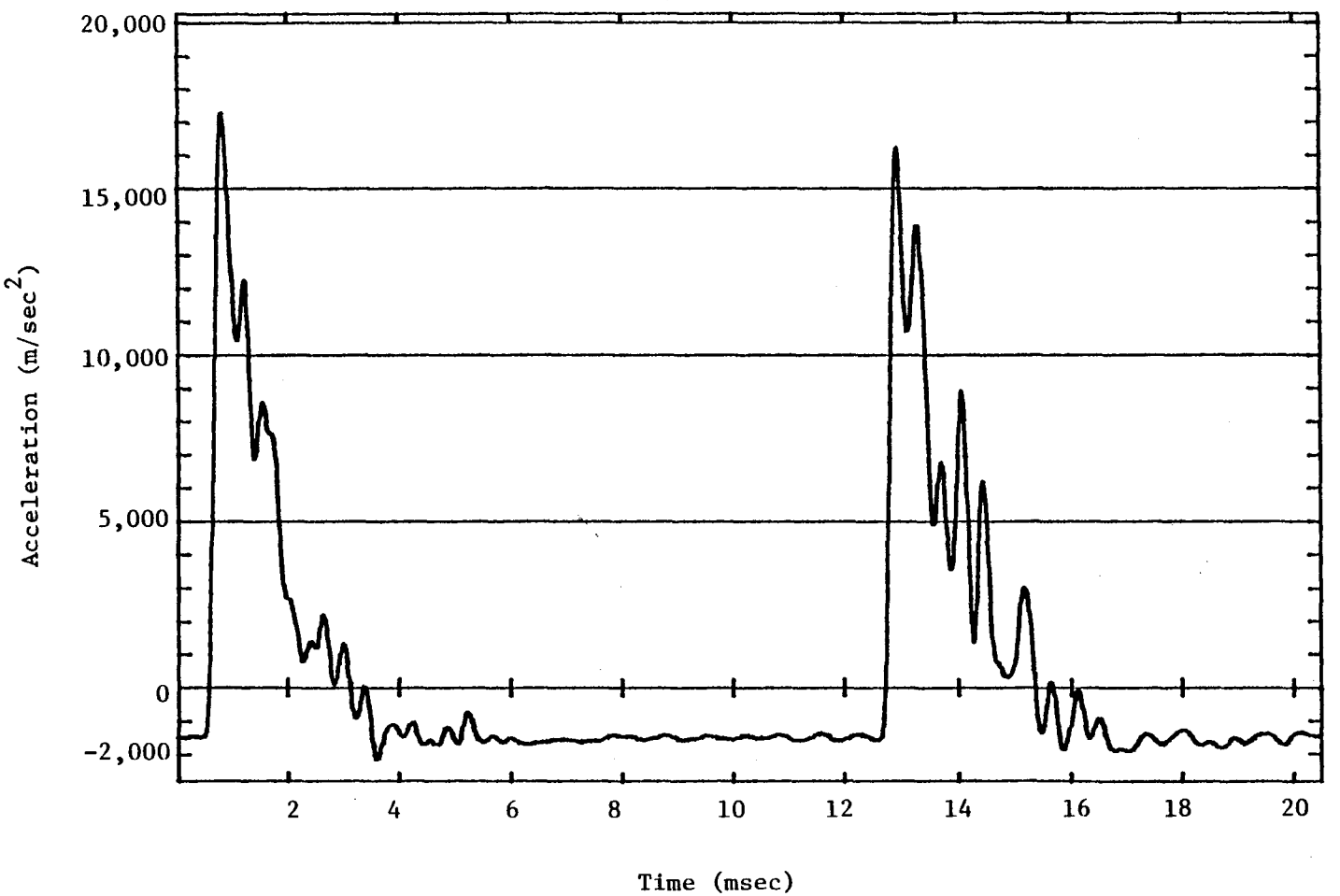

Figure E-5. Acceleration time history for chisel of small chipping hammer used to carve limestone. Chipping hammer operated at full throttle.

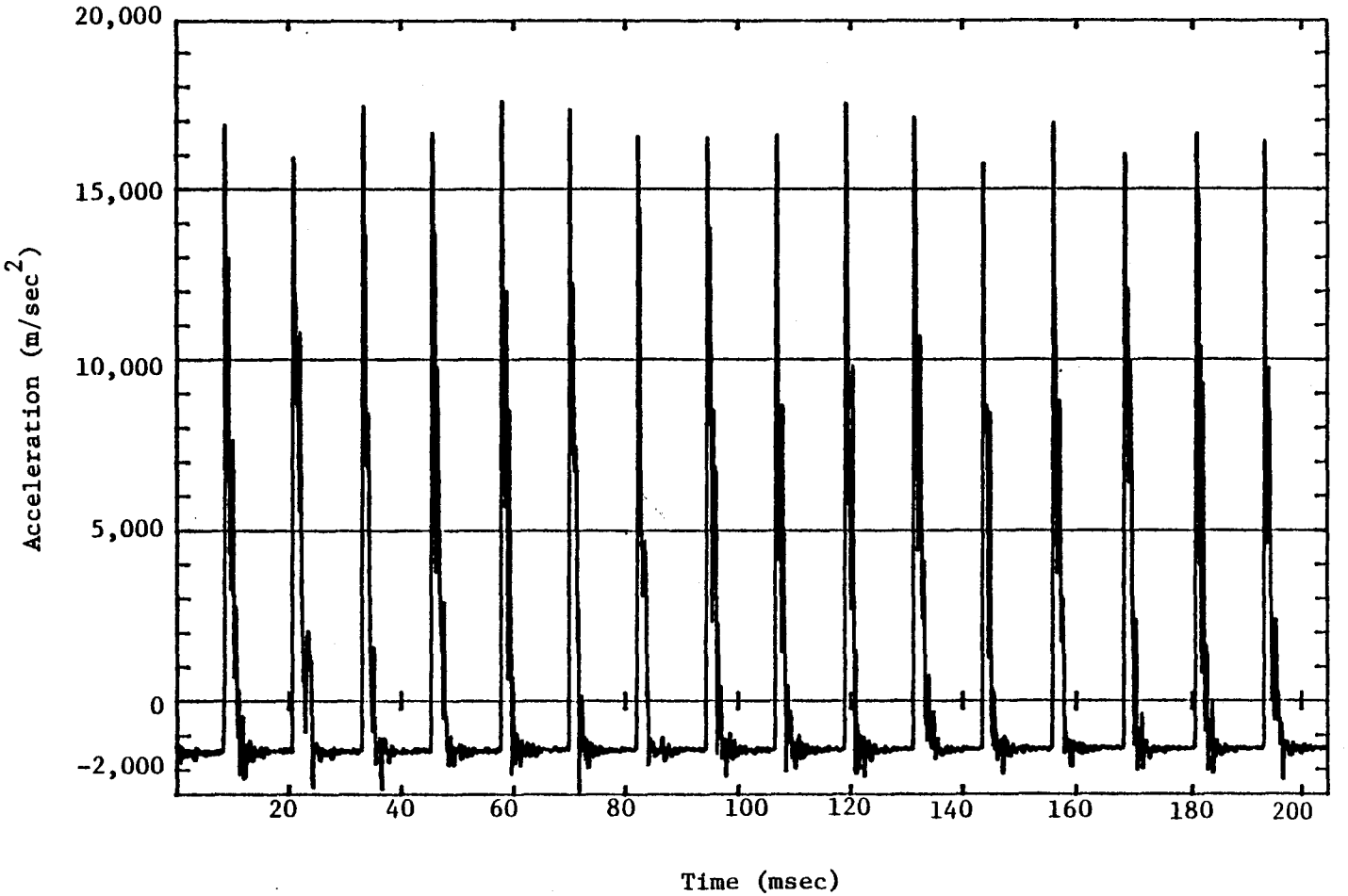

Figure E-6. Condensed time scale acceleration time history for chisel of small chipping hammer used to carve limestone. Chipping hammer operated at full throttle.

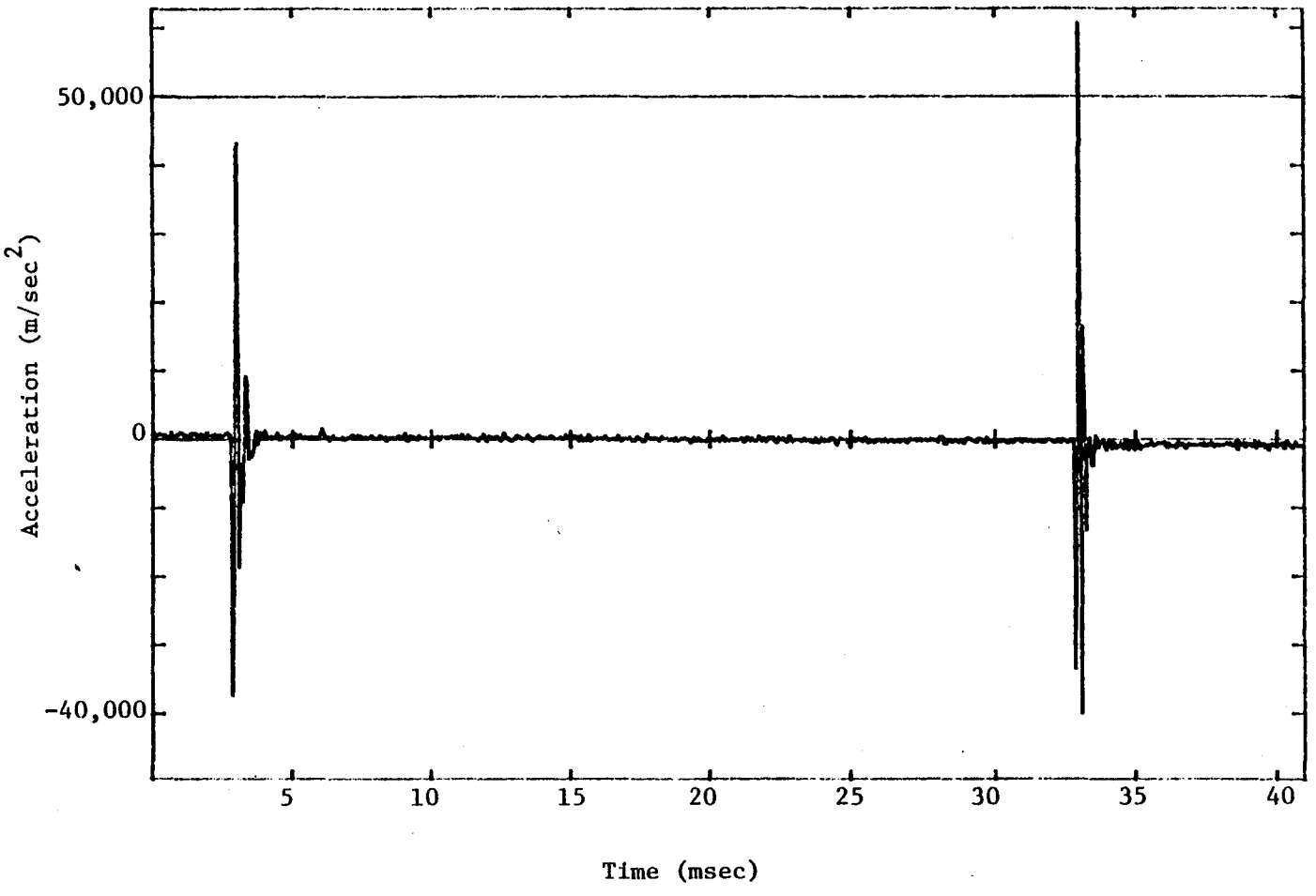

Figure E-9. Acceleration time history for chisel of chipping hammer D used to shape propeller blades. Chipping on Ni-Al-Br. Chipping hammer operated at 1/2-3/4 throttle.

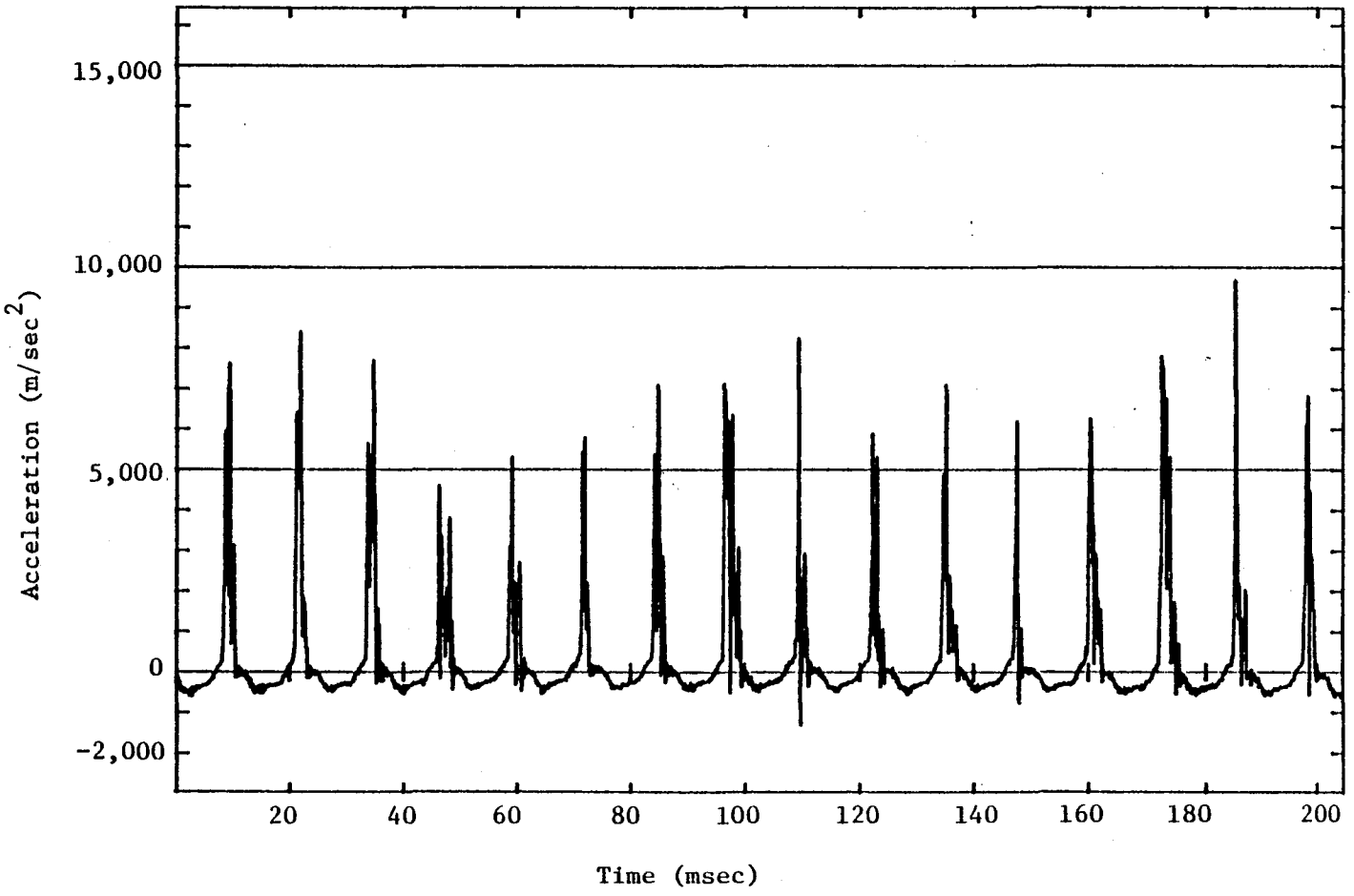

Figure E-8. Condensed time scale acceleration time history for barrel of small chipping hammer used to carve limestone. Chipping hammer operated at full throttle.

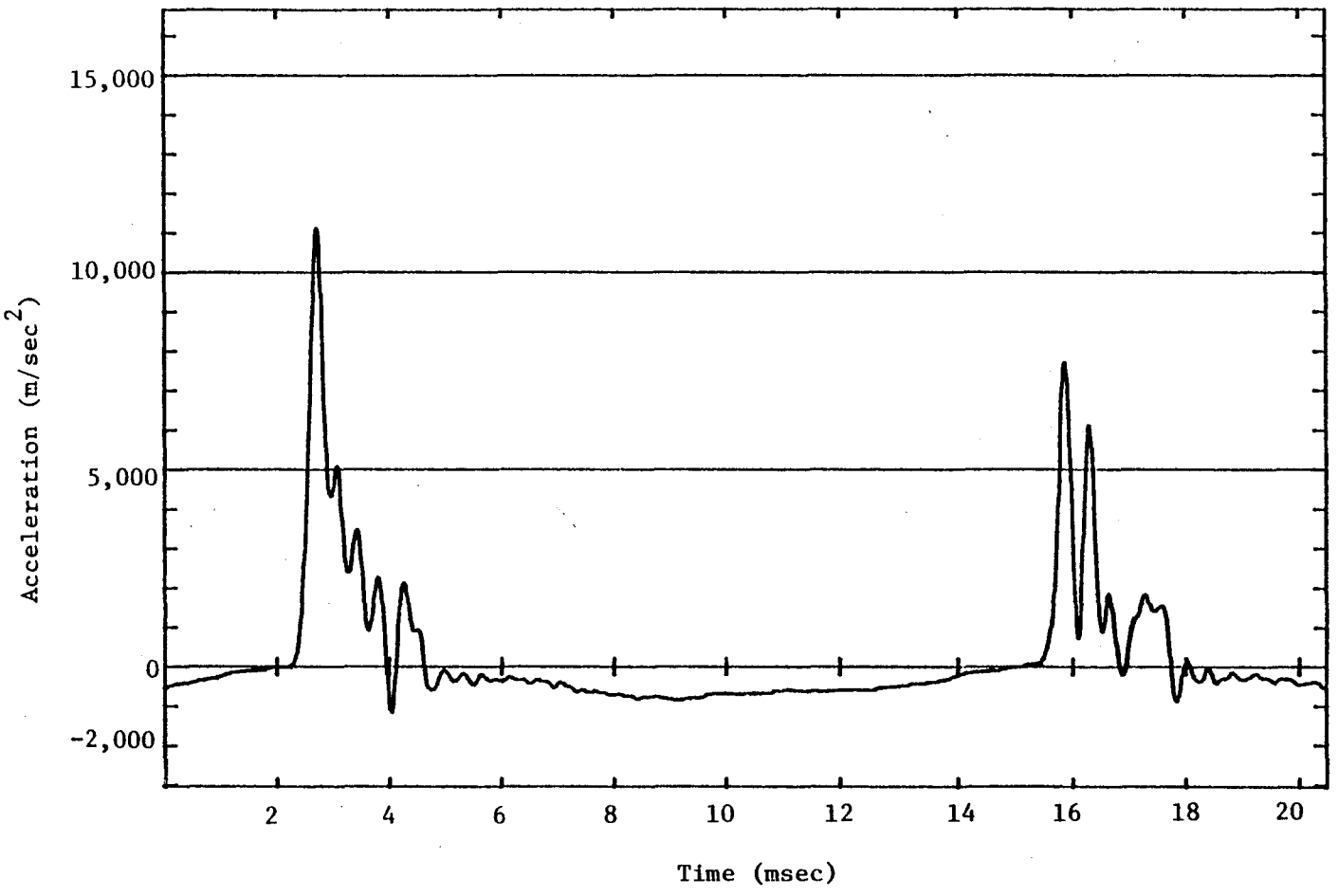

Figure E-7. Acceleration time history for barrel of small chipping hammer used to carve limestone. Chipping hammer operated at full throttle.

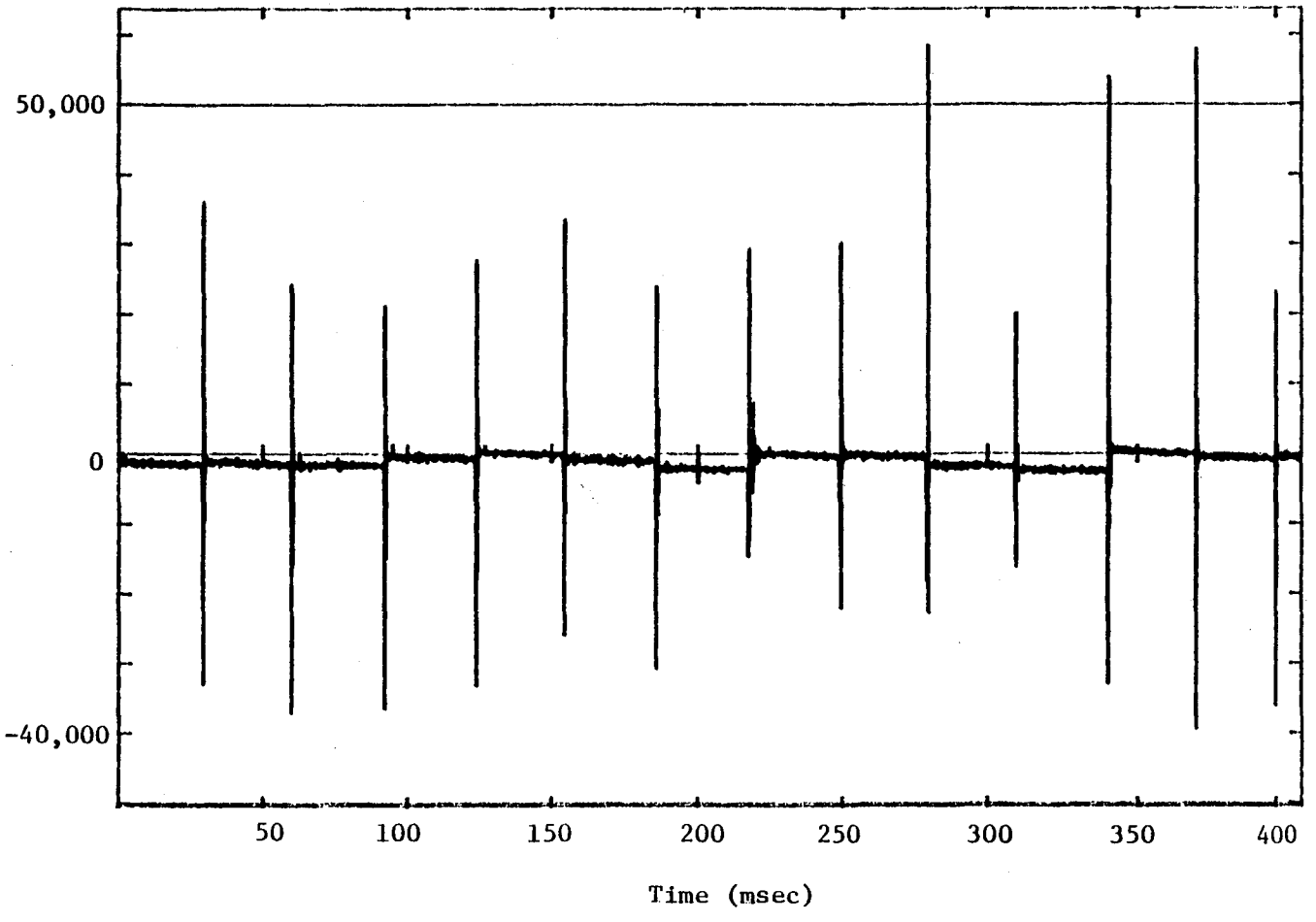

Figure E-10. Condensed time scale acceleration time history for chisel of chipping hammer D used to shape propeller blades. Chipping on Ni-Al-Br. Chipping hammer operated at 1/2-3/4 throttle.

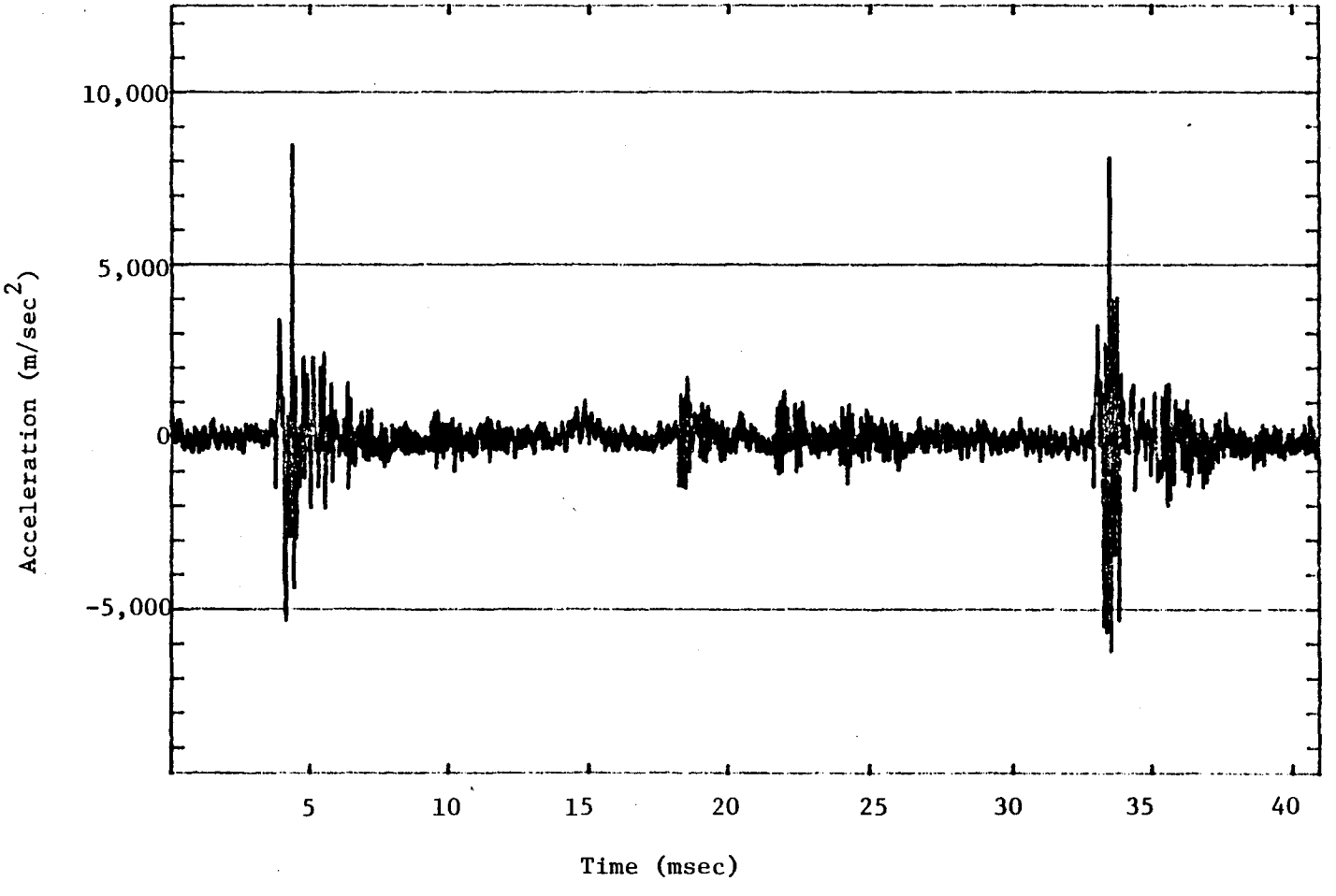

Figure E-11. Acceleration time history for handle of chipping hammer D used to shape propeller blades. Chipping on Ni-Al-Br. Chipping hammer operated at 1/2-3/4 throttle.

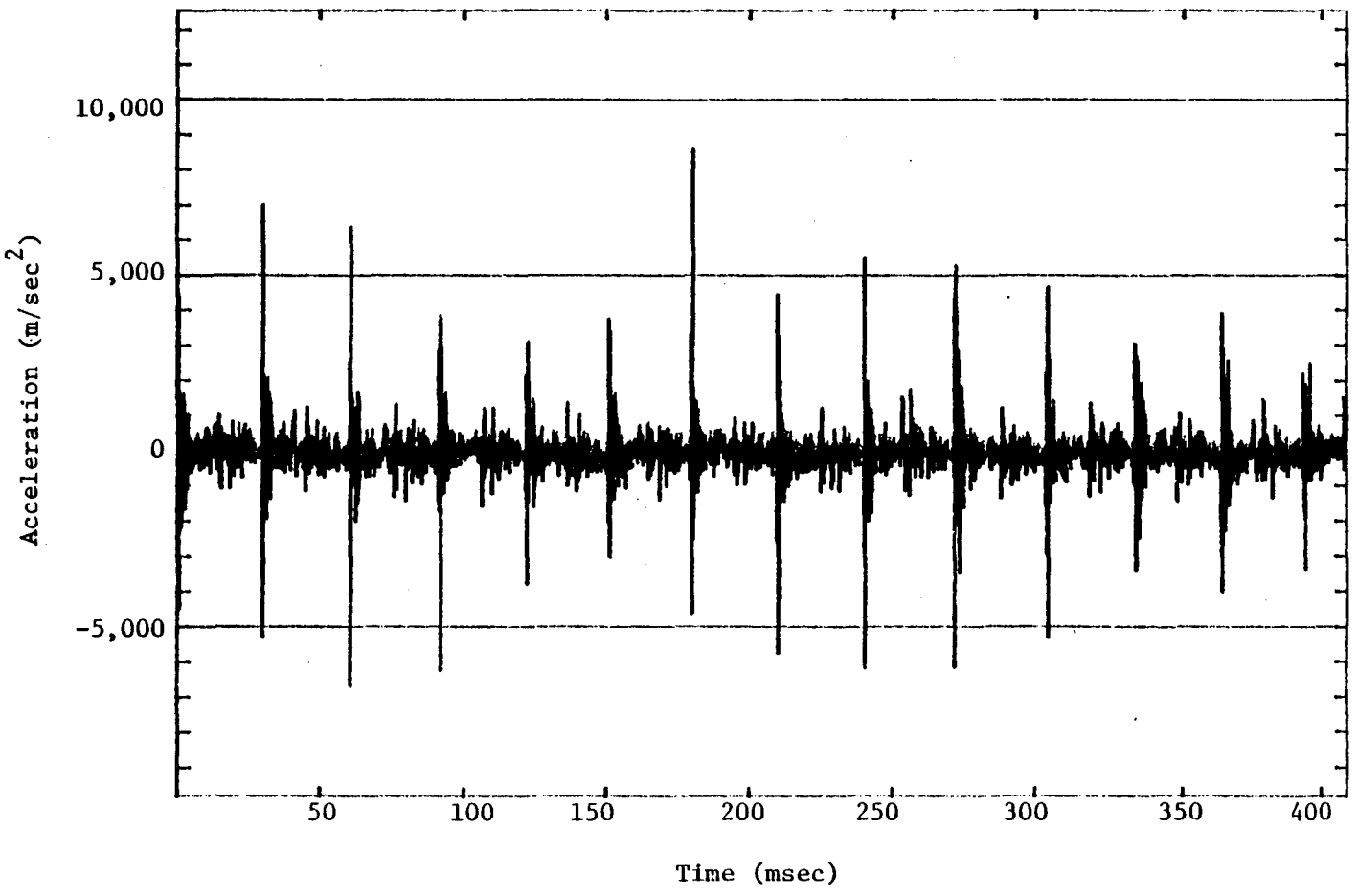

Figure E-12. Condensed time scale acceleration time history for handle of chipping hammer D used to shape propeller blades. Chipping on Ni-Al-Br. Chipping hammer operated at 1/2-3/4 throttle.

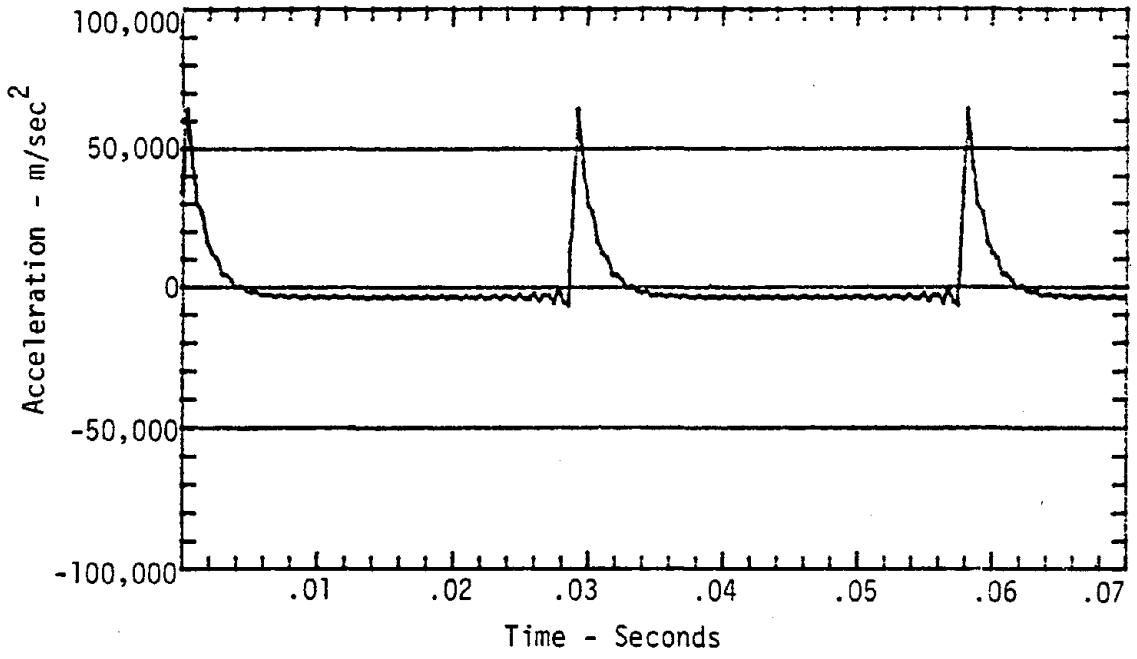

a) Acceleration Time History

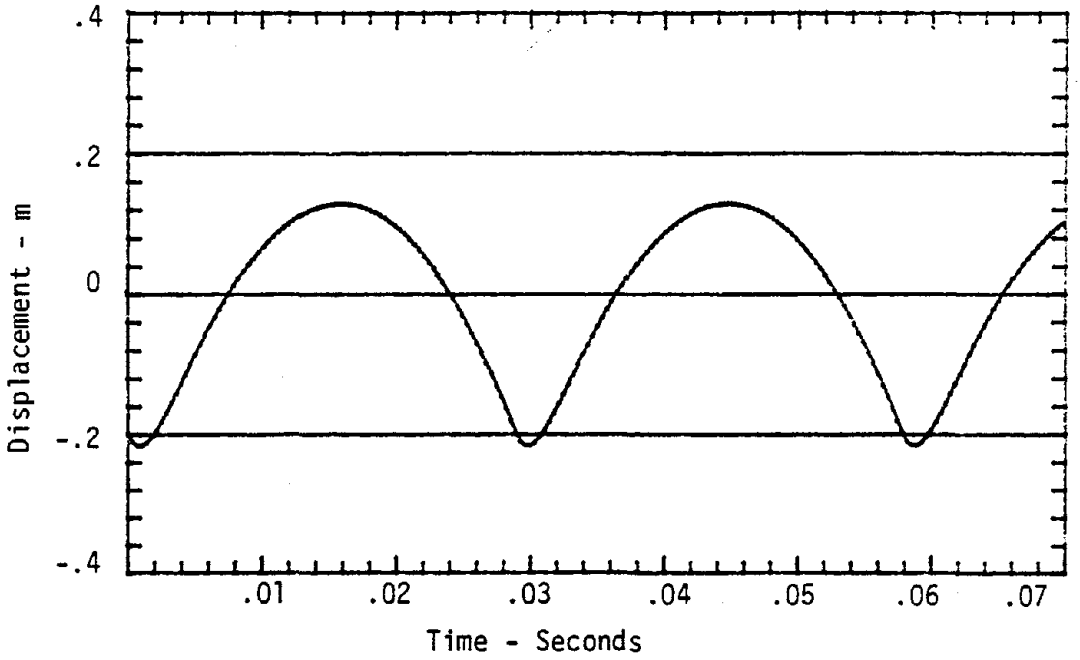

b) Displacement Time History

Figure E-13. Acceleration and displacement time history calculated using Fourier series for chisel of chipping hammer A used to clean castings. Slot chipping on nodular cast iron.

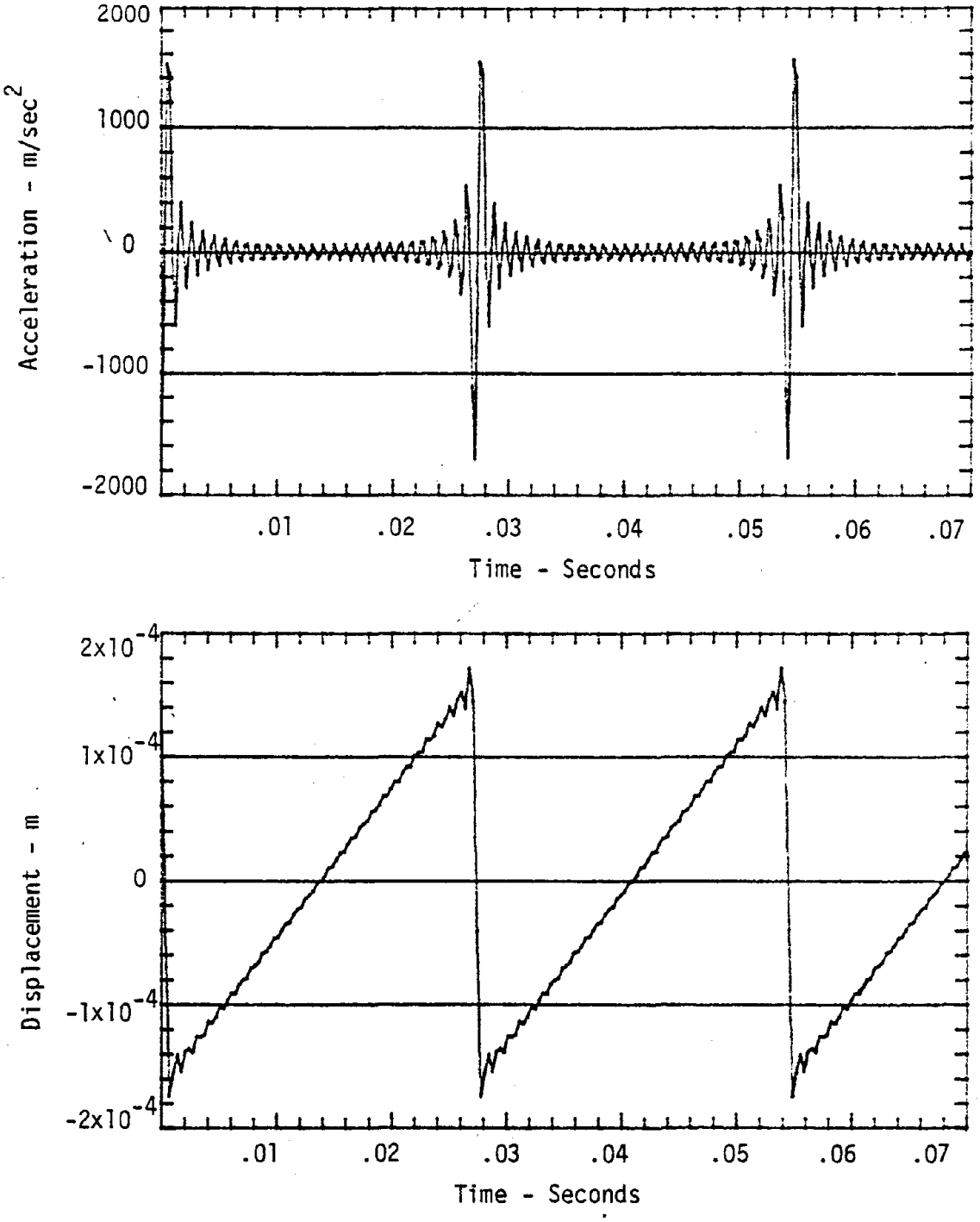

Figure E-14. Acceleration and displacement time history calculated using Fourier series for handle of chipping hammer A used to clean castings. Slot chipping on nodular cast iron.

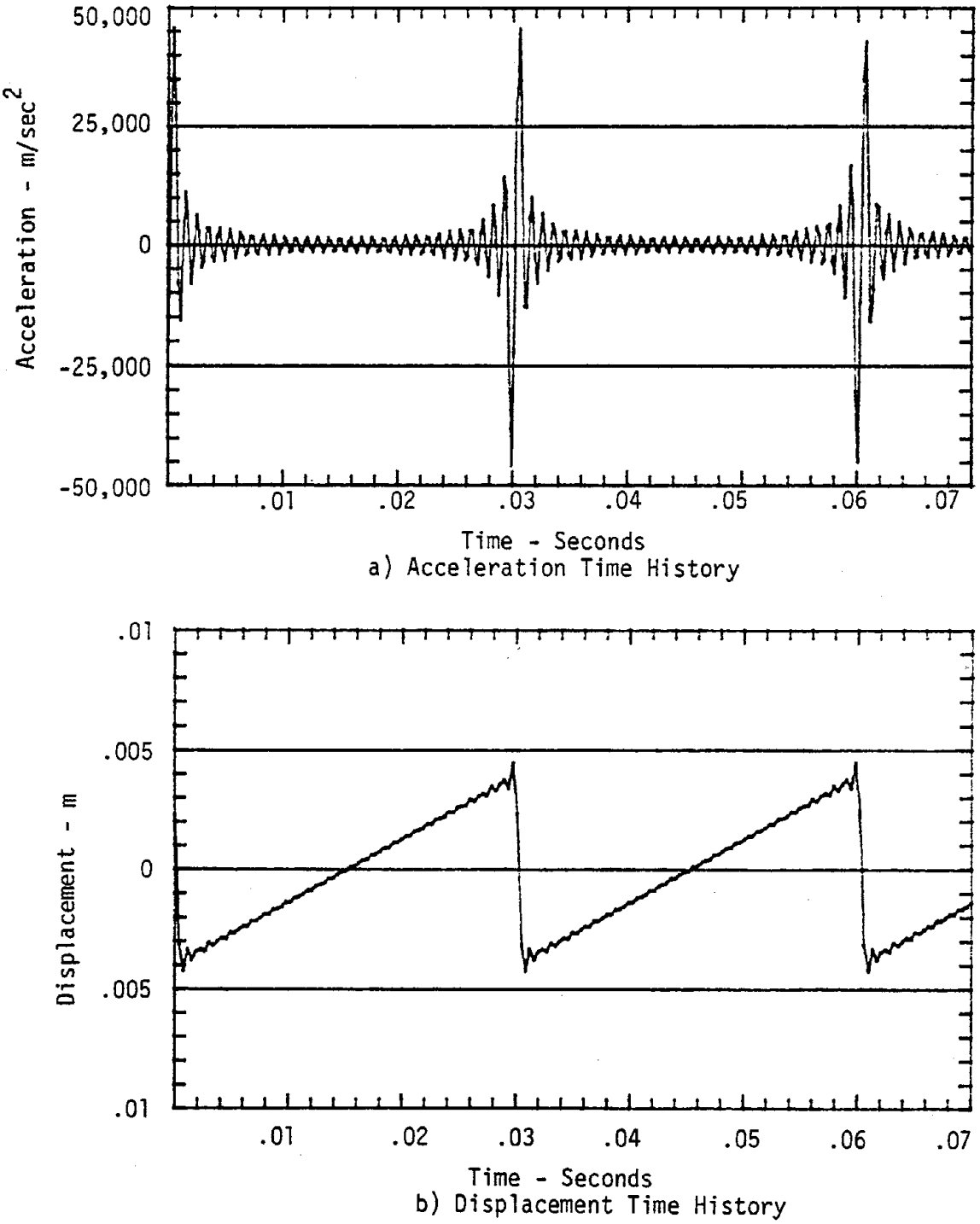

Figure E-15. Acceleration and displacement time history calculated using Fourier coefficients for chisel of chipping hammer D used to shape propeller blades. Chipping on Ni-Al-Br.

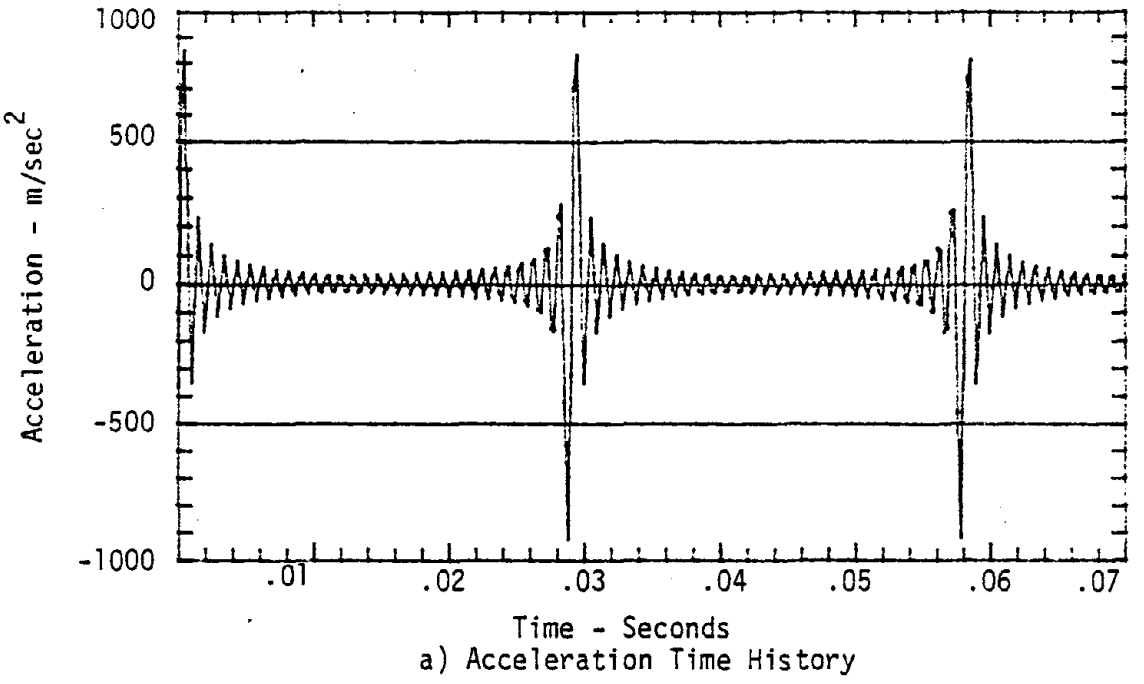

a) Acceleration Time History

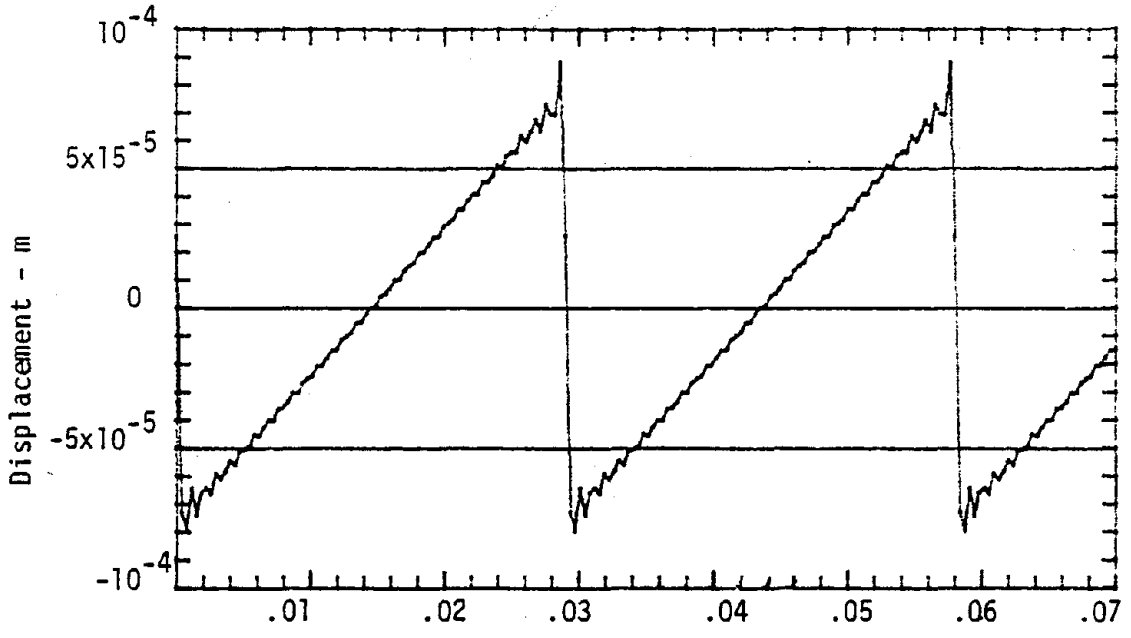

b) Displacement Time History

Figure E-16. Acceleration and displacement time history calculated using Fourier series for handle of chipping hammer D used to shape propeller blades. Chipping on Ni-Al-Br.

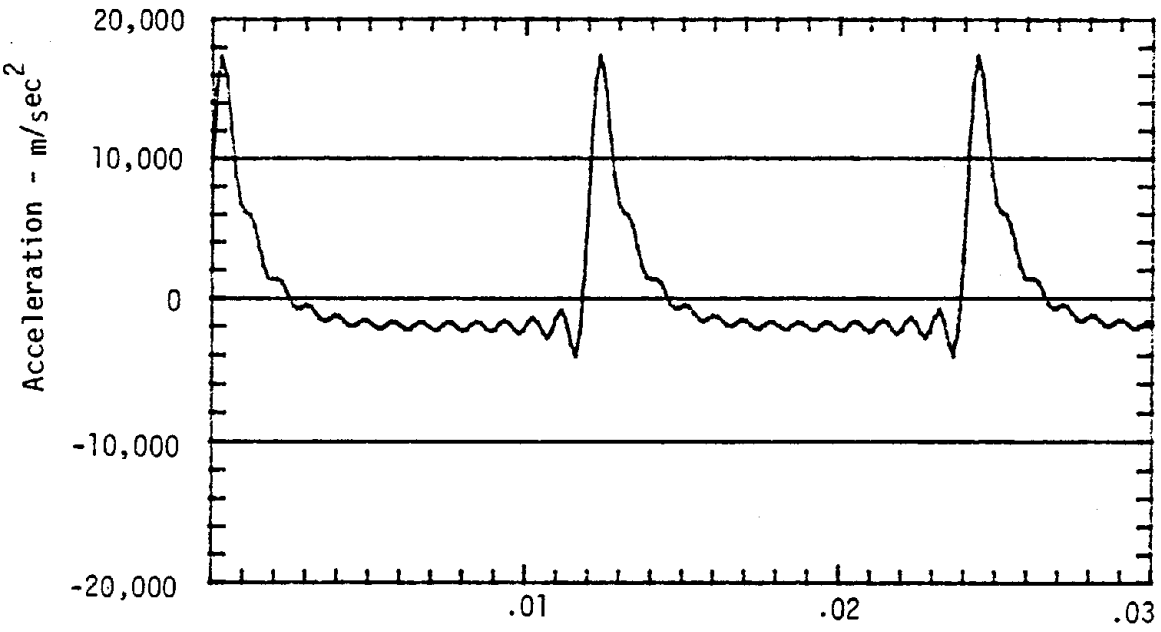

a) Acceleration Time History

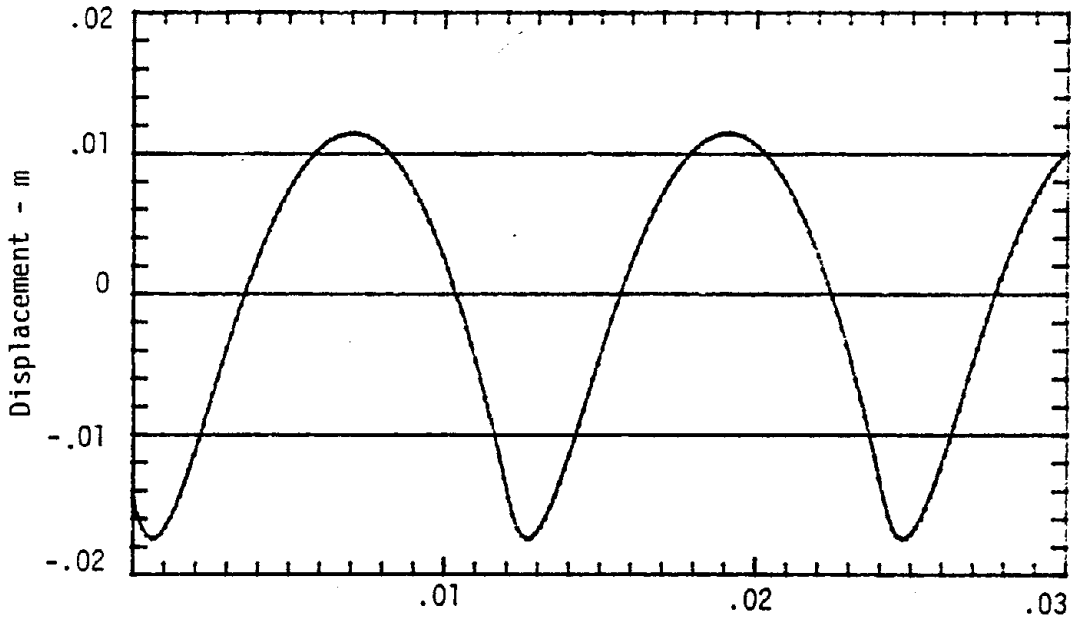

b) Displacement Time History

Figure E-17. Acceleration and displacement time history calculated using Fourier series for chisel of small chipping hammer used to carve limestone.

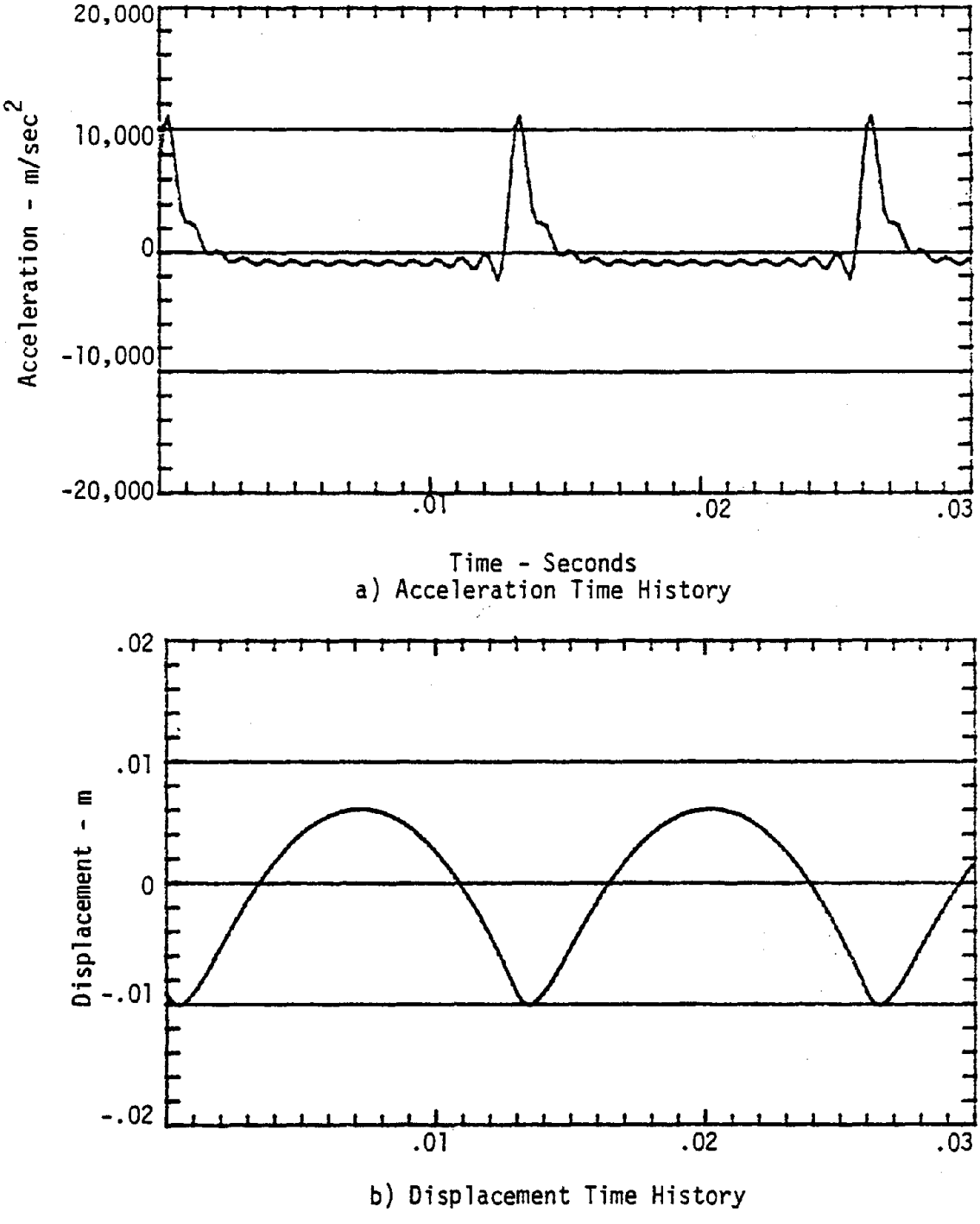

Figure E-18. Acceleration and displacement time history calculated using Fourier series for barrel of small chipping hammer used to carve limestone.

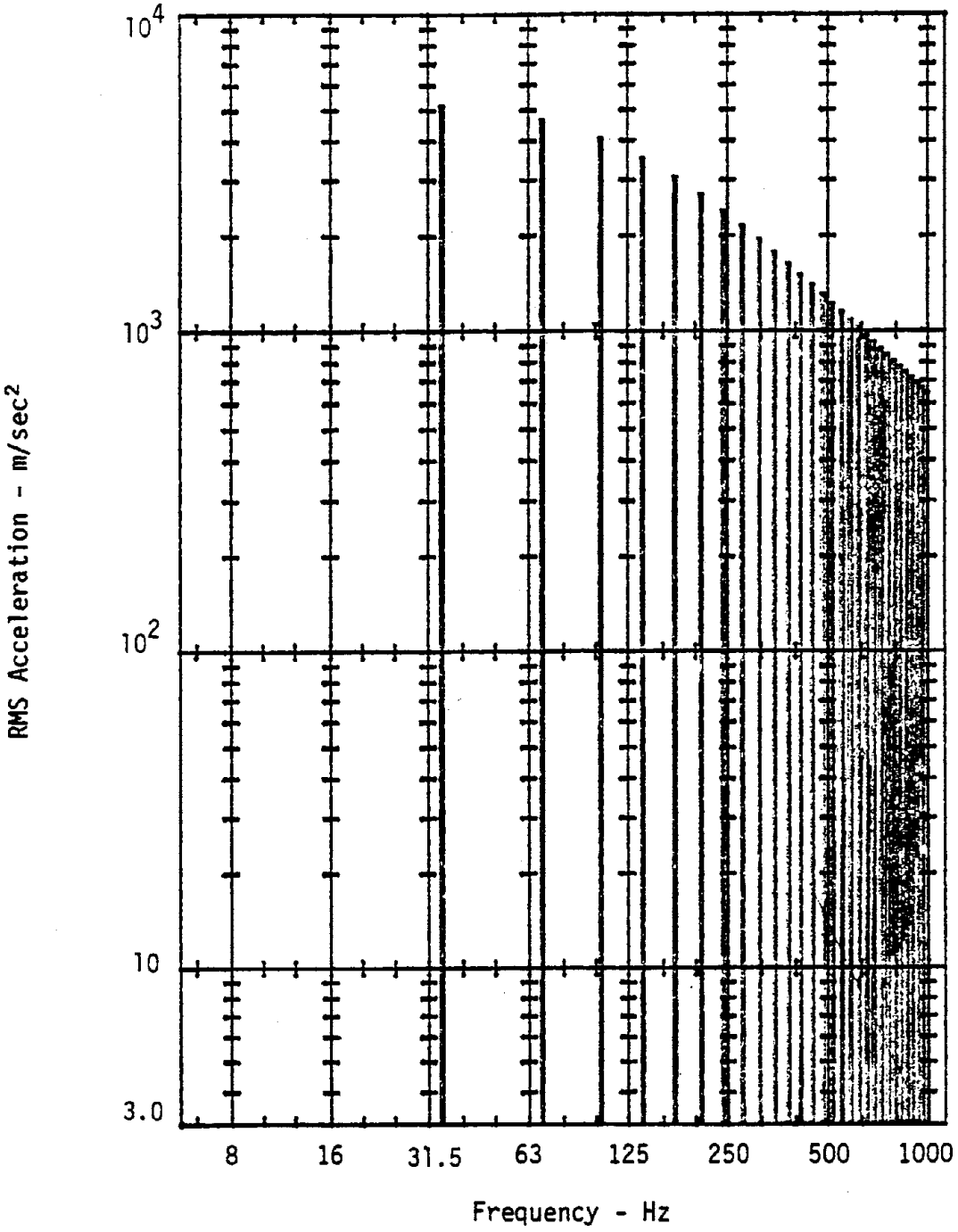

Figure E-19. RMS Fourier coefficients for acceleration of chisel of chipping hammer A used to clean castings. Slot chipping of nodular cast iron.

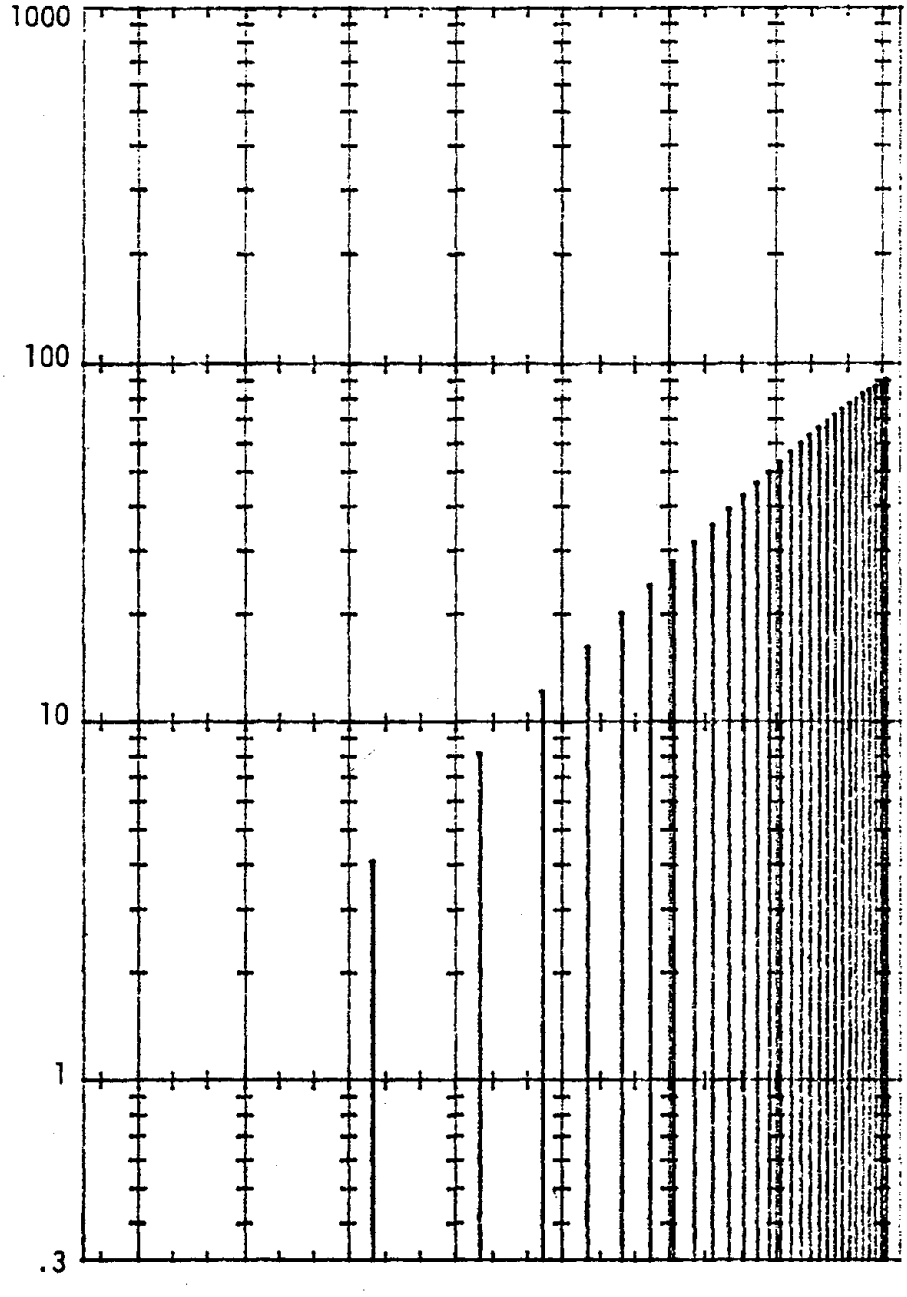

Figure E-20. RMS Fourier coefficients for acceleration of handle of chipping hammer A used to clean castings. Slot chipping on nodular cast iron.

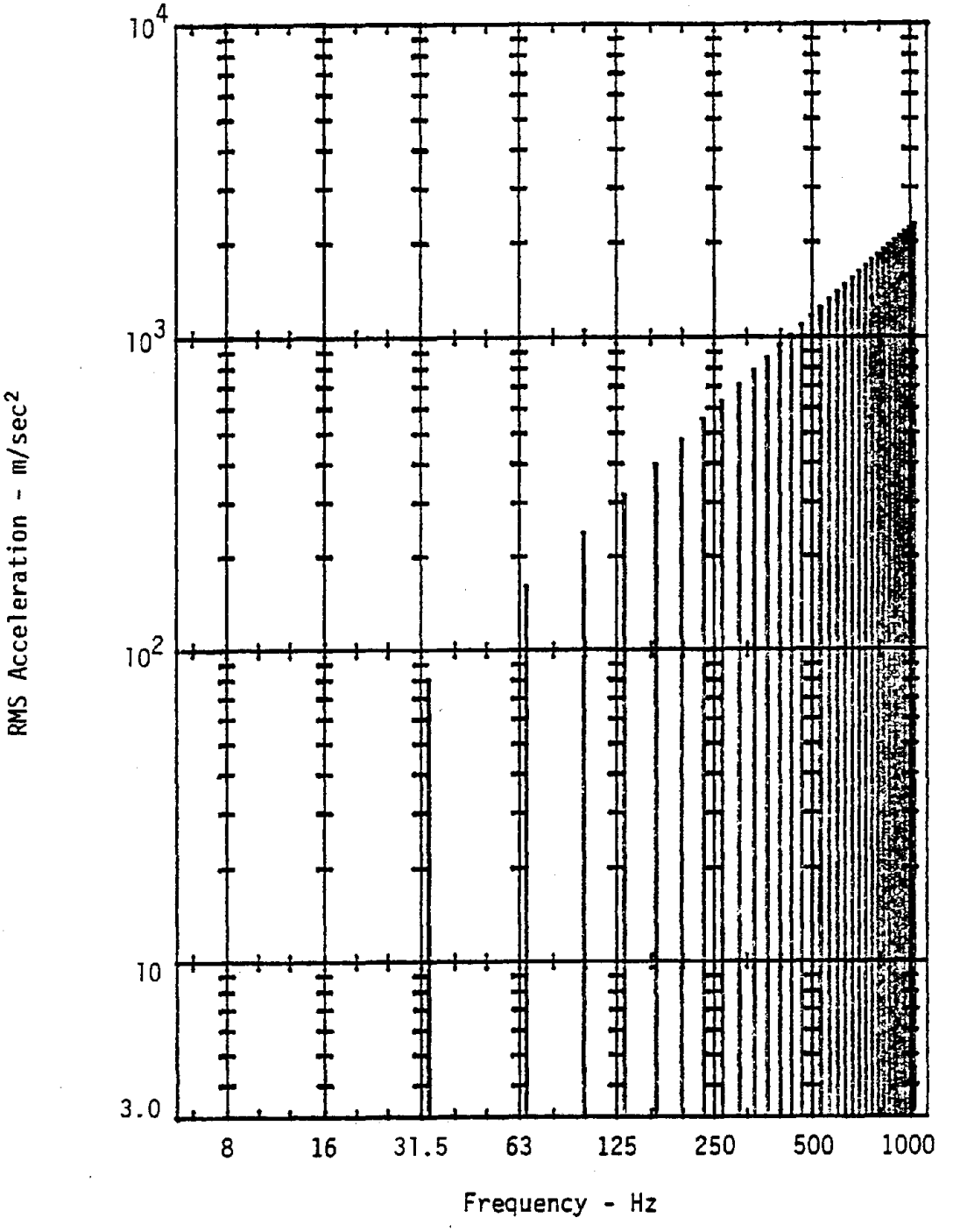

Figure E-21. RMS Fourier coefficients for acceleration of chisel of chipping hammer D used to shape propeller blades. Chippings are Ni-Al-Br.

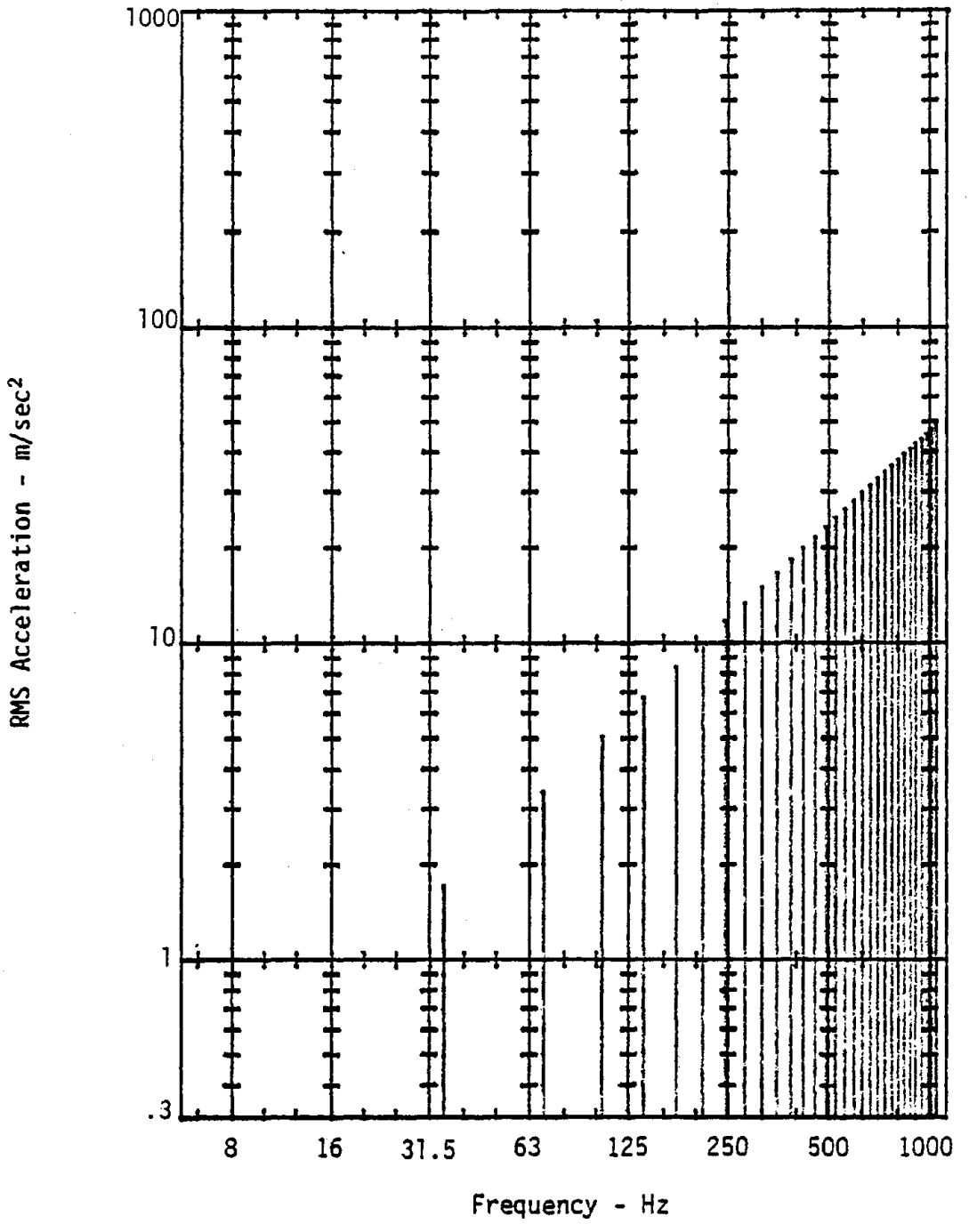

Figure E-22. RMS Fourier coefficients for acceleration of handle of chipping hammer D used to shape propeller blades. Chipping on Ni-Al-Br.

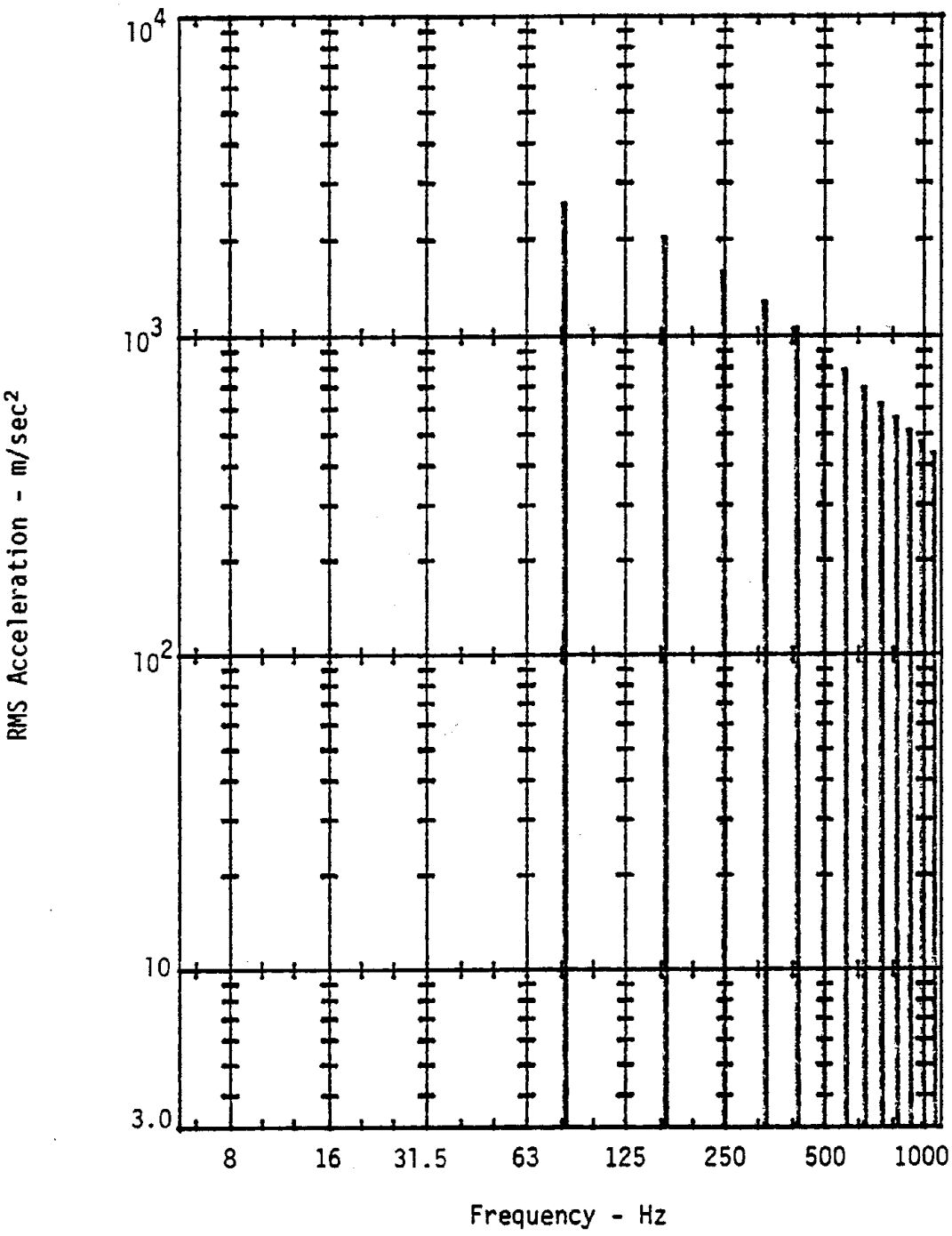

Figure E-23. RMS Fourier coefficients for acceleration of chisel of small chipping hammer used to carve limestone.

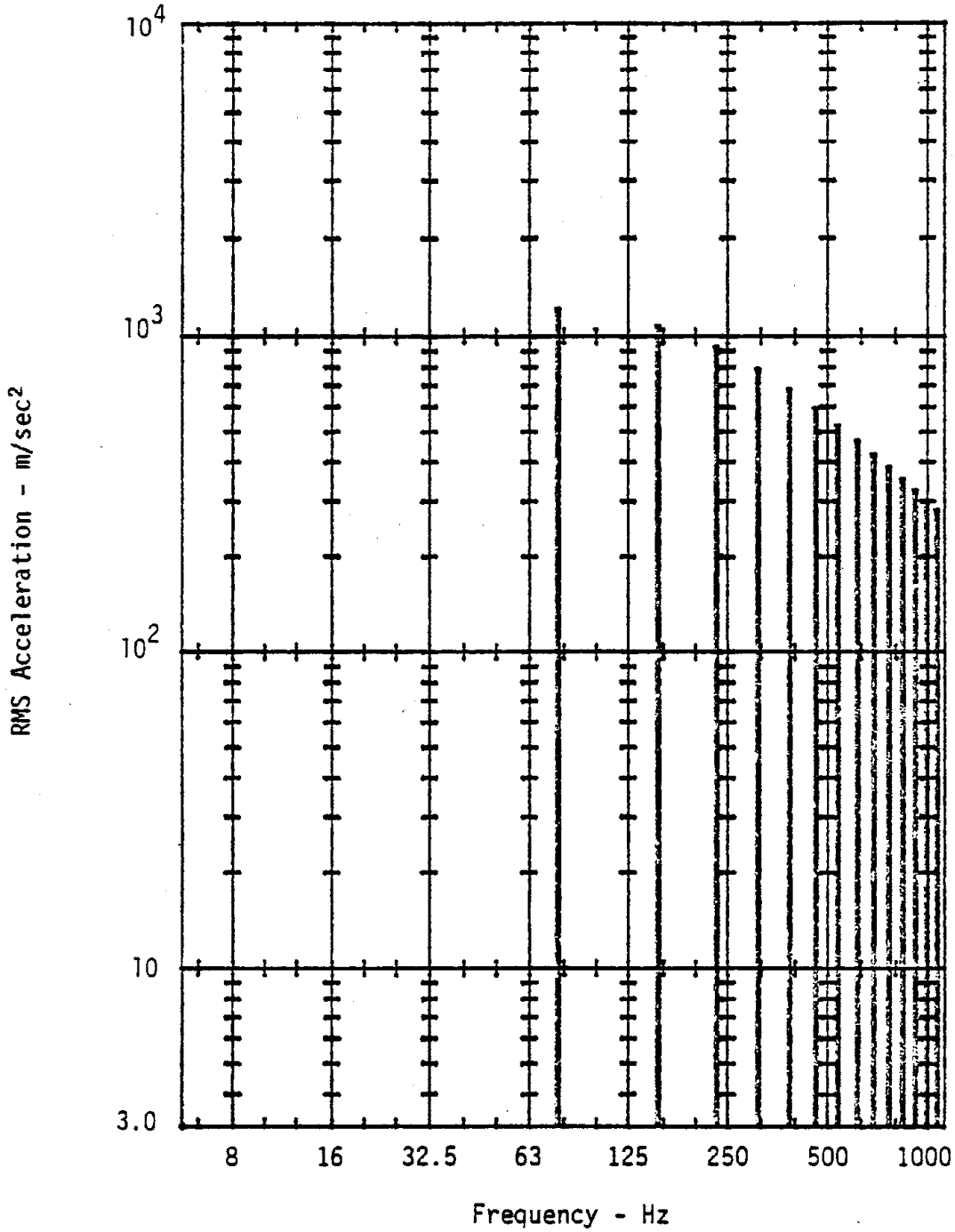

Figure E-24. RMS Fourier coefficients for acceleration of barrel of small chipping hammer used to carve limestone.

APPENDIX F

WORK PER UNIT TIME PLOTS

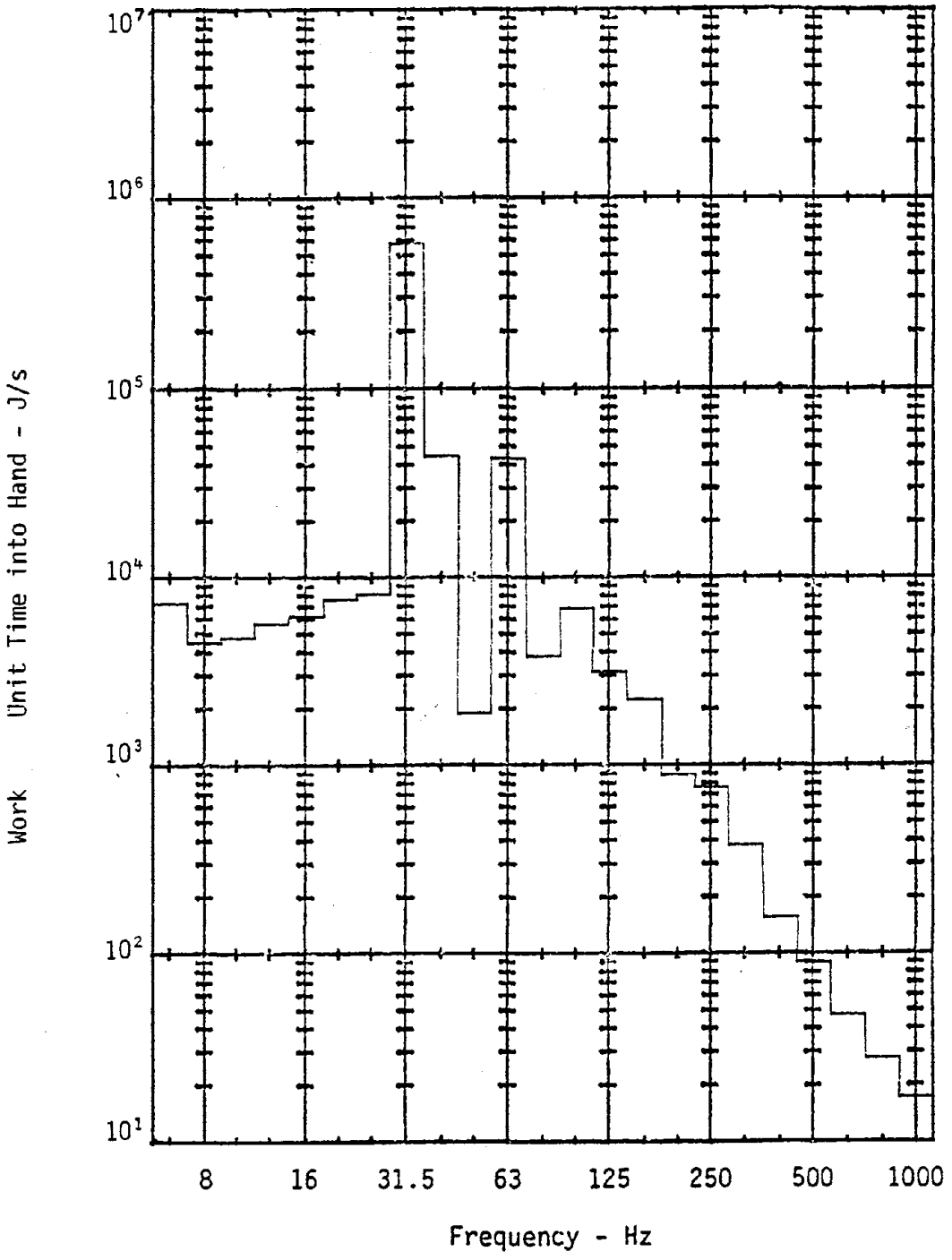

Figure F-1. RMS amplitude of work per unit time directed into hand from the chisel of chipping hammer A used to clean castings. Slot chipping on nodular cast iron. Chipping hammer operated at full throttle.

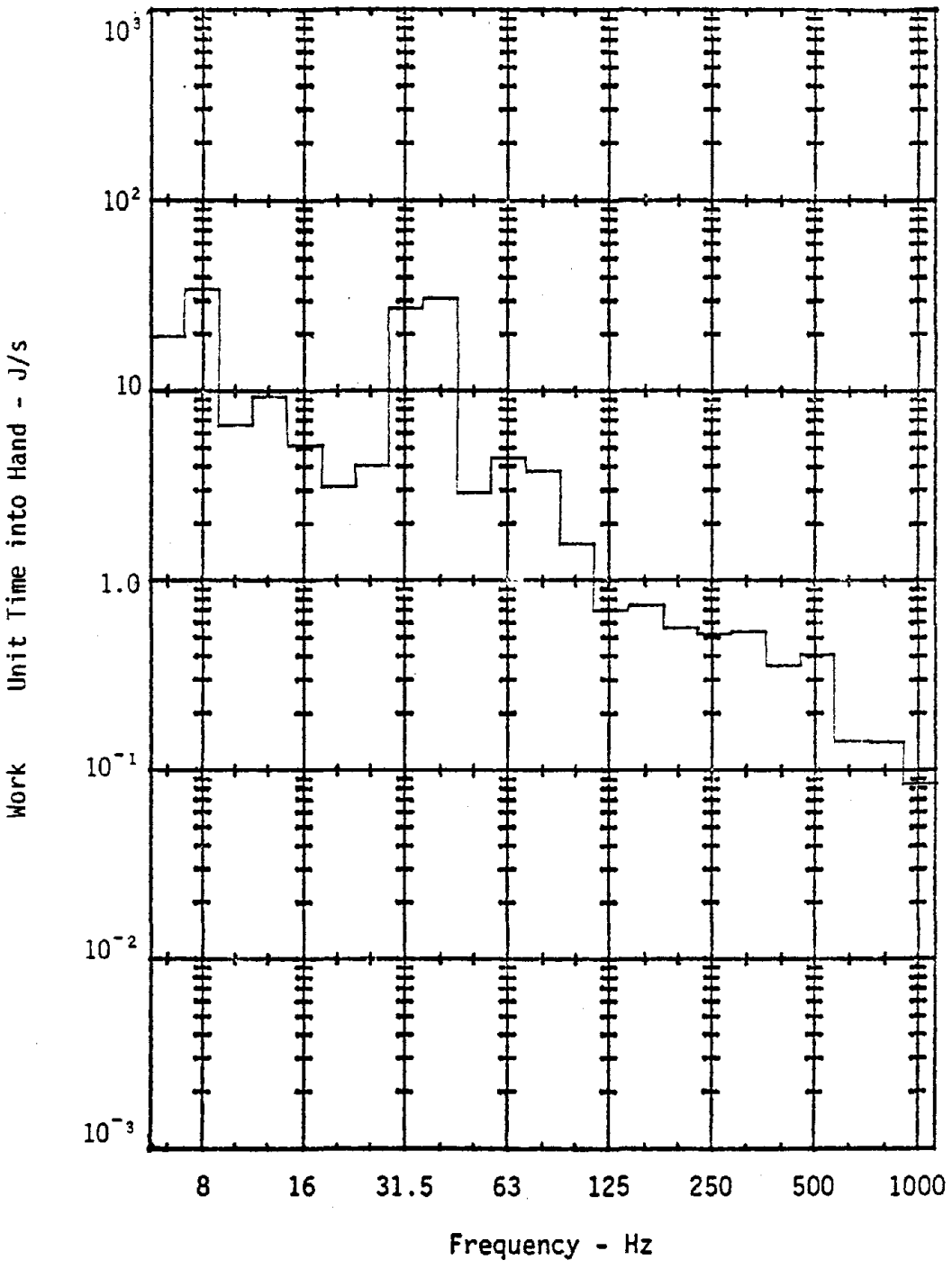

Figure F-2. RMS amplitude of work per unit time directed into hand from the handle of chipping hammer A used to clean castings. Slot chipping on nodular cast iron. Chipping hammer operated at full throttle.

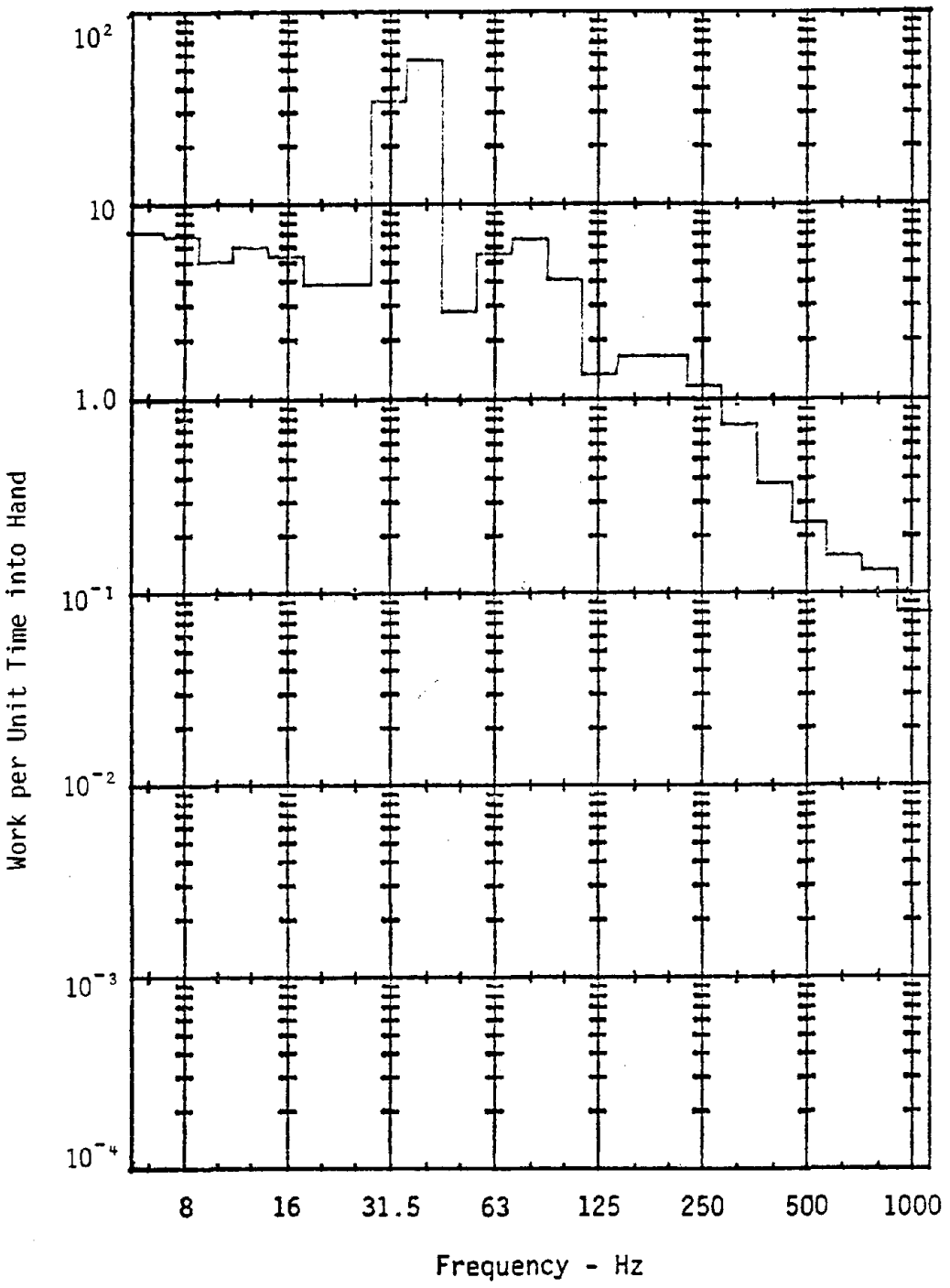

Figure F-3. RMS amplitude of work per unit time directed into hand from the handle of chipping hammer B used to clean castings. Slot chipping on nodular cast iron. Chipping hammer operated at full throttle.

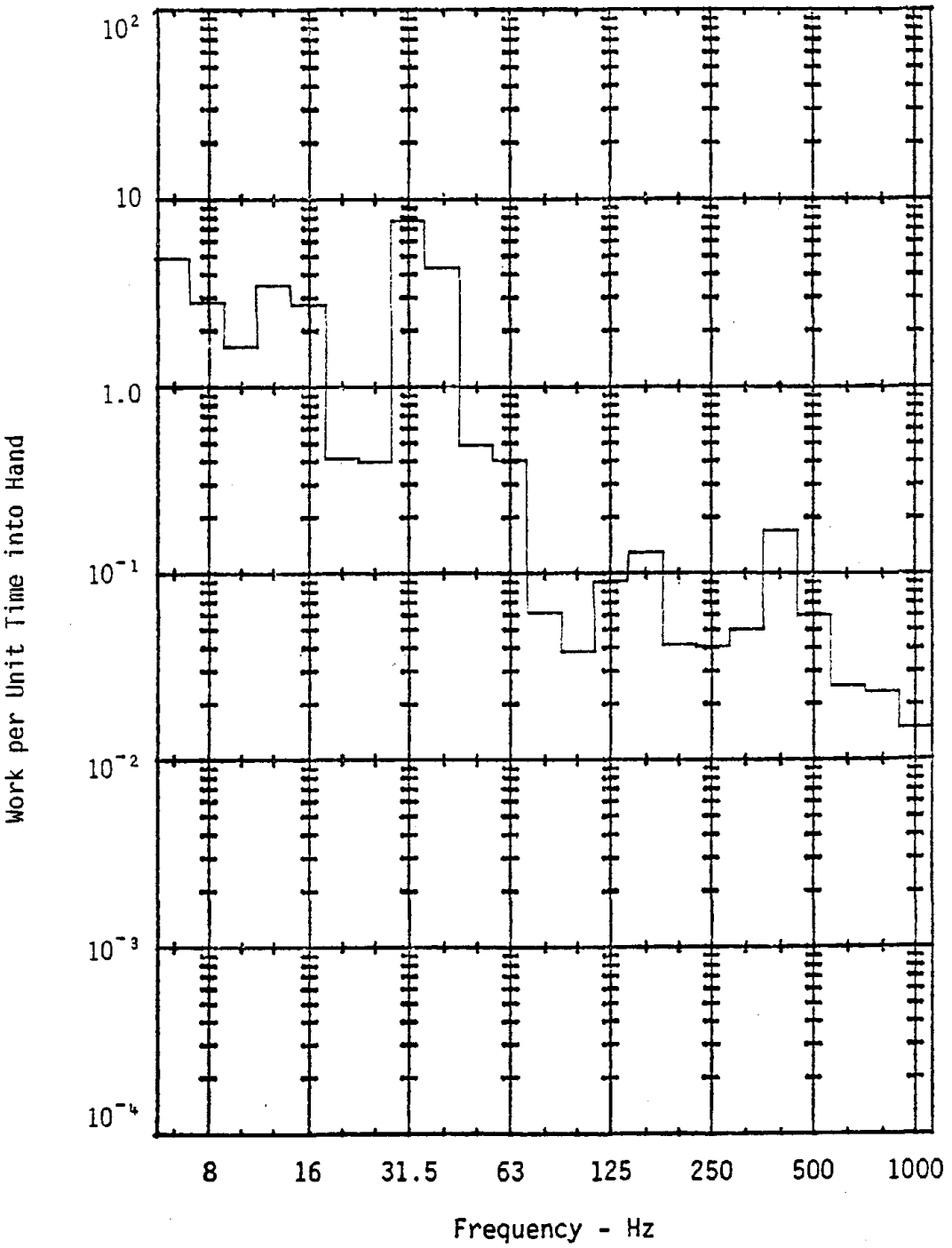

Figure F-4. RMS amplitude of work per unit time directed into hand from the handle of chipping hammer C used to clean castings. Slot chipping on nodular cast iron. Chipping hammer operated at full throttle.

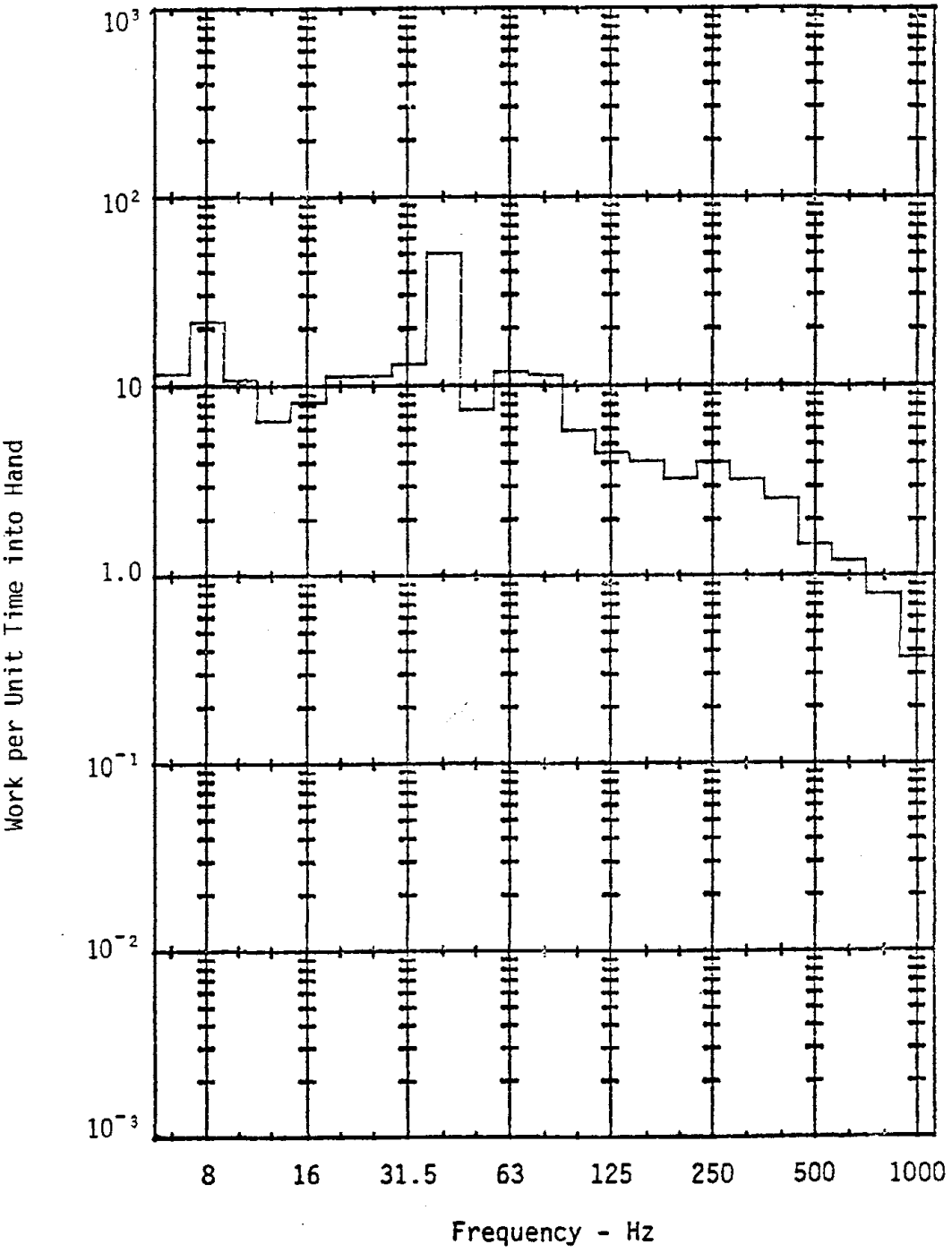

Figure F-5. RMS amplitude of work per unit time directed into hand from the handle of chipping hammer D used to shape propeller blades. Slot chipping on cast iron. Chipping hammer operated at full thr throttle.

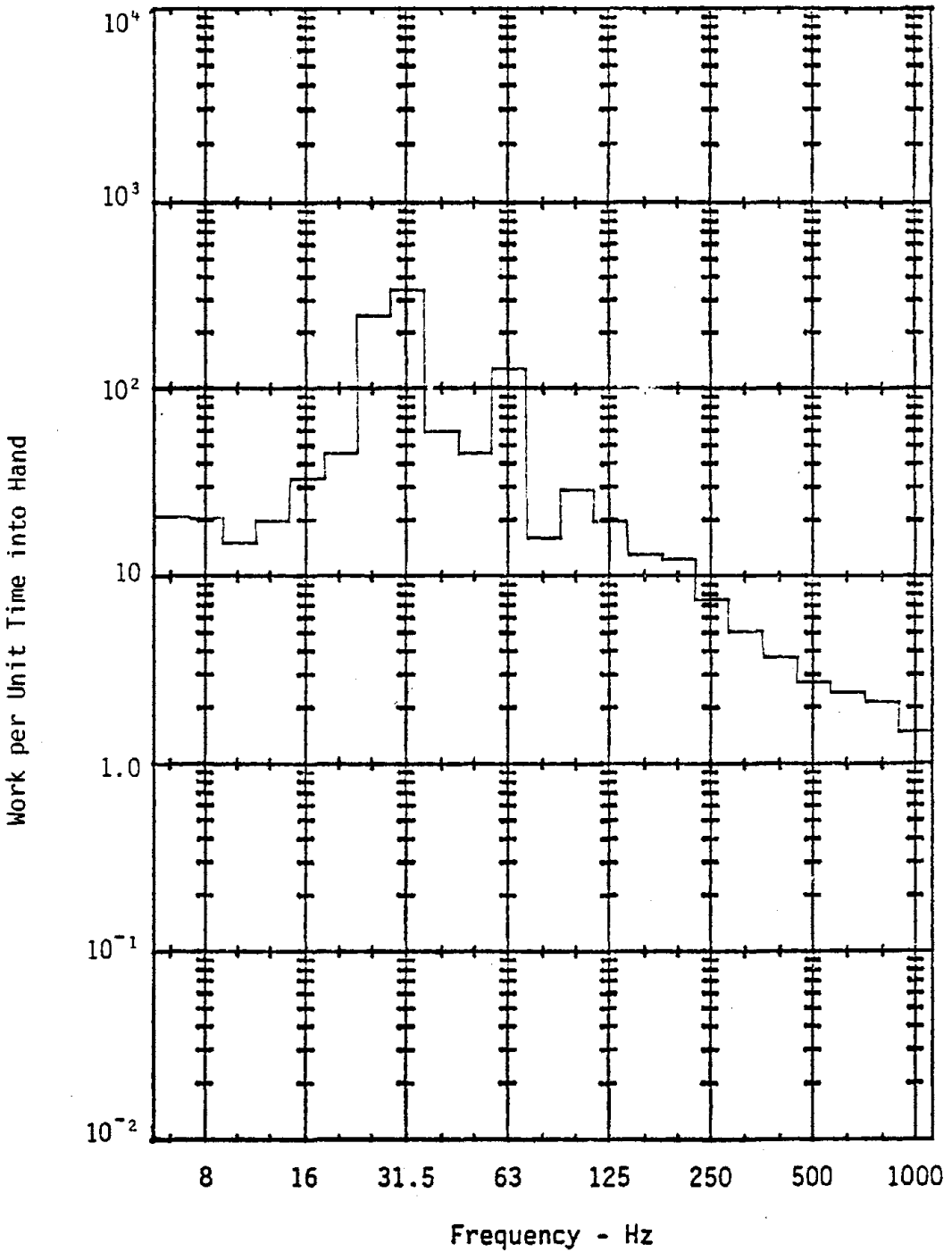

Figure F-6. RMS amplitude of work per unit time directed into hand from the chisel of chipping hammer D used to shape propeller blades. Chipping on mild B steel. Chipping hammer operated at 1/2-3/4 throttle.

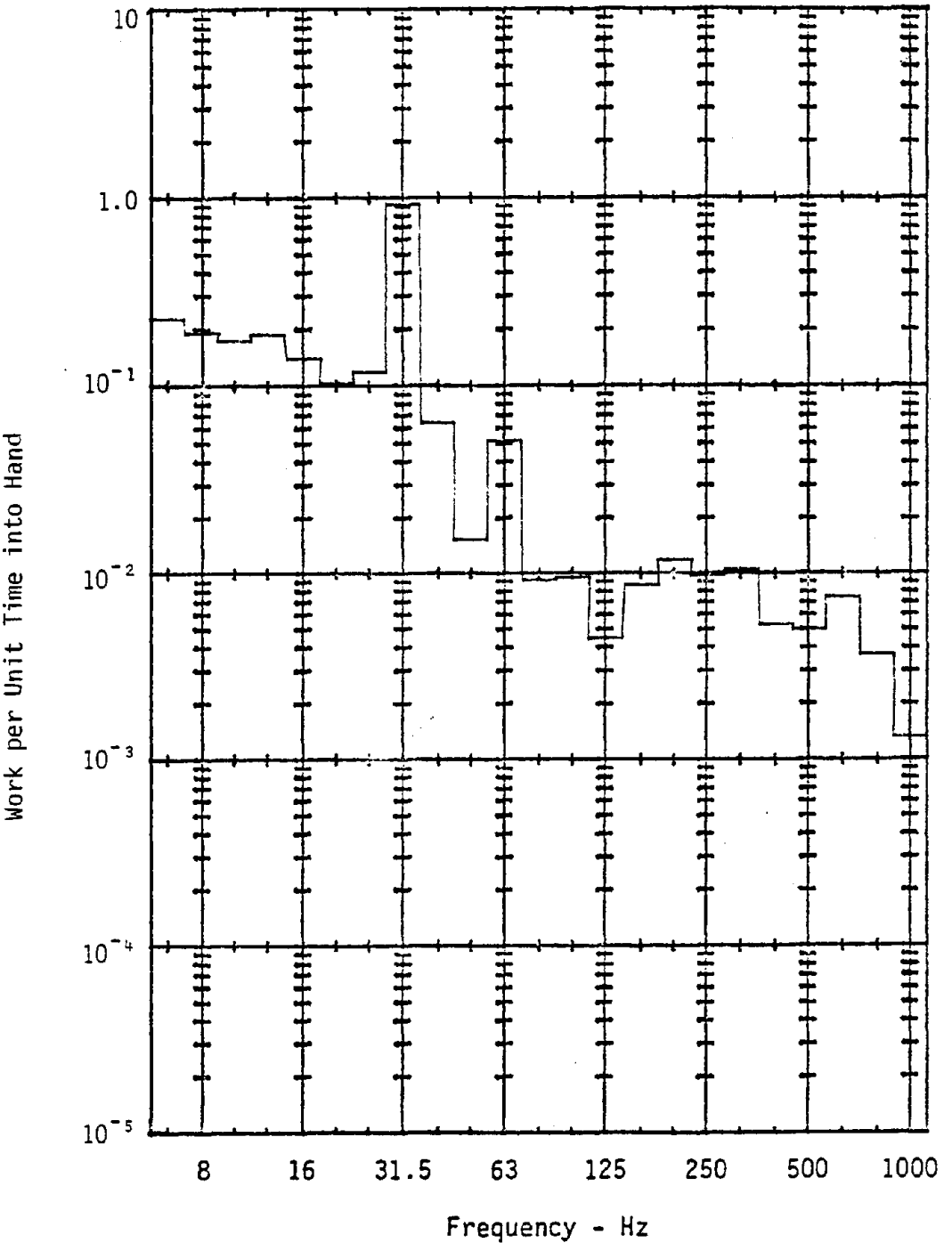

Figure F-7. RMS amplitude of work per unit time directed into hand from the handle of chipping hammer D used to shape propeller blades. Chipping on mild B steel. Chipping hammer operated at 1/2-3/4 throttle.

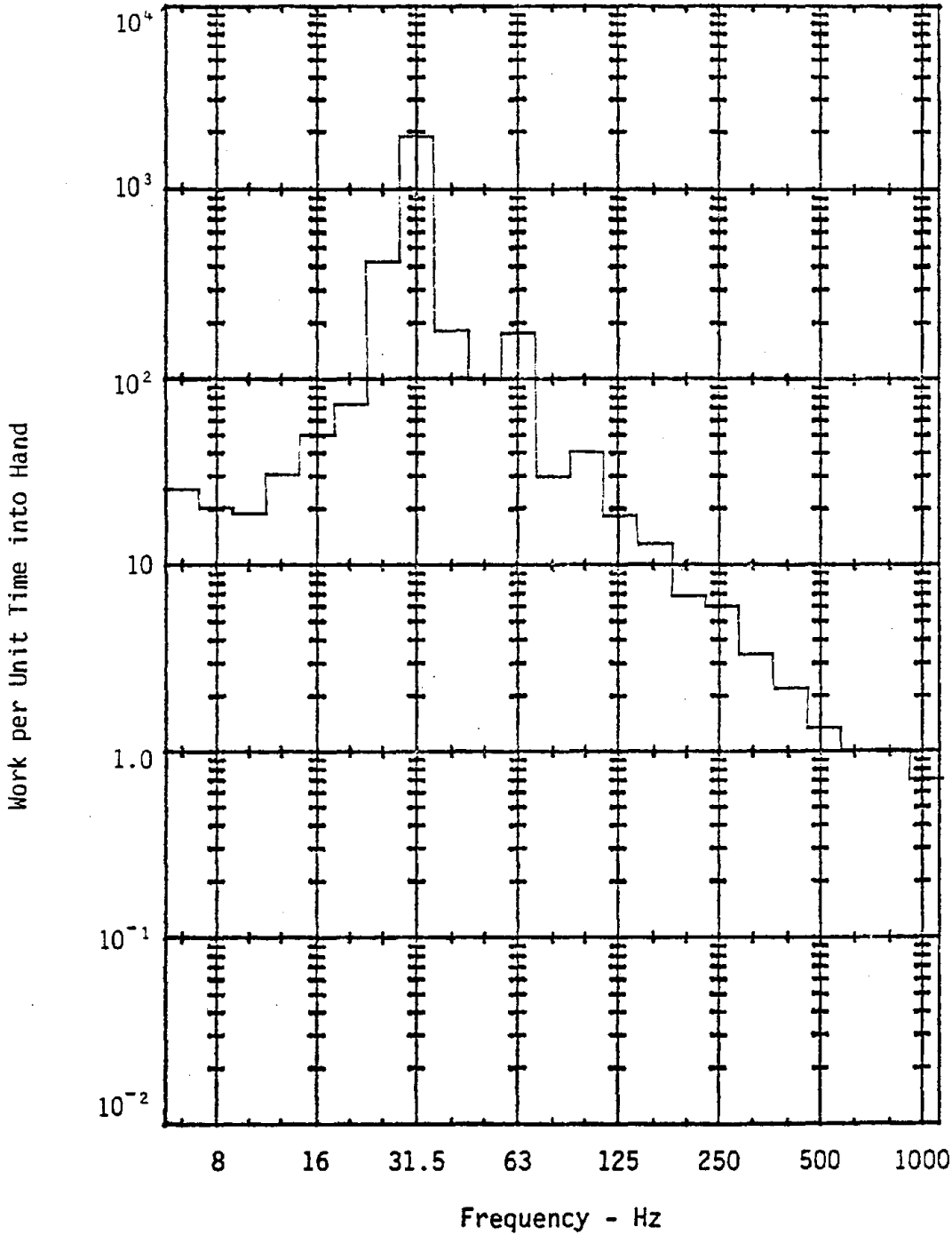

Figure F-8. RMS amplitude of work per unit time directed into hand from the chisel of chipping hammer D used to shape propeller blades. Chipping on Ni-Al-Br. Chipping hammer operated at 1/2-3/4 throttle.

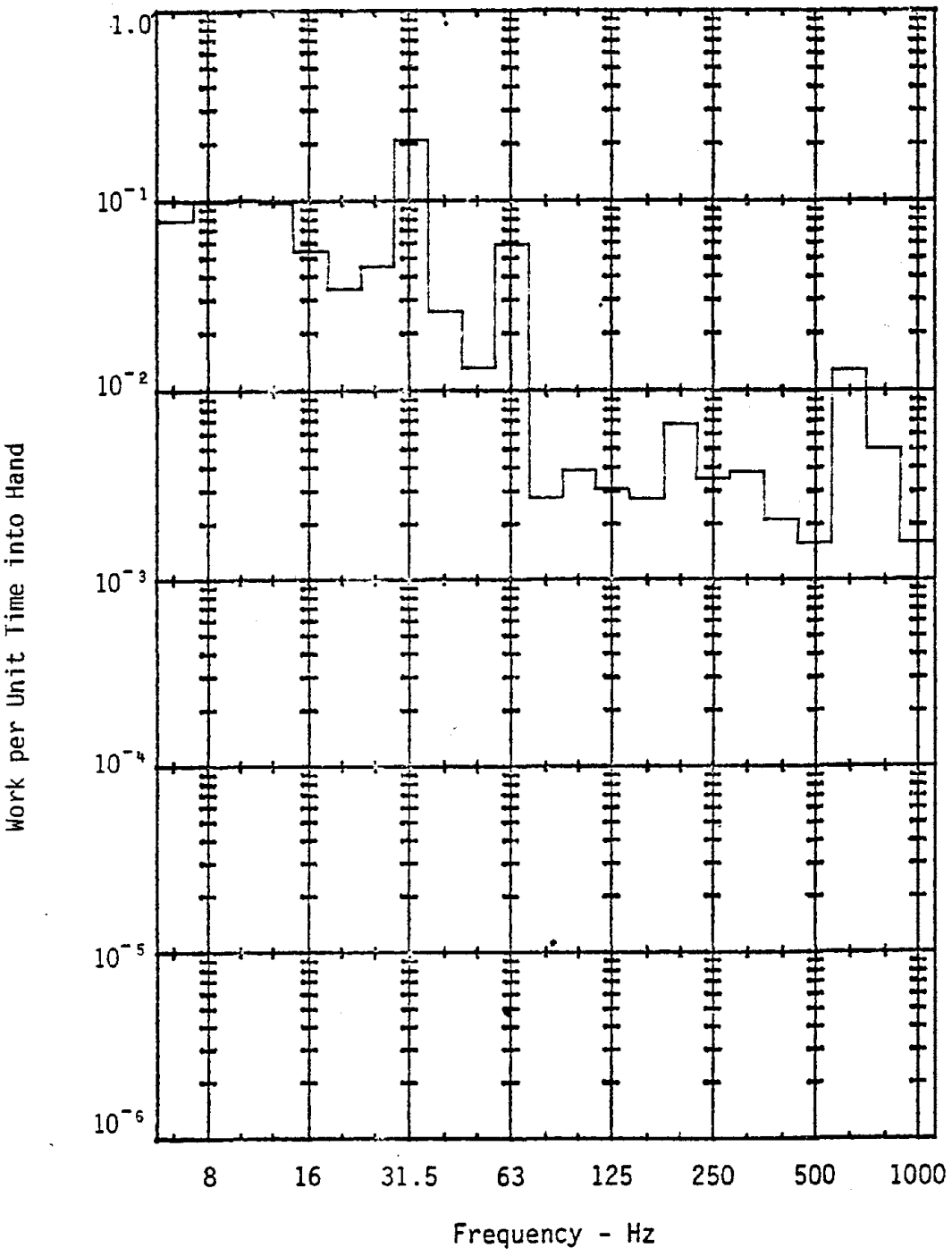

Figure F-9. RMS amplitude of work per unit time directed into hand from the handle of chipping hammer D used to shape propeller blades. Chipping on Ni-Al-Br. Chipping hammer operated at 1/2-3/4 throttle.

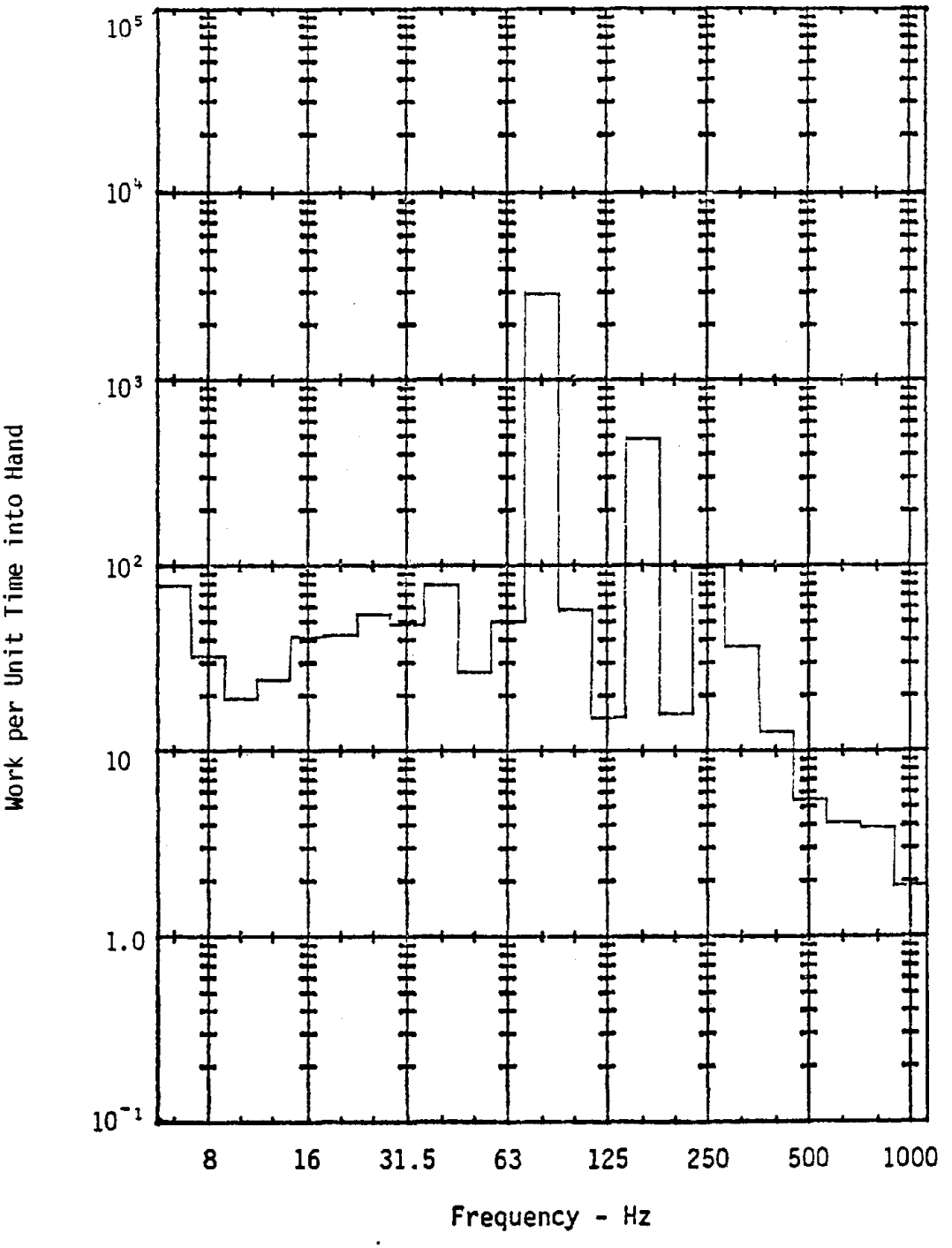

Figure F-10. RMS amplitude of work per unit time directed into hand from the chisel of small chipping hammer used to carve limestone. Chipping hammer operated at full throttle.

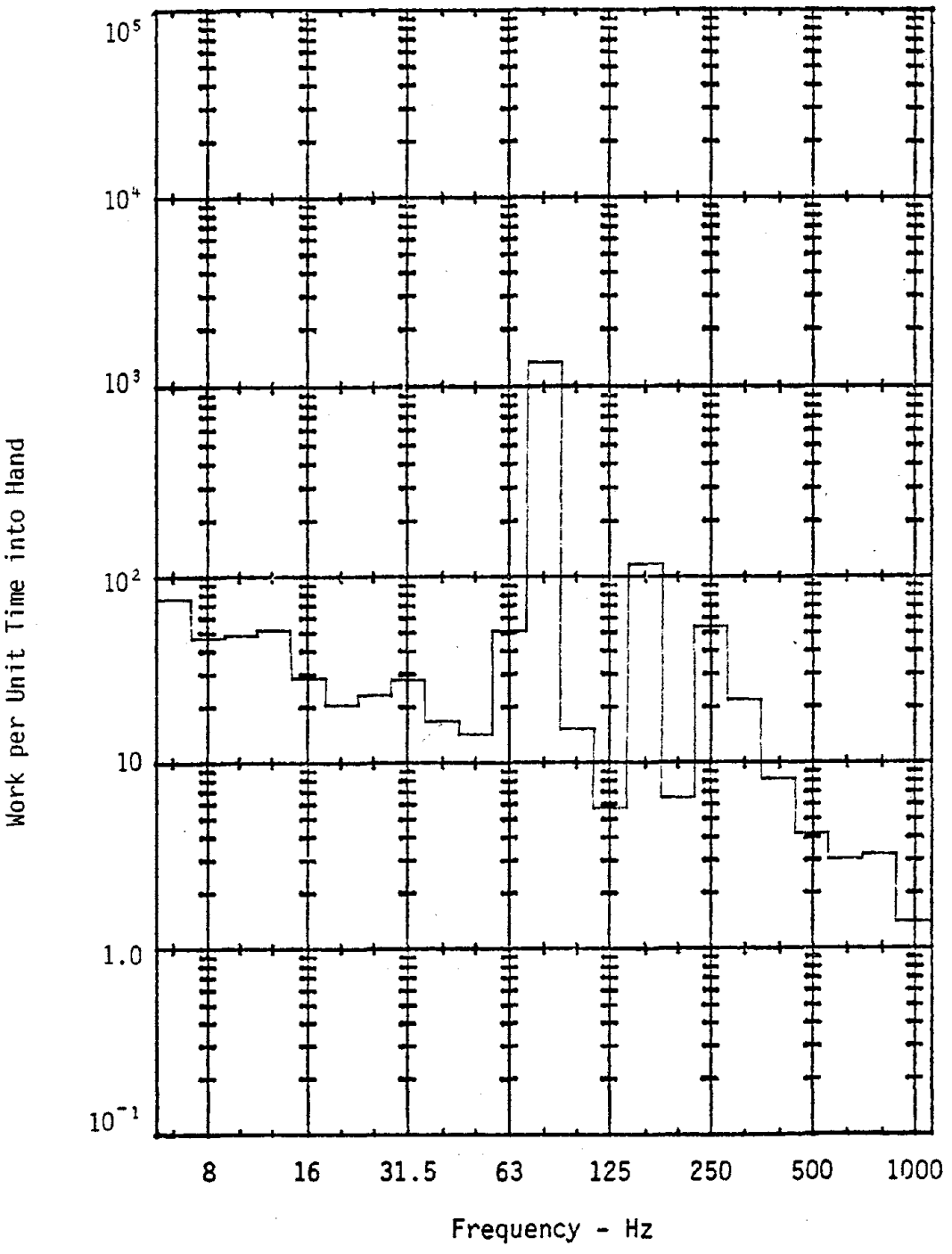

Figure F-11. RMS amplitude of work per unit time directed into hand from the handle of small chipping hammer used to carve limestone. Chipping hammer operated at full throttle.

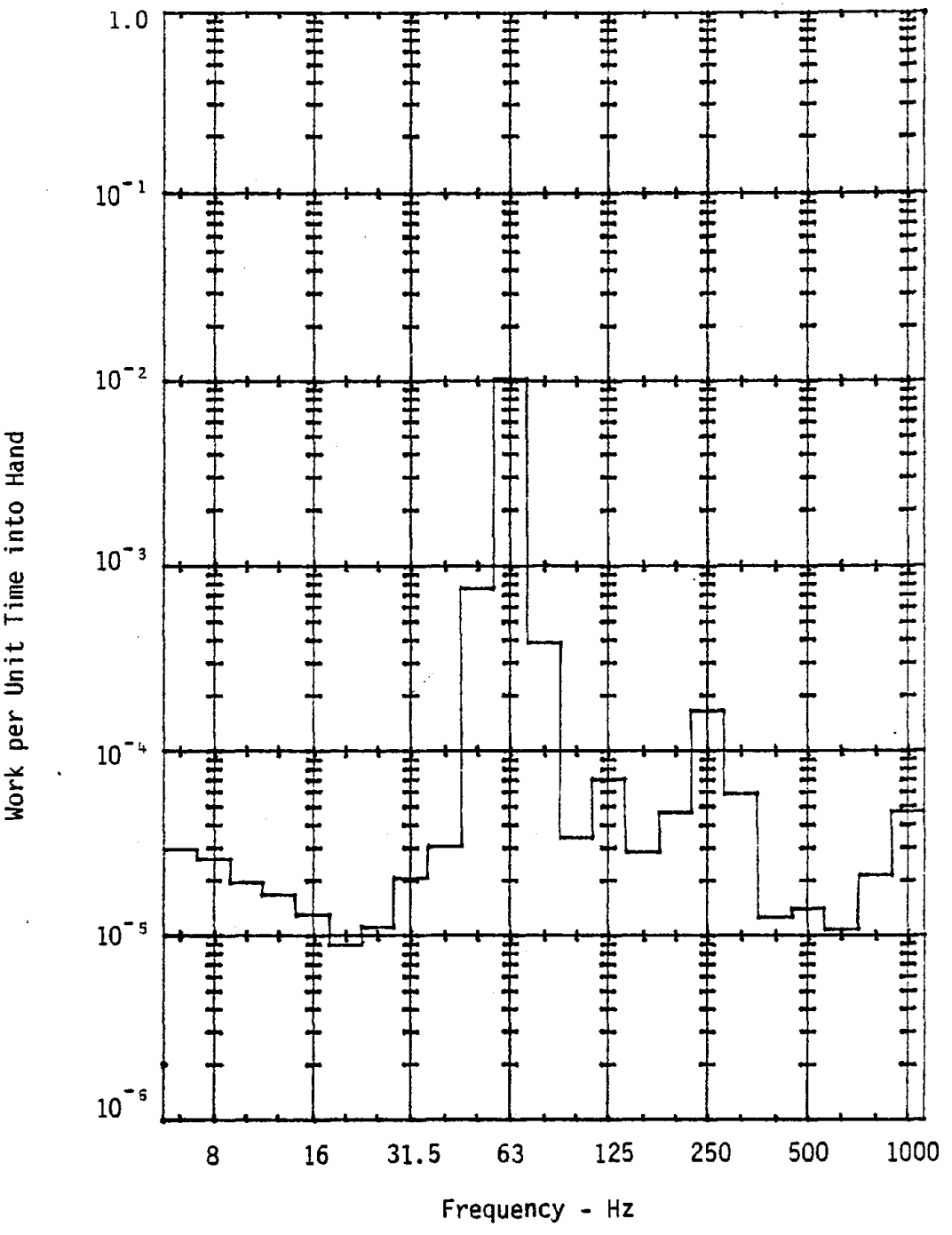

Figure F-12. RMS amplitude of work per unit time directed into hand from horizontal grinder with coarse radial wheel. Right hand, X-direction.

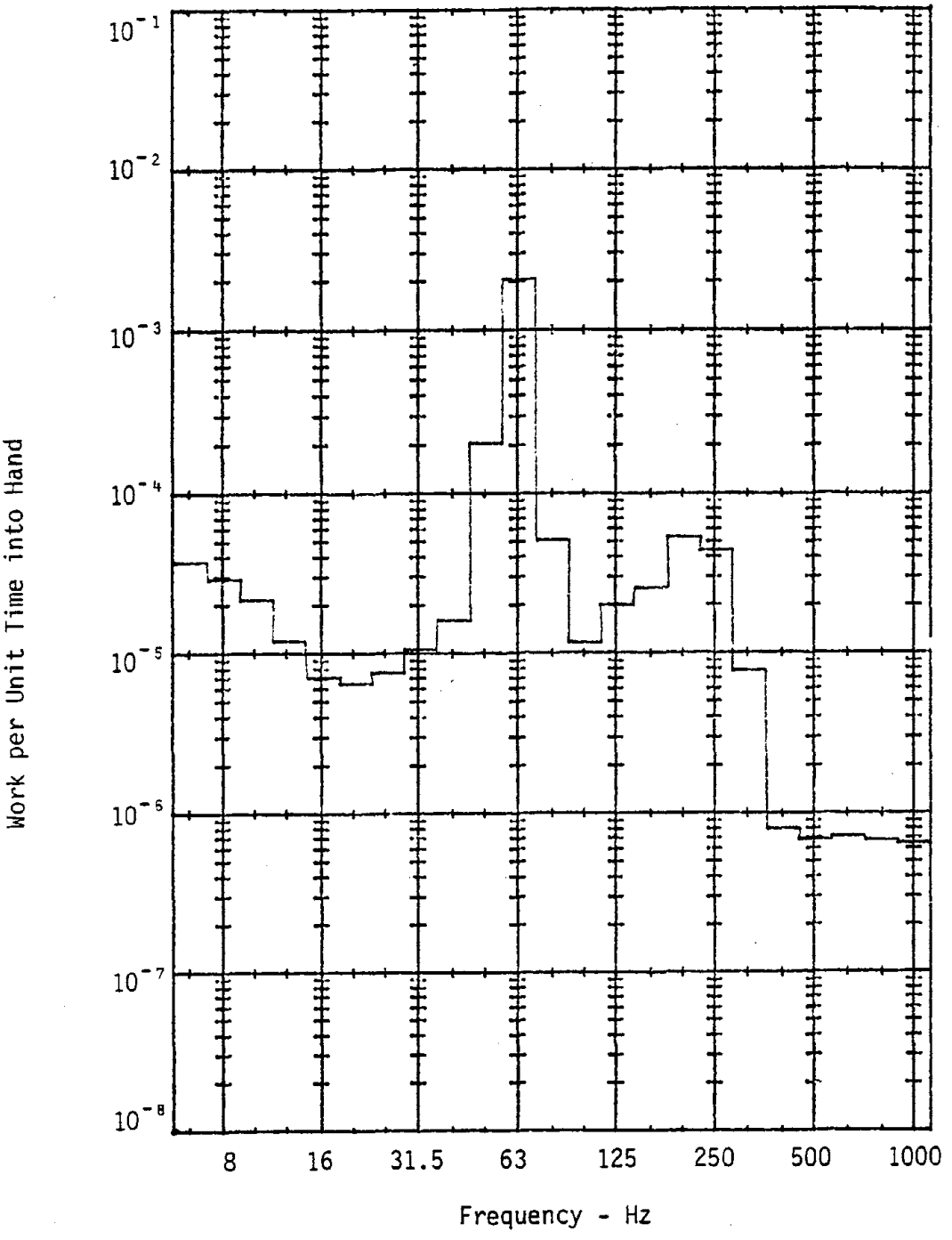

Figure F-13. RMS amplitude of work per unit time directed into hand from horizontal grinder with coarse radial wheel. Right hand, Y-direction.

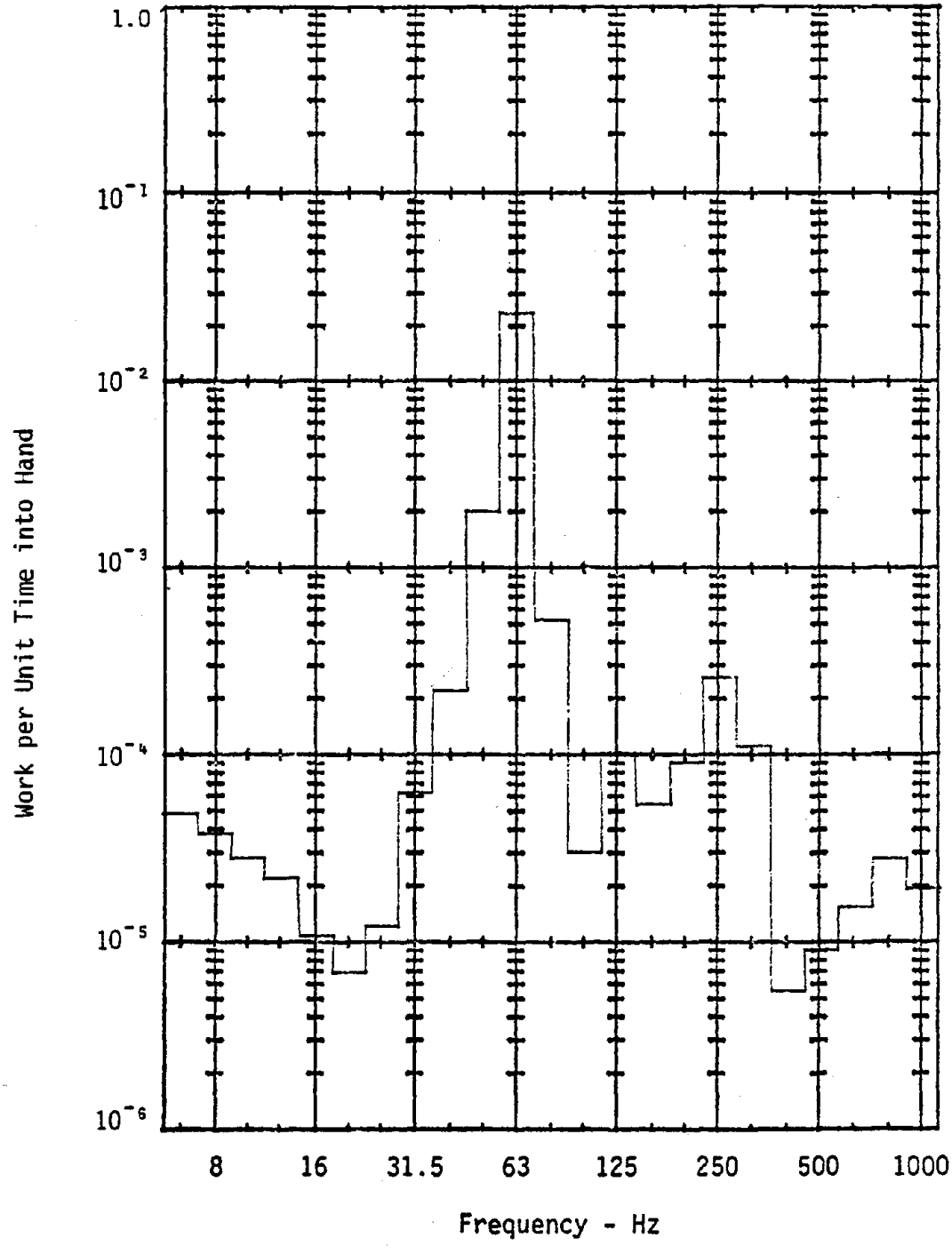

Figure F-14. RMS amplitude of work per unit time directed into hand from horizontal grinder with coarse radial wheel. Right hand, Z-direction.

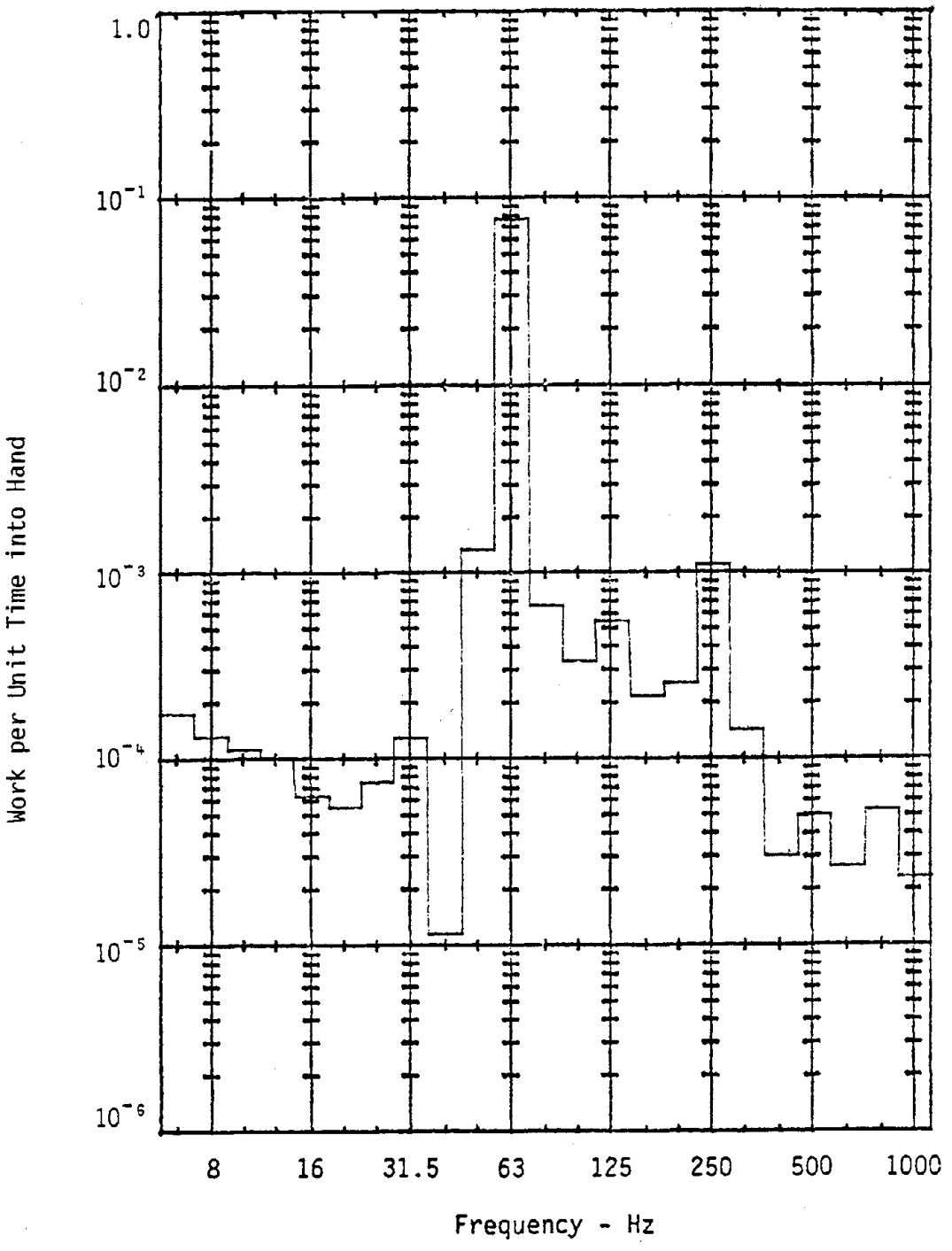

Figure F-15. RMS amplitude of work per unit time directed into hand from horizontal grinder with coarse radial wheel. Left hand, X-direction.

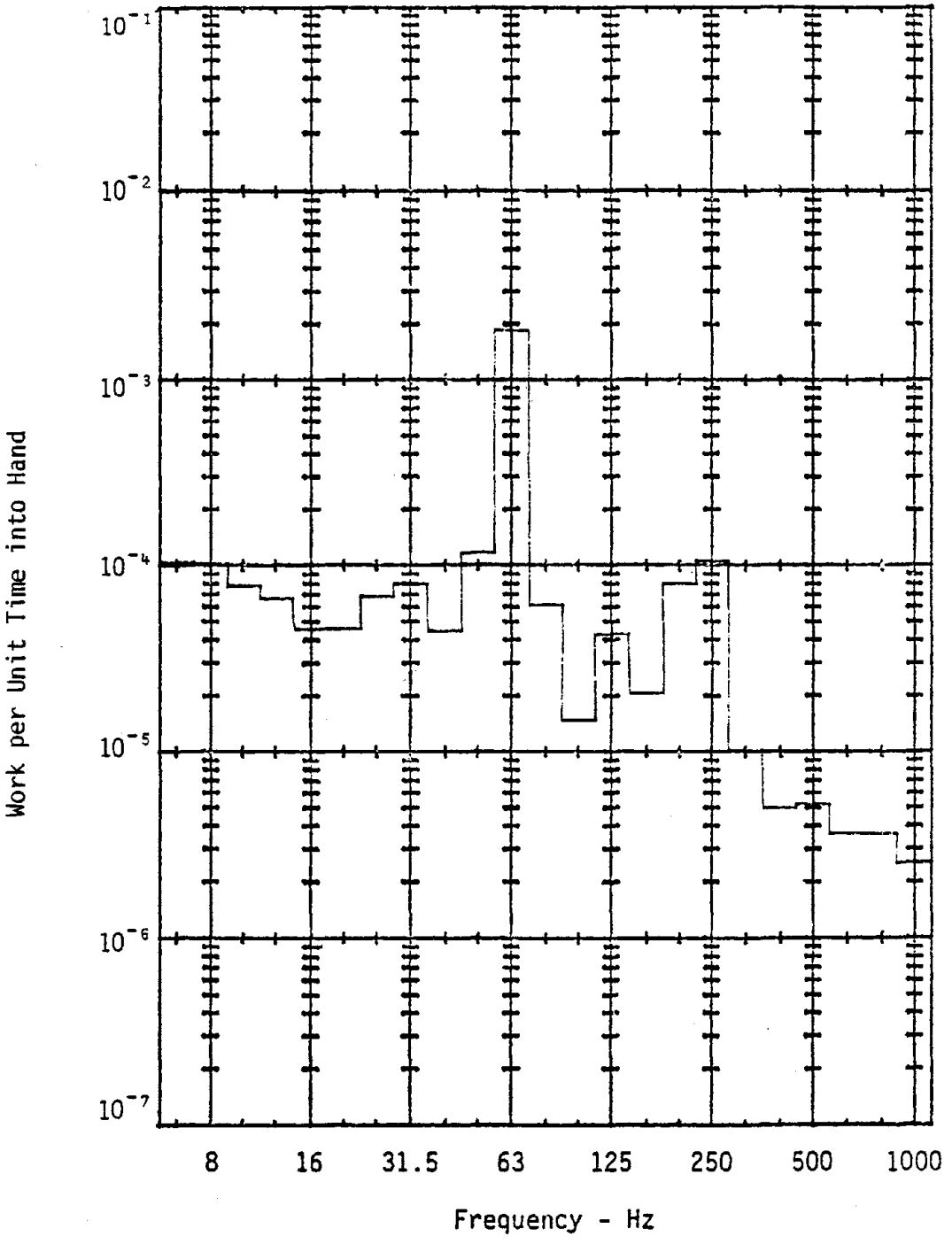

Figure F-16. RMS amplitude of work per unit time directed into hand from horizontal grinder with coarse radial wheel. Left hand, Y-direction.

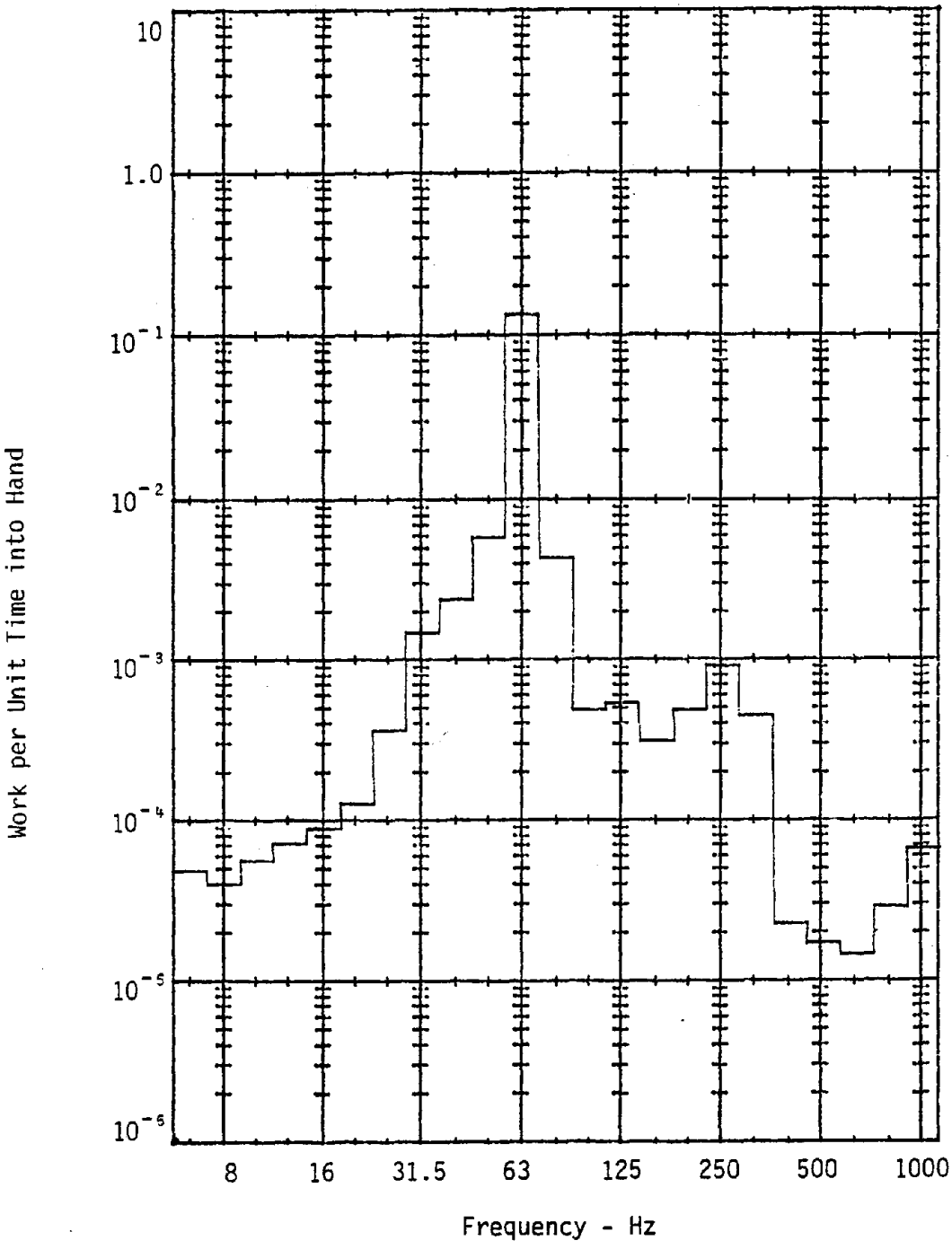

Figure F-17. RMS amplitude of work per unit time directed into hand from horizontal grinder with coarse radial wheel. Left hand, Z-direction.

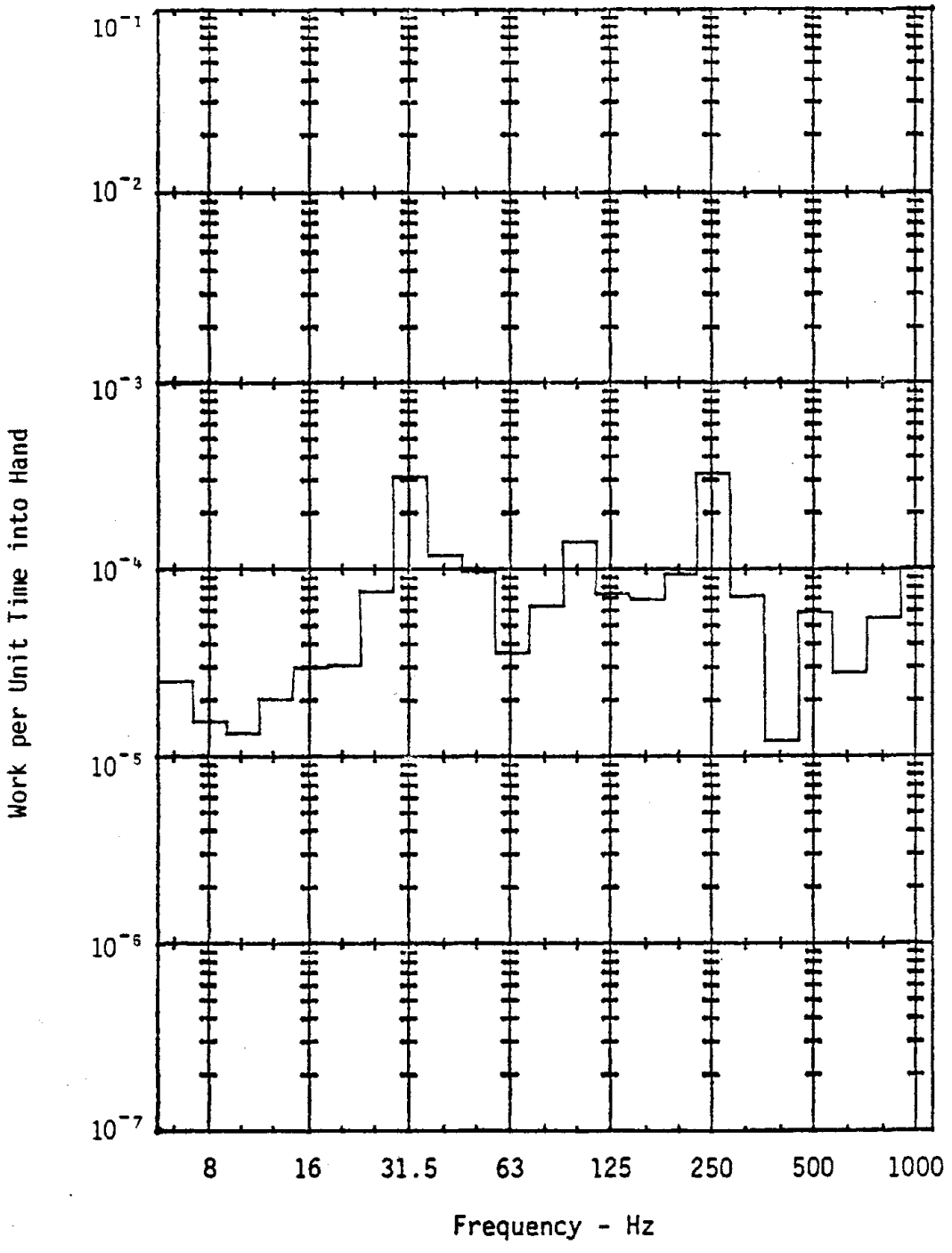

Figure F-18. RMS amplitude of work per unit time directed into hand from horizontal grinder with fine radial wheel. Right hand, X-direction.

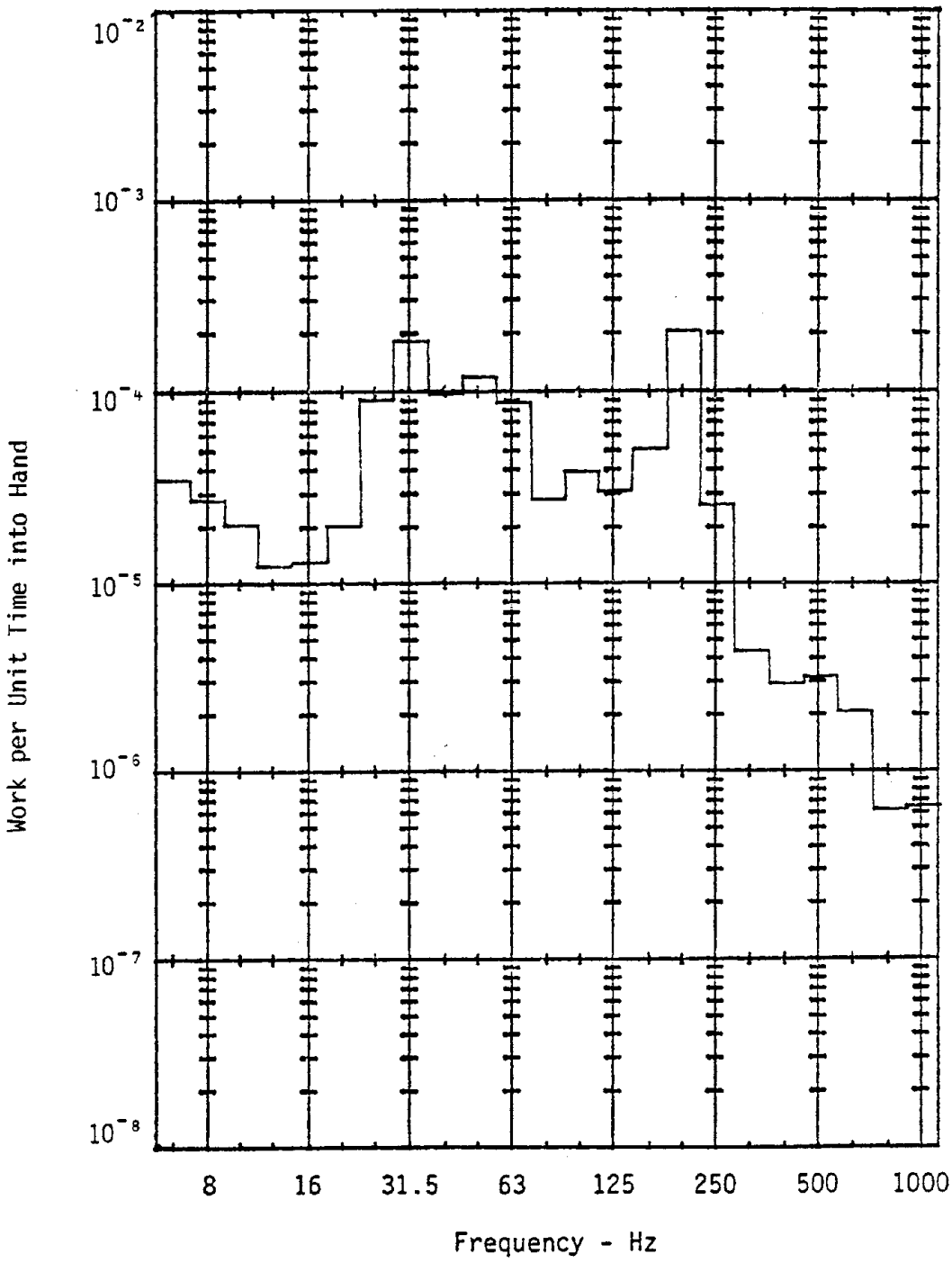

Figure F-19. RMS amplitude of work per unit time directed into hand from horizontal grinder with fine radial wheel. Right hand, Y-direction.

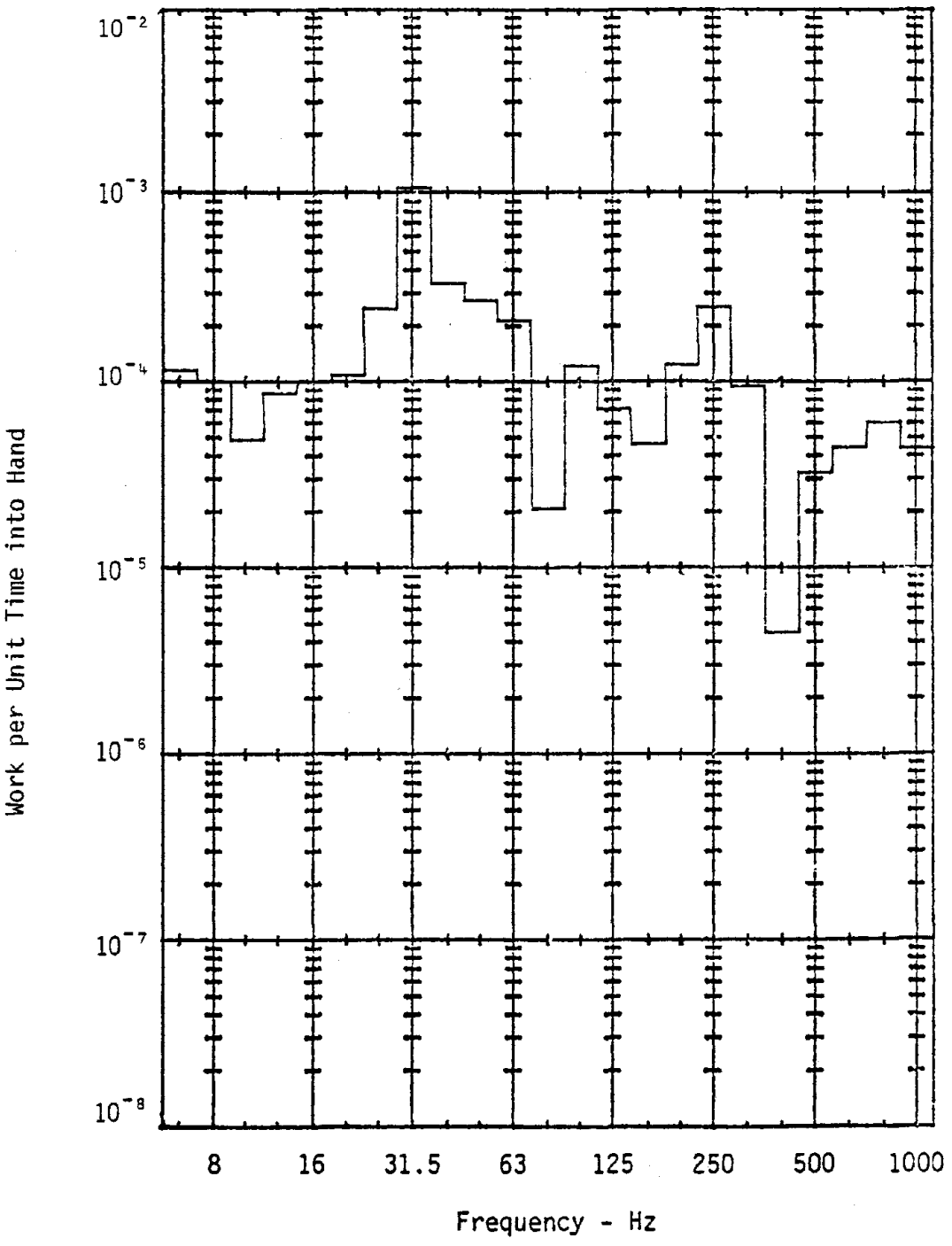

Figure F-20. RMS amplitude of work per unit time directed into hand from horizontal grinder with fine radial wheel. Right hand, Z-direction.

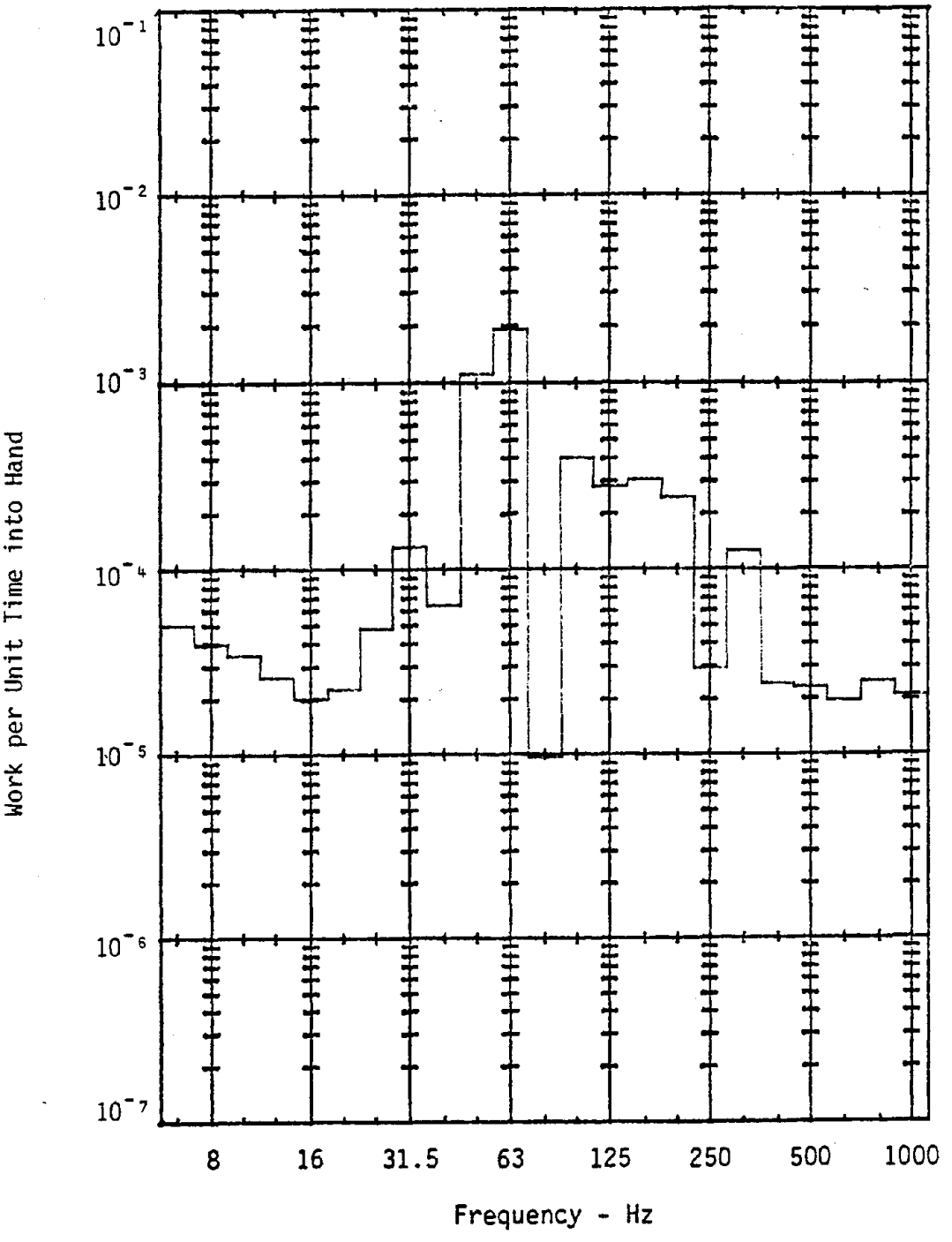

Figure F-21. RMS amplitude of work per unit time directed into hand from horizontal grinder with fine radial wheel. Left hand, X-direction.

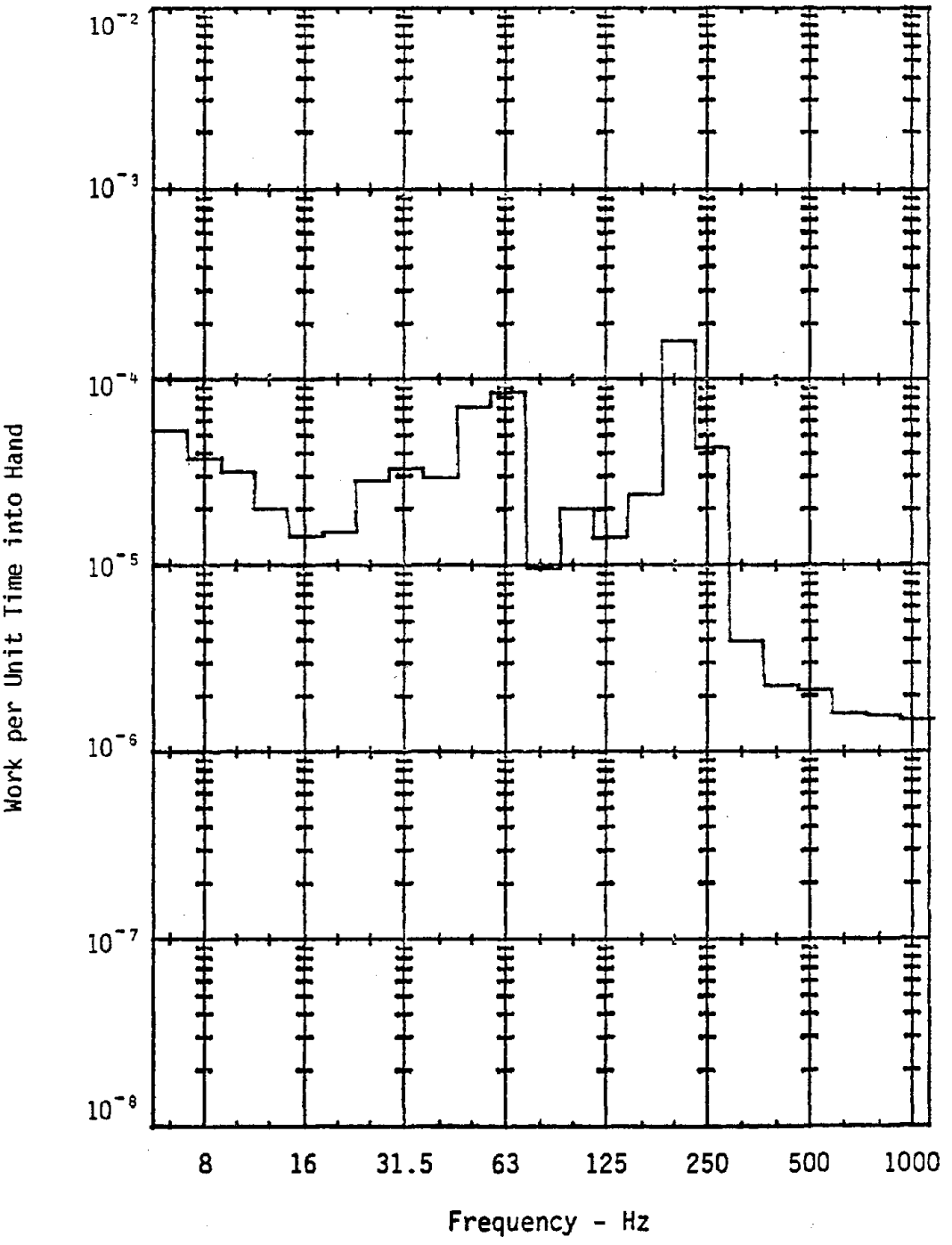

Figure F-22. RMS amplitude of work per unit time directed into hand from horizontal grinder with fine radial wheel. Left hand, Y-direction.

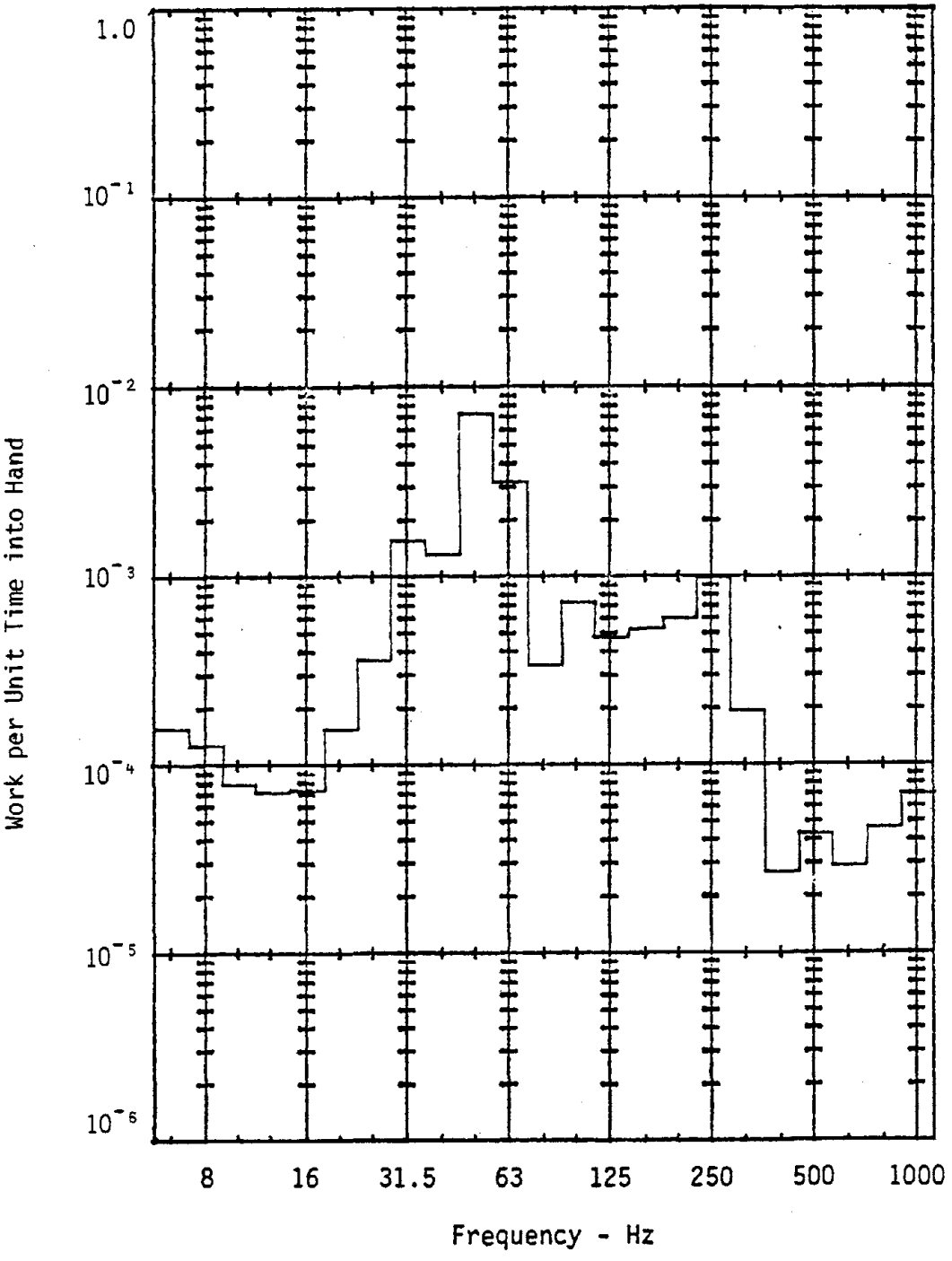

Figure F-23. RMS amplitude of work per unit time directed into hand from horizontal grinder with fine radial wheel. Left hand, Z-direction.

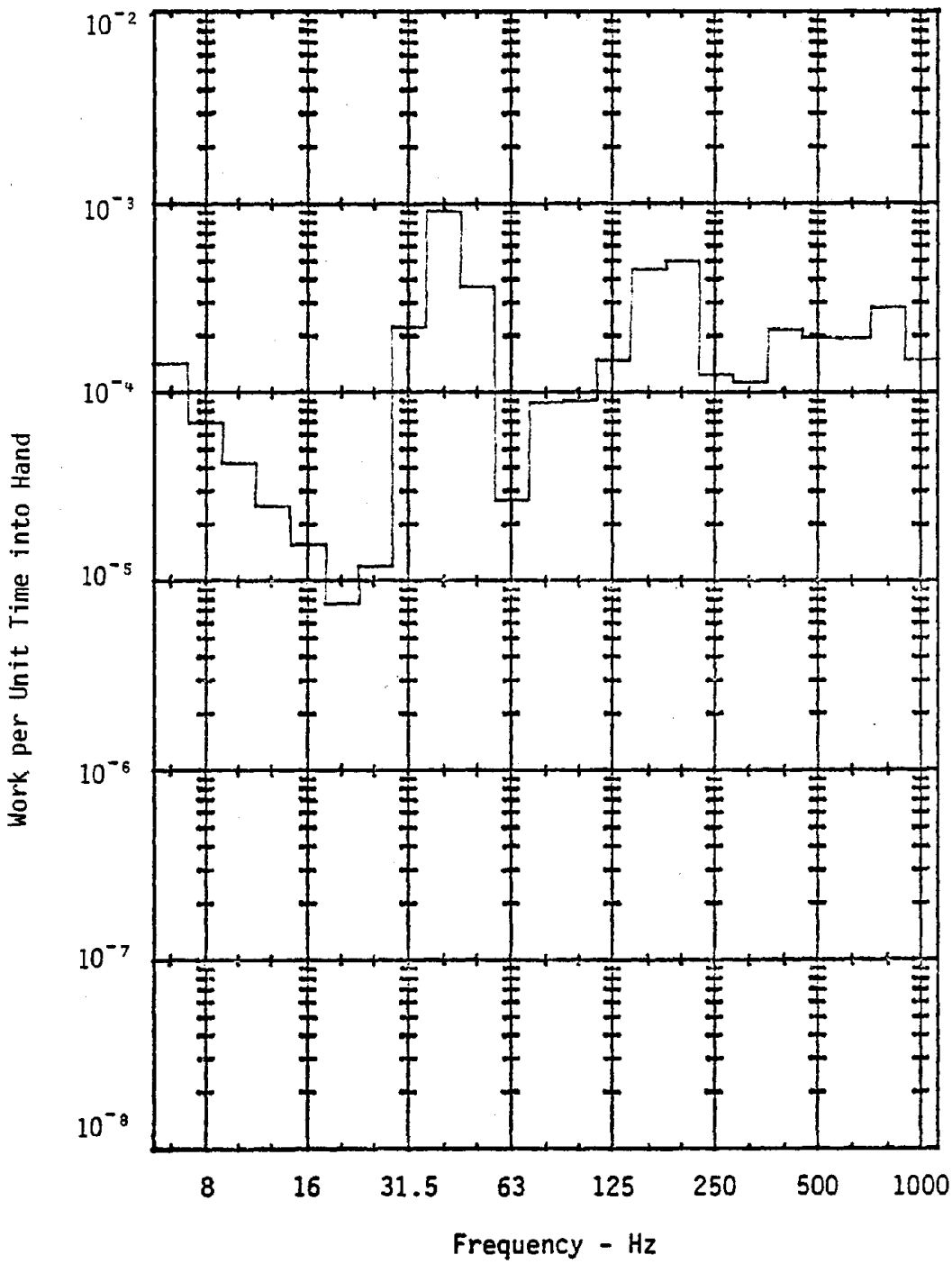

Figure F-24. RMS amplitude of work per unit time directed into hand from horizontal grinder with coarse flared cup wheel. Right hand, X-direction.

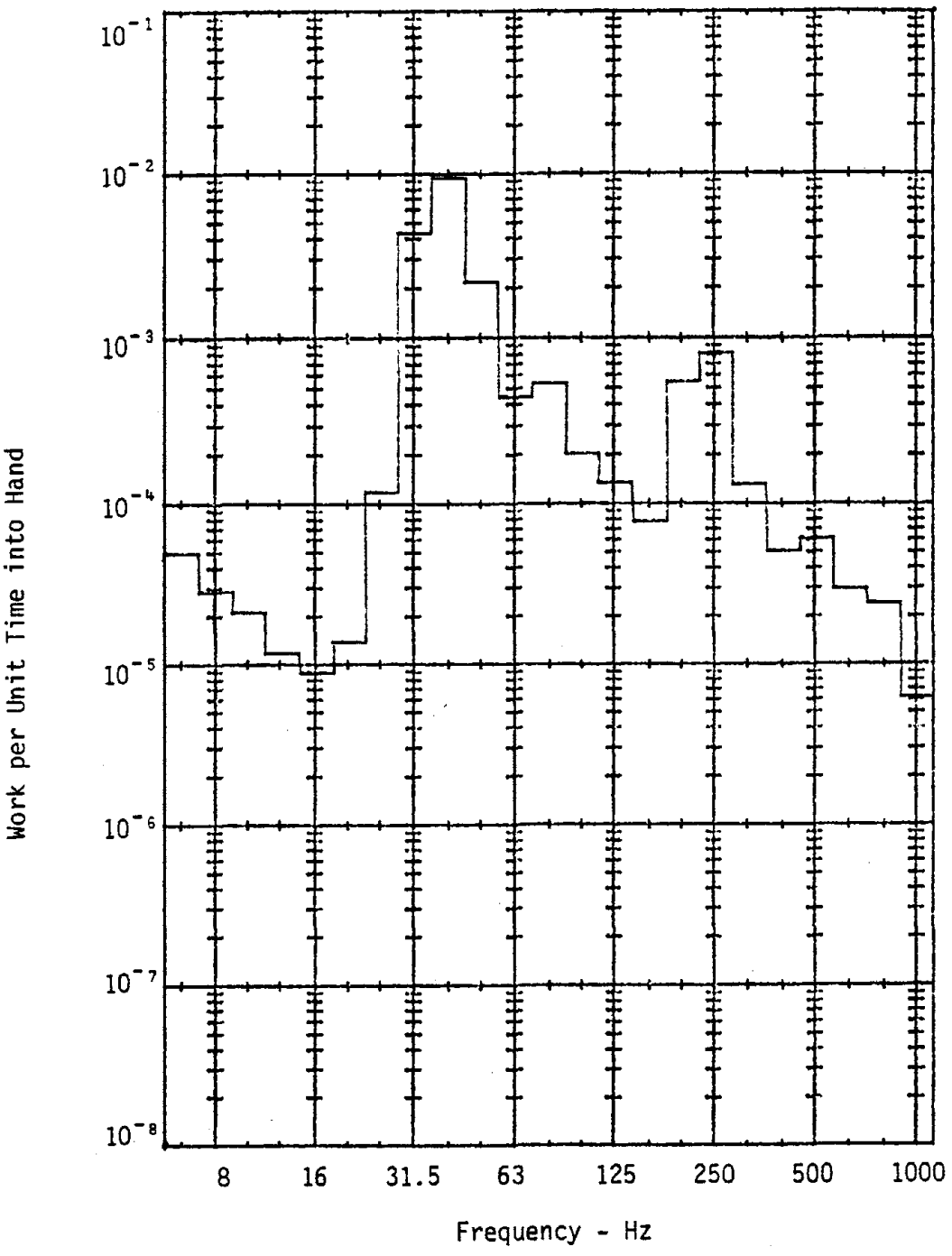

Figure F-25. RMS amplitude of work per unit time directed into hand from horizontal grinder with coarse flared cup wheel. Right hand, Y-direction.

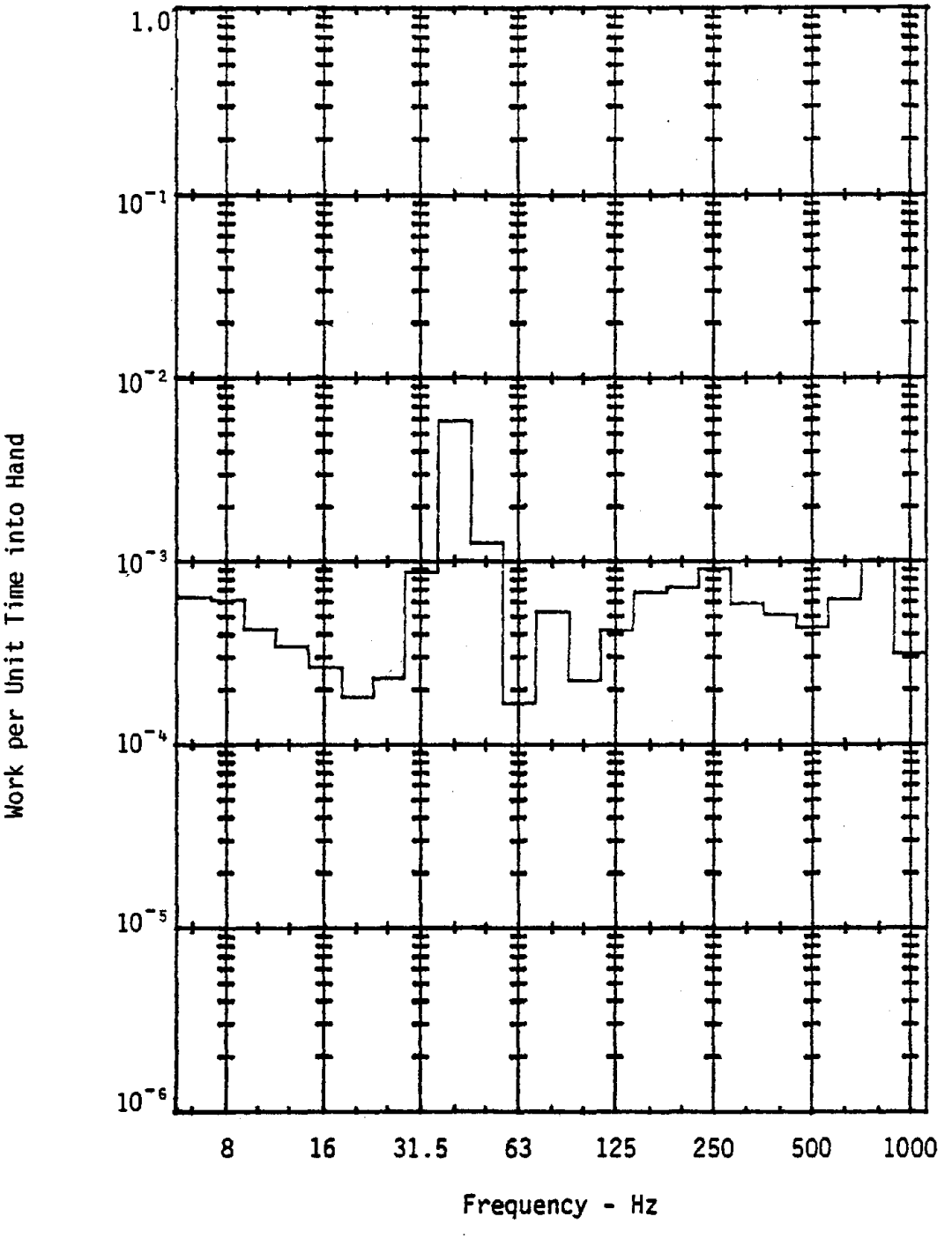

Figure F-26. RMS amplitude of work per unit time directed into hand from horizontal grinder with coarse flared cup wheel. Right hand, Z-direction.

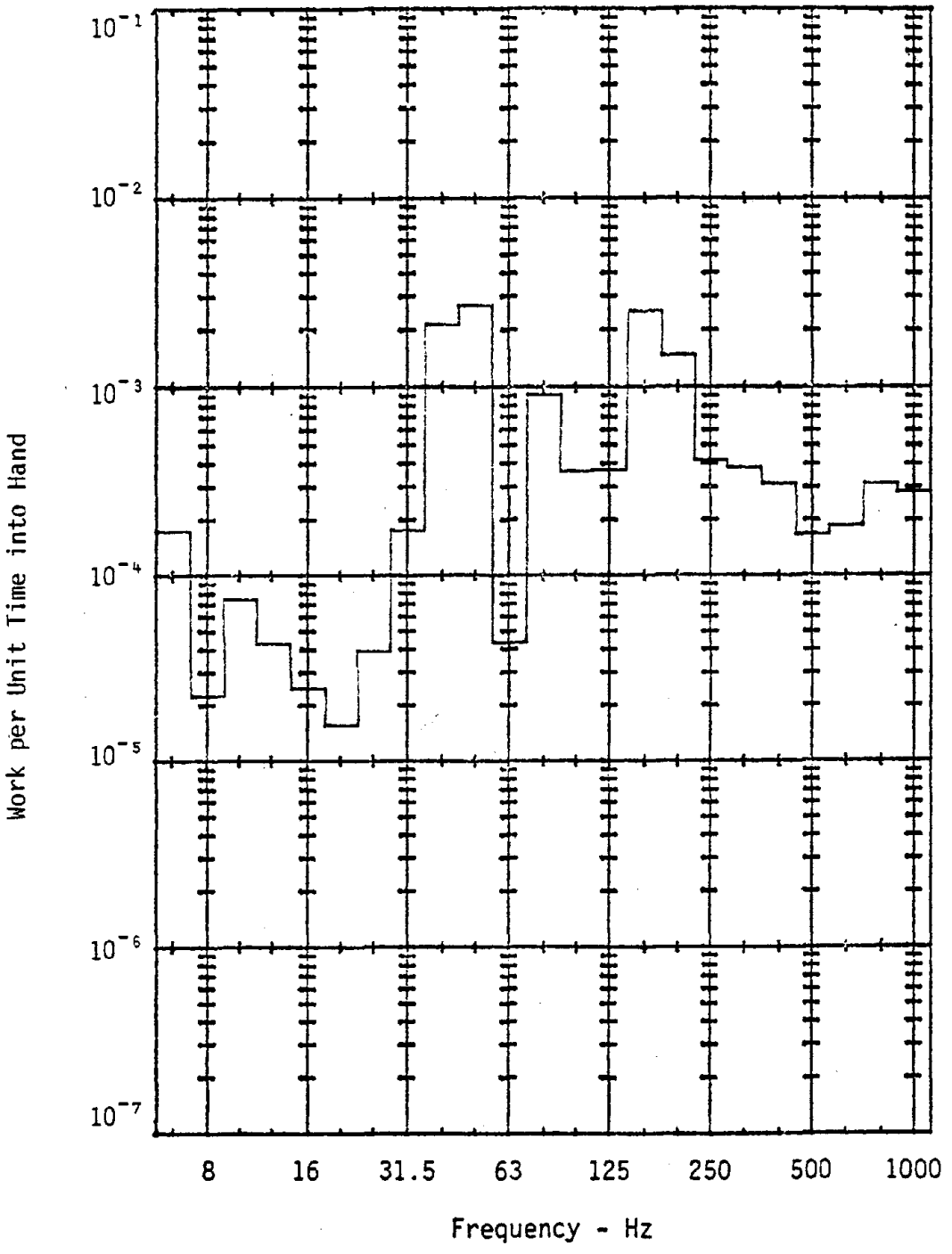

Figure F-27. RMS amplitude of work per unit time directed into hand from horizontal grinder with coarse flared cup wheel. Left hand, X-direction.

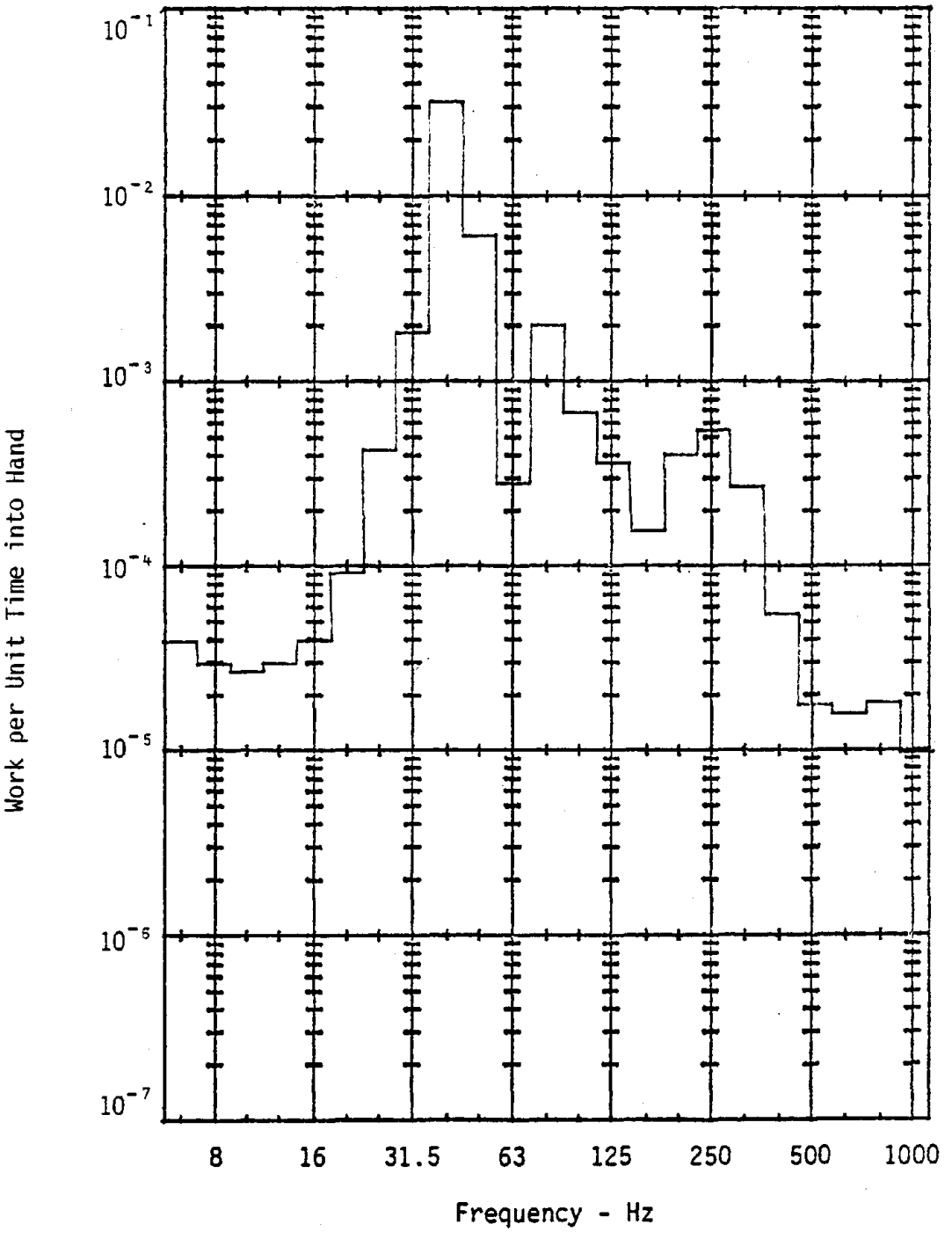

Figure F-28. RMS amplitude of work per unit time directed into hand from horizontal grinder with coarse flared cup wheel. Left hand, Y-direction.

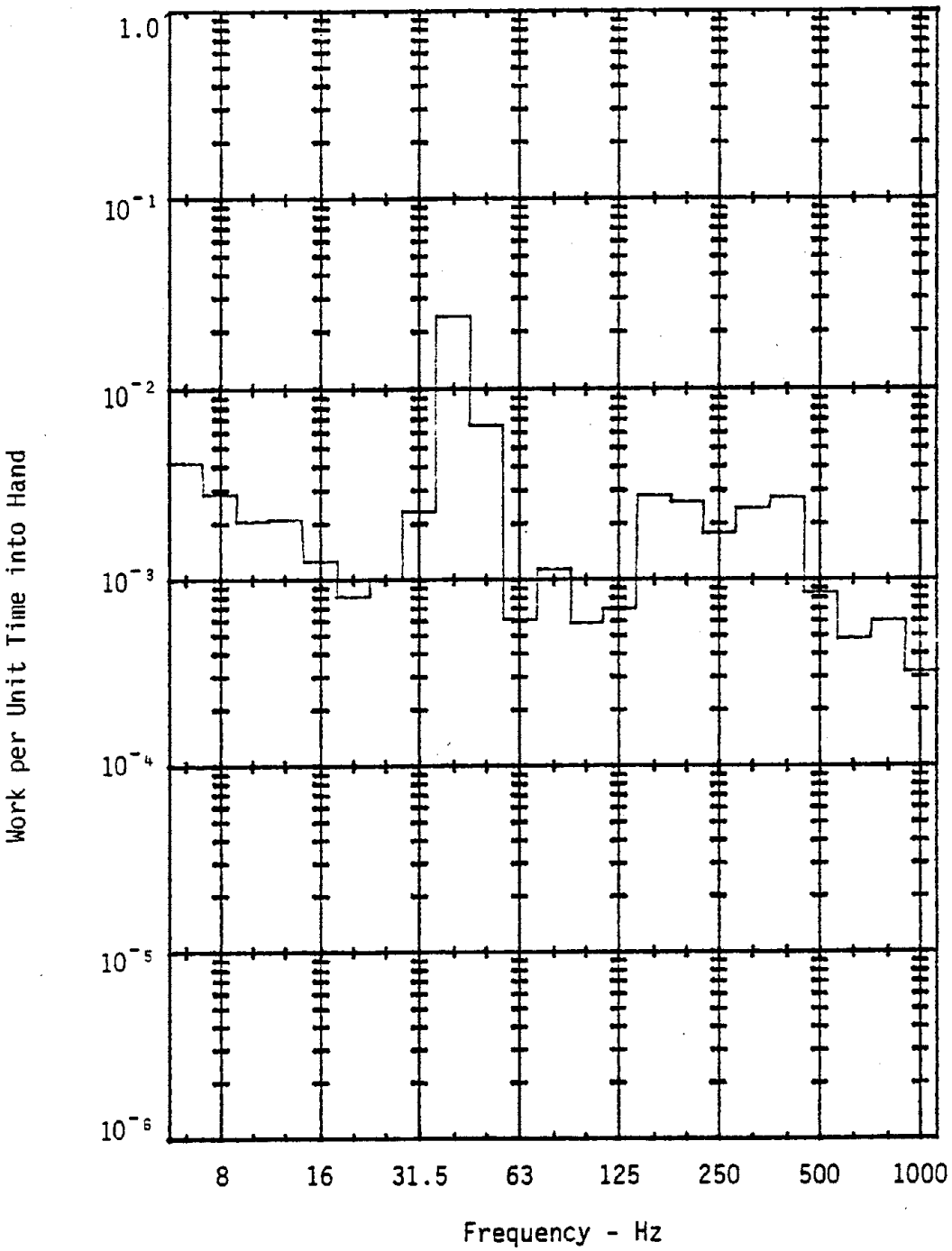

Figure F-29. RMS amplitude of work per unit time directed into hand from horizontal grinder with coarse flared cup wheel. Left hand, Z-direction.

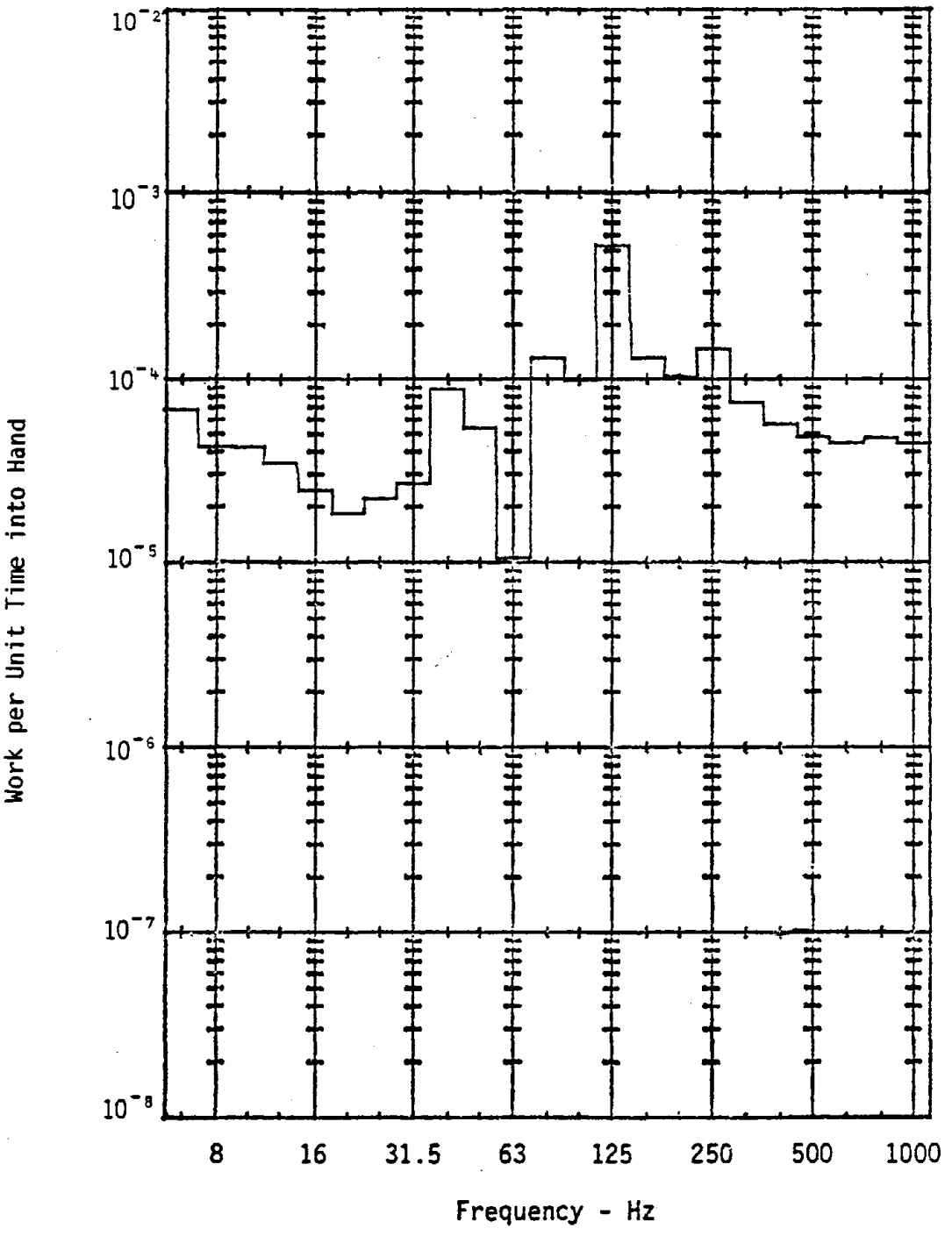

Figure F-30. RMS amplitude of work per unit time directed into hand from vertical grinder with sanding pad, medium paper. Right hand, X-direction.

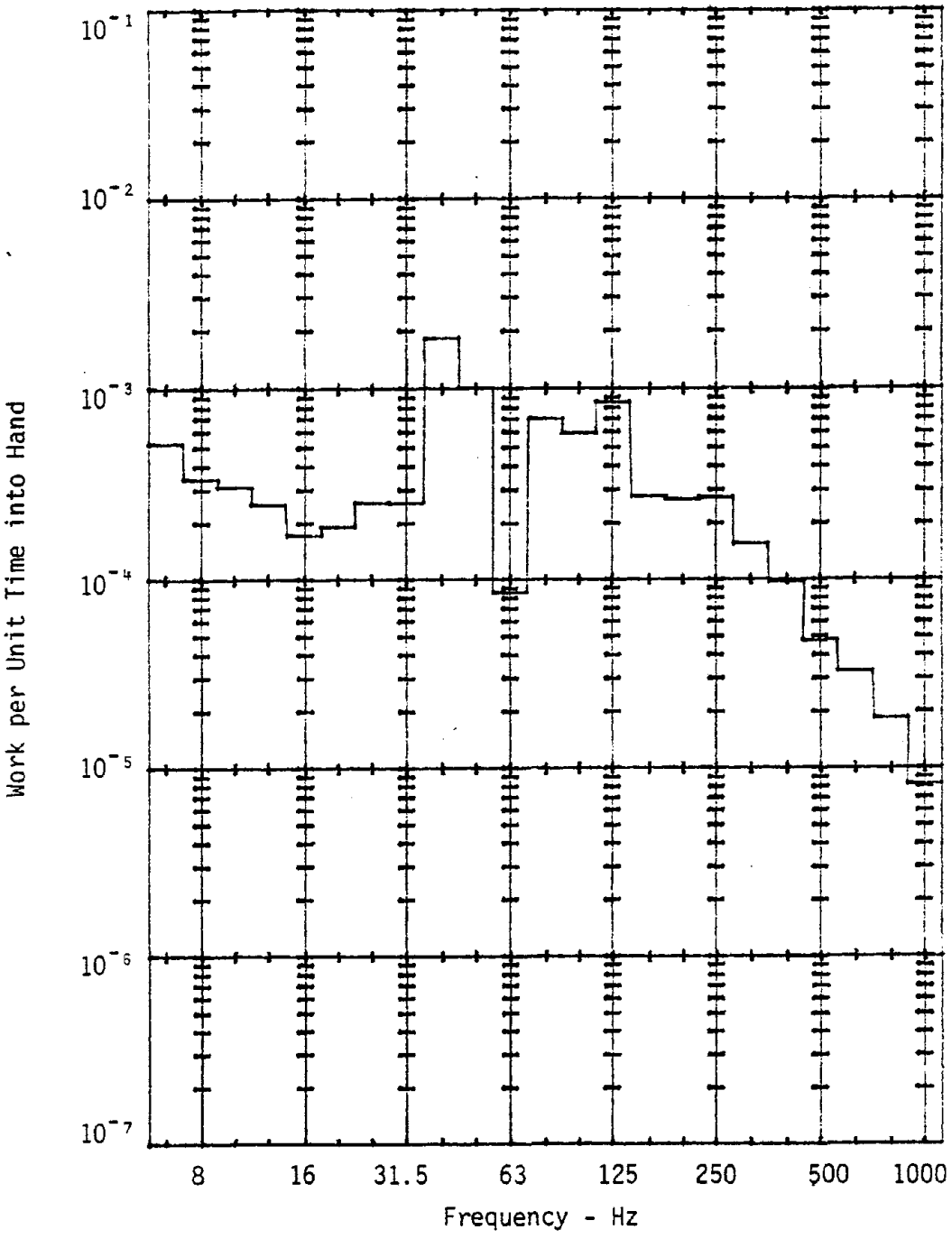

Figure F-31. RMS amplitude of work per unit time directed into hand from vertical grinder with sanding pad, medium paper. Right hand, Y-direction.

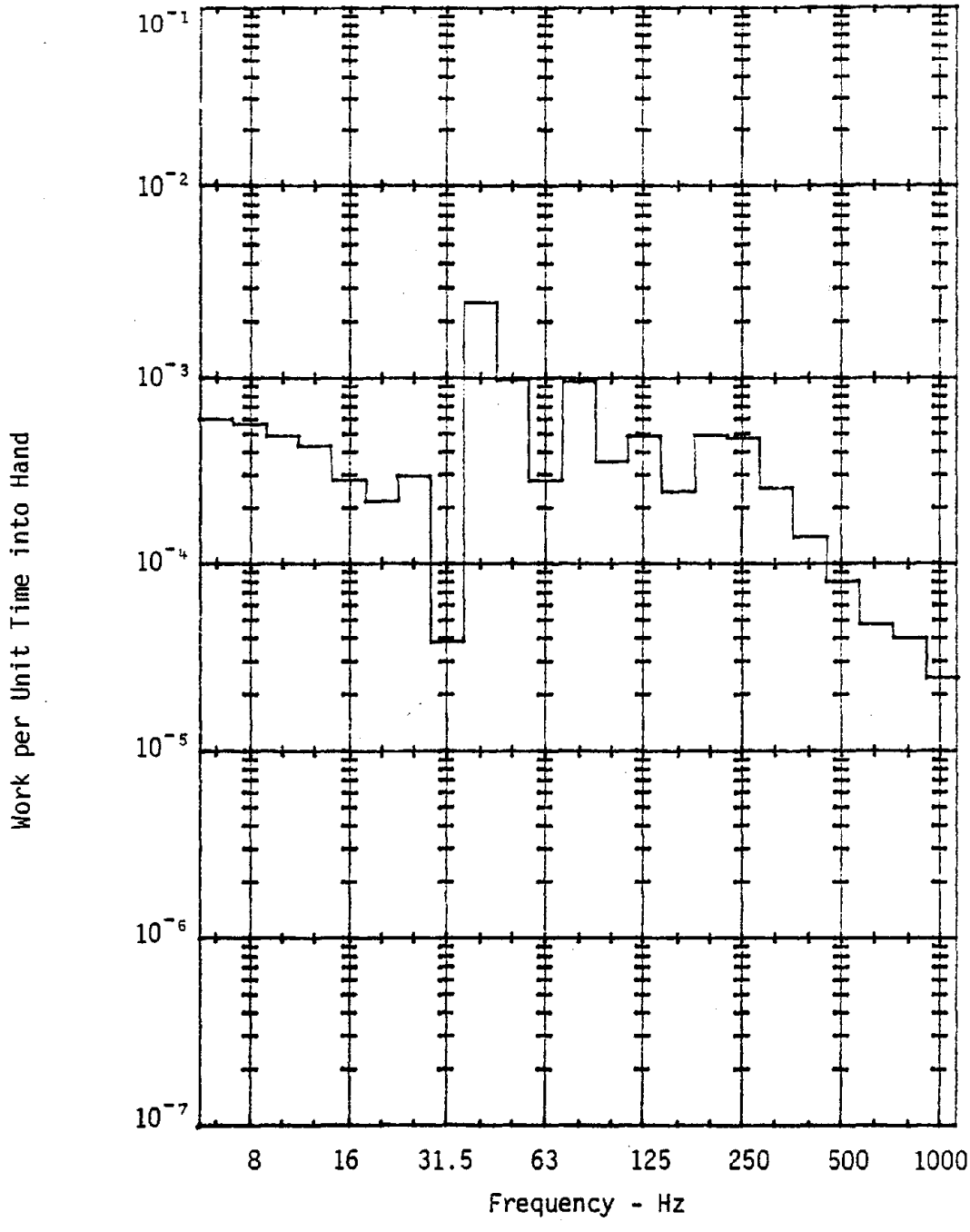

Figure F-32. RMS amplitude of work per unit time directed into hand from vertical grinder with sanding pad, medium paper. Right hand, Z-direction.

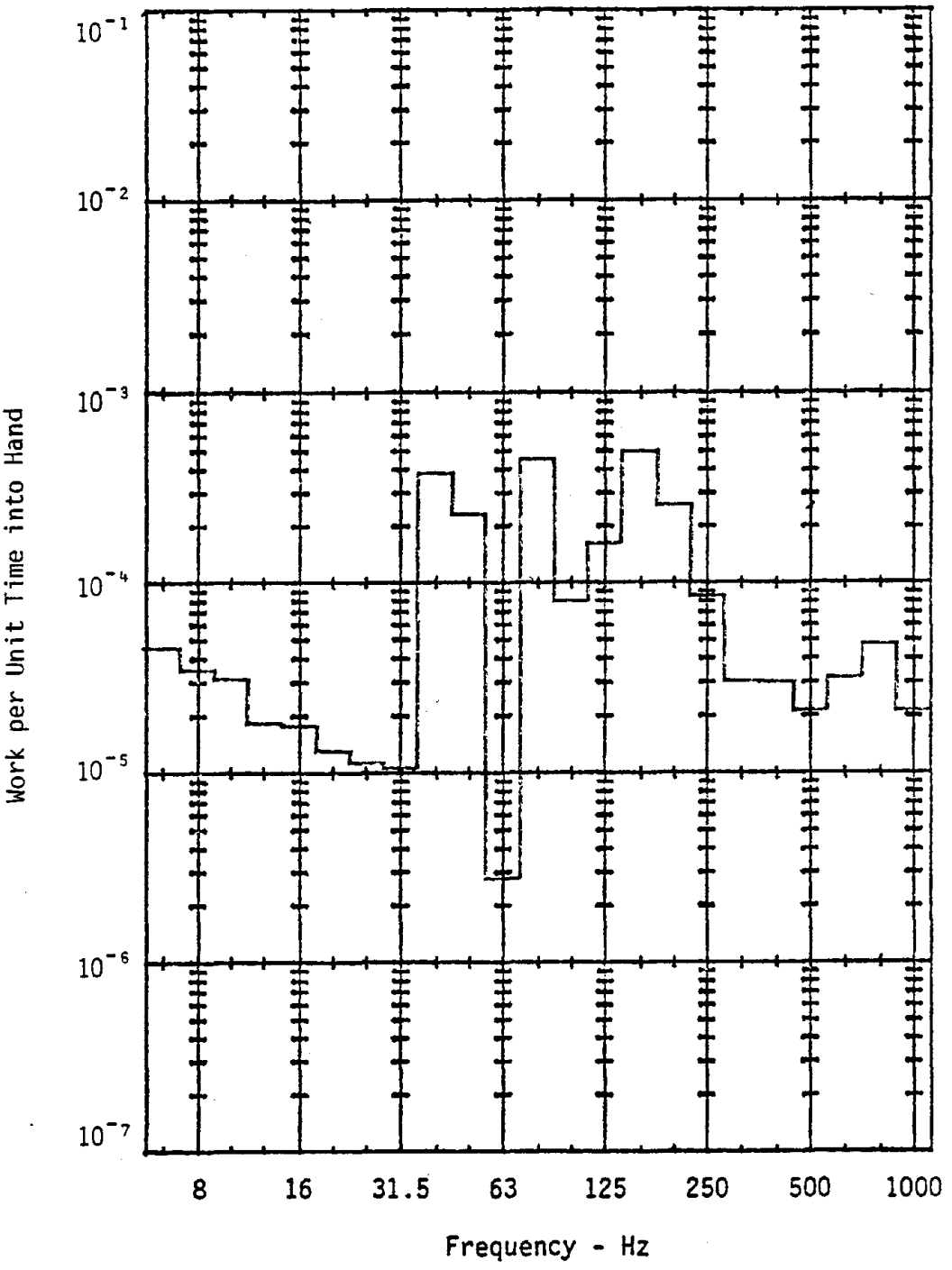

Figure F-33. RMS amplitude of work per unit time directed into hand from vertical grinder with sanding pad, medium paper. Left hand, X-direction.

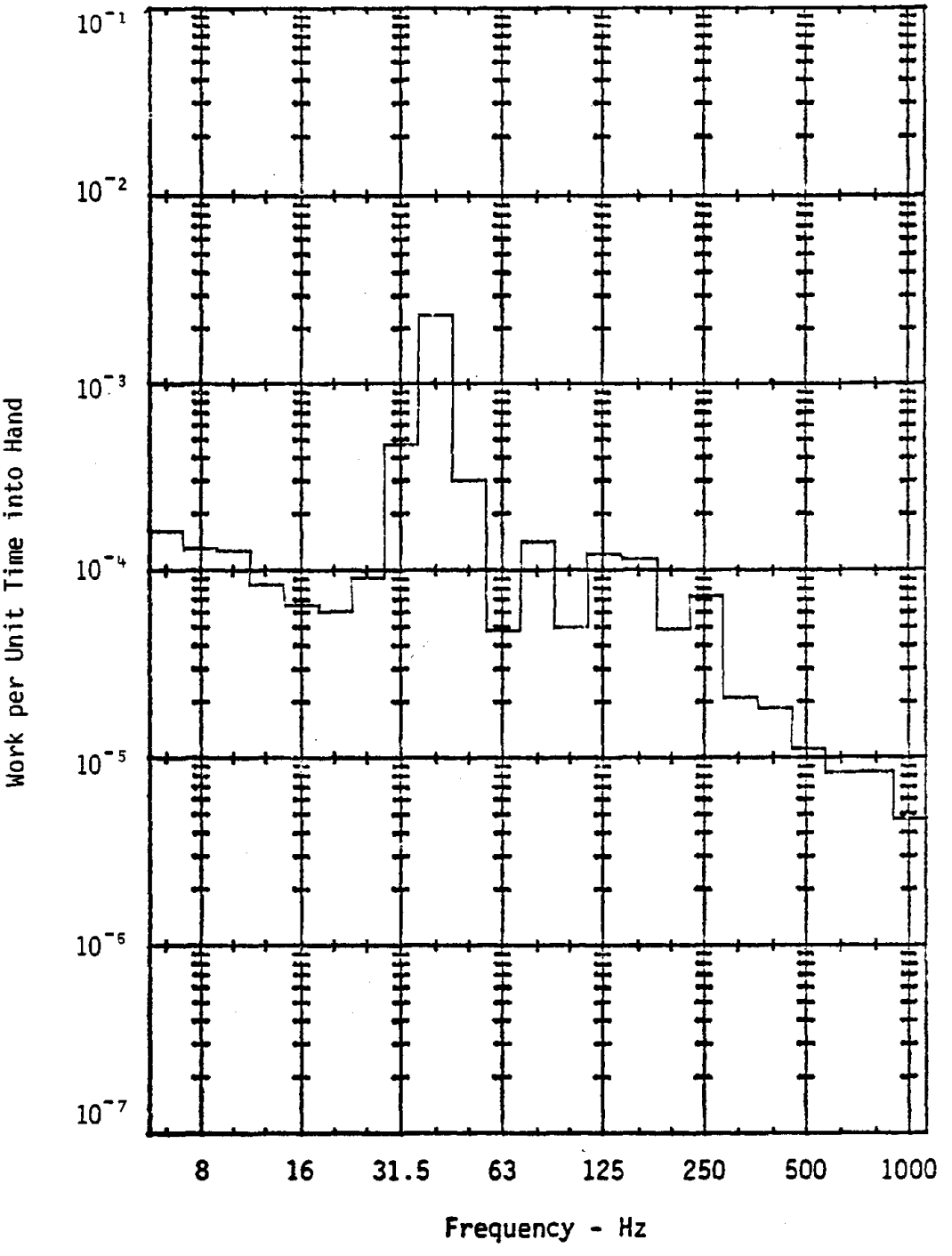

Figure F-34. RMS amplitude of work per unit time directed into hand from vertical grinder with sanding pad, medium paper. Left hand, Y-direction.

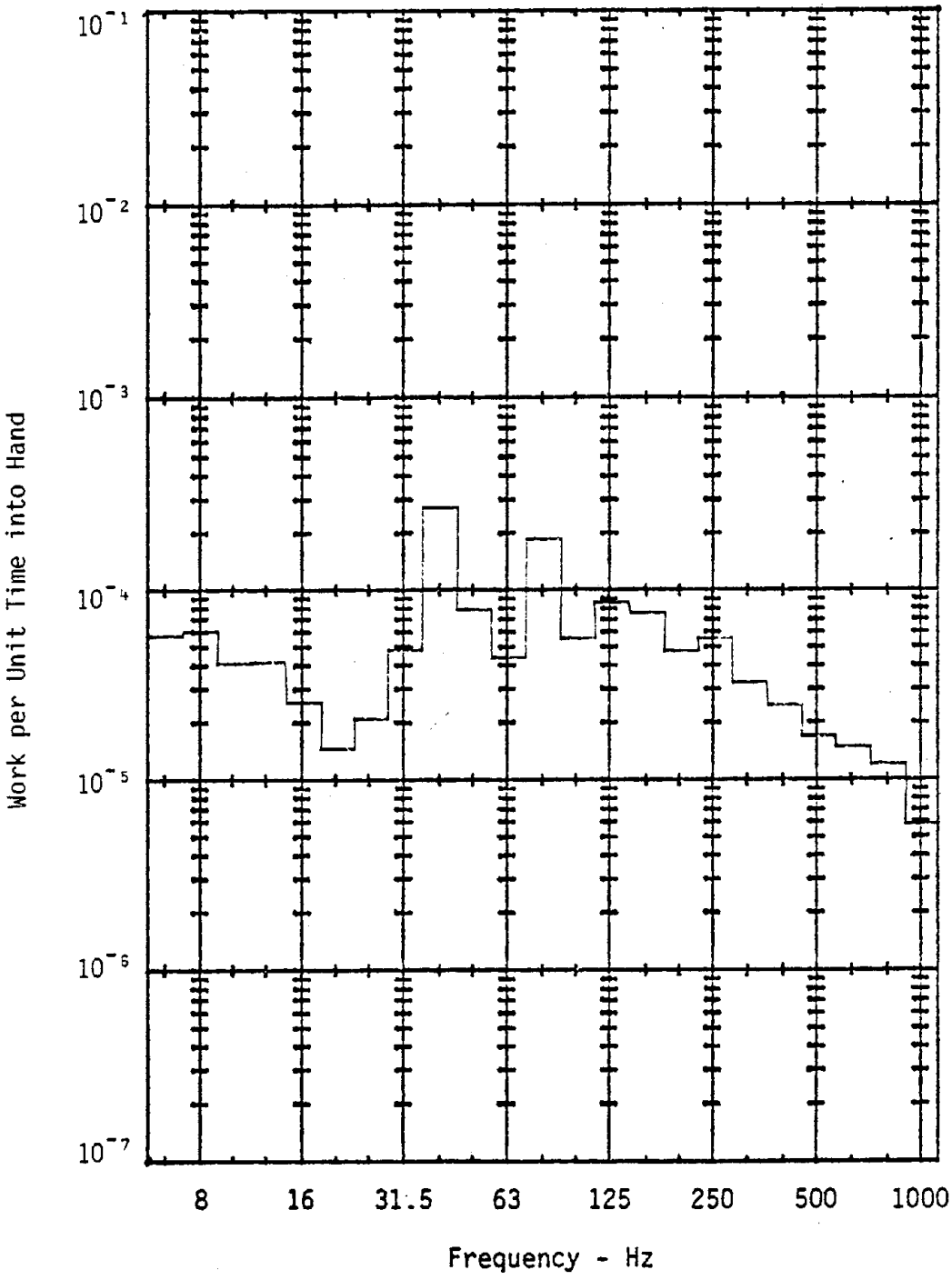

Figure F-35. RMS amplitude of work per unit time directed into hand from vertical grinder with sanding pad, medium paper. Left hand, Z-direction.

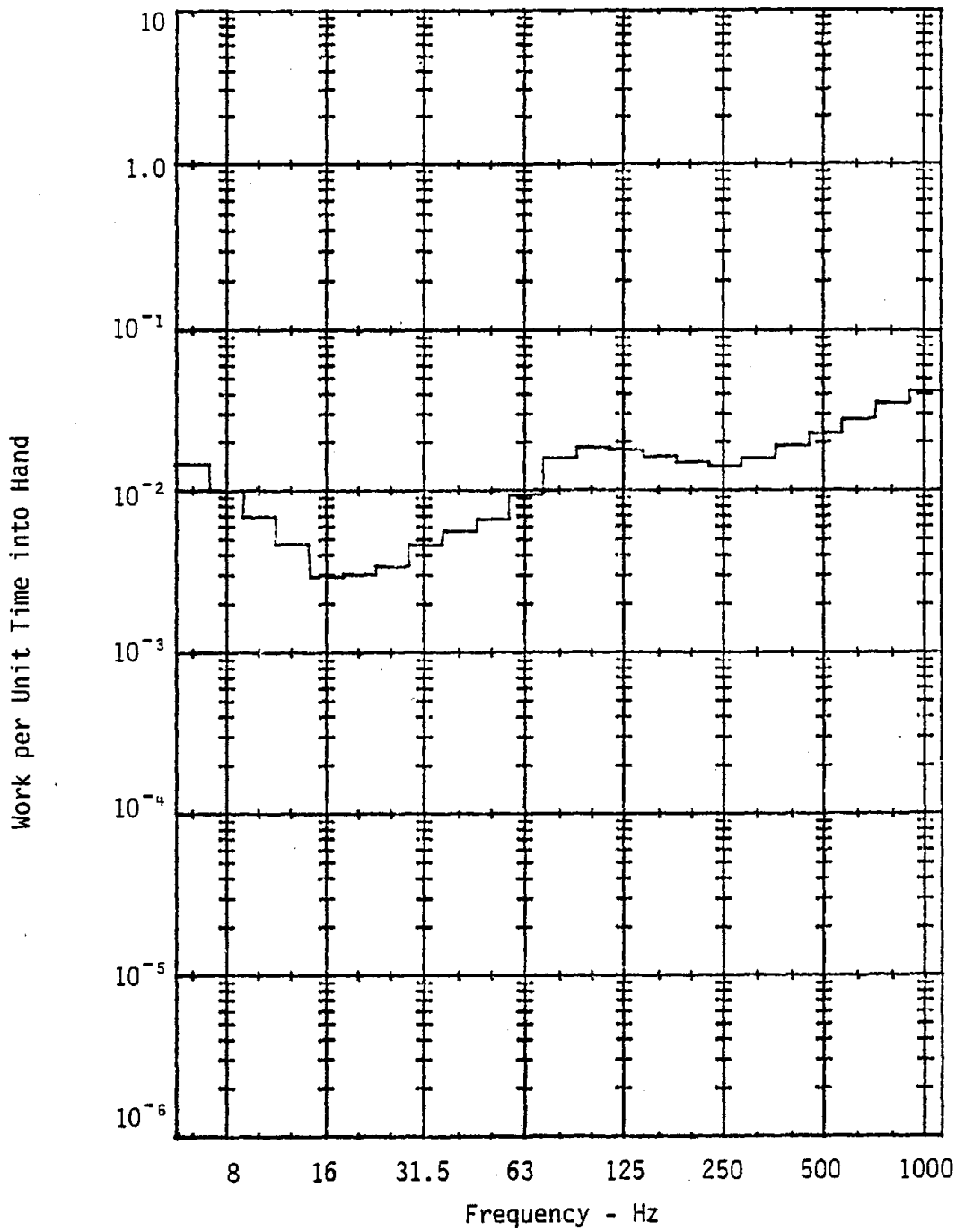

Figure F-36. RMS amplitude of work per unit time based on proposed ISO 8 hour acceleration limits. 3.8 cm handle, X-direction.

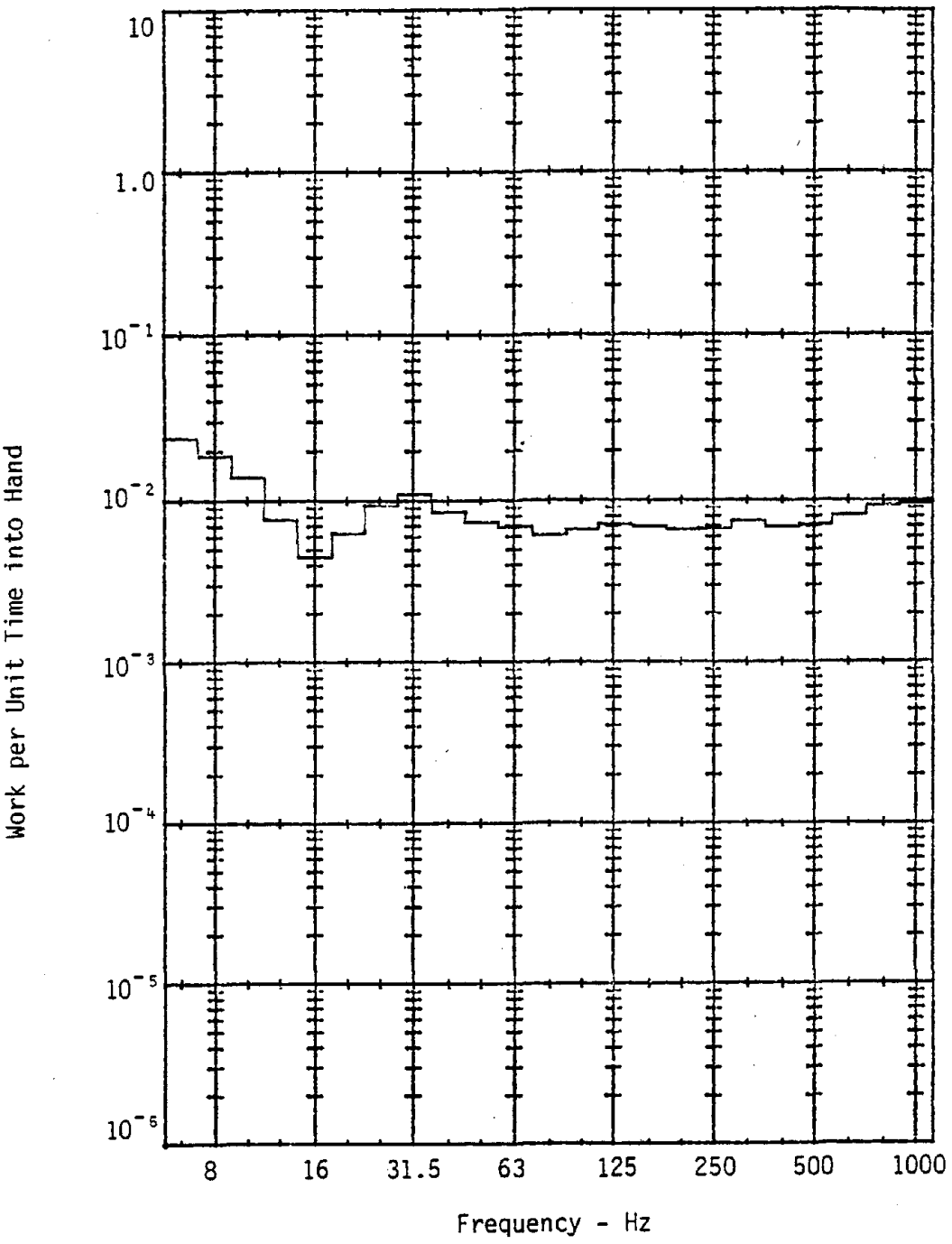

Figure F-37. RMS amplitude of work per unit time based on proposed ISO 8 hour acceleration limits. 3.8 cm handle, Y-direction.

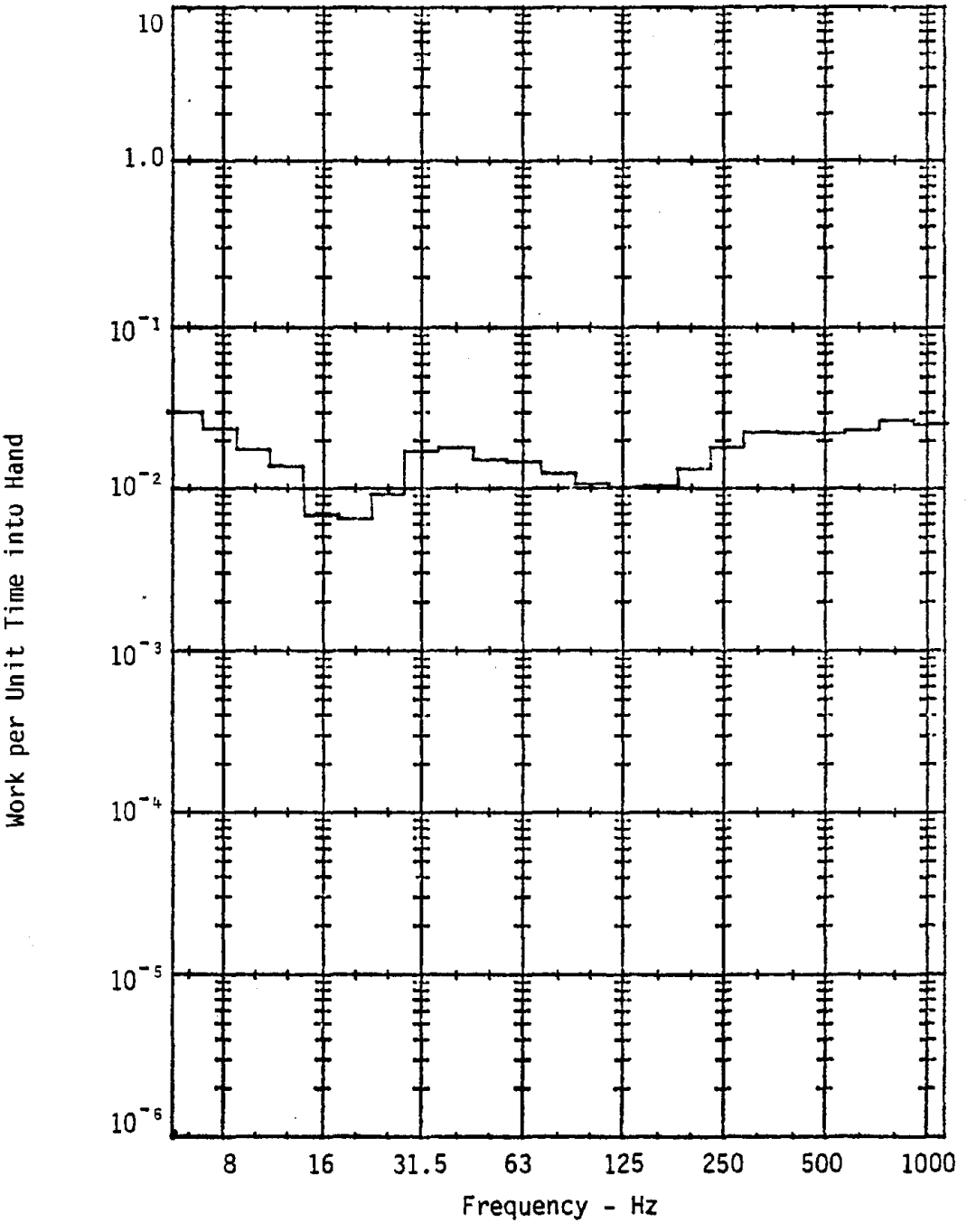

Figure F-38. RMS amplitude of work per unit time based on proposed ISO 8 hour acceleration limits. 3.8 cm handle, Z-direction.

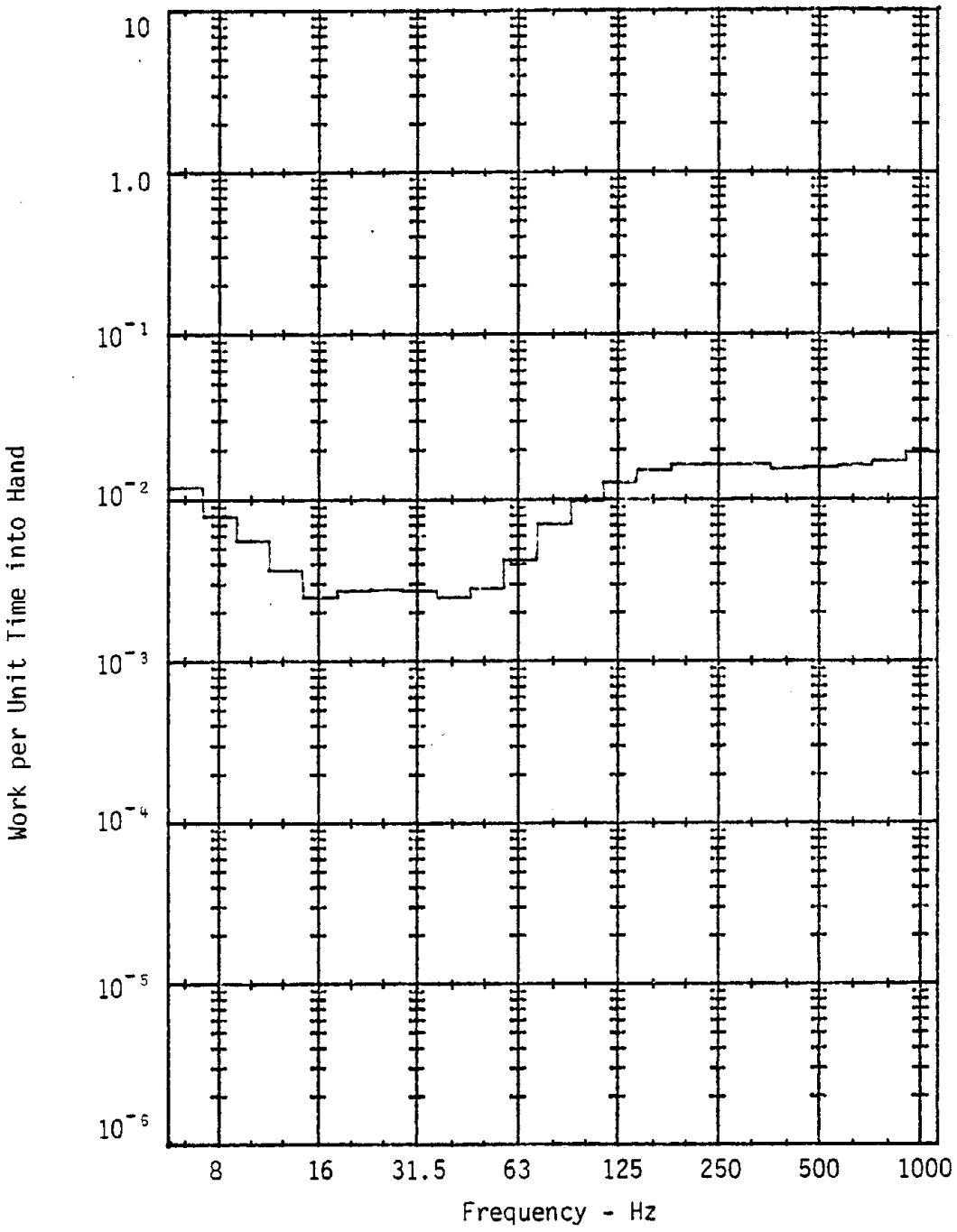

Figure F-39. RMS amplitude of work per unit time based on proposed ISO 8 hour acceleration limits. 1.9 cm handle, X-direction.

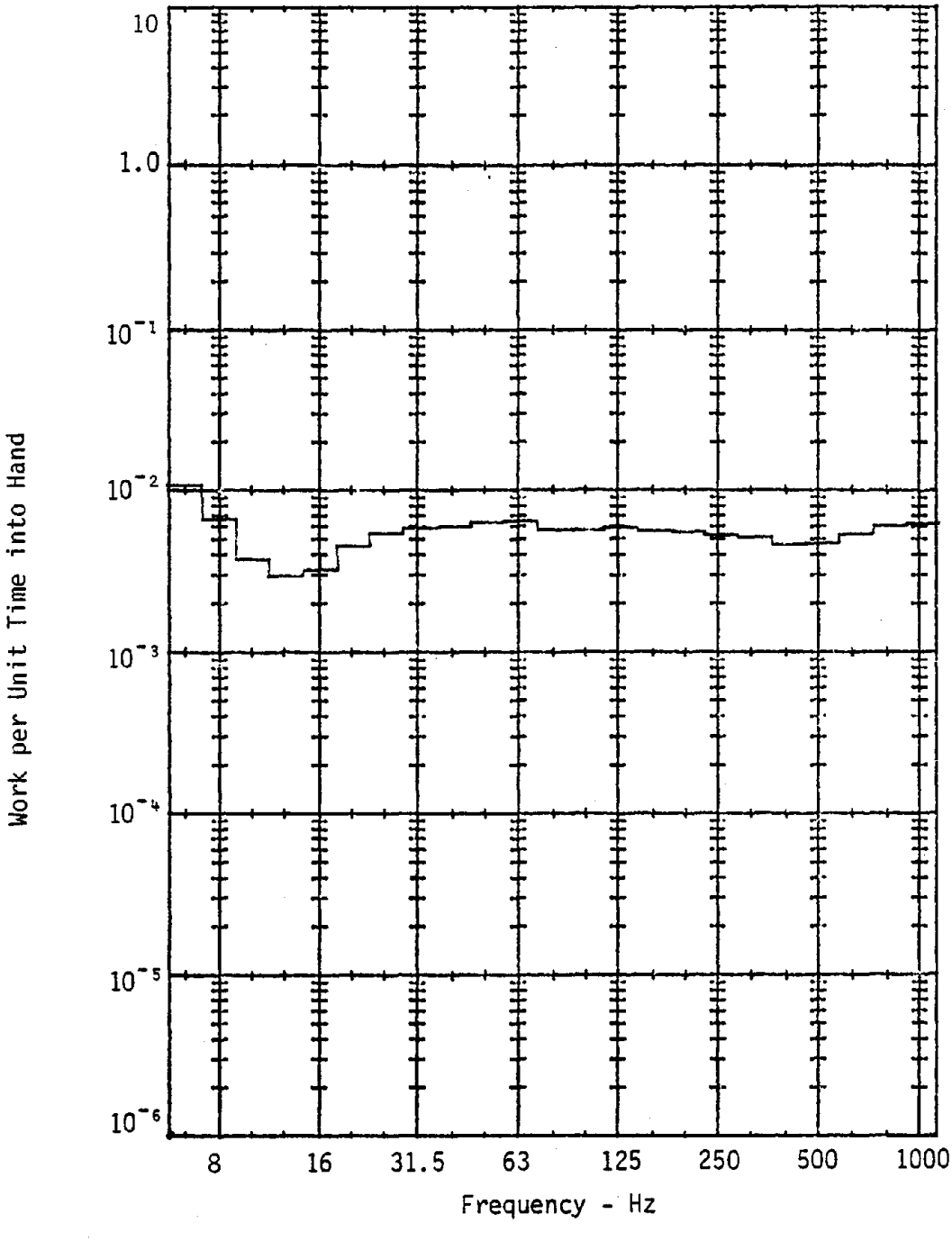

Figure F-40. RMS amplitude of work per unit time based on proposed ISO 8 hour acceleration limits. 1.9 cm handle, Y-direction.

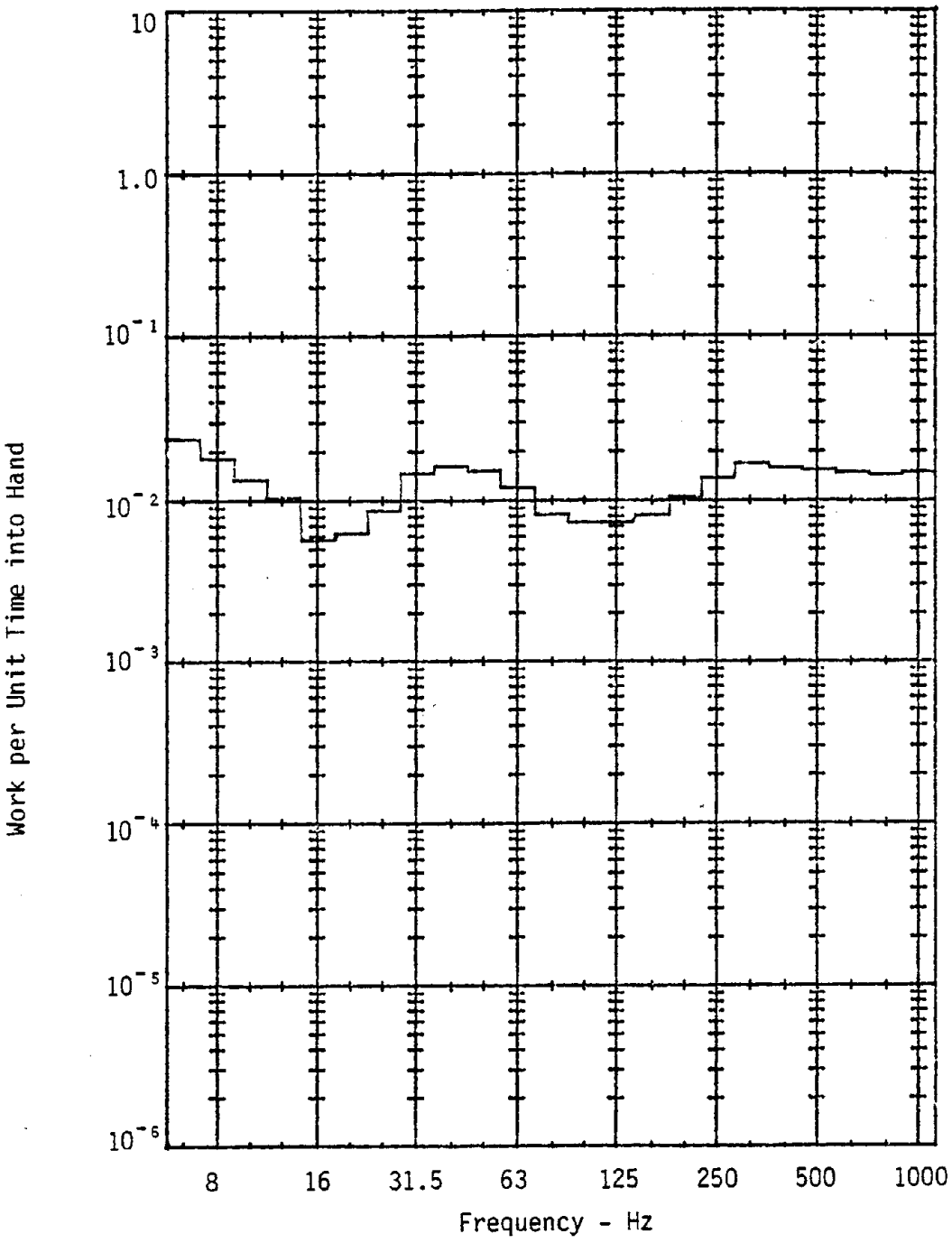

Figure F-41. RMS amplitude of work per unit time based on proposed ISO 8 hour acceleration limits. 1.9 cm handle, Z-direction.

APPENDIX G

DESCRIPTION OF WORKSITES, WORKPRACTICES & TOOLS USED ON THE JOB

Appendix G: Description of Worksites, Workplaces, and Tools Used on the Job

A total of 415 male workers from four workplace sites were investigated in this study: two gray-iron foundries, a shipyard, and the stoneworks of Bedford, Indiana. The pneumatic tools used by workers in the study of foundries and a shipyard were the Type 2 chipping hammer and a vertical and horizontal grinder. These same tool types are competitively made by various manufacturers.*

The chipping tool (also called an impact hammer) generally produces 2100 blows/ minute (corresponding to a 35 Hz repetition rate). It weighs about 12 pounds (5.45 kg) and its length can vary from 12 to 15 inches (30 to 37.5 cm) (depending on the manufacturer). The diameter of the rear handle is approximately 1.5 inches (3.75 cm). The diameter of the chisels used with these hammers is approximately 0.75 inch (1.875 cm) and the length can vary from a few inches to 2 foot. The characteristics of the working end of the chisels differ somewhat depending on the chisel application. Most importantly, so the worker can change chisels quickly, the chisel is inserted freely into the bore of the chipping hammer and is not usually retained while in use, i.e., the chisel, if not guided by the operator's hand and not working against resistance, is free to shoot out of the chipping tool. This is the main reason why the operator must place one hand around the chisel.

The foundries studied used pneumatic horizontal grinders accommodating 6 or 8 inch (15 to 20 cm) grinding wheels. These units rotate from 4500 to 6000 rpm (corresponding to 75 to 100 Hz). They weigh about 14 pounds (6.36 kg) and their length is from 20 to 25 inches (50 to 62.5 cm). The vertical grinders used in the shipyard accommodated similar grinding wheels, ran at about the same speed as the horizontal grinders and weighed about 8 pounds (3.64 kg).

For all these pneumatic tools, usable air pressure was in the 90 to 110 psi range. Each of the three worksites studied had a central tool crib and repair/maintenance station for these tools.

A description of the work situation for each of the foundries and shipyard follows.

Foundry # 1 - Foundry # 1 was a large, high volume production, gray iron foundry manufacturing large castings weighing more than 100 pounds (45.45 kg), such as vehicular castings (engine blocks, transmission cases, etc.). The casting metal used was a gray iron that falls under the Class 30 Gray Iron designation. This type of metal is a pearlitic (nodular) iron having a minimum of 30,000 psi tensile strength with a general hardness range of 187 to 255 BHN (Burnell Hardness Number).

* Ingersol-Rand Company, Chicago Pneumatic Company, Dresser Industries, Thor Corporation, The Dallet Company, Atlas-Copco Company, Rotor Corporation, and others.

We observed several workers using pneumatic chipping and grinding tools and discussed with various department supervisors and foremen how a worker uses both chipping and grinding tools interchangeably.

The men worked in teams of two and each team's work station consisted of a semi-enclosed cubicle (approximately 10 foot long x 5 foot (300 cm x 150 cm) wide). Approximately 20 of these stations were lined up side by side. Compressed air (90 psi) was brought to each work station to power two Type 2 chipping hammers (with assorted chisels, each from 1 to 3 foot (30 to 90 cm) long) and two rotary grinders (with 6 and 8 inch (15 and 20 cm) grinding wheels). Each cubicle had a waist-high steel table. Above this table was an electric hoist used to manipulate large castings. In operation, large castings were brought to each of these two-man work stations via a continuous overhead moving chain conveyor or by a forklift truck containing pallets of castings.

The men on these teams were paid on a piecework basis and worked very quickly. After they received the casting at their steel table, one man immediately began chipping the burrs off the visible faces of the casting and the other man followed next by grinding the area just chipped. After doing 1 to 3 surfaces, they would interchange tools. Sometimes both chipped simultaneously (e.g., one on the surface metal and the other in the deep cyclinder cavities of an engine block). After all visible surfaces were chipped and ground, they then hoisted it on the table to work on the remaining surfaces. A team could completely chip and grind an 800 pound transmission case, for example, in an average of 54 minutes. On occasion, some castings were "burnt" -- sand from the mold had impregnated itself on the casting. These were extremely difficult castings to chip and grind and were, as a rule, sent back to a single "reclaim/salvage chipper/grinder" (paid as an hourly employee, not as a pieceworker) who spent all the necessary time it took to do this difficult job. The ratio of two-man teams to reclaim/salvage chipper/grinders was 10 teams to 1 reclaim man.

These two-men teams worked very hard and very fast while operating their chipping and grinding tools, virtually all of the time at full tool throttle. They clasped the chipping tool (both at the chisel and rear end) with a tightly coupled wrap around palm grip (grip strength 5.7 pounds (25.4N) of force for each hand). The hand holding the chisel was usually gloved (to reduce the heat to the hand). The hand holding the rear handle was occasionally gloved, depending on operator preference. The method of hand clasping the pneumatic grinder was essentially the same as that for the chipping tool. Since the same operator interchangeably used both chipping and grinding tools, operator preference with regard to gloves did not change.

The gloves themselves were of medium weight leather or similar man-made materials and, we believe, did very little to attenuate the vibration except at the very high frequencies (above 500 Hz) when some absorption into the material undoubtedly took place. All chipper and grinders wore hearing protection and each wore a ventilated hood connected to a filtered, compressed air supply line. The hood also prevented flying metal and dirt particles from striking the eyes.

Based on our observations and discussions with supervisors, we estimate that in a normal 8 hour shift each chipper and grinder spent an average of 3.5 hours chipping, 2.5 hours grinding, 1.5 hours manipulating and moving castings, 0.5 hour break time. The reclaim/salvage chipper/grinder (hourly) worker averaged about the same time as the pieceworkers (except that he worked longer on much fewer castings). In this plant, there were about five or six different types of castings.

Foundry # 2 - Foundry # 2 is another large, high volume production, gray-iron foundry manufacturing small (less than 100 pounds (45.45 kg)) vehicular castings (oil pans, manifolds, etc.). The casting metal was the same type as that used in Foundry # 1.

Here we examined 66 chippers and grinders and 79 machine shop set-up men who were not exposed to either hand-arm or whole-body vibration. In this plant, the chippers and grinders were not teamed. Each man was paid on a piecework basis and the foundry operation was composed of many such workers. Castings were brought to the work station via forklift truck and pallet. A variety of types of small castings were handled with more grinding than chipping taking place. The same types of tools used in Foundry # 1 were used here. Chisel lengths varied from 3 to 12 inches (7.5 to 30 cm) and were not, as a rule, as long as those used in Foundry # 1.

The men in Foundry # 2 were also incentive workers and worked very quickly. Chipping and grinding time varied depending on the casting type, e.g., an 85 pound (38.6 kg) oil pan took about 10 minutes to complete, whereas a 44 pound (20 kg) manifold took about 1.5 minutes to complete. Here, again, there were a few hourly paid reclaim/salvage chipper/grinder operators (10 pieceworkers for each reclaim/salvage operator).

Each man wore hearing protection as well as a ventilated hood. As a rule, at least one glove was worn and, at times, both hands were gloved, depending on operator preference. The estimated work time was 4 hours grinding, 3 hours chipping, 0.5 hour casting manipulation, 0.5 hour break time.

We discussed with supervisors in both foundries the training given to their workers. They were brought up gradually as their skill level increased. This was by placing a new worker on the midnight to 8:00 a.m. shift where the workload is lighter than on the other two shifts. As his skill level increased, the trainee was eventually transferred to another shift. There appeared to be little specific training as to a preferred or a more appropriate method of working with the vibrating tools. Thus, each operator chose a working method that seemed to suit him.

Shipyard - The large shipyard operation we investigated employed about 10,000 workers. Large ships and ship propellers of all descriptions were built, repaired, modified, etc., at this location. These workers used the same chipping hammer used by the foundry workers (Type 2 chipping hammers) and a rotary type grinder not very different from the foundry type grinder.

We observed workers using pneumatic chipping and grinding tools and talked with supervisors in two departments to determine how the workers used these tools. Department X included men who worked in the holes of ships. Department Y included workers who chipped and ground propellers. All worked on a single daily work shift. The metals chipped by workers in both departments were: nickel-aluminum; bronze alloy; and mild steel,

Department X - The men in this department worked in the holes of ships and used both pneumatic chippers and grinders. An average 8 hour work day consisted of 4 hours of chipping, 2 hours of grinding, and 2 hours of performing other non-vibratory activities. On occasion, the chipping could extend to 5.5 hours per day. The workers were under continuous pressure to complete the work quickly and accurately.

One man trained all of the men in this department on the use of pneumatic chipping hammers. All chippers were instructed to use their body for leverage and thereby absorb some of the vibration energy from the chipping hammer. Their arms were to be held close to the body with the arm being braced by the body, knee, etc., for extra leverage. Generally, the chipping hammer chisel was guided with the first finger and thumb or the flat palm of the hand. The chisel was rarely in complete contact with the fingers. The chippers were trained to work holding the chipping hammer in either the right or left hand according to preference. The workers always wore leather gloves on BOTH HANDS, principally for heat reduction. Generally, they operated the chipping hammers for 15 to 20 minute stretches without resting. They also sharpened their own chisels, customizing them to suit themselves. The length of the chisel was from 3 to 5 inches (7.5 to 12.5 cm).

The men in this department basically performed two types of chipping operations: tamp and cut. The tamping operation included tamping and packing metal and other calking compounds into holes. Welders initially welded metal into a hole and the chippers finished the job by tamping the metal down to even it out and form a smooth surface. The chisel was held and guided by the flat part of the palm of the hand. The back handle was loosely clasped with the fingers. The workers leaned into the chipping hammer, pushing on the back handle with the palm of their hand and using their bodies as leverage. They interchanged hands frequently while holding the chipping hammer and chisel.

Using the chipping hammer for cutting involved removing metal, cleaning welds, etc. Sometimes workers used chisels to cut through bulkheads. For these operations, the workers guided the chisel with the flat part of the palm of the hand and gripped the back handle fairly tightly. They also used their body for leverage and interchanged hands frequently while holding the hammer and chisel. Frequently, they had to hold the chipping hammer over their head to perform some cutting operations. During nearly all of the chipping, the worker used the chipper at full throttle. The workers used pneumatic grinders to do finishing work. Both horizontal and vertical grinders were used.

Department Y - The men in this department cleaned and formed ship propellers. The workers spent about 3 hours of their time chipping, 3 hours grinding, and 2 hours in other activities. Because of the high precision required for finishing propellers, the workers worked very slowly. It was not unusual for a worker to work from 40 to 50 weeks on a newly cast propeller. Normally, a worker worked first on one side of a propeller. He first chipped the entire surface of the propeller and then ground the surface. When these operations were completed on one side, the propeller was turned over and the operations were repeated on the other side. These chipping and grinding operations generally occurred continuously over a several-week period before changing to another operation.

Chipping a propeller is very demanding and tiring work. The worker leaned into the chipping hammer with his body, pushing on the back handle of the hammer with the palm of his hand. He then guided the chisel with the flat part of the palm of his hand. Thus, his fingers never contacted the surface of the chisel and rarely contacted the back handle. In many cases, the worker rested the hand that guided the chisel on the front end of the chipping hammer. Thus, no part of his hand came in contact with the chisel. Each worker wore a glove only on the one hand that was used to guide the chisel. The hand that pushed against the back handle remained ungloved so that the worker's hand was free to "feel" the throttle trigger of the hammer. The workers mostly operated this tool at 1/2 to 3/4 throttle and chipped in 15 to 30 second bursts with a 2 to 3 minute rest period between bursts.

Workers indicated that the general maintenance of the tools (obtained from a central supply tool crib) was poor. They claimed that this, along with bent chisels, usually resulted in higher vibration levels.

The table given below summarizes the time estimates for chipping and grinding in an 8 hour day and on a yearly basis (assuming no overtime and a two week vacation period) at each of the three worksites studied. Estimates of time spent chipping, grinding, and in non-vibratory activity for each of the worksites studied in daily hours and total hours/year.*

	FOUNDRY					
	No. 1		No. 2		Shipyard	
Activity	hr/d	hr/y	hr/d	hr/y	hr/d	hr/y
Chipping	3.5	840	3	720	3	720
Grinding	2.5	600	4	960	3	720
No vibration	2	480	1	240	2	480

* Assuming an 8 hour day (40 hours/week), and a yearly work schedule of 50 weeks/year (2 week vacation period).

Limestone Workers

There are two types of limestone workers who use pneumatic tools: (a) cutters and carvers; and (b) drillers. Cutters and carvers are true artisans who use a myriad of chipping chisels, most no longer than 6 inches (15 cm) with a smaller impact hammer. These workers frequently change chisels and grip the chisel and barrel of the chipping tool very tightly. The tool is usually operated at full throttle without the benefit of a trigger grip throttle control. The thumb of the dominant hand (barrel hand) controls the tool throttle by pressing on a small exhaust hole. An operator uses the tool for 5-6 hours/day or a total of 1500 hours/year vibration exposure.

Drillers, unlike carvers and cutters, work in the quarry operations. Drillers use an impact hammer type of tool with a 3 foot (90 cm) pointed chisel. After the face of the limestone block to be quarried is exposed, the driller then drills a line of holes (spaced a few feet apart) across and down the sides of this face. Another worker then inserts wood wedges into these holes. The wedges are next driven into the limestone by sledge hammers, thus splitting the limestone into the desired dimensions. A crane next lifts the limestone block onto a flatbed truck for delivery to the mill where the carvers and cutters then form the finished piece. The driller uses the tool for 2-2.5 hours/day or 600 hours/year.

APPENDIX H

VIBRATION MOBILE UNIT

Appendix H: NIOSH Vibration Mobile Unit

The engineering vehicle to be briefly described here has been used for both whole-body and hand-arm vibration measurements -- either as a stationary vehicle (as was used in this study), or as a moving data collection center. Because we needed a versatile, rugged, on-off road mobile unit, reasonably small and compact, that could virtually go anywhere, under any road conditions, a four-wheel drive, military ambulance was selected and customized to meet our particular needs as a mobile control and data acquisition center.

Four modes of conducting a vibration field study are provided by the unit:

1. A stationary condition where the mobile unit would be parked adjacent to a building or a fixed structure, such as a foundry or quarry, and be for use in making segmental or whole-body field measurements, or both.

2. An off-road stationary condition, e.g., at a construction site, when various moving heavy equipment vehicles are sequentially monitored.

3. An off-road moving condition where, for example, the mobile unit would follow behind a scraper or other vehicle over an unpaved haul-road or other off-road area.

4. An on-road moving condition where, for example, the mobile unit would follow behind a tractor-trailer truck on a paved highway for a distance of several miles.

The vehicle (25 feet long x 10 feet high x 7 feet wide) is a converted Dodge 56-W200-126 4-wheel drive, former military ambulance. Major modifications included installing vibration and shock mounting (Barry Controls SLM-3) of three mutually braced instrumentation racks (Bud relay racks - Model RR1364) across the rear of the vehicle; raising the inside vehicular height from 5 to 6 feet; installing an internal air conditioning system and side viewing windows; installing vibration isolated seats (Bostrom-type thin line and T-bar seats); installing wide profile snow-type tires (from 8-17.5 to 10-16.5) for increased stability while in motion; and installing an underside tread plate, an auxillary gasoline tank, a rooftop tripod mount (for use with video equipment), two yellow beacon flashers for safety, and an access ladder to the roof area. Special TV mobile-unit-type cable reels were installed in the vehicle to accomodate the several hundred feet of cabling used for stationary operation of the mobile unit.

So that the reader will obtain an appreciation for the versatility of this vehicle, a brief description of its multiple uses is described.

When the mobile unit is used for whole-body vibration measurements, it is used in conjunction with a 14-channel 216.5 MHz telemetry transmitter mounted near a vehicle operator. Measuring transducers from both the vehicle and human subject under test are wired to this transmitter that, in turn, transmits the multi-channel data to the mobile unit. Vehicle speed is also measured (using a Doppler police radar unit) as well as TV observation of the subject and vehicle under test. The mobile unit thus contains a custom

designed base-loaded telemetry receiving antenna mounted on a modified three-section telescoping 19 foot antenna mount (Radio Shack 15-5065) with the lower part of the mount welded to the rear of the mobile unit. Since the telemetry is operated at 216.5 MHz, line-of-sight transmission and reception is the preferred mode of operation. Using a telescoping antenna ensures maximum signal-to-noise ratio under hilly and obstructive conditions. A 5000-watt, 100 VAC single-phase (50 amp) alternator (Generac Model XP-50140, 6207-5) is installed with the air intake line to the alternator remotely positioned to roof level (passenger side rear); this is done to minimize failure of the alternator in dusty conditions during field studies, especially in off-road areas. The alternator is operated from an auxillary 12-volt battery and does not interfere with the truck's normal 12-volt battery. Because the alternator automatically charges this auxillary battery, the vehicle has 110 VAC single-phase power, as well as auxillary DC power for use with special low-power (30 W) interior fluorescent lamps (Sears 28AB49347) and the Doppler radar unit. Our carpentry shop designed several unique storage containers and fittings so that we could maximize the use of existing interior space. The truck is air-conditioned (Frigiking Chiller 10 unit, 10,000 BTU).

During whole-body field studies, the mobile unit normally carries a three-man crew; all work assignments are related. Functionally, a single operator completely controls the major electronics system (i.e., receivers, video tape recorder, Fourier minicomputer, instrumentation, tape system, etc.) from a single command position situated just behind the vehicle driver and passenger, facing the electronics racks. A second person operates the roof video camera chain, and the third person doubles as the mobile unit driver and operator of the Doppler speed-measuring unit. Much of the electronic instrumentation and mechanical fixtures used in the field studies was designed and built in-house by our NIOSH group. Details of the vehicle's use in whole-body vibration studies are given elsewhere*.

The mobile unit was used for most of the engineering testing in this study. This was accomplished in part by using a rack-mounted Spectral Dynamics Model SD1002EP-1A Portable Mechanical Impedance System in conjunction with a swivel base mounted in the vehicle cab and consisting of three orthogonal Oinishakers (as described in the engineering section) mounted with the sets of three removable handles. Between each shaker and its respective handle was affixed an impedance "head" transducer. During this study, acceleration measurements were obtained from the vibrating pneumatic tools while being used. Also, dynamic compliance using the above Spectral Dynamics System was measured and recorded on 75 subjects selected by the medical team.

In conclusion, this mobile unit has a great deal of versatility with its cabability for capturing, storing, and analyzing a variety of environmental data on-site under a variety of field conditions.

---

* Wasserman, D., T. Doyle, and W. Asburry. 1978. Whole-Body Exposure of Workers During Heavy Equipment Operation. DHEW (NIOSH) Publication No. 78-153.

* U.S. GOVERNMENT PRINTING OFFICE: 1981 -559-093/3612